ELECTROCHEMISTRY RESEARCH LABORATORIES

DEPARTMENT OF CHEMISTRY
JOHN SCHOFF MILLIS SCIENCE CENTER
CASE WESTERN RESERVE UNIVERSITY
CLEVELAND, OHIO 44106

FINAL REPORT

CATALYSTS FOR ELECTROCHEMICAL GENERATION OF OXYGEN

Report prepared by: P. Hagans and E. Yeager

Project Director: Ernest Yeager

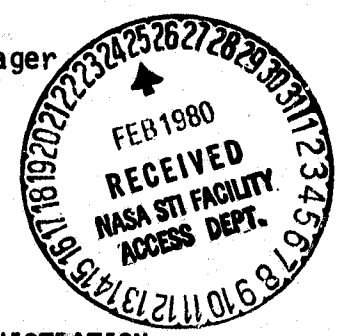

NATIONAL AERONAUTICS & SPACE ADMINISTRATION

NASA-Ames Grant No. NGR 36-027-050

TABLE OF CONTENTS

Chemistry Department
Case Western Reserve University
Cleveland, Ohio 44106

CATALYSTS FOR THE ELECTROCHEMICAL GENERATION OF OXYGEN

Final Report for 1972 to 1979

Sponsor: NASA-Ames

Grant No.: NGR 36-027-050

I. PRIMARY OBJECTIVES

To find new, more effective catalysts for the electrolytic evolution of oxygen and to understand the mechanism and kinetics for the electrocatalysis in relation to the surface electronic and lattice properties of the catalyst.

II. SPECIFIC OBJECTIVES FOR THIS REPORT

This report concludes all research performed under NASA Grant 36-027-050. A short summary of all work is presented, followed by an Appendix containing all published research papers which pertain to the work performed under the grant.

III. SUMMARY OF THE WORK

The objective of the research was the development of high active electrocatalysts for O_2 generation in life support systems. Edisonian methods have not proved effective in earlier work carried out by various industrial laboratories and consequently the present work was in good part directed to establishing a predictive base and particularly identifying the relation of the mechanisms and rate constants to the surface electronic properties and morphology. The energy efficiency of O_2 electrogeneration is adversely affected by the overvoltage at both the oxygen generating anode and the hydrogen counter electrode used in the water electrolysis cell. The research has included O_2 as well as H_2 electrocatalysis with principal emphasis on the former.

The early phase of the research concentrated on the examination of the kinetics of the O_2 generation reaction on a number of surfaces including various defect oxides. Several oxide catalysts were found to be considerably more active for O_2 anodic generation than platinum. These include RuO_x, IrO_x and La_xCoO_y on substrates such as titanium metal. The O_2 generation proceeds with a much lower Tafel slope on these surfaces than on Pt, indicating a different rate controlling step. Platinum, however, can be in very high area form and remains one of the most effective electrocatalysts for both the O_2 anode and H_2 cathode.

In the more recent phase of the research the electrochemical properties of Pt have been examined in alkaline and acid electrolytes in considerable detail. Special emphasis has been placed on the electrosorption of hydrogen and anodic film formation on Pt since these play a critical role in water electrolysis with Pt electrodes. The research has shown that the competitive adsorption of various anions has a pronounced effect on hydrogen electrosorption and anodic film formation and in turn influences H_2 as well as O_2 generation. In alkaline solutions, the presence of divalent cations was found to influence the behavior of the anodic films. This information is of considerable help in understanding the electrocatalytic properties of Pt.

A key question in electrocatalysis is the role of the surface morphology. Various workers including our group have attempted to examine electrosorption and electrode kinetics for the O_2 and H_2 electrode reactions on specific surfaces of single crystal metals including Pt but the results have been questionable. While the bulk electrodes were single crystal, the surfaces have generally not corresponded to a single crystal plane. Further, such studies have usually been complicated by surface impurities such as carbon. Modern surface physics techniques can be used to produce and characterize

single crystal surfaces of known morphology, free of impurities. This offers an exciting opportunity for electrochemical studies of such surfaces, provided the transfer between the electrochemical and ultrahigh vacuum environments can be carried out in such a way to avoid restructuring and contamination of the electrode surfaces. A special transfer system was developed for transferring single crystal electrode surfaces directly from the ultrahigh vacuum of a LEED-Auger system into the electrochemical environment within a thin layer electrochemical cell. This system was then used to examine hydrogen electrosorption on the low index planes of Pt single crystals during 1976 and 1977. These studies clearly demonstrated that the electrosorption of hydrogen and hence the electrocatalytic properties are strongly dependent on the surface morphology.

Within the last two years, the LEED-Auger thin-layer electrochemical cell system has been used to examine an underpotential deposited foreign metal layer on a noble metal substrate, in particular lead on gold. Such systems are of special interest because of thin catalytic properties. The three low index planes of Au [(100), (111) and (110)] and one stepped surface (410) were studied. Special emphais was placed on returning the Au single crystals back to the LEED-Auger chamber after the electrochemistry was completed. The voltammetric results indicate that each surface is highly specific toward Pb adsorption at mono- and submonolayer levels. Various processes including phase transitions within the underpotentially deposited Pb layer and reconstruction of the Au surface were identified. This research resulted in a Ph.D. thesis which is presented in the Appendix.

In the past two months new studies were begun using the LEED-Auger thin-layer electrochemical cell system to examine oxide formation on Au and Pt single crystals using HF as the electrolyte. Very preliminary post-LEED results have been obtained which indicate that, for the case of Au (100),

potential cycling into the oxide region appears to be an annealing effect on the clean, reconstructed (5x20) surface. However, for Pt (111), as little as three cycles into the oxide region has a strong perturbance on the Pt surface as is indicated by gross modification of the hydrogen adsorption-desorption region in the voltammetry curves. The effect is not as dramatic with the Pt (100) surface but the hydrogen region shows new structure not previously seen in the earlier experiments with the H_2SO_4 electrolyte. No conclusive post-LEED work has been obtained with the Pt surfaces as of yet. These results are extremely preliminary and further work is now in progress to verify or disprove this new data.

Also during the past year various transition metal oxides with spinel structures have been prepared in conjunction with a DOE supported project involving O_2 electroreduction catalysts for chlor-alkali cell and air-consuming battery applications. These oxides may also prove active as O_2 generation catalysts. Consequently two more promising spinels ($NiCo_2O_4$ and Co_3O_4) are being examined for O_2 generation as part of this NASA project.

IV. SUMMARY OF PAPERS PUBLISHED UNDER NASA SUPPORT

1. "Ruthenium Oxide Catalysts for the Oxygen Electrode," W. O'Grady, C. Iwakura, J. Huang and E. Yeager, in Proceedings of the Symposium on Electrocatalysis, M. Breiter, ed., The Electrochemical Society, Princeton, N.J., 1974, pp. 285-302.

2. "Oxygen Electrode Kinetics on Various Electrode Surfaces," E. Yeager, Proceedings of Fuel Cell Catalysis Workshop, Electric Power Research Institute, A. Fickett, Ed., 1975, pp. 49-60.

3. "Theory of Charge Transfer at Electrochemical Interfaces," in Annual Review of Physical Chemistry, 26, 287 (1975).

4. "Mechanisms of Electrochemical Reactions on Non-Metallic Surfaces," National Bureau of Standards Publ. 455, 1976, pp. 203-219.

5. "Oxygen Electrocatalysis for Life Support Systems," by W. O'Grady, C. Iwakura and E. Yeager, ASME Publication 76-ENAs-37, pp. 1-12, 1976.

6. "Electrode Surface Studies by LEED-Auger," by W. O'Grady, M. Woo, P. Hagans and E. Yeager, J. Vac. Sci. Technol., 14, 101 (1977).

7. "The Effects of Cations and Anions on Hydrogen Chemisorption at Pt," by J.C. Huang, W. O'Grady and E. Yeager, J. Electrochem. Soc., 124, 1732-1737 (1977).

8. "Recent Advances in the Understanding of Electrocatalysis and Its Relation to Surface Chemistry," by Ernest Yeager, in Electrode Material and Processes for Energy Conversion and Storage, J.D.E. McIntyre, S. Srinivasan and F.G. Will, eds., The Electrochemical Society, Princeton, N.J., 1977, pp. 149-171.

9. "Electrochemical Hydrogen Adsorption on the Pt (111) and (100) Surfaces", by W. O'Grady, M.Y.C. Woo, P. Hagans and Ernest Yeager, in Electrode Material and Processes for Energy Conversion and Storage, J.D.E. McIntyre, S. Srinivasan and F.G. Will, eds., The Electrochemical Society, Princeton, N.J., 1977, pp. 172-184.

10. "Hydrogen Adsorption on Single Crystal Platinum", by E. Yeager, W. O'Grady, M.Y.C. Woo, and P. Hagans, J. Electrochem. Soc., 125, 348-349 (1978).

11. "LEED-Auger Thin-Layer Electrochemical Study of the Underpotential Deposition of Pb onto Au Single Crystals," P.L. Hagans, Ph.D. Thesis, Case Western Reserve University, Cleveland, Ohio (1979).(To be published).

12. "Non-Traditional Approaches to the Study of the Solid-Electrolyte Interface: Problem Overview", by E. Yeager, presented at the International Conference, Non-Traditional Approaches to the Study of the Solid-Electrolyte Interface, held September 24-27, 1979 in Snowmass, Colorado. Proceedings to be published.

V. APPENDIX

Publications attached.

Reprinted from Electrocatalysis

RUTHENIUM OXIDE CATALYSTS FOR THE OXYGEN ELECTRODE

W. O'Grady, C. Iwakura,* J. Huang, and Ernest Yeager

Department of Chemistry, Case Western Reserve University
Cleveland, Ohio 44106

Abstract

The electrochemical properties of ruthenium oxide on Ti and other substrates have been examined using linear sweep voltammetry. The oxygen electrode kinetics have been studied in alkaline solutions on RuO_x on Ti using principally the rotating disk technique. O_2 reduction involves the formation of peroxide in the solution phase. O_2 generation occurs at low overpotentials and the kinetics are characterized by a Tafel slope of 0.040V/decade and a first order dependence on OH^- concentration. Mechanisms are proposed to explain the experimental results.

I. Introduction

Ruthenium oxide on a titanium substrate has found wide application in the clor-alkali industry as an electrocatalyst with low overpotential and long life for the anodic generation of Cl_2. Various workers have reported that RuO_x on Ti (1) as well as Ru metal and metal blacks (2-4) have low anodic O_2 overpotential in acid solutions. The present study has involved the examination of RuO_x on substrates such as Ti as a catalyst for the O_2 electrode, principally in alkaline solutions.

Bulk RuO_2 had metallic like conductivity (5) as a result of the overlapping partially filled π^* bands with a Fermi energy close to the top of the filled t_{1g} states (6). Cyclic voltammetry, electronic conductivity, and x-ray diffraction measurements, however, indicate substantial differences between single crystal RuO_2 and the film produced by thermal decomposition of $RuCl_3$ in air or O_2 on substrates such as Ti (1). The RuO_x surface films are most likely highly defect and non-stoichiometric. In contact with aqueous solutions, the RuO_x surface film is expected to contain bound water as a result of proton penetration into the oxide lattice. Kuhn and Mortimer (7) have proposed that the RuO_x films on Ti behave as semiconductors (probably n-type) and that the semiconductor properties strongly influence the polarization curves for Cl_2 generation, with a substantial portion of the potential drop across a space charge region within the RuO_x film.

---

* Present address: Department of Applied Chemistry, Faculty of Engineering, Osaka University, Suita, Osaka, Japan.

The electrochemical studies of the RuO_x catalyst reported in this paper have involved two types of measurements: 1) preliminary characterization of the catalyst using linear slow sweep voltammetry without special precautions to control purity and 2) anodic and cathodic polarization measurements, essentially steady state with the rotating disk technique under much better controlled conditions, particularly with respect to the elimination of possible impurities. These electrochemical measurements have been complemented by X-ray photoelectron (ESCA) studies of the RuO_x catalyst both before and after electrochemical treatment. The ESCA spectra yield information concerning the valency state as well as elemental composition of the catalyst. Although the electrochemical and ESCA studies of the RuO_x catalyst system have not yet been completed at the time of preparation of this paper, interesting features are already evident from the available data and are herein reported.

II. Experimental

1. Preparation of electrode surfaces

The RuO_x films have been formed on titanium by a thermal decomposition method similar to that reported in the patent literature (8) for the DSA anodes used in the chlor-alkali industry. For the preliminary voltammetry measurements, flat Ti sheet (5 cm x 1 cm x 0.1 cm) was used for the substrate while 0.5 cm diameter Ti rod stock was used for the preparation of the rotating disk electrodes (in both instances 99.95% Ti, supplied by Research Organics/Inorganics). After polishing the Ti with emery and thorough cleaning, including degreasing by refluxing in isoproponal vapor, the surface was coated with a solution of reagent grade $RuCl_3$ (Fisher) in 20% HCl. In the earlier work, sufficient concentrated H_2O_2 was added to oxidize the ruthenium to Ru IV, but this addition was found to have no observable effect on the final catalyst and the H_2O_2 addition was not made for the remainder of the work.

In order to vary the catalyst loading on the electrode surface while maintaining an essentially constant preparative procedure, varying amounts of the original solution (0.1M Ru) were diluted to the same volume and this solution then applied to the substrate in six repetitive coatings or alternatively the number of coatings varied. After each coating, the solution was dried at a moderate temperature (110°C in a drying oven for 5 min) and then placed in a preheated furnace at 350°C for 10 min. After the final coating, the temperature of the furnace was raised to 450°C for 1 hour. The catalyst loadings examined in the present work ranged from 10^{-9} to 10^{-5} moles of Ru per cm^2.

The X-ray diffraction characteristics of this catalyst were examined and found to be essentially the same as reported by Pizzini *et al.* (21) for RuO_x produced at 400-500°C. Line breadth indicates a domain size of several hundred Angstroms. No change was detected in the X-ray diffraction before and after use as an electrode.

The disk electrodes were press fitted into a Teflon mounting which attached to the shaft of the rotating disk electrode assembly. With the flat sheet electrodes, the geometric area exposed to the solution was reduced to 1 cm x 1 cm on one side by using a vinyl copolymer resin lacquer[1] to mask off the remainder of the electrode.

An attempt was also made to examine the O_2 overpotential on ruthenium metal in alkaline solutions using both single crystal ruthenium (supplied by Research Organic/Inorganic) and electrodeposited Ru in a Pt substrate. The single crystal measurements were carried out both on the basal plane [0001] and the general faces [kh10] of the hexagonal structures, using the masking lacquer to restrict the surface of the single crystal exposed to the electrolyte. The electrodeposited Ru was electroplated from a solution of $(NH_4)_2Ru(H_2O)Cl_5$ on to Pt wire at a current density of 70 ma/cm^2 for 10 min using the procedure of Galizziole and Trasatti (9).

Unfortunately, active dissolution of either type of Ru metal electrodes begins at ~1.3 V vs. RHE[2] in the 4M KOH solutions with no indication of passivation in the slow sweep voltammetry curves at more anodic potentials. On the basis of the color imparted to the solution near the electrode and the Pourbaix diagram (10), the dissolution product appears to be RuO_4^{-2}.

2. Electrochemical cells and procedures

The rotating disk experiment was carried out in an all Teflon cell (11) consisting of a main compartment containing the working electrode and two separate compartments for the reference and counter electrodes, both of which were Pd-H in the form of Pd diaphragms supplied with H_2 from the back side. The reference compartment was connected to the main working electrode compartment by a Teflon Luggin capillary positioned at 4 mm from the rotating disk electrode surface on the axis of rotation. The electrolyte in the main compartment was usually saturated with purified O_2 gas (12).

The majority of the measurements have been carried out with 4M KOH prepared from reagent grade KOH (Baker, 0.2% carbonate) and triply distilled water (second stage from alkaline permanganate). For the pH dependence studies, different ratios of 1M KOH and 0.5 M K_2SO_4 were used. For the rotating disk experiments, the solutions were pre-electrolyzed in a separate Teflon cell between bright nickel electrodes (7 cm^2 each) at a current density of 1 ma/cm^2 for a minimum of 24 hr with agitation obtained using purified helium gas (12).

The measurements with the flat RuO_x/Ti electrodes were carried out in a Pyrex cell with a Teflon cap without pre-electrolysis, using a

---

[1] Microshield Stop-Off Lacquer (Michigan Chrome and Chemical Co.)

[2] Unless otherwise indicated, all electrode potentials are expressed relative to a reversible hydrogen electrode (RHE) in the same solution.

bright platinum counter electrode and a glass Luggin capillary with electrochemically charged α-Pd-H as the reference. From time to time, the reference was checked against a calomel or Hg-HgO reference.

A Wenking potentiostat, a linear sweep generator and Houston x-y recorder were used to carry out the electrochemical measurements. The essentially steady state polarization data were obtained with very slow voltage sweeps (1 mV/sec) and in some instances also with point by point measurements (e.g., 3 min per point) as a check. The IR drop corrections, needed at higher current densities, were determined using the current interrupter technique with a high pressure hydrogen, mercury-wetted relay to interrupt the current.

III. Results

1. Electrochemical area

The Zn^{2+} ion adsorption technique, developed by Kozawa (13) has been used to obtain an estimate of the ratio of true-to-apparent area for the RuO_x on Ti electrodes. This method is preferred to the usual BET measurements since pores that may not necessarily be electrochemically accessible may contribute to the BET areas.

The Zn^{2+} adsorption method is based on the concept that the Zn^{2+} will ion exchange with H^+ bound to surface $O^=$, releasing H^+ into the solution. The assumption is made that the surface coverage with Zn^{2+} is near or at saturation and that the area per Zn^{2+} has a specific value. Kozawa has demonstrated the validity of the method for battery oxides such as MnO_2 with the Zn^{2+} adsorption measured by the decrease in Zn^{2+} concentration in a $ZnCl_2$-NH_4Cl solution and the area taken to be 17 $Å^2$ per adsorbed Zn^{2+}.

In the present study, the Zn^{2+} ion adsorption was measured on the RuO_x coated flat titanium electrodes by placing them in a 0.5M NH_4Cl solution containing 0.005M Zn^{+2} at a pH of 7.25. Overnight was allowed for equilibrium and an alloquote of the solution, then titrated with EDTA using Erichrome Black T as the indicator.

As a check on the question of whether the Zn^{2+} coverage was close to the saturation value of the adsorption isotherm, the adsorption was checked in 0.002M $ZnCl_2$ and 0.010M $ZnCl_2$ with both solutions containing 0.5M NH_4Cl at pH of 7.25 and the electrodes at an open-circuit potential of 0.21 to 0.22 V vs. SCE. The Zn^{2+} adsorption was the same within the reproducibility of the method (± 10%).

Using an area of 20 $Å^2/Zn^{2+}$, the ratio of true-to-apparent surface areas is typically 60-80 for a catalyst loading of 1 x 10^{-5} moles Ru/cm^2 of geometry area. Using krypton BET, Kuhn and Mortimer (7) found a ratio of 240 for their RuO_x on Ti electrodes. While the technique used to prepare their electrodes is similar to that in the present work, their catalyst loading is not specified. Since more concentrated Ru

solutions (0.4M) were used by Kuhn and Mortimer for coating their electrodes, the thickness of the RuO_x coatings on their electrodes may well have been several fold greater.

2. Voltammetry curves for RuO_x

Typical slow sweep voltammetry curves are shown in Figure 1 in N_2-saturated alkaline and acid solutions. Some minor features of the curves in the voltage range 0.6 - 1.0 V are associated with the O_2/H_2O_2 couple. The peak at ~1.3 V in the alkaline solution is only slightly irreversible at the sweep rate of 50 mV/sec. This peak has also been observed with RuO_x on nickel, platinum, and gold substrates, and hence is not associated with the substrate. This peak is much suppressed or almost absent for mixed oxide layers of Ru + Ti as well as Ru + Ir and Ru + Pt, produced by thermal decomposition on a Ti substrate (see Fig. 2). Thus the peak is associated with the RuO_x.

At slow sweep rates (e.g., 10 mV/sec) this peak is essentially reversible with the anodic and cathodic peak potentials coinciding. The peak current is directly proportional to the sweep rate over the range examined (1 to 300 mV/sec) and the charge under the peak (subtracting the background) is independent of sweep rate over this range. The estimated value for the charge ~5 x 10^{-3} C/cm^2 (apparent area) represented a very small fraction of the total charge ~1C/cm^2 required to change the valency state of all the ruthenium in the coating by one oxidation state. Consequently, this peak probably corresponds to a change of the valency state of only surface Ru. For a true-to-apparent area ratio of 50, the charge associated with this peak corresponds to ~100μC/cm^2 of true area, which is reasonable for a change of surface ruthenium by one charge state.

On the basis of the voltammetry curves, it appears that the RuO_x can be reduced and reoxidized over a substantial range of potentials in both acid and alkaline solution. The oxidation and reduction products appear to involve a single phase in view of having the voltammetry current density high over the wide potential range of the sweep rather than having the charge associated with a single voltammetry peak, even at very low sweep rates. After correction for the Faradaic currents associated with O_2 and small amount of H_2O_2 produced in the electrolyte, the shape of the voltammetry curves is essentially the same for sweep rates from 1 to 50 mV/sec with the current density approximately proportional to the sweep rate. The corresponding current density for uncoated Ti electrodes is at least an order of magnitude less. The total charge associated with the area under the voltammetry curves in the cathodic or anodic sweeps between 0.1 and 1.4 V is approximately 0.1 C/cm^2 of apparent area for the electrodes with 1 x 10^{-5} moles Ru/cm^2, or approximately one-tenth of that required to change the valency state by one electron per Ru atom in the oxide coating.

Kozawa (14) has reported that porous bulk hydrated RuO_2 can be reduced rather reversibly over an extended voltage range when mixed

with carbon in both alkaline and acid solutions. The reduction of the porous anhydrous RuO_2 was far less reversible, but this difference may be associated with the 8 fold larger pore area of the hydrated material. The reduction of the oxide with the reactant and product in a single oxide phase requires the introduction of protons into the oxide lattice. If the proton mobility within the oxide is low, the rate of the reduction as well as oxidation of the RuO_x may be proportional to the surface area.

The initial open-circuit voltage observed by Kozawa starting with near stoichiometric RuO_2 was +0.5 V and +0.8 V vs. RHE for the anhydrous and hydrated materials, respectively. Even considering the question of the reversibility of these potential measurements, it appears likely that the O_2 evolution reaction on RuO_x on Ti occurs in a potential range where at least the surface Ru ions of the catalyst are in a higher valency state than +4.

A large cathodic peak was observed in the voltammetry curves for the RuO_x on Ti electrodes in N_2 saturated KOH solutions in the potential range 0.6 to 0.9 V when the anodic limit of the sweep was extended beyond 1.4 V (see Fig. 3). Saturation of the solution with O_2 rather than N_2 increased this peak. The potential range corresponds to that expected for O_2 reduction to HO_2^-. The assignment of this peak to the reduction of O_2 to peroxide was confirmed by adding the H_2O_2 to the solution and observing complementary cathodic and anodic peaks (see Fig. 4). Thus in alkaline solutions, O_2 reduction on RuO_x/Ti electrodes involves solution phase HO_2^- as an intermediate.

3. ESCA measurements

A few preliminary ESCA spectra have been obtained for the RuO_x/Ti surfaces before and after electrochemical treatment at 1.45 V in 4M KOH for up to 1 hr using a Varian IEE-15 spectrometer with a modified high intensity X-ray source. The instrumental line width was controlled by the width of the Al K_α radiation used to produce the photoelectrons and was 1 eV as measured by the width at half maximum of the Au 4f lines. Complications have been encountered because of peak interferences and limited resolution. The interference-free Ru $3d_{5/2}$ peak at a binding energy of 280 eV for the RuO_x/Ti surface does not show any appreciable shift following the electrochemical treatment at 1.45 V and thus the valency state of most of the Ru in the oxide layer appears to remain unchanged. This evidence must be interpreted with some caution, however, since it is possible that the oxide was transformed to a higher valency state during the polarization at 1.45 V but after loss of potential control, during the subsequent rinsing and drying in air, was reduced back by the Ti metal to the valency state prevailing before the electrochemical treatment. Further work is planned to check on this possibility.

4. Polarization measurements with the rotating disk electrode

Fig. 5 indicates the log current density vs potential data obtained potentiostatically for a RuO_x/Ti electrode with a very slow sweep (1 mV/sec) in O_2 saturated 4M KOH at a rotation rate of 8800 rpm.

The hysteresis evident in this type of plot is very pronounced at low current densities because of the small currents associated with intrinsic changes in the oxidation state of the catalyst even at such slow sweep rates. The anodic branch for O_2 generation is free of hysteresis effects above 5×10^{-3} A/cm^2 (apparent area) and exhibits a Tafel slope of 0.040 V/decade over at least 3 decades after IR drop correction. Measurements in KOH-K_2SO_4 solutions of varying pH with constant K^+ ion concentration indicate a reaction order of 1.0 with respect to OH^- for the O_2 generation reaction over the pH range 11 to 14 (see Fig. 6). With the electrode stationary and control of the boundary layer by O_2 bubble evolutions, a limiting current density has been observed in the KOH-K_2SO_4 electrolytes, which is directly proportional to the OH^- ion concentration from pH 10 to 14, amounting to ~0.02 A/cm^2 (apparent area) at pH 11.8. Above the limiting current density, the discharge is from water with a Tafel slope of ~0.13 V/decade, indicating a change in mechanism.

Unfortunately the stoichiometric number cannot be obtained for the O_2 generation reaction in the alkaline solutions because of the interference from the intrinsic electrochemistry of the RuO_x/Ti electrode surface at low current densities near the reversible potential for the 4-electron reaction.

The Tafel slopes are independent of the catalyst loading over the ranges 10^{-8} to 10^{-5} moles Ru/cm^2 and the apparent exchange current densities are approximately proportional to the catalyst loading over this range (see Fig. 7). Such a proportion is to be expected since the true-to-apparent area ratio is also approximately proportional to the catalyst loading.

The current density passes through zero in the anodic sweep and increases very substantially cathodically during the cathodic sweep at approximately 0.90 V as a consequence of the $O_2 - HO_2^-$ reaction. The dependence of the O_2 reduction current density on rotation rate (f) at constant potential indicates that the O_2 reduction is under combined diffusion and kinetic control (see Fig. 8). The linear relationship between $1/i$ vs. $1/\sqrt{f}$ indicates that the reduction is first order in the diffusing reactant with the intercept corresponding to the current density with pure kinetic control and the slope only a function of the diffusion coefficient and bulk concentration of the diffusing reactant, according to the Levich treatment (15). The slope changes with potential, however, according to Fig. 8.

This can be explained in terms of the following two reduction processes:

<u>Reaction 1</u>: $O_2 + H_2O + 2e^- \xrightarrow{k_1} HO_2^- + HO^-$ (1)

<u>Reaction 2</u>: $HO_2^- + H_2O + 2e^- \xrightarrow{k_2} 3HO^-$ (2)

At potentials equal to and more cathodic than 0.80 V, the back reactions for both processes are negligible compared to the forward reactions for the conditions prevailing in the present experiments. Under these circumstances, assuming first order kinetics in O_2 and HO_2^- for reactions 1 and 2, respectively, the cathodic current density can be expressed as

$$i = \left[\frac{1}{\frac{1}{(i_d)_1} + \frac{1}{(i_k)_1}} + \frac{1}{\frac{2}{(i_d)_2} + \frac{1}{(i_k)_2}}\right] \cdot \left[\frac{\frac{2}{(i_d)_2} + \frac{1}{(i_k)_2}}{\frac{1}{(i_d)_2} + \frac{1}{(i_k)_2}}\right] \qquad (3)$$

where

$$(i_k)_1 = \vec{k_1} C^\circ_{O_2} \; ; \; (i_k)_2 = \vec{k_2} C^\circ_{HO_2^-} \qquad (4a,b)$$

with $C^\circ_{O_2}$ and $C^\circ_{HO_2^-}$ the bulk concentrations and $\vec{k_1}$ and $\vec{k_2}$ the first order potential-dependent rate constants. The quantities $(i_d)_1$ and $(i_d)_2$ are the diffusion limiting current densities for the independent reduction of O_2 and HO_2^-, respectively, and are related to the diffusion coefficients D_{O_2} and $D_{HO_2^-}$ and the Nernst diffusion layer thickness δ by the equations[2]

$$(i_d)_1 = 2 F D_{O_2} C^\circ_{O_2}/\delta \qquad (5)$$

and

$$(i_d)_2 = 2F D_{HO_2^-} C^\circ_{HO_2^-}/\delta \qquad (6)$$

where F is the Faraday.

For the measurements represented on Fig. 8, the only bulk HO_2^- present is that produced by O_2 reduction during the measurements. Consequantly $(i_d)_2$ and $(i_k)_2$ should be very small compared to $(i_d)_1$ and $(i_k)_1$, respectively. Therefore,

$$\frac{1}{\frac{2}{(i_d)_2} + \frac{1}{(i_k)_2}} \ll \frac{1}{\frac{1}{(i_d)_1} + \frac{1}{(i_k)_1}} \qquad (7)$$

in the first factor on the right hand side of eq. (3), and

$$\frac{1}{I} = \left[\frac{1}{(i_d)_1} + \frac{1}{(i_k)_1}\right] \cdot \left[\frac{\frac{1}{(i_d)_2} + \frac{1}{(i_k)_2}}{\frac{2}{(i_d)_2} + \frac{1}{(i_d)_2}}\right] \qquad (8)$$

As the cathodic overpotential for O_2 reduction increases, $(i_k)_2$ will become larger because of the potential dependence of k_2 while $(i_d)_2$ is independent of potential. Therefore, consider the following

situations:

Case I: $(i_k)_2 \ll (i_d)_2$. Eq. (8) becomes

$$\frac{1}{i} = \frac{1}{(i_d)_1} + \frac{1}{(i_k)_1} = \frac{1}{B\sqrt{f}} + \frac{1}{(i_k)_1} \qquad (9)$$

where f is the rotation rate and B is given by Newman (16) as

$$B = 2\sqrt{2\pi}\, A\nu^{1/2} C^{o}_{O_2} [0.621\, S^{-2/3}/(1+0.298\, S^{-1/3} + 0.145\, S^{-2/3})] \qquad (10)$$

where f is the rotation rate in rps, A is the electrode area, ν is the kinematic viscosity, and S is the Schmidt number (ν/D_{O_2}). The overall O_2 reduction current is then entirely controlled by Reaction 1 with combined kinetic and O_2 diffusion control. This appears to be the situation for the 0.80 V curve in Fig. 8. The slope is 12 ma cm^{-2} $(rps)^{-1/2}$ as compared with a value of 11.9 ma cm^{-2} $(rps)^{-1/2}$ obtained from the limiting current density vs. rotation rate data reported by Yeager et al. (17) for O_2 reduction on pyrolytic graphite rotating disk electrodes in 4M KOH at 25°C under conditions where the reduction proceeds quantitatively to only the peroxide.

Case II: $(i_k)_2 \gg (i_d)_2$. For this case eq. (8) yields

$$\frac{1}{i} = \frac{1}{2(i_d)_1} + \frac{1}{2(i_k)_1} = \frac{1}{2B\sqrt{f}} + \frac{1}{2(i_k)_1} \qquad (11)$$

Thus, as the potential becomes more cathodic, the slope should approach 1/2 of the value at less cathodic potentials where Case I is applicable. Further, the intercept corresponds to only 1/2 of $1/(i_k)_1$. The slope does decrease as the potential becomes more cathodic in Fig. 8 as predicted by eq. (11). The intercept 1/i has also approached 1/2 of the value at 0.8 V. This is somewhat surprising since, if $(i_k)_1$ had the usual exponential dependence on potential, the value would have been expected to be several orders of magnitude higher than the value at 0.8 V and hence the 1/i intercept to have been effectively zero for the plot in Fig. 8. This then implies that the O_2 reduction has a kinetic limiting current density and therefore that the reduction proceeds through a multiple step mechanism, one of which is potential insensitive and becomes rate controlling at higher overpotentials. A similar situation has been encountered for O_2 reduction on carbon and graphite.(12).

The change in slope in Fig. 5 can also be explained with a parallel rather than series mechanism involving the 4e reduction; i.e.,

Reaction 1: $O_2 + H_2O + 2e^- \xrightarrow{k_1} HO_2^- + HO^-$ (12)

Reaction 3: $O_2 + 2H_2O + 4e^- \xrightarrow{k_3} 4HO^-$ (13)

Reaction 1 would need to be predominant at 0.8 V and Reaction 3 at 0.5 V. Further to explain the failure of the 1/i intercept to be far smaller at 0.5 V than at 0.8 V, it is again necessary to involve some relatively potential insensitive step as becoming rate controlling for both Reactions 1 and 3 rather than just Reaction 1.

Since the O_2 reduction involves the formation of HO_2^- in alkaline solutions on the RuO_x/Ti electrode, the rotating ring-disk method is needed to characterize the mechanism and kinetics. This technique will be used for the on-going research on this system.

IV. Discussion

Since the cathodic and anodic branches for the oxygen electrochemistry on RuO_x/Ti in alkaline solutions are distinctly different, the results for each will be discussed separately.

1. Cathodic branch

The parallel and series reaction schemes represented by eqs. (11-13) can be considered as part of the overall scheme shown in Fig. 9 for alkaline solutions. The difference between the series and parallel mechanisms then is just a matter of the reversibility of the adsorption-desorption of HO_2^- (step C). If this step is very irreversible, then the parallel scheme is the more appropriate representation.

The $4e^-$ overall reducation of O_2 may also proceed by a parallel reaction which does not involve a peroxide species on the surface. In view of the strength of the O-O interaction in O_2, this seems rather unlikely.

The assumption has been made in Fig. 9 that the O_2 must be first adsorbed on the electrode prior to the first electron step but the adsorption may be electrochemical; i.e., simultaneous adsorption-electron transfer:

$$O_2 + e^- \longrightarrow O_2^-(ads) \qquad (14)$$

or

$$O_2 + HOH + e^- \longrightarrow HO_2(ads) + HO^- \qquad (15)$$

A separate O_2 adsorption step, preceding the first electron transfer step, however, provides a convenient potential insensitive step to explain the minor dependence of the intercept 1/i on potential in Fig. 8. The possible reduction of O_2 and HO_2^- without adsorption at a position equivalent to the outer Helmholtz plane has not been included in Fig. 9 on the basis that strong interaction is required with the electrode surface for the electron transfers to proceed at a resonable rate.

2. Anodic branch

Several of the reaction paths for O_2 generation tabulated by Damjanovic (18) for acid solutions can have Tafel slopes corresponding to $dV/d \ln i = 2RT/3F$ or 0.040 V/decade when modified to a form suitable

for alkaline solutions. All have the common feature that the rate controlling step is a second electron rather than first electron transfer. With judicious choice of H_2O vs. OH^- as the reactant in the first and second electron transfer steps or proceeding proton transfer steps, it is possible to have the kinetics also first order in OH^-.

With electrode surfaces involving species with ionic character, the authors prefer to write the mechanism in such a way as to indicate the possibility of changes in the effective valency state of the catalyst sites. A simple mechanism compatible with the observed Tafel slope and reaction order is as follows:

$$\underline{\text{Step a}}: \quad S^z + OH^- \underset{k_{-a}}{\overset{k_a}{\rightleftharpoons}} (SOH)^z + e^- \text{ (fast)} \tag{16}$$

$$\underline{\text{Step b}}: \quad (SOH)^z \xrightarrow{k_b} (SOH)^{z+1} + e^- \text{ (slow)} \tag{17}$$

followed by subsequent processes yielding finally O_2 and regenerating the site S^z; for example,

$$\underline{\text{Step c}}: \quad \begin{matrix} (SOH)^{z+1} \\ + \\ (SOH)^{z+1} \end{matrix} \begin{matrix} OH^- \\ \longrightarrow \\ OH^- \end{matrix} \begin{matrix} S-O-H--OH^- \\ \\ S-O-H--OH^- \end{matrix} \longrightarrow \begin{matrix} S^z \\ + \\ S^z \end{matrix} \begin{matrix} O \\ \| \\ O \end{matrix} + \begin{matrix} HOH \\ \\ HOH \end{matrix} \tag{18}$$

The sites are probably Ru^{4+} but also could be higher valency state Ru ions or Ti ions. There sites are undoubtedly hydrated although the waters of hydration are not shown in the mechanism. With the Step b rate controlling, negligible back reactions and the coverage of $(SOH)^z$ and $(SOH)^{z+1}$ low, the current density is

$$i = 4F \cdot \frac{k_a k_b}{k_{-a}} C_{OH^-} \cdot \exp\frac{(1+\beta_2)FE}{RT} \tag{19}$$

where E is the electrode potential against an arbitrary pH insensitive reference electrode; k_a, k_{-a}, and k_b are the rate constants for Steps a and b at E = 0; and β_2 is the transfer coefficient for Step b. For the usual value of $\beta_2 = 1/2$, the Tafel slope then is (2RT/3F) (2.30) or 0.040 V/decade with i first order in C_{OH^-}. If Step b is followed by the reaction indicated by Step c, then the stoichiometric number should be 2. Unfortunately the stoichiometric number is not known experimentally.

In Step a, the site S is a Ru ion of the oxide lattice. Step a involves the oxidation of the Ru to a higher valency state with partial transfer of electron charge from the OH species to Ru forming a $(RuOH)^z$ complex. Such a process should require much less energy than the formation of an OH free radical or a rather weakly adsorbed OH radical. Step b involves the further oxidation to $RuOH)^{z+1}$, possibly followed by the formation of $(RuO)^z$ before proceeding with Step c. The RuO_x/Ti elec-

trode surface may have some of the same features as the $Ru(NH_3)_5ORu(NH_3)_4ORu(NH_3)_5^{7+}$ ion, reported by Earley and Razavi (19,20) to oxidize OH^- homogeneously to form O_2. These species have the structure Ru-O-Ru-O-Ru^{7+}. Earley and Razavi have pointed out that Ru has a tendency to form species of coordination number 7 and that there are low lying antibonding π^* orbitals which can accept electron charge from OH^-. Thus the $(RuOH)^+$ intermediate (other species in the inner coordination sphere not shown) seems reasonable.

Acknowledgements: This research has been supported by NASA and the Office of Naval Research. The authors are pleased to acknowledge the help of Prof. G. Mateescu in the ESCA studies.

References:

1. S. Trasatti and G. Buzzanca, J. Electroanal. Chem. 29, App. 1 (1971).
2. J. Llopis and M. Vazquez, Electrochim. Acta 11, 633 (1966).
3. L. Burke and T. O'Meara, J.C.S. Faraday Trans. I 68, 839 (1972).
4. L. Burke and T. O'Meara, J. Electroanal. Chem. 36, 25 (1972).
5. D. Rogers, R. Shannon, A. Sleight, and J. Gillson, Inorg. Chem. 8, 841 (1969).
6. J. Goodenough in Progress in Solid State Chemistry, Vol. 5, H. Reiss, ed., Pergamon Press, Oxford, 1971, p. 362.
7. A. Kuhn and C. Mortimer, J. Electrochem. Soc. 120, 231 (1973).
8. e.g., South African Pat. 68/7371, 68/7482 (1968). German Pat. 2021422 (1969); 2014746, 1915951 (1970); British Pat. 1206863 (1970).
9. D. Galizzioli and S. Trasatti, J. Electroanal. Chem. 44, 367 (1973).
10. M. Pourbaix "Atlas of Electrochemical Equilibria in Aqueous Solutions", Pergamon Press, Oxford, 1966, pp. 343-349.
11. R. Zurilla and E. Yeager, "Oxygen Electrode Kinetics on Gold", ONR Tech. Rept. 23, Case Western Reserve, Cleveland, 1969.
12. I. Morcos and E. Yeager, Electrochim Acta 15, 953 (1970).
13. A. Kozawa, J. Inorg. Nucl. Chem. 21, 315 (1961).
14. A. Kozawa, "Electrochemical Reduction of RuO_2", Abstract No. 29, National Meeting Electrochemical Soc., Boston, Oct. 1973.
15. V. Levich, Acta Phys. Chim. USSR 17, 257 (1952); Physico-chemical Hydrodynamics, Prentice Hall, Englewood Cliffs, N.J., 1962.
16. J. Newman, J. Phys. Chem. 70, 1327 (1966).
17. E.Yeager, P. Krouse, and K. Rao, Electrochim. Acta 9, 1057 (1964).
18. A. Damjanovic in Modern Aspects of Electrochemistry, Vol. 5, J. Bockris and B. Conway, eds., Chapt. 5, Plenum Press, N.Y., 1969.
19. J. Earley and H. Razavi, Inorg. Nucl. Chem. Letters 9, 331 (1973).
20. J. Earley and T. Fealey, Inorg. Chem. 12, 323 (1973).
21. S. Pizzini, G. Buzzanca, C. Mari, L. Rossi, and S. Torchio, Mat. Res. Bull. 7, 449 (1972).

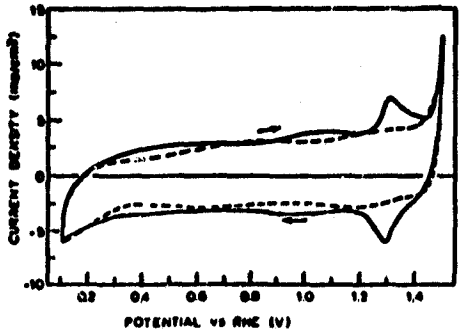

Fig. 1. Cyclic voltammogram for RuO_x on Ti substrate in N_2- saturated 4 M KOH (solid curve) and 2 M $HClO_4$ (dashed curve). Sweep rate: 50mV/sec; catalyst loading: 1x10-5 moles Ru/cm^2; temp. ~ 22°C.

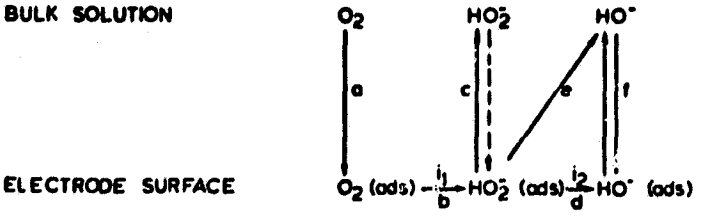

Fig. 9. Simplified representation of series and parallel mechanism involving peroxide.

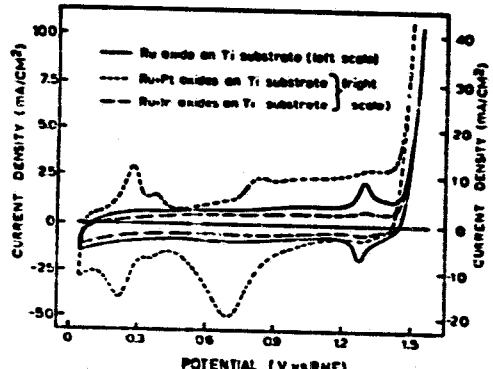

Fig. 2. Cyclic voltammograms of Ru, (Ru + Ir) and (Ru + Pt) oxides on Ti electrodes in 4M KOH (O_2 saturated). Sweep rate: 10mV/sec for RuO_x; 50mV/sec for (Ru + Ir) Ox and (Ru + Pt)Ox.

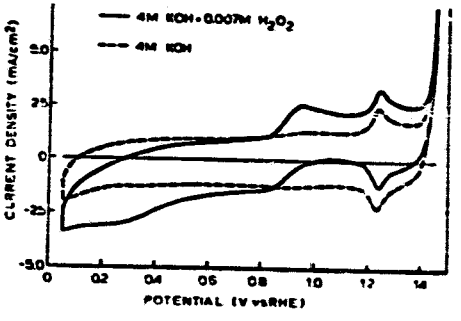

Fig. 4. Effect of hydrogen peroxide on the cyclic voltammograms of Ru oxide on Ti electrode in 4M KOH (N_2 saturated) Sweep rate: 50mV/sec; temp. 22°C.

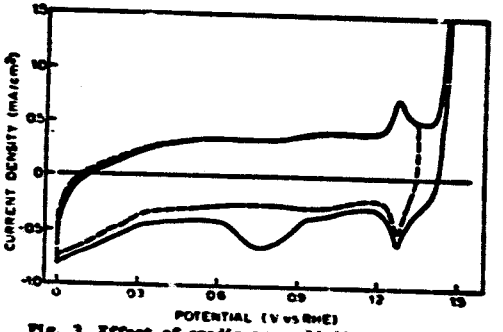

Fig. 3. Effect of anodic sweep limit on the cyclic voltammograms of Ru oxide on Ti electrode in 4M KOH (N_2 saturated). Sweep rate: 10mV/sec; temp. 22°C.

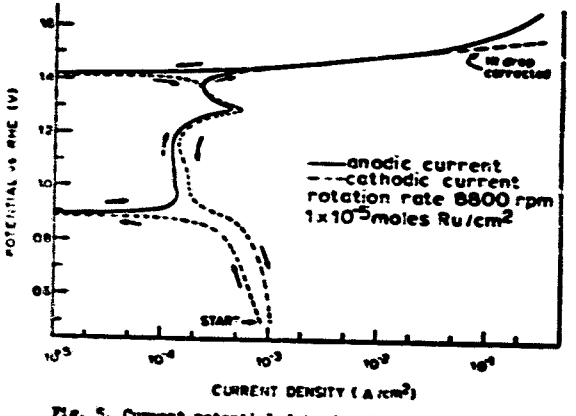

Fig. 5. Current-potential data for RuO_x on Ti. Data obtained with sweep rate of 2mV/sec with rotating disk technique. Electrolyte: 4M KOH (O_2 saturated)

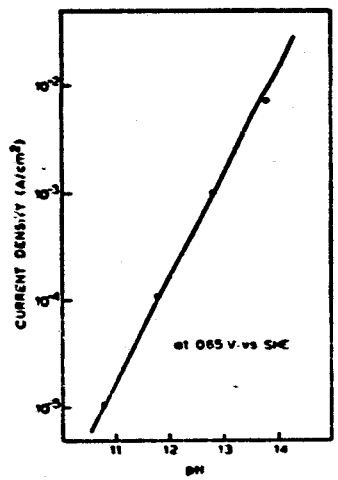

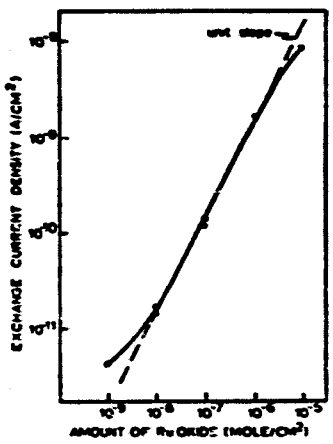

Fig. 6. pH dependence of current density at 0.65V vs SHE. in KOH - K_2SO_4 solutions with K^+ = 1 M; temp.: ~ 22°C. Stationary electrode.

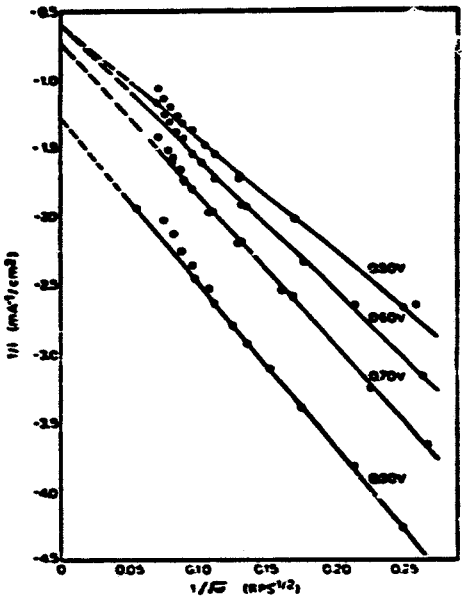

Fig. 7. Exchange current densities for O_2 generation on catalyst loading for RuO_x/Ti electrodes; temp. ~ 22°C; electrolyte 4 M KOH.

Fig. 8. Dependence of current density on rotation rate for O_2 reduction on the RuO_x/Ti electrode. Electrolyte: 4 M KOH (O_2-saturated); catalyst loading: 1×10^{-5} moles Ru/cm^2; temp. ~ 22°C. (Open and solid circles correspond to two different experiments).

B.E. Conway, Chemistry Department, University of Ottawa:

Could Professor Yeager comment further on the significance of the broad region of the anodic/cathodic current-potential profile for his RuO_2 electrode over potentials more cathodic than ca. 0.9V? Beyond this, a small peak appears in the anodic and cathodic curves which he attributed to oxidation of Ru to higher states but most of the charge is associated with the broad region. Is the effect associated with charging a highly porous electrode surface? It is known that commercially prepared RuO_2 DSA electrodes have very large areas.

E. Yeager, Department of Chemistry, Case Western Reserve University:

The charge under the voltammetry curve over the range 0.1V to 1.4V for the RuOx/Ti electrode appears too large to explain on just the basis of high surface area. For example, for RuOx/Ti electrodes with a catalyst loading of 10^{-5} moles Ru/cm^2 (apparent area) the charge from integration of the voltammetry curve over this voltage range is 0.1 C/cm^2 (apparent area), while the ratio of true-to-apparent area is typically 60 to 80 using the Zn^{2+} adsorption method. If this charge were entirely associated with the surface, this would be equivalent to $\sim$1000 μC/cm^2 (true area), which is too high by almost an order of magnitude. While some doubt may exist as to the accuracy of the absolute electrochemical area values from the Zn^{2+} adsorption measurements, it is doubtful if they are off by a sufficient amount to explain such a discrepancy.

The total charge under the voltammetry curve, however, only amounts to one tenth of that required to change the valency state of the Ru by one electron/Ru atom. We propose that this charge occurs principally in the bulk of the oxide and is accompanied by proton penetration from the electrolyte into the oxide to compensate charge with no phase change in the oxide.

The charge under the small peak at 1.3V in the voltammetry curves does seem reasonable for a change in the valency state of just surface Ru.

R. Woods, CSIRO, Division of Mineral Chemistry:

I was interested to note that you explained the voltammogram for RnO_2 in terms of stoichiometry charges. We have found a fresh irridium electrode to behave in a similar manner to other noble metals but voltammetric current peaks grow on continuous cycling and give a charge up to 60e/bare metal site. We have explained this behvior in terms of stoichiometry changes in an oxide species formed irreversibly on cycling.

E. Yeager, Chemistry Department, Case Western Reserve University

We explain the peak in the voltammetry curve in alkaline solutions in terms of a change in the valency state of the ruthenium at the surface but attribute the charge under the remainder of the voltammetry curves to a change in the bulk valency state, as indicated in the manuscript. The total charge is just too large (e.g., 0.1 coulombs/cm^2 of apparent electrode area) to attribute only to surface ruthenium, taking into account the measured area factor of ~50 for these electrodes.

The cyclic voltammetry curves are invariant over a large number of cycles, indicating no appreciable progressive changes in the oxide layer with layers containing e.g., 10^{-5} moles Ru/cm^2 (apparent electrode area).

Reprinted from
ANNUAL REVIEW OF PHYSICAL CHEMISTRY
Volume 26, 1975

THEORY OF CHARGE TRANSFER AT ELECTROCHEMICAL INTERFACES

R. K. Sen, E. Yeager, and W. E. O'Grady
Chemistry Department, Case Western Reserve University, Cleveland, Ohio 44106

INTRODUCTION

The theory of charge transfer is central to a molecular level understanding of electrode processes. Since the 1964 review of this topic by Marcus (1) in the *Annual Review of Physical Chemistry*, considerable progress has been made in understanding the mechanism of the elementary act of both electron and proton charge transfer. Much of the theoretical effort in the last decade has been made by the Levich, Dogonadze, and Kuznetsov (LDK) and the Bockris-Conway schools. The approaches followed by these two groups are quite different and, in fact, represent two opposite poles. The former group has stressed the importance of solvent polarization fluctuations, whereas the latter group, following a more traditional approach, has emphasized the bond stretching contribution to the activation process. Several review articles have recently been published by both groups, describing their own points of view (2–5). This review attempts to present an overview. Principally, the work carried out subsequent to Marcus' (1) article is reviewed.[1] Electrode processes on metals only are considered, although these theories are also applicable with minor modification to electrode processes on semiconductors [see e.g. Myamlin & Pleskov (6) and Gerischer (7)] and oxide-covered electrodes [see e.g. Schultze & Vetter (8, 9)].

HISTORICAL BACKGROUND

Gurney (10) in 1931 suggested that heterogeneous electron transfer reactions can be considered as tunneling of electrons between the electrode and a solution phase species through a potential barrier at the metal-electrolyte interface, whose height depends on the interaction between the reactant and the electrode surface. The reaction considered by Gurney was the discharge of a proton at the interface. The importance of taking into consideration the Franck-Condon principle in the electron transfer accompanying this proton discharge had been pointed out by Fowler (11) in 1934. Horiuti & Polanyi (12) developed a theory for the discharge step of the hydrogen electrode reaction within the framework of the activated complex theory,

[1] An attempt has been made to incorporate the published research through the end of 1974.

using the concepts already suggested by Gurney (10). The potential energy barrier for the reaction in this model is generated by the gradual stretching of the O–H bond in H_3O^+ or H_2O. The hydrogen discharge step can then proceed by thermal activation over the barrier or by proton tunneling. This approach to the calculation of the activation barrier for the hydrogen discharge reaction has been further developed in more recent years by Christov (13–15), Salomon & Conway (16), and Bockris and his co-workers (4). Based on the concepts of activated complex theory, similar approaches for outer sphere electron transfer reactions have been developed by Marcus, Zwolinski & Eyring (17, 18) and also by Sacher & Laidler (19, 20). These approaches treat the solution as a static dielectric and represent one pole in the controversy concerning the theoretical aspects of charge transfer reaction.

The other pole emerged from a suggestion by Libby (21) in 1952 that for homogeneous outer sphere electron transfer reactions, a considerable part of the activation barrier arises from nonequilibrium solvent polarization fluctuations. Platzman & Franck (22) essentially used the same idea to describe homogeneous charge transfer reactions within the framework of radiationless transition theory. These workers described the charge transfer processes in solution in terms of the polaron concept, originally developed for polar crystals by Pekar (23) and extended to polar solvents by Davydov (24). Using essentially the same model, Marcus (1, 25–28), Hush (29–31), and the LDK group (32–36) have made extensive quantitative calculations for both the outer sphere homogeneous electron transfer process and the corresponding reactions at metal electrodes. In their earlier papers, Marcus and LDK assumed that the metal ion with its inner coordination sphere can be treated as a conducting sphere with all the activation barrier associated with solvent polarization fluctuation. Marcus (25–28) developed the model using a classical statistical mechanical description of the solvent, whereas the LDK group developed a quantum statistical mechanical description (32–36). Various authors (18, 19), including Marcus (1, 28), pointed out that the neglect of bond stretching contributions from the inner sphere may be serious, and Marcus (28, 37) and Hush (29–31) have taken this into account. The LDK group (3, 38), on the other hand, has omitted the inner sphere contributions on the ground that the vibrational modes of the inner sphere have $h\omega \gg kT$, and consequently these bonds require multiple phonon interactions involving far too many phonons to have a reasonable probability of being excited. This reasoning, however, has been questioned by Bockris and his co-workers (see e.g. 5, 39).

Recently Schmidt (40, 41) and Schmickler & Vielstich (42, 43) have further developed the solvent fluctuation model, the former by presenting a more generalized nonequilibrium statistical mechanical picture and the latter by considering more specifically the effect of the inner coordination sphere.

OUTER SPHERE ELECTRON TRANSFER REACTIONS

The Marcus Treatment and Related Approaches

Marcus (1, 25–28, 37) uses a general classical statistical mechanical approach with the rate constant given by

$$k = \kappa Z \exp -(\Delta G^*/RT) \qquad 1.$$

where κ is the electron transmission coefficient in the activated state, Z is the collision number for the reaction, and ΔG^* is the free energy of activation. For the homogeneous case Marcus takes $Z = 2.5 \times 10^{11}\ M^{-1}\ sec^{-1}$ and for the heterogeneous case $Z \approx 10^{-4}$ cm sec^{-1}. The free energy of activation includes the following contributing terms

$$\Delta G^* = \Delta G_w^{\ddagger} + \Delta G_o^{\ddagger} + \Delta G_i^{\ddagger} + \Delta G_e^{\ddagger} \qquad 2.$$

where $\Delta G_o^{\ddagger}$ and $\Delta G_i^{\ddagger}$ are the reorganizational free energy contributions from the outer and inner solvation spheres, $\Delta G_w^{\ddagger}$ is the work term associated with bringing the reacting ions together or to the electrode surface, and $\Delta G_e^{\ddagger}$ corresponds to an entropy term associated with any change in the electronic multiplicities in the initial and final states.

Marcus assumes the electron transfer process to be only moderately adiabatic—to the extent that the transmission coefficient κ is approximately unity but not so strongly adiabatic that the activated state has appreciable resonance stabilization. Marcus uses nonequilibrium dielectric polarization theory involving continuum concepts to calculate $\Delta G_o^{\ddagger}$. The term $\Delta G_i^{\ddagger}$ is expressed in terms of the vibrational contributions of the inner solvation sphere to the partition function of the activated complex and the corresponding zero-point energies. The principal configurational changes in the inner sphere are the changes in bond lengths from the inner sphere solvent molecules to the central ion, and therefore $\Delta G_i^{\ddagger}$ is approximately equal to the difference of the zero-point energy of the breathing mode in the activated and initial states. This difference can be estimated from the force constants for the breathing mode of the inner sphere in the initial and final states, as has been done by Marcus (37) and Sutin (44), or from the potential energy functions for the initial and final states (see e.g. 29, 45).

For electrode reactions involving metals, Marcus assumes that the electronic energy levels of the metal contributing to the reaction are confined to within $\pm kT$ of the Fermi level. He then considers the distribution of activated complexes corresponding to radiationless electron transfer to or from various electronic energy levels in the metal to be equivalent to a single activated complex corresponding to the Fermi level. Contributions to $\Delta G_o^{\ddagger}$ arising from the action of the image forces in the metal on the solvent polarization are also taken into account.

One of the more important outcomes of the Marcus treatment is the relationship between the heterogeneous electron transfer rate constant k_{el} and the homogeneous homonuclear electron exchange rate constant k_x. When the electrostatic work terms are low or corrections are applied for them

$$(k_{el}^2/k_x) = (Z_{el}^2/Z_x) \approx \text{constant} \qquad 3.$$

The Marcus treatment also predicts a transfer coefficient of $\beta = 0.5$ for heterogeneous outer sphere electron transfer at relatively low and moderate overpotentials, with deviations from this value at high overpotentials.

The various assumptions involved in the Marcus treatment impose significant

limitations. The estimation of inner sphere contributions by Marcus in the classical limit, considering only symmetric breathing modes, is probably a substantial oversimplification. In recent years, however, efforts by several authors (43, 47) to consider the inner sphere quantum mechanically unfortunately have met with only limited success. Particularly questionable is the separation of the reorganizational contributions into inner and outer solvation sphere values, with one handled in terms of discrete vibrational states and the other with dielectric continuum theory. Sacher & Laidler (19, 20) have avoided this rather arbitrary division of the inner-outer solvation contributions by considering changes in the total solvation energy as the radius of the inner coordination sphere changes, but this approach involves continuum concepts.

The collision number in the Marcus treatment of both the homogeneous and heterogeneous electron transfers has been estimated rather crudely. More refined estimates are available for the homogeneous case in the literature relating to second order diffusion-controlled reactions (see e.g. 48).

The assumption of negligible resonance stabilization in the activated state limits the Marcus treatment to redox systems in which the interaction between the reacting ions and electrode is weak. In contrast, Hush (29) has assumed that the resonance stabilization is sufficient for the transferred electron to become delocalized and distributed between the reacting ions in the homogeneous case or between the reacting ion and the electrode in the heterogeneous case. Hush then considers the fraction of the electron charge transferred to or from the reacting ions or electrode. The Marcus treatment is probably more appropriate for outer sphere electron transfer electrode reactions in which the reacting central ion is separated from the electrode surface by its own inner coordination sphere as well as by a layer of adsorbed solvent molecules on the electrode surface. In instances where the reacting ion is specifically adsorbed, even with its inner coordination sphere intact, the Hush approach may become more appropriate. Under such circumstances, however, a bridge mechanism may need to be considered.

The Levich, Dogonadze, and Kuznetsov (LDK) Approach

In their initial publications (32, 33, 35), Levich, Dogonadze, and Kuznetsov considered the reacting ion with its inner coordination sphere as a frozen system, which does not contribute in any way to the activation process. The potential energy of the electron in this frozen system, however, depends on the polarization of the solvent near the ion. Since the molecules of the solvent are in continuous thermal movement, the polarization P of the solvent surrounding the ion fluctuates with time until a state of polarization is reached where a radiationless electron transfer can take place between the ion and electrode by tunneling. After the electron transfer, the polarization of the solvent surrounding the ion is the same as the polarization prior to the transfer and then decays as the system reverts to the equilibrium polarization of the final state.

The electrode reduction current is written by LDK in the general form

$$i = e \iint_{x\varepsilon} C(x) n(\varepsilon) \rho(\varepsilon) W(\varepsilon, x)\, d\varepsilon\, dx \qquad 4.$$

where $C(x)$ is the concentration of reacting ions at a distance x from the electrode surface, $n(\varepsilon)$ is the Fermi distribution function, and $\rho(\varepsilon)$ is the electron density of states in the metal. $W(\varepsilon, x)$ is the transition probability of the system to pass from the initial to the final states. LDK assume that the electron transfer probability is highest when the reacting ion is at a distance x_0 from the electrode surface. The integral over x can then be removed and equation 4 becomes

$$i = eC(x_0)\int_{\varepsilon} n(\varepsilon)\rho(\varepsilon)W(\varepsilon, x_0)\,d\varepsilon \qquad 5.$$

According to first order perturbation theory, the transition probability of the system from the initial state i in the mth level to the final state f is

$$W_{if} = \frac{2\pi}{\hbar}\sum_n \left|\int \psi^*_{fn} v \psi_{im}\,dv\right|^2 \delta(E_{im} - E_{fn}) \qquad 6.$$

where v is the perturbation operator, δ is the Dirac delta function, and ψ_{fn} and ψ_{im} are wavefunctions of the final state in the level n and the initial state in the level m, with corresponding energies of E_{fn} and E_{im}. The Franck-Condon principle is assumed to apply to this system. Further, by using the Born-Oppenheimer approximation to separate the electronic and heavy particle wavefunctions and the Condon approximation, which argues the gradual monotonicity of the electronic matrix element, equation 6 can be written as

$$W_{if} = \left(\frac{2\pi}{\hbar}\right)L^2\sum_n \left|\int \Phi^*_{fn}(q)\Phi_{im}(q)\,dR\right|^2 \delta(E_{im} - E_{fn}) \qquad 7.$$

where L is the electronic matrix element given as

$$L = \left|\int \chi^*_{fn}(r, R) v \chi_{im}(r, R)\,dr\right|^2 \qquad 7a.$$

where χ is the electronic wavefunction, r is the electron coordinate, R is the inter-reactant coordinate, Φ is the solvent wavefunction, and q is the solvent normal coordinate. The thermally averaged transition probability W in equation 5 involves a statistical averaging over all initial states and is given as

$$W = \sum_m \rho(\varepsilon_m) W_{if} \qquad 8.$$

where $\rho(\varepsilon_m)$ is the Gibbs distribution function.

The Hamiltonian of the heavy particle system needed to solve the solvent matrix element in equation 7 is written by LDK as

$$\mathcal{H} = \mathcal{H}_s + \varepsilon_{el}(q) \qquad 9.$$

where $\mathcal{H}_s$ is the solvent Hamiltonian and $\varepsilon_{el}(q)$ is the energy of the electronic subsystem, which depends on the solvent coordinates. The LDK treatment considers the solvent to be a dielectric continuum, in which thermal fluctuations produce a set of standing polarization waves whose frequency spectrum can be approximated by a single characteristic angular frequency ω_0. LDK take the value of ω_0 to be $\sim 10^{12}$ rad/sec for water, corresponding to the Debye dielectric relaxation frequency.

This model yields a Hamiltonian identical with the Landau-Pekar Hamiltonian obtained for polarons in crystals

$$\mathcal{H}_s = \sum_k \frac{\hbar\omega_0}{2}\left(q_k^2 - \frac{\partial^2}{\partial q_k^2}\right) \qquad 10.$$

where q_k are the dimensionless normal coordinates of the solvent oscillator.

It is further assumed (2) that the change in energy of the electronic subsystem, due to changes in the solvent coordinates, is a linear function of the displacement, i.e.

$$\Delta\varepsilon_{el} = \varepsilon_{el}(q_k) - \varepsilon_{el}(q_k^0) = \sum_k \left(\frac{\partial\varepsilon_{el}}{\partial q_k}\right)_{q_k = q_k^0}(q_k - q_k^0) \qquad 11.$$

where q_k^0 is the equilibrium solvent coordinate. From equations 10 and 11 the complete Hamiltonian for the heavy particle subsystem can be obtained.

Using harmonic oscillator wavefunctions, the thermally averaged transition probability is then solved with the help of Feyman calculus (50) to yield

$$W = \frac{2\pi}{\hbar^2}\, L^2 I_M(z) \exp\left[-\left(\frac{\hbar\omega_0 M}{2kT}\right) - z\cosh\left(\frac{\hbar\omega_0}{2kT}\right)\right] \qquad 12.$$

where I_M is a Bessel function of Mth order, and

$$M = \frac{(J_f - J_i)}{\hbar\omega_0} \qquad 12a.$$

$$z = \tfrac{1}{2}\,\mathrm{cosech}\left(\frac{\hbar\omega_0}{2kT}\right)\sum_k [(q_k^0)_i - (q_k^0)_f]^2 \qquad 12b.$$

where J_i and J_f are the equilibrium energies, and $(q_k^0)_i$ and $(q_k^0)_f$ are the equilibrium solvent coordinates of the initial and final states, respectively.

The general solution can be simplified for two limiting cases. In the high temperature limit, i.e. $kT \gg \hbar\omega_0$, equation 12 reduces to

$$W = \left(\frac{\pi}{\hbar E_s}\right)^{1/2} L^2 \exp\left[-\frac{(J_f - J_i + E_s)^2}{4E_s kT}\right] \qquad 13.$$

where E_s is the solvent reorganization energy and is given by

$$E_s = \left(\frac{\hbar\omega_0}{2}\right)\sum_k [(q_k^0)_i - (q_k^0)_f]^2 \qquad 13a.$$

The physical process involved in the high temperature case is shown in Figure 1*A*, where the energy-solvent coordinate profile is schematically presented. Here, the energy of the initial system changes due to solvent polarization fluctuations until the solvent configuration attains the coordinate q^*. At this point a radiationless electron transfer occurs. Subsequently the polarization fluctuation decays to produce the final state in the equilibrium configuration.

On the other hand, in the low temperature limit, i.e. $kT \ll \hbar\omega_0$, equation 12 reduces to

$$W = \frac{2\pi(L^2)}{\hbar^2\omega_0[(J_f - J_i)/(\hbar\omega_0)]!}\left(\frac{E_s}{\hbar\omega_0}\right)^{J_f - J_i/(\hbar\omega_0)} \exp\left[-\frac{E_s}{\hbar\omega_0}\right]\exp\left[-\frac{J_f - J_i}{kT}\right] \quad 14.$$

The physical process involved in this case is shown in Figure 1*B*. This situation involves a quantum mechanical tunnel transition from the initial state to the equilibrium configuration of the final state.

Using the transition probability obtained for the high temperature limit in equation 5 and integrating gives the exchange current density

$$i_0 = \kappa\bar{\rho}\left(\frac{\pi}{\hbar^2 kTE_s}\right)^{1/2} L^2 \exp\left[-\frac{E_s}{4kT}\right]\exp\left[\frac{V_{rev}\beta e}{kT}\right] \quad 15.$$

where $\bar{\rho}$ is an effective density of states, V_{rev} is the reversible electrode potential, and β is the transfer coefficient.

The description of the solvent polarization waves and the consideration of only a single effective frequency ω_0 in the early papers of the LDK group (33–36) are at best only a coarse approximation. Even within this simplified model, Schmickler & Vielstich (42) have questioned the appropriateness of using a value for ω_0 cor-

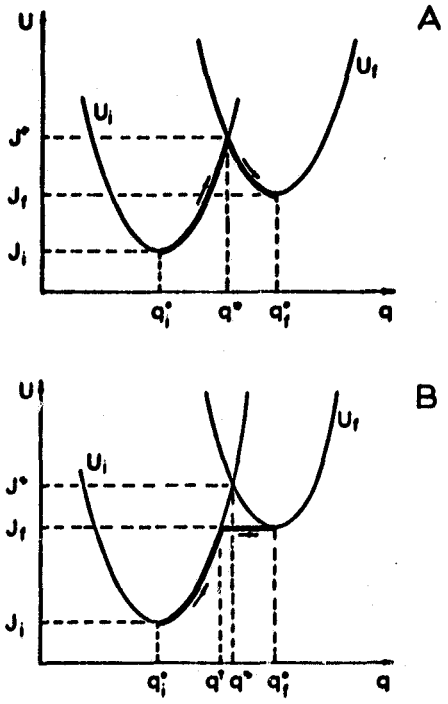

Figure 1 Outer sphere electron transfer according to the LDK model. *A*: High temperature behavior ($\hbar\omega_0 \ll kT$). *B*: Low temperature behavior ($\hbar\omega_0 \gg kT$). Ordinate: energy of electron; abscissa: generalized solvent polarization coordinate (2).

responding to the Debye dielectric relaxation frequency and have pointed out that ω_0 probably changes appreciably in the vicinity of the ions.

Recently Dogonadze et al (3, 50-52) have made a sustained effort to refine the solvent model and have now taken into account both local contributions (single dipole performing orientational vibrations at a limiting frequency ω_0) and nonlocal contributions (interactions of polarization at different points in space) to the potential energy of the solvent. The latter effect is considered in terms of space correlation functions of the dipole moments of solvent molecules. The Hamiltonian obtained from this model accounts for dispersion effects in both frequency and momentum space and has the general form

$$\mathcal{H}_s = \sum_k \frac{\hbar\omega_i(k)}{2}\left[q_k^2 - \frac{\partial^2}{\partial q_k^2}\right] \qquad 16.$$

where $\omega_i(k)$ is complex and has a spectrum of values depending on the correlation functions. Vorotyntsev et al (53, 54) have solved for the transition probability for an electron transfer process, using the Hamiltonian given in equation 16, without taking into consideration any contribution from the inner coordination sphere. Up to the time of preparation of this review, no rigorous test of this modified solvent model has been published. Dogonadze and co-workers (52), however, have used it to estimate the solvation energy of alkali metal cations with reasonable success.

The LDK treatment does not include any contribution from the inner solvent sphere. Schmickler & Vielstich (42), Kestner et al (47), Hale (64), and Bockris et al (5, 39) have recently pointed out the importance of taking such effects into account. This has been done in the Marcus treatment (1, 37). Dogonadze (3) and Vorotyntsev et al (55-57), however, still continue to advocate the view that the degrees of freedom for which $\hbar\omega \gg kT$ take part only in the transfer process in a quantum mechanical sense (tunneling) and their effects are manifested in only the pre-exponential factor, whereas degrees of freedom with $\hbar\omega \ll kT$ take part in the activation process. Since most of the stretching frequencies in the inner solvent sphere have $\hbar\omega \gg kT$, they do not contribute to the activation process according to these authors. Dogonadze & Kuznetsov (58) have considered the effect of inner sphere degrees of freedom with $\hbar\omega \simeq kT$ and have shown that the transition probability W_{if} is decreased by a factor that depends on the frequencies and normal coordinates of the inner coordination sphere modes.

Other Treatments

Three different groups, namely Schmickler & Vielstich (42, 43), Kestner, Logan & Jortner (47), and Schmidt (40, 41, 46), have examined the theory of outer sphere electron transfer reactions, using essentially the LDK model. Different formalisms have been attempted and improvements in the original model have been made.

THE SCHMICKLER-VIELSTICH APPROACH Schmickler & Vielstich (42, 43) have examined the LDK model in some detail. Using the same model and an analogous approach, they obtained expressions for the transition probability which were identical with the original Levich-Dogonadze (35) expression for the high

temperature limit but different for the low temperature approximation. Schmidt (59) investigated this discrepancy and has shown that the Schmickler-Vielstich results (42) are in error because they neglected to consider the quantum mechanical non-commutivity of the solvent system Hamiltonians for the initial and final states. Although both Schmickler & Vielstich (42) and Levich & Dogonadze (32) started from the same formal expression, the latter authors make subsequent use of the Feynman calculus (49), which recognizes this commutation problem.

Schmickler (43) also has tried to improve the original LDK model by incorporating inner coordination sphere contributions. The total heavy particle system Hamiltonian in this case is written as

$$\mathscr{H} = \mathscr{H}_{in} + \mathscr{H}_{out} \qquad 17.$$

where $\mathscr{H}_{out}$ is the Hamiltonian without any inner sphere effects and is identical with that used by Levich & Dogonadze (32). The Hamiltonian $\mathscr{H}_{in}$ for the inner sphere is expressed as

$$\mathscr{H}_{in} = \sum_{\mu=1}^{n} \left(\frac{\hbar^2}{2m_\mu} \frac{\partial^2}{\partial s_\mu^2} + \frac{m_\mu}{2} \omega_\mu^2 s_\mu^2 \right) \qquad 18.$$

where the sum is taken over all normal modes μ of the inner sphere; ω_μ, s_μ and m_μ are frequencies, normal coordinates, and reduced masses of the normal modes. Only symmetrical breathing modes are considered in the final calculation.

First order perturbation theory is then used to calculate the transition probability and subsequently the exchange current. No analytical solutions are obtained, but computer calculations show that the influence of the inner coordination sphere lowers the exchange current by a factor of two to three. Just how reliable this factor may be, however, is open to question because this treatment also includes the non-commutation error pointed out by Schmidt (59) in the Schmickler-Vielstich paper (42).

THE KESTNER, LOGAN, AND JORTNER (KLJ) APPROACH The KLJ approach (47) is more or less an extension of the LDK treatment. Although KLJ have limited their calculations so far to homogeneous electron transfer, the salient features of their approach can be projected to the heterogeneous reaction. They consider both the initial and final states consisting of the reacting species and the solvent to be in their ground electronic and vibronic states. The electron transfer process is then visualized as the irreversible decay of the initial states into the manifold of the final states. Such a model is valid only if the total width of each of the acceptor states is large relative to their spacing. KLJ (47) show that such is the case in polar liquids.

Second order perturbation theory is used to calculate the transition probability. The thermally averaged transition probability is then solved, using the generating function method of Kubo & Toyozawa (60) and Engelman & Jortner (61) to yield

$$W = \frac{V^2}{\hbar} \left(\frac{2\pi}{\hbar^2 D^2} \right)^{1/2} \cdot \exp[(\Delta E - E_s)^2/(2D^2\hbar^2)] \qquad 19.$$

where ΔE is the difference in the energy of the initial and final states in their equilibrium configuration and

$$E_s = \tfrac{1}{2}\sum_j m_j\omega_j^2[(q_j^0)_i-(q_j^0)_f]^2 \qquad 20.$$

where m_j and ω_j are the reduced mass and frequency of the jth normal mode of the system $(q_j^0)_i$ and $(q_j^0)_f$ are the equilibrium coordinates of the jth normal mode in the initial and final states, and

$$D^2 = \tfrac{1}{2}\sum_j(2m_j+1)\omega_j^2[(q_j^0)_i-(q_j^0)_f] \qquad 21.$$

The term V in equation 19 is the electronic matrix element involving the initial and final state electronic wavefunctions. This matrix element is separated out from the vibrational overlap term in the second order perturbation matrix element using the Condon approximation. The expression for the transition probability in the high temperature limit reduces to the equation obtained by LDK (35) as well as by Marcus (37). KLJ do take into account the frequency dispersion in the solvent.

This formalism has so far dealt completely with the generalized nuclear coordinates of various normal modes of the system. In principle therefore this approach should take into account inner sphere effects as well. KLJ (47), however, show that this approach is valid only when the vibrational quantum number of any normal mode is much greater than unity. This condition is met for the low frequency solvent modes but not for the inner sphere modes. To take inner sphere effects into account, KLJ modified the approach slightly. The total potential energy of the system was written as the sum of the inner sphere and the solvent contribution, with the latter estimated using the LDK Hamiltonian. The inner sphere part was estimated considering only the symmetric breathing mode on the nearest solvent molecules in the harmonic approximation.

The transition probability was then calculated using the methods already described to yield a rather complicated result. At the temperatures involved in most experiments, the KLJ results show that there is a significant temperature-dependent contribution from the first coordination layer.

THE SCHMIDT APPROACH The use of perturbation theory by the LDK group restricts the validity of their approach to the weak coupling cases. Furthermore, the LDK and, for that matter, all the other formalisms have failed to develop a unified formal treatment of electron transfer, which holds for the adiabatic and nonadiabatic limits and all intermediate cases. In order to avoid these drawbacks, Schmidt (40, 41) has developed the theory of homogeneous and heterogeneous outer sphere electron transfer reactions on the basis of Yammamoto's (62) general expression for the rate of a chemical reaction, obtained using linear response theory. It has been shown that the rates of constants obtained by this formalism are completely general and should be valid for any degree of coupling between the participating subsystems.

The general expression for the rate of a chemical reaction in the Yammamoto (62) approach is given as

$$k = [V/(2\langle N_a\rangle_0\langle N_b\rangle_0)]\int_{-\infty}^{\infty} dt\,\langle\dot{N}(O)\dot{N}(t)\rangle \qquad 22.$$

where $\langle N_a \rangle_0$ and $\langle N_b \rangle_0$ are equilibrium number concentrations of the reactants A and B and the term within the brackets $\langle \ldots\ldots \rangle$ in the integrand indicates the trace operation with respect to the equilibrium density operator; i.e.

$$\langle \ldots\ldots \rangle = \text{trace}\,\{\rho(\ldots\ldots)\} \qquad 23.$$

where ρ is the density operator. Furthermore N in equation 22 is the occupation number operator, given as

$$N = \sum_i a_i^\dagger a_i \qquad 24.$$

where $a_i^\dagger$ and a_i are the creation and annihilation operators for the reactant state. The time derivative of the occupation number operator N is given by

$$\dot{N} = (ih)^{-1}[N, \mathscr{H}] \qquad 25.$$

which is the well-known Heisenberg equation of motion, with $\mathscr{H}$ being the Hamiltonian of the system. An inspection of equations 22–25 indicates that knowing the complete Hamiltonian of the system would allow the calculation of the rate.

Schmidt (40, 41, 59) has shown that this general nonequilibrium statistical mechanical approach yields the same results as obtained by Marcus (37) and the LDK group (35) with their approaches when the approximations involved in these treatments are incorporated in the linear response formulation.

Recently Schmidt (46) has used this approach to extend the LDK model for outer sphere electron transfer reactions to include inner sphere vibronic degrees of freedom. The description of the solvent is identical with that used in the later LDK papers (50, 51), where the frequency dispersion of the solvent is taken into account. The inner sphere vibronic terms are considered in the harmonic approximation, and it is further assumed that there is no coupling between the inner sphere vibrations and the neighboring solvent. The total wavefunction is then expressed as the product of the wavefunctions of the electronic, inner sphere vibronic, and solvent subsystems. Following the LDK approach (35), the total Hamiltonian of the system is written as

$$\mathscr{H} = \mathscr{H}_m + \mathscr{H}_s + \mathscr{H}_{int} \qquad 26.$$

where $\mathscr{H}_m$ is the contribution from electronic and nuclear motions, $\mathscr{H}_s$ is the solvent Hamiltonian identical with the one shown in equation 16, and $\mathscr{H}_{int}$ describes the coupling between the solvent system and the transferring electron.

The rate expression calculated in this manner shows interesting effects of the inner sphere vibronic terms. The nature of the effect depends on whether the vibrational potential energy surfaces for the donor and acceptor species undergo severe displacement, distortion, or both, and also on whether the fundamental frequencies of the inner sphere normal modes are greater or less than $4kT$. Three cases can be distinguished; namely

(*a*) In the high temperature limit ($h\omega \ll 4kT$), if there is negligible displacement of the inner sphere vibrational potential energy surfaces but strong distortion, the inner sphere effect enters through the pre-exponential part of the rate constant expression.

Table 1 Comparison of the Marcus theory with experimental free energies of activation and the transfer coefficients for various redox couples at electrodes [data as listed by Hale (64)]

System	Electrode	Electrolyte	Solvent	Temperature (°C)	$\Delta G_s^{\ddagger}$ (eV)	$\Delta G_i^{\ddagger}$ (eV)	$\Delta G_{theor}^{\ddagger}$ (eV)	$\Delta G_{exp}^{\ddagger}$ (eV)	β_{exp}
$V(H_2O)_6^{3+}$	Hg	1 M $HClO_4$	W	20	0.288	0.101	0.389	0.379	0.54
$Cr(H_2O)_6^{3+}$	Hg	0.1 M $HClO_4$	W	25	0.287	0.146	0.432	0.541	0.45
$Mn(H_2O)_6^{3+}$	Pt	4 M $HClO_4$	W	22	0.287	0.180	0.467	0.427	0.26
$Fe(H_2O)_6^{3+}$	Pt	1 M $HClO_4$	W	20	0.285	0.115	0.400	0.373	0.42
$Co(H_2O)_6^{3+}$	Pt	5.6 M $HClO_4$	W	2	0.287	0.103	0.390	0.586	0.47
$Ce(H_2O)_6^{3+}$	Pt	1 M $HClO_4$	W	22	0.267	0.026	0.293	0.515	0.25
$Fe(CN)_6^{3-}$	Pt	1 M KCl	W	20	0.215	0.095	0.310	0.299	0.5
$Co(NH_3)_6^{3+}$	Hg	0.1 M $NaClO_4$	W	25	0.298	0.054	0.352	0.551	0.61
WO_4^{2-}	Pt	1 M H_3PO_4	W	25	0.314	0.062	0.376	0.355	—
Naphthalene	Hg	0.1 M TBAI	DMF	30	0.236	0.011	0.247	0.237	0.56
Anthracene	Hg	0.1 M TBAI	DMF	25	0.217	0.006	0.223	0.2	—
Tetracene	Hg	0.1 M TBAI	DMF	30	0.203	0.013	0.216	0.224	0.52
Perylene	Hg	0.1 M TBAI	DMF	25	0.198	0.012	0.210	0.2	—
Cyclo-octatetraene	Hg	0.1 M TPAP	DMF	25	0.234	0.161	0.375	0.359	—
Trans-stilbene	Hg	0.1 M TBAI	DMF	30	0.199	0.007	0.206	0.235	0.58
Azobenzene	Hg	0.1 M TEAP	DMF	—	0.199	0.017	0.216	0.255	0.37

(*b*) In the low temperature limit ($h\nu \gg 4kT$), the effect of the inner sphere vibronic terms is negligible and only the solvent modes contribute in the rate constant expression, in agreement with the claims of the LDK group (3).

(*c*) At both high and low temperature limits, if there is a strong displacement and strong distortion in the vibrational potential energy surfaces, the inner sphere effect manifests itself in both the pre-exponential and the exponential part of the rate expression. This is a situation closer to the inner sphere type of electron transfer reactions.

Schmidt (63) has examined the effect of damping on the rate by introducing a damping factor as a parameter in the solvent Hamiltonian. Two types of damping effects are considered: namely, state damping, arising from the interaction of the reacting system in some arbitrary state with a number of loss or attenuating systems, and damping due to the attenuation of the polarization energy modes of the dielectric continuum. In either case, Schmidt (63) has shown that the damping processes result in an effective increase in the activation energy of the process. It should, however, be mentioned that the modified LDK solvent Hamiltonian (equation 16) takes both frequency dispersion and damping effects into account implicitly. The results obtained using that Hamiltonian should show the same tendencies as observed by Schmidt (63).

In overall perspective, the approach used by Schmidt, although mathematically cumbersome, appears to be more rigorous and valid over a considerably wider range than the other existing approaches for the theory of charge transfer reactions.

Comparison of Theory and Experiment

Most comparisons of experiment with prediction for outer sphere electron transfer electrode reactions have been carried out using the Marcus treatment. These comparisons are somewhat compromised by uncertainties as to how the solvent polarizability terms contributing to $\Delta G_\delta^\ddagger$ are influenced by the double layer and the electrode boundary itself as well as by a lack of reliable data for the force constants associated with the inner sphere breathing mode and the change in bond distances within the inner sphere. One such comparison is given in Table 1, in which theoretical and experimental values of the free energies of activation as compiled by Hale (64) are tabulated. He has evaluated the experimental values $\Delta G_{exp}^\ddagger$ from the rate constants using equation 1 with $Z = 1 \times 10^{-4}$ cm sec^{-1}. The theoretical values, $\Delta G_{theor}^\ddagger$, have been calculated by Hale (64) using the Marcus theory, assuming that the work term and multiplicity contributions $\Delta G_w^\ddagger$ and $\Delta G_j^\ddagger$ in equation 2 are small and that the electrostatic image-solvent polarization terms can be neglected because of the shielding effects of the supporting electrolyte for ions in the outer Helmholtz plane. The latter assumption is questionable and probably results in high estimated values of $\Delta G_\delta^\ddagger$ and hence $\Delta G_{theor}^\ddagger$ in Table 1.

Only those systems are included from the Hale compilation that should come close to fulfilling the conditions of the Marcus treatment, i.e. proceed by outer sphere electron transfer without strong interaction of the reacting species with the electrode (no specific adsorption). The organic reductions have been restricted to those for which the first electron transfer is believed to be rate controlling and specific

adsorption does not occur. With aromatic systems, this limits the comparison to neutral reductants in nonaqueous solvents such as dimethyl formamide (65, 66), as pointed out by Hale (64).

The agreement between $\Delta G^{\ddagger}_{theor}$ and $\Delta G^{\ddagger}_{exp}$ in Table 1 is surprisingly good with the exception of reductions for which there are doubts as to whether they proceed by an outer sphere mechanism [e.g. $Cr(H_2O)_6^{2+}$] or for which spin conservation problems may be involved [e.g. $Co(H_2O)_6^{3+}$]. On the other hand, the values for the outer sphere terms $\Delta G_o^{\ddagger}$ listed in Table 1 are considerably larger and the inner sphere $\Delta G_i^{\ddagger}$ values are considerably smaller than those calculated by Bockris (67) using essentially the Marcus treatment. In any event, with neither of these compilations can $\Delta G_i^{\ddagger}$ or $\Delta G_o^{\ddagger}$ be generally neglected. The LDK (2, 3) treatment will give essentially the same value for $\Delta G^{\ddagger}_{theor}$ for only couples whose inner sphere contributions $\Delta G_i^{\ddagger}$ in equation 2 are small. From Table 1, it appears that such may be the case with aromatic species in which the bond lengths and force constants undergo only small changes.

Many of the redox couples for which comparisons between theory and experiment have been attempted in the literature (e.g. see 68) may involve one or more of the following features which disqualify them for comparison with the Marcus theory: bridged charge transfer, strong interaction with the electrode, multiple electron transfer with other than the first step rate controlling, and spin conservation problems.

Various workers, including Marcus (1), Sutin (69), and Vleek (70), have used equation 3 to compare experimental data for heterogeneous and homogeneous electron transfer reactions. The comparison is reasonably good for a number of outer sphere electron transfer couples in the absence of specific adsorption of the reacting species on oxide-free electrode surfaces.

Most theoretical treatments of outer sphere electron transfer electrode reactions predict a potential-dependent transfer coefficient with a value of $\beta = 1/2$ at low and moderate overpotentials. A substantial number of couples have this value (see Table 1). The evidence for a potential-dependent transfer coefficient, however, is far less clear. The LDK group cite as evidence for such a potential-dependent β the work of Frumkin, Petrii & Nikolaeva-Fedorovich (71) on the $Fe(CN)_6^{3-}/Fe(CN)_6^{4-}$ couple, which indicates some deviation from Tafel behavior after double layer corrections have been taken into account. Parsons & Passeron (72) have reported a potential-dependent transfer coefficient for $Cr(H_2O)_6^{2+}/Cr(H_2O)_6^{3+}$, but Anson, Rathjen & Frisbee (73) have criticized this work on the basis of the high pH of the solutions used by Parsons & Passeron (72) and the need for unusually high precision in the measurement of β. Anson et al (73) failed to find any such potential dependence.

BRIDGE-ASSISTED ELECTRON TRANSFER REACTIONS

Homogeneous outer sphere electron transfer reactions are often catalyzed by the presence of alkali metal cations in solutions (see e.g. 74). For example, the MnO_4^-/MnO_4^{2-} (75) and $Fe(CN)_6^{3-}/Fe(CN)_6^{4-}$ systems (76) are catalyzed by alkali

metal cations with the rate increasing with increasing intrinsic cation radius. Such catalytic effects are usually explained by assuming that the alkali metal cations reduce the coulombic repulsion between the reactants (i.e. decrease the electrostatic work terms in the Marcus approach) and/or that these cations serve as a bridge for the electron transfer and thus reduce the activation energy for the overall process. Although no detailed attempt to calculate the effects of the work terms have been carried out, it is commonly assumed (77) that they are usually small and that the primary catalytic effect is due to bridging. A third factor apparently neglected up to this time, however, is that the cation changes the polarizability of the environment surrounding the reacting ions through both the cations' intrinsic polarizability and its field effects on the surrounding medium.

Similar catalytic effects of alkali metal cations also have been found for the heterogeneous case. The $Fe(CN)_6^{3-}/Fe(CN)_6^{4-}$ electrochemical reaction (78-81) is catalyzed by the alkali metal cations, with the exchange current density decreasing in the order $Cs^+ > K^+ > Na^+ > Li^+$. Bindra, Gerischer & Peter (80) have shown rather conclusively that double layer effects involving work terms are not sufficient to explain such an effect. Dogonadze, Ulstrup & Kharkats (82) have used the bridging concept to explain the catalytic effect.

The majority of the theoretical work on these bridge-assisted outer sphere electron transfers has been done for both homogeneous and heterogeneous reactions by the Levich-Dogonadze theoretical group at the Institute of Electrochemistry in Moscow (77, 82–87). For the homogeneous reactions these workers consider two limiting cases:

1. the push-pull mechanism, in which an electron is first transferred from the reacting ion A to the bridging species C and then from C to the other reacting ion B; and
2. the pull-push mechanism, in which an electron is first transferred from the bridging species C to the ion B, followed by the transfer of an electron from A to C.

Second order perturbation theory is then used to calculate the transition probability of both mechanisms. The use of this approach implies that the intermediate states considered in the two limiting mechanisms are virtual states with no need to include energy conservation factors for the intermediate states. In a sense, the lifetime of the intermediate state is so short that its energy is very broadened by the uncertainty principle.

Using the LDK solvent polarization fluctuation approach for outer sphere electron transfer, Volkenshtein et al (84) have treated the quasiclassical, high temperature limit ($\hbar\omega \ll kT$) for the homogeneous reaction, assuming that the initial, intermediate, and final states each have their own potential energy surfaces which are linear and noninteracting. Levich, Madumarov & Kharkats (85) have extended this treatment by using parabolic noninteracting potential energy surfaces for the high temperature limit. No inner sphere effects were taken into account. Dogonadze, Ulstrup & Kharkats (77) have further extended this treatment to the case where the intermediate state has a continuous distribution of electronic energy levels.

Dogonadze, Ulstrup & Kharkats (82) have treated heterogeneous bridge outer

sphere electron transfer using the push-pull and pull-push mechanisms, considering the quasicontinuous distribution of electron energy states of the metal. The total transition probability for electron transfer from the reacting ion through the bridge to the metal is

$$W = \sum_{\varepsilon_j} \{[1 - n(\varepsilon_j)] W_{if}(\varepsilon_j)\} \qquad 27.$$

where $W_{if}(\varepsilon_j)$ is the transition probability for electron transfer from the reacting ion via the bridge to a particular electronic energy level ε_j in the metal, and $n(\varepsilon_j)$ is the Fermi distribution function. The heterogeneous rate constant, neglecting double layer effects, is proportional to W. For the push-pull mechanism, the transition probability $W_{if}(\varepsilon_j)$ is in turn given as

$$W_{if}(\varepsilon_j) = L_{ik}^2 L_{kf}^2 K(\varepsilon_j) \exp\{[-E_{kw}(\varepsilon_j) - I_i]/kT\} \qquad 28.$$

where L_{ik} and L_{kf} are the electronic matrix elements obtained from second order perturbation theory for the initial (i), final (f), and intermediate (k) states of the push-pull mechanism (i.e. electrons in the bridge); $K(\varepsilon_j)$ is a slowly varying function of ε_j; $E_{kw}(\varepsilon_j)$ is the energy of the intersection point of the potential energy surfaces between the initial and intermediate, or intermediate and final states, depending on which is highest; and I_i is the equilibrium ground state energy of the initial state. An analogous equation can be written for the pull-push mechanism. The activation energy $[E_{kw}(\varepsilon_j) - I_i]$ and its potential dependence are evaluated in essentially the same way as in the LDK approach with heterogeneous nonbridged electron transfer. The potential distribution across the interface relative to the positions of the reacting ion and the bridge species, however, is of particular importance. Two limiting cases are considered by Dogonadze, Ulstrup & Kharkats (82), as shown in Figure 2. The question of whether the bridged species is hydrated must also be taken into account.

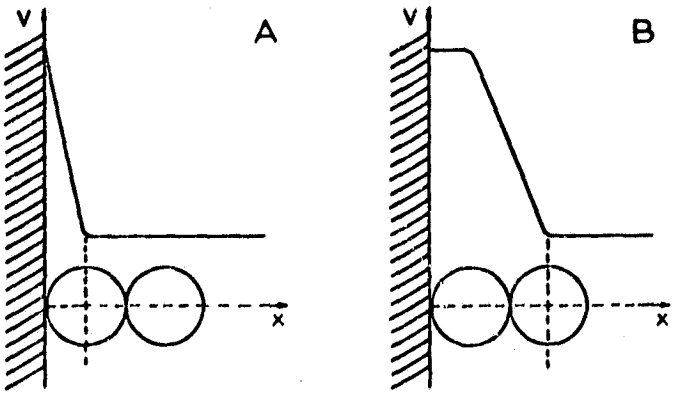

Figure 2 Potential distribution models for bridge-assisted electron transfer for two limiting cases in the treatment of Dogonadze et al (82).

This theoretical treatment leads to various types of current-voltage behavior depending on the energy of the Fermi level of the metal relative to the intersection point of the potential energy surfaces for the initial and intermediate states and intermediate and final states. This in turn is a function of the overpotential. For example, for the push-pull mechanism and the potential distribution shown in Figure 2*B*, the cathodic branch of the current-voltage curves should have the normal Tafel behavior with $\beta = 1/2$ at relatively low overpotentials, but should make a transition at higher overpotentials to an activationless region corresponding to $\beta = 0$. Dogonadze et al (82) cite the decrease in the experimentally observed transfer coefficient for the reduction of the ferricyanide in the presence of alkali metal cations at high overpotentials as evidence of such a transition. Uncertainties about double layer corrections and the possibility of changes in potential distribution across the interface make this evidence somewhat questionable. Recently Dogonadze, Ulstrup & Kharkats (83) have extended this treatment to the case where the virtual intermediate state also has a quasicontinuous distribution of electronic energy levels.

These treatments of bridged outer sphere electron transfer at metal electrodes represent a major advance but suffer from oversimplifications which may not be appropriate for most experimental systems. The use of second order perturbation theory to calculate $W_{if}(\varepsilon_r)$ involves the assumption that there are no strong interactions between the electronic energy levels of the reacting ion, bridge species, and the metal. This assumption is particularly questionable if the bridging species is specifically adsorbed on the electrode. Further, the models in Figure 2 used to calculate the effects of the potential distribution at the interface on the activation energies are at best qualitative and in many instances may not even be that. In addition, no account is taken of the effects of the bridging ion on the polarizability of the environment surrounding the ion, as cited earlier. The increase in the rate constants for the ferrocyanide oxidation encountered in going from Li^+ to Cs^+ as the cation may well be due principally to this effect, since the electrode is quite anodic to the potential of zero charge (pzc) and a bridge mechanism therefore seems unlikely.

In a somewhat preliminary treatment, Schmidt (88) has considered the homogeneous inner sphere bridge electron transfer reaction (without atom transfer) by assuming that a radiationless electron transfer occurs within the bridge molecular complex. The bridged complex is assumed to be in equilibrium with the reactants, and the electron transfer alone is assumed to control the reaction rate. The rate for such a process was then calculated using the linear response formalism developed by Yammamoto (62) in a manner similar to that used by Schmidt for the homogeneous (46) and heterogeneous (41) outer sphere electron transfer (without bridge). The expressions involved in the Schmidt treatment are quite complex. For purposes of simplification in this preliminary treatment, Schmidt has assumed no strong interactions between the reacting ions and the bridge species—certainly a doubtful assumption for inner sphere electron transfer. In principle, however, this formalism can be extended to the strong interaction case, as pointed out by Schmidt (88).

PROTON TRANSFER ELECTRODE REACTION

The Activated Complex Approach

Since the pioneering work of Horiuti & Polanyi (12), various authors (see e.g. 89–92) have used the activated complex approach involving the stretching of the OH bond in H_3O^+ to form a transition state of the form O—H—Metal. Of critical importance is the model of the interface, particularly the position of the H_3O^+ or H_2O from which the proton transfer occurs. Bockris & Matthews (93, 94) have proposed the model shown in Figure 3. The initial state of the system is a solvated H_3O^+ ion at the outer Helmholtz plane. One of the protons associated with the H_3O^+ ion then transfers to one of the solvation waters [number 2 in Figure 3] situated at a distance δ_r, estimated by Bockris & Matthews to be ~3.8 Å. Further Grotthus-type transfer of a proton to a water molecule immediately adjacent to the surface is not considered because these authors believe that the strong negative charge of the electrode surface preferentially orients the water molecules on the electrode surface and therefore impedes further proton transfer to these molecules.

Bockris & Matthews consider the electron to be transferred by tunneling in the activated state because the barrier height is otherwise too high for classical transfer. They then use the Morse curves for $[H_2O–H]^+$ and H–M to construct the potential energy surface along the reaction coordinate (Figure 4). The vertical transition ΔE_0 in Figure 4 corresponds to transferring an electron from the Fermi level of the metal to the H_3O^+ (number 2 in Figure 3) in its ground electronic state with no change in the reaction coordinate. At the intersection point of the two Morse curves, radiationless electron transfer from the metal to a vibrationally excited H_3O^+ becomes possible. The various electronic energy levels in the metal correspond to the vertical translation of the Morse curve for the initial state $[H_3O^+ + e\ (metal)]$, with a different intersection point for each electronic energy level in the metal.

Bockris & Matthews (93) calculate the electron tunneling probability in the

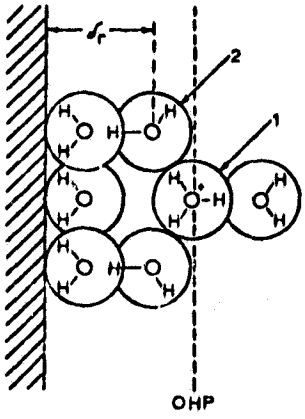

Figure 3 Bockris-Matthews model (4) for the electrode interface in proton discharge from H_3O^+.

activated state by considering the number of electrons of the particular energy E in the metal striking the surface per unit time, the probability of electron tunneling at this energy, and the probability of the electron colliding with a proton. Taking into account the Fermi distribution in the metal, they obtain for the discharge current density for proton transfer over the barrier the equation

$$i = (C_{H_3O^+})\frac{\pi r_H^2}{3}\cdot\frac{4\pi m_e e_0 kT}{h^3}\cdot W_e \int \frac{\exp -[\beta(E_0 - E)/RT]}{1+\exp[(E-E_1)/RT]}\,dE \qquad 29.$$

where $C_{H_3O^+}$ is the surface concentration of H_3O^+ located at the appropriate position relative to the electrode surface (position 2 in Figure 3), r_H is the effective radius of the proton for electron capture, m_e is the effective electron mass, W_e is the effective electron tunneling probability (averaged about the Fermi level), E_1 is the energy of the initial system $[H_3O^+ + e\ (\text{metal})]$ with the electron at the Fermi level, E_0 is the ground state energy of the system with the electron on the proton,

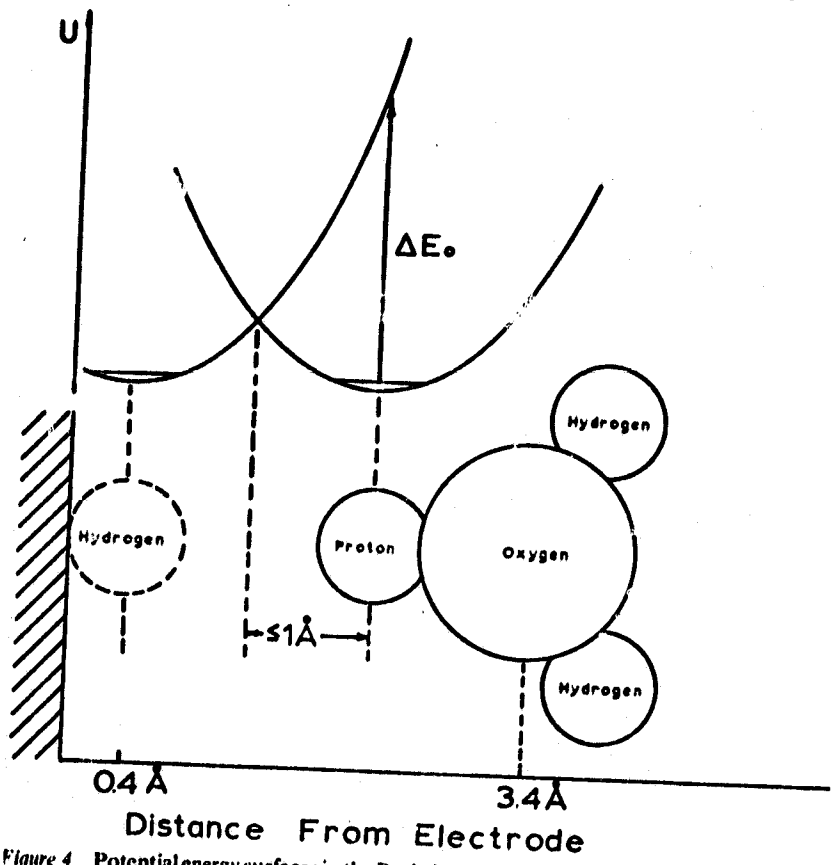

Figure 4 Potential energy surfaces in the Bockris-Matthews model for proton discharge (4).

and β is the transfer coefficient. The principal contribution to the discharge current is from the tunneling of electrons at or near the Fermi level, with the contribution dropping off rapidly as $|E - E_{f}|$ becomes large compared to RT. Under such circumstances, equation 29 reduces to an Arrhenius form; i.e.

$$i = (C_{H_3O^+}) \cdot \frac{\pi r_H^2}{3} \cdot \frac{4\pi m_e e_0 kT}{h^3} \cdot (1-\bar{\beta}) \cdot \exp - \frac{\Delta E^{\ddagger}}{RT} \qquad 30.$$

where the energy of activation $\Delta E^{\ddagger}$ is given by $\Delta E^{\ddagger} = \bar{\beta}\Delta E$, with ΔE corresponding to the difference in the energies of the initial and final states, and $\bar{\beta}$ is an averaged value of the symmetry factor.

As an alternative to proton transmission over the barrier, various authors have considered the possibility of proton tunneling through the barrier. As early as the 1930s, Topley & Eyring (95) and Bawn & Ogden (96) attempted to evaluate the relative rates of proton and deutron discharge: the former using a parabolic barrier of 1.5 Å thickness and the latter a symmetrical Eckart barrier of the same effective thickness. The question of proton tunneling has been more recently examined by Conway (27), Christov (13–15), and Bockris & Matthews (94), using various potential energy barriers.

For proton discharge from H_3O^+, the proton tunneling current density is (see e.g. 94)

$$i_{tun} = k_1 (C_{H_3O^+}) \int_{\varepsilon_0}^{\infty} \exp[-(\varepsilon - \varepsilon_0)/kT] P(\varepsilon)\, d\varepsilon \qquad 31.$$

where k_1 is a frequency factor, $C_{H_3O^+}$ is the surface concentration of the proton, ε_0 is the zero point energy level for the $[H_2O\text{–}H]^+$ stretching, and $P(\varepsilon)$ is the probability of proton tunneling at the energy level ε. For the calculation of $P(\varepsilon)$, Bockris & Matthews (94) use an asymmetric Eckart barrier of the form

$$U(x) = \frac{A \exp(2\pi x/d)}{1+\exp(2\pi x/d)} + \frac{B \exp(2\pi x/d)}{[1+\exp(2\pi x/d)]^2} \qquad 32.$$

where $A = A_0 + e\eta$, $B = 2E^{\ddagger} - A + 2[E^{\ddagger}(E^{\ddagger} - A)]$, and $E^{\ddagger} = E_0^{\ddagger} + \beta e_0 \eta$, with A_0 and $E_0^{\ddagger}$ corresponding to the energy of reaction and activation energy at an overpotential of $\eta = 0$, and $2d$ corresponds to the effective Eckart barrier width. The asymmetric Eckart barrier is a poor approximation to the actual potential energy surface and some uncertainty exists as to the relation of the Eckart barrier width $2d$ to the real proton transfer distance. Bockris & Matthews (94) have attempted to show that the real barrier width for the proton transfer is approximately half the Eckart barrier width ($2d$). The tunneling probability is quite sensitive to the barrier parameters, particularly the thickness (dropping off exponentially with thickness), and hence it is difficult to predict the extent to which the reaction proceeds by tunneling on purely theoretical grounds.

On the basis of the isotopic separation factor S and its potential dependence on Hg over a potential range for which β is constant, Bockris & Matthews (94) conclude that up to 70% of the observed current at low overpotentials is associated with tunneling. From experimental data for S and its potential dependence, Bockris, Srinivasan & Matthews (98) have estimated these parameters

to have the approximate values of $2d = 4$ Å, $E_0^{\ddagger} \cong 1.0$ eV, and $A_0 = 0.3$ eV. This value of 4 Å for the Eckart barrier thickness appears reasonable for the model shown in Figure 4 if the ratio of the real barrier width to the Eckart barrier width is $\sim 1/2$.

Conway (97) has also treated proton tunneling using an asymmetric Eckart barrier, but in contrast to Bockris & Matthews, he assumed that the proton transfer would take place from water molecules immediately adjacent to the surface and therefore used a very thin barrier ($2d = 0.5$ Å). With such thin barriers, the tunneling probability for protons is high and the Conway treatment leads to a Tafel slope of ~ 0.25 V/decade at low overpotential and nonlinear Tafel behavior greater than $\eta = -0.5$ V. Such behavior has generally not been observed.

Christov (13–15, 102) has also investigated the question of proton tunneling using various types of barriers (symmetrical and asymmetrical Eckart and parabolic) without developing a detailed physical model. For each, the effect of a linear potential energy drop across the interface was considered. In each instance, with judicious choice of barrier parameters, Christov finds the tunneling model to fit the experimental data, including the linear Tafel behavior, the temperature dependence of the exchange current density, and the isotopic separation factor. On this basis, Christov reaches a conclusion similar to that of Bockris et al concerning the importance of proton tunneling in hydrogen discharge on Hg.

In contrast, Conway & Salomon (99) have concluded that proton tunneling is not significant because the activation energy for proton transfer in methanol is independent of temperature down to -110°C. The anomalous temperature dependence of the Tafel slopes observed in these studies has been attributed by Conway & Mackinon (100) to double layer effects. At this time the importance of proton tunneling in hydrogen discharge appears far from settled.

Conway & Salomon (91, 92) have developed a treatment involving an analysis of the vibrational modes of the transition state and have concluded that the hydrogen-tritium separation factor on Hg and possibly on Ni and Fe cathodes can be adequately explained on the basis of slow proton discharge without involving tunneling. Their treatment takes into account the symmetrical stretch mode in the activated complex. They suggest several possible qualitative explanations for the potential dependence of the separation factor on Hg. For the most part these involve the interactions of the electric field across the interface with either the vibrational modes of the activated complex or the solvent adjacent to it.

In considering electron and proton tunneling at electrodes, various authors have used the Gamov equation which involves implicitly the WKB approximation. Levich (2) has questioned the validity of this approach on the grounds that the derivation of the Gamov equation involves the assumption that the spatial distribution of the potential field does not change during the course of the transition. He points out that the energy levels of the initial and final states are changing because of solvent polarization changes. Sen & Bockris (101) have examined the tunneling times for electron and proton tunneling through a rectangular barrier using the barrier height-width parameters of the Bockris-Matthews model of proton transfer, and they concluded that the tunneling times are considerably shorter than the 10^{-13} sec involved with solvent polarization fluctuations. Consequently they

do not believe this error to be significant in the Bockris-Matthews treatment. It is important to note, however, that the tunneling times are sensitive to the barrier parameters, and hence their conclusions should not be generalized.

In the Bockris-Matthews treatment of proton transfer, resonance interaction at the top of the barrier was not included. Salomon, Enke & Conway (103) and Sen (104) have attempted to take into account strong interaction in the activated state by using the semiempirical bond energy bond order (BEBO) method for calculating potential energy surfaces. This approach was first proposed by Paar & Johnston (105) to construct the potential energy (PE) profile along the reaction coordinate for the gas phase $H + H_2$ reaction. According to this approach, the total bond order of the three-center bond involving the proton as it moves through reaction coordinate space is assumed to be constant and equal to the initial value of unity in the prereaction state. The Bockris-Sen treatment considers the model

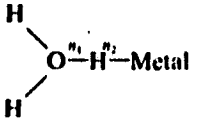

where $n_1 + n_2 = 1$. The remainder of the treatment is similar to that for the gas phase reaction $H + H_2$. Using the data of Parsons & Bockris (90) for the proton solvation energy and M–H bond energy, Bockris & Sen obtain a value of 15 kcal/mol for the height of the energy barrier. These workers consider the proton transfer process to occur by proton tunneling. Using the asymmetrical Eckart barrier in a manner analogous to Bockris & Matthews (94), they calculate the potential dependence of the transfer coefficient and the isotopic separation factor ratio for hydrogen discharge on Hg. Using the BEBO value of 15 kcal/mol for the barrier height and $2d = 4.0$ Å, they obtain values for the isotopic separation factor and its potential dependence in reasonable agreement with experiment.

The Salomon-Enke-Conway (SEC) treatment (103) of proton transfer using the BEBO method differs from the Bockris-Sen treatment in that the reaction is considered to proceed entirely by proton transfer *over* the barrier. SEC take the final state following the slow proton transfer to be $Hg–H^+$ and then use the bond energy of the $Hg–H^+$ as an adjustable parameter. Using the experimental activation energy on Hg, they find this bond energy to be ~155 kcal/mol, a value that they feel argues for $Hg–H^+$ rather than Hg–H as the final state of the slow step. Using these values they calculate the ratio of the pre-exponential values for proton and deutrium discharge on Hg and find reasonable agreement with experiment.

These BEBO treatments have several shortcomings. In the construction of the potential energy surface, various interactions other than those associated with O···H—M have not been considered adequately or have been omitted altogether. These other interactions include modifications in the other O–H bonds of the hydronium ion as the proton is withdrawn, electronic band interactions within the metal surface, modifications of such attending the H–M bond formation, and reorganization of the solvent interacting with the electrode surface and the hydronium ion during the proton transfer.

Marcus (106) has used the BEBO approach in his treatment of the kinetics of atom, proton, and strong-overlap electron transfers in solution. He has taken into account solvent effects including the addition or removal of solvent molecules to and from reactants, vibrational changes in strongly interacting solvent molecules immediately adjacent to the reacting species, and solvent reorientation-polarization effects arising from changes in the charge distribution in the reacting system. The solvent polarization effects are treated as the equivalent of partial dielectric saturation. The solvent free energy contribution from this source is a quadratic function of the fluctuations in solvent polarization, just as the harmonic potential energy term for vibrational coordinates is a quadratic function of fluctuations in these coordinates. It appears attractive to extend these additional features of the Marcus BEBO treatment to the proton transfer reactions at electrodes.

The Nonequilibrium Solvent Polarization Model

Dogonadze, Kuznetsov & Levich (107, 108) have extended the theoretical formalism, which they developed for outer sphere electron transfer, to proton transfer at electrodes. For the discharge step, these authors state that activation by stretching of the $[H_2O{-}H]^+$ and H–M bonds is sufficiently improbable to be neglected on the basis that for these bonds $\hbar\omega \gg kT$. They treat the proton as well as the electron as part of a fast subsystem with the solvent being the slow system. Their model assumes that activation can arise only due to nonequilibrium solvent polarization, in a manner similar to that for their outer sphere electron transfer model. By using a double adiabatic approximation, this approach separates the electron and proton wavefunctions from the solvent wavefunctions and treats the electron and proton as a quantum subsystem and the solvent as a classical subsystem.

The potential energy surface assumed for the discharge reaction is schematically shown in Figure 5, where R is the proton coordinate and q is the solvent coordinate

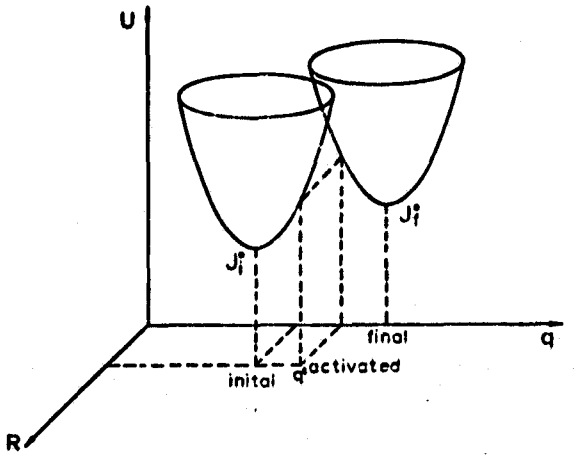

Figure 5 Potential energy surfaces for proton discharge according to the DKL model (2). q: solvent coordinate, R: proton coordinate.

indicating the state of polarization of the solvent. Due to solvent polarization fluctuations, as the coordinate q changes values, the potential energy of the initial state of the system changes and the system moves continuously along the energy surface $U(q, R_0)$, preserving the constant value of $R = R_0$; i.e. the vibrations along the bond $[H_2O\text{-}H]^+$ remain unexcited. At $q = q^*$, the energy of the initial state equals that of the final state and the system undergoes a quantum transition involving proton tunneling from the ground vibrational state of H_3O^+ to the ground state of H-M. The solvent then relaxes to the equilibrium configuration around the final $H_2O + H\text{-}M$ state. The rate of the discharge reaction is written as

$$i = e(C_{H_3O^+}) \int n(\varepsilon)\rho(\varepsilon)W(\varepsilon)\,d\varepsilon \qquad 33.$$

where $C_{H_3O^+}$ is the surface concentration of protons, $n(\varepsilon)$ is the Fermi distribution, $\rho(\varepsilon)$ is the electronic density of states, and $W(\varepsilon)$ is the thermally averaged transition probability. $W(\varepsilon)$ is related to the transition probability of the system passing from the mth vibrational level of the initial state to the nth vibrational level of the final state $W_{if}(\varepsilon)$ by a relation of the form of equation 8. First order perturbation theory is then used to calculate $W_{if}(\varepsilon)$. Thus $W_{if}(\varepsilon)$ is given by the expression shown in equation 6.

The DKL approach then uses the Born-Oppenheimer approximation to express the wavefunctions of the initial and final states as a product of the electronic, proton, and solvent wavefunction. The assumption implicit in such a separation of the proton and solvent wavefunctions is that the proton subsystem is fast compared to the solvent subsystem. DKL justifies this assumption on the ground that the vibration frequencies of the proton attached to the hydronium ions in the initial state and the hydrogen atom adsorbed on the metal surface in the final state are orders of magnitude higher than the frequencies of the solvent orientational modes. Using the Condon approximation twice, once for the electronic subsystem and once for the proton subsystem, DKL expresses $W_{if}(\varepsilon)$ as

$$W_{if}(\varepsilon) = \frac{2\pi}{\hbar} L^2 \sum_n \langle \chi^*_{fn}(R,q)\chi(R,q)\rangle^2 \langle \phi^*_{fn}(q)\phi_{im}(q)\rangle^2 \delta(\varepsilon_{im} - \varepsilon_{fn}) \qquad 34.$$

where L^2 is the electronic matrix element, the χ and ϕ quantities are the proton and solvent wavefunctions, R and q are the proton and solvent coordinates, and the subscripts fn and im represent the final state in the vibrational level n and the initial state in the vibrational level m, respectively. Equation 34 is then solved using harmonic oscillator wavefunctions. The solvent Hamiltonian used in this calculation is identical with the one used in the early LDK papers (35) for outer sphere electron transfer reactions (see equation 10).

The current density-overpotential relation obtained from this approach shows three distinct regions with different values of the transfer coefficient. At very low overpotentials, the transfer corresponds to an activationless type (see Figure 6*C*) with the transfer coefficient $\beta \simeq 1$. At moderate overpotentials the system exhibits a normal Tafel-type behavior with a transfer coefficient $\beta = 1/2$ (Figure 6*B*). Finally at very high overpotentials, the transfer coefficient becomes zero and the transition is barrierless (Figure 6*A*).

Comparisons between the predictions of this approach and the experimental results are only possible if the reorganization energy E_r in the theory can be estimated with any accuracy. Unfortunately such is not the case. However, Levich has compared the current-voltage behavior predicted by this theory to experimental results, assuming that the reorganization energy of the system is equal to 2eV. The very low overvoltage region with a transfer coefficient of $\beta = 1$ predicted by this theory has not been observed experimentally on Hg. This region is not readily accessible for accurate measurements, however, because of the very low current densities involved. Moderately good agreement is obtained in the normal Tafel region. Krishtalik (109, 110) has reported that at very high overpotentials the system does pass into a barrierless region for Hg.

Within the framework of this approach, German et al (111) have investigated the potential dependence of the isotopic separation factor. They have shown that there are two contributions to the separation factor. The first is the difference in zero point energies between the O–H^+ and O–D^+ bonds. This contribution,

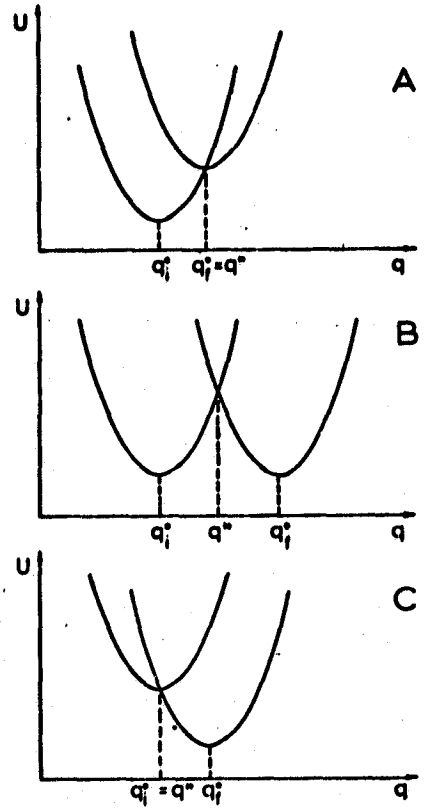

Figure 6 Potential energy surfaces for proton discharge according to the DKL treatment (2) for low (*A*), intermediate (*B*), and high (*C*) overpotentials.

however, does not depend on potential. The second factor arises from differences in the transmission coefficients for the proton/deutrium/tritium transfer. This contribution depends on the distance of closest approach of the discharging species to the electrode. German et al concluded that the proton and the deutrium approach distances are different as well as potential dependent and this is what causes the potential dependence of the separation factor. Although this approach has not been developed to the extent where a quantitative comparison with experimental results can be carried out, the shape of the separation factor-potential curve obtained from this approach is analogous to the one experimentally observed.

In effect, the DKL treatment considers activation to be achieved by the accumulation of energy through phonon interactions in a solvent volume of dimensions large compared to the solvated hydronium ion and with almost a continuum of low frequency modes. The conventional activated complex theory with or without tunneling considers the accumulation of the energy of activation to occur in a single vibrational mode through multiple phonon interactions. The DKL group claims that the hydronium ion with its small volume is just too "hard," in terms of potential energy, to be effective for such accumulation. The extent to which either of these two views is valid remains to be established but it seems likely that both types of contributions to the activation energy will prove to be important. There is a need for an overall treatment of both contributions for the heterogeneous proton transfer.

ACKNOWLEDGMENT

The authors express appreciation to the Office of Naval Research and NASA for financial support during the preparation of this review.

Literature Cited

1. Marcus, R. A. 1964. *Ann. Rev. Phys. Chem.* 15:155
2. Levich, V. G. 1970. *Physical Chemistry; An Advanced Treatise*, ed. H. Eyring, D. Henderson, W. Jost, 9B: Chap 12. New York: Academic
3. Dogonadze, R. R. 1971. *Reactions of Molecules at Electrodes*, ed. N. S. Hush, Chap 3. New York: Wiley
4. Matthews, D. B., Bockris, J. O'M. 1971. *Mod. Aspects Electrochem.* 6: Chap 4
5. Appleby, A. J., Bockris, J. O'M., Sen, R. K., Conway, B. E. 1972. *MTP-International Review of Science and Technology*, ed. J. O'M. Bockris. London: Butterworths
6. Myamlin, V. A., Pleskov, Y. V. 1967. *Electrochemistry of Semiconductors*. New York: Plenum
7. Gerischer, H. See Ref. 2, 9A: Chap 5
8. Schultze, J. W., Vetter, K. J. 1973. *Electrochim. Acta* 18:889
9. Vetter, K. J., Schultze, J. W. 1973. *Ber. Bunsenges. Phys. Chem.* 77:945
10. Gurney, R. W. 1931. *Proc. Roy. Soc. London A* 134:137
11. Fowler, R. H. 1934. *Electrolytes*, ed. H. Falkenhagen (transl. R. Bell), Appendix. London: Oxford Univ. Press
12. Horiuti, J., Polanyi, M. 1935. *Acta Physicochim. URSS* 2:505
13. Christov, St. G. 1958. *Z. Elektrochem.* 62:567
14. Christov, St. G. 1961. *Electrochim. Acta* 4:306
15. Christov, St. G. 1968. *J. Res. Inst. of Catal. Hokkaido Univ.* 16:169
16. Salomon, M., Conway, B. E. 1965. *Discus. Faraday Soc.* 39:223
17. Marcus, R. J., Zwolinski, B. J., Eyring, H. 1954. *J. Phys. Chem.* 58:432
18. Marcus, R. J., Zwolinski, B. J., Eyring, H. 1955. *Chem. Rev.* 55:157
19. Sacher, E., Laidler, K. J. 1964. *Mod. Aspects Electrochem.* 3: Chap 1
20. Sacher, E., Laidler, K. J. 1963. *Trans. Faraday Soc.* 59:396
21. Libby, W. 1952. *J. Phys. Chem.* 56:863

22. Platzman, R., Franck, J. 1954. *Z. Physik* 138:411
23. Pekar, S. I. 1951. *Investigations of the Electronic Theory of Crystals*. Moscow
24. Davydov, A. S. 1948. *Zh. Eksp. Teor. Fiz.* 18:913
25. Marcus, R. A. 1956. *J. Chem. Phys.* 24:966
26. Marcus, R. A. 1957. *J. Chem. Phys.* 26:867
27. Marcus, R. A. 1959. *Can. J. Chem.* 37:155
28. Marcus, R. A. 1960. *Discus. Faraday Soc.* 29:21
29. Hush, N. S. 1961. *Trans. Faraday Soc.* 57:557
30. Hush, N. S. 1958. *J. Chem. Phys.* 28:962
31. Hush, N. S. 1957. *Z. Elektrochem.* 61:734
32. Levich, V. G., Dogonadze, R. R. 1959. *Dokl. Akad. Nauk SSSR* 124:123
33. Dogonadze, R. R., Chizmadzhev, Y. A. 1962. *Dokl. Akad. Nauk SSSR.* 144:1077
34. Dogonadze, R. R., Kuznetsov, A. M., Chizmadzhev, Y. A. 1964. *Zh. Fiz. Khim.* 38:1195
35. Levich, V. G., Dogonadze, R. R. 1961. *Coll. Czech. Chem. Commun.* 29:193
36. Levich, V. G. 1966. *Advan. Electrochem. Electrochem. Eng.* 4: Chap 5
37. Marcus, R. A. 1965. *J. Chem. Phys.* 43:679
38. Dogonadze, R. R., Kuznetsov, A. M. 1974. *Proceedings of the Symposium on Electrocatalysis*, ed. M. W. Breiter. The Electrochemical Society. 195 pp.
39. Bockris, J. O'M., Sen, R. K., Conway, B. E. 1972. *Nature Phys. Sci.* 240:143
40. Schmidt, P. P. 1972. *J. Chem. Phys.* 56:2775
41. Schmidt, P. P. 1973. *J. Chem. Phys.* 58:4290
42. Schmickler, W., Vielstich, W. 1973. *Electrochim. Acta* 18:883
43. Schmickler, W. 1973. *Ber. Bunsenges. Phys. Chem.* 77:991
44. Sutin, N. 1962. *Ann. Rev. Nucl. Sci.* 12:285
45. Reynolds, W. L., Lumry, R. W. 1966. *Mechanism of Electron Transfer*. New York: Ronald
46. Schmidt, P. P. 1973. *J. Chem. Soc. Faraday Trans. II* 69:1104
47. Kestner, N. R., Logan, J., Jortner, J. 1974. *J. Phys. Chem.* 78:2148
48. Noyes, R. M. 1961. *Progr. React. Kinet.* 1:129
49. Feynman, R. P. 1951. *Phys. Rev.* 84:108
50. Dogonadze, R. R., Kuznetsov, A. M. 1971. *Elektrokhimiya* 7:763
51. Dogonadze, R. R., Kornyshev, A. A. 1972. *Phys. Stat. Solidi B* 53:439
52. Dogonadze, R. R., Kornyshev, A. A. 1974. *J. Chem. Soc. Faraday Trans. II* 7:1121
53. Vorotyntsev, M. A., Dogonadze, R. R., Kuznetsov, A. M. 1971. *Electrokhimiya* 7:306
54. Dogonadze, R. R., Kuznetsov, A. M., Vorotyntsev, M. A. 1972. *Croat. Chem. Acta* 44:257
55. Dogonadze, R. R., Kuznetsov, A. M., Vorotyntsev, M. A. 1972. *Phys. Stat. Solidi B* 54:125
56. Dogonadze, R. R., Kuznetsov, A. M., Vorotyntsev, M. A. 1972. *Phys. Stat. Solidi B* 54:425
57. Vorotyntsev, M. A., Katz, V. M., Kuznetsov, A. M. 1971. *Elektrokhimiya* 7:1
58. Dogonadze, R. R., Kuznetsov, A. M. 1967. *Elektrokhimiya* 3:1324
59. Schmidt, P. P. 1974. *J. Phys. Chem.* 78:1684
60. Kubo, R., Toyozawa, Y. 1955. *Progr. Theor. Phys.* 13:161
61. Engelman, R., Jortner, J. 1970. *Mol. Phys.* 18:145
62. Yammamoto, T. 1960. *J. Chem. Phys.* 33:281
63. Schmidt, P. P. 1973. *J. Chem. Soc. Faraday Trans. II* 69:1122
64. Hale, J. See Ref. 3, Chap 4
65. Dietz, R., Peover, M. 1968. *Discus. Faraday Soc.* 45:154
66. Aylward, G., Garnett, J., Sharp, J. 1967. *Anal. Chem.* 39:457
67. Bockris, J. O'M. See Ref. 38
68. Bockris, J. O'M., Mittal, K. L., Sen, R. K. 1971. *Nature Phys. Sci.* 234:118
69. Sutin, N. 1966. *Ann. Rev. Phys. Chem.* 17:119
70. Vlcek, A. A. 1961. *Sixth International Conference on Coordination Chemistry*, ed. S. Kirschner, 590–603. New York: Macmillan
71. Frumkin, A. N., Petrii, O. A., Nikolaeva-Fedorovich, N. V. 1963. *Electrochim. Acta* 8:177
72. Parsons, R., Passeron, E. 1966. *J. Electroanal. Chem.* 12:524
73. Anson, F. C., Rathjen, N., Frisbee, R. D. 1970. *J. Electrochem. Soc.* 117:477
74. Basolo, F., Pearson, R. 1968. *Mechanism of Inorganic Reactions*, 488–89, New York: Wiley. 2nd ed.
75. Gjertsen, L., Wahl, A. C. 1959. *J. Am. Chem. Soc.* 81:1572
76. Shporer, M., Ron, G., Loewenstein, A., Navon, G. 1965. *Inorg. Chem.* 4:362
77. Dogonadze, R. R., Ulstrup, J., Kharkats, Y. I. 1973. *J. Theor. Biol.* 40:259
78. Schearer, G., Willig, F. 1974. *Extended Abstracts 25th Meeting ISE* Brighton,

England, 81
79. Kuta, J., Yeager, E. 1968. *Extended Abstracts 19th CITCE Meeting*, Detroit, 116–20
80. Bindra, P., Gerischer, H., Peter, L. M. 1974. *J. Electroanal. Chem.* 57:435
81. Nikolaeva-Fedorovich, N. V., Frumkin, A. N., Keis, Kh. E. 1971. *Coll. Czech. Chem. Commun.* 36:722
82. Dogonadze, R. R., Ulstrup, J., Kharkats, Y. I. 1973. *J. Electroanal. Chem.* 39:47
83. Dogonadze, R. R., Ulstrup, J., Kharkats, Y. I. 1973. *J. Electroanal. Chem.* 43:161
84. Volkenshtein, M. V., Dogonadze, R. R., Madumarov, A. K., Kharkats, Y. I. 1971. *Dokl. Akad. Nauk SSSR* 199:124
85. Levich, V. G., Madumarov, A. K., Kharkats, Y. I. 1972. *Dokl. Akad. Nauk SSSR* 203:1351
86. Kharkats, Y. I., Madumarov, A. K., Vorotyntsev, M. 1974. *J. Chem. Soc. Faraday Trans. II* 70:1578
87. Kharkats, Y. I., Madumarov, A. K., Ulstrup, J. 1974. *Extended Abstracts 25th Meeting ISE* Brighton, England, 51–54
88. Schmidt, P. P. 1974. *Z. Naturforsch. A* 29:880
89. Butler, J. A. V. 1936. *Proc. Roy. Soc. London A* 157:423
90. Parsons, R., Bockris, J. O'M. 1951. *Trans. Faraday Soc.* 47:914
91. Conway, B. E., Salomon, M. 1964. *J. Phys. Chem.* 68:2009
92. Conway, B. E., Salomon, M. 1964. *Ber. Bunsenges. Phys. Chem.* 68:331
93. Bockris, J. O'M., Matthews, D. B. 1966. *Proc. Roy. Soc. London A* 292:479
94. Bockris, J. O'M., Matthews, D. B. 1966. *J. Chem. Phys.* 44:298
95. Topley, B., Eyring, H. 1933. *J. Am. Chem. Soc.* 55:5053
96. Bawn, C. E. H., Ogden, G. 1934. *Trans. Faraday Soc.* 30:432
97. Conway, B. E. 1959. *Can. J. Chem.* 37:178
98. Bockris, J. O'M., Srinivasan, S., Matthews, D. B., 1965. *Discus. Faraday Soc.* 39:239
99. Conway, B. E., Salomon, M. 1964. *J. Chem. Phys.* 41:3169
100. Conway, B. E., Mackinon, D. J. 1969. *J. Electrochem. Soc.* 116:1665
101. Sen, R. K., Bockris, J.O'M. 1973. *Chem. Phys. Lett.* 18:166
102. Christov, St. G. 1964. *Electrochim. Acta* 9:575
103. Salomon, M., Enke, C., Conway, B. E. 1965. *J. Chem. Phys.* 43:3989
104. Sen, R. K. 1972. PhD thesis. Univ. of Pennsylvania
105. Paar, C., Johnston, H. 1963. *J. Am. Chem. Soc.* 85:2544
106. Marcus, R. A. 1968. *J. Phys. Chem.* 72:891
107. Dogonadze, R. R., Kuznetsov, A. M., Levich, V. G. 1967. *Elektrokhimiya* 3:739
108. Dogonadze, R. R., Kuznetsov, A. M., Levich, V. G. 1968. *Electrochim. Acta* 13:1025
109. Krishtalik, L. I. 1968. *Electrochim. Acta* 13:1045
110. Krishtalik, L. I. 1970. *Advan. Electrochem. Electrochem. Eng.* 7:283
111. German, E. D., Dogonadze, R. R., Kuznetsov, A. M., Levich, V. G., Kharkats, Y. I. 1970. *Elektrokhimiya* 6:342

National Bureau of Standards Special Publication 455, *Electrocatalysis on Non-Metallic Surfaces*, Proceedings of Workshop held at NBS, Gaithersburg, Md., December 9-12, 1975. (Issued November 1976)

Mechanisms of Electrochemical Reactions on Non-Metallic Surfaces

Ernest Yeager
Department of Chemistry
Case Western Reserve University
Cleveland, Ohio 44106

Oxygen electrocatalysis has assumed new importance because of the involvement of the O_2 electrode in various fuel cells and electrolyzer systems. For O_2 electroreduction to proceed at reasonable current densities requires the adsorption of the O_2 molecule or ion on the electrode surface. Various models for the interaction of such O_2 species with surfaces and the corresponding pathways for the electroreduction are considered. Generally peroxide mechanisms are predominant in aqueous solutions on non-metallic as well as metal surfaces but this leads to less favorable operating potentials for O_2 cathodes. A number of reasonably effective O_2 electroreduction catalysts have been identified for alkaline solutions but so far only high area platinum appears to combine reasonable activity and stability in acid electrolytes. Various electrocatalysts for which results have been reported in the literature are summarized. The electrochemical behavior of various carbons and graphites, lithiated NiO and various defect metal oxides including RuO_2/Ti is considered in some detail relative to O_2 generation as well as reduction kinetics.

Key words: Carbon; electrocatalysis; nickel oxide; semiconductor electrodes; oxide electrodes; oxygen electrochemistry.

1. Introduction

With the energy problems facing many nations, renewed interest has developed in electrochemical energy conversion and storage, and among the various electrochemical devices, particularly fuel cells and water electrolyzers. An important part of most such devices is the oxygen electrode. Unfortunately it is one of the more troublesome parts. The irreversibility of the oxygen electrode leads to excessive voltage losses and restrictions on power densities of the cells. Furthermore, in an effort to achieve an acceptable level of performance, it has been necessary to resort to expensive precious metal oxygen electrocatalysts in very high area forms, which are difficult to maintain over long operating times.

In light of the importance of O_2 electrodes and problems associated with oxygen electrocatalysis, this lecture will be directed principally to oxygen electrode reactions on nonmetallic surfaces.

2. General features of oxygen electrode reactions

The pronounced irreversibility of the oxygen electrode reactions at moderate temperatures has severely complicated mechanistic studies. The exchange current densities for the oxygen electrode are very low--typically 10^{-10} to 10^{-11} A/cm^2 on an effective catalytic surface such as platinum. Consequently the current densities near the reversible potential are generally too low to permit measurements under conditions where the kinetics are sensitive to the reverse as well as forward reactions. Further, the experimentally accessible

portions of the cathodic and anodic branches of the polarization curves are sufficiently separated in potential that the surface conditions differ very substantially. Therefore, the cathodic and anodic processes under these conditions are probably not the reverse of each other. To complicate the situation further, the oxygen electrode reactions may proceed through a large number of pathways. This explains why the mechanisms for O_2 generation and reduction are still not fully understood even on platinum, the most extensively used and most studied O_2 electro-reduction catalyst.

Before discussing O_2 electrocatalysis on specific non-metallic surfaces, some of the general features of the possible electrode mechanisms will be considered. O_2 reduction in aqueous solutions requires a strong interaction of O_2 with the electrode surface for the reaction to proceed at a reasonable rate. Three types of models for such interaction have been proposed [1,35][1]. These are shown in figure 1, together with the corresponding reaction

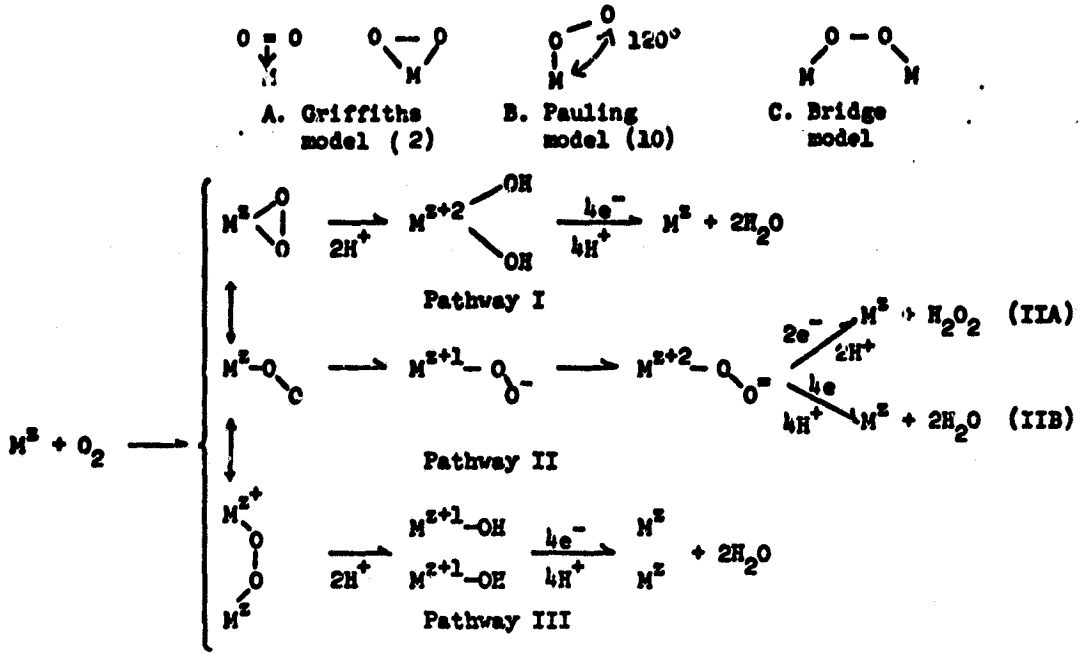

Figure 1. Models for adsorbed O_2 and corresponding reaction pathways for O_2 electroreduction.

pathways for O_2 reduction. The Griffiths model [2] involves a lateral interaction of the π orbitals of the O_2 interacting with empty d_{z^2} orbitals of a transition element, ion or metal atom with back bonding from at least partially filled d_{xz} or d_{yz} orbitals of the transition element to the π^* orbitals of the O_2. This type of interaction should lead to a weakening of the O-O bond with a corresponding lengthening of this bond. The Vaska complexes [e.g., $Ir(O_2)Cl(CO)(PPh_3)_2$] appear to form such complexes with O_2 [3,4]. These compounds are selective oxidation catalysts for cyclic olefins [5]. The formation of a strong metal-to-oxygen interaction results in a weakening of the O-O bond and an increment in the length of this bond [6]. Sufficiently strong interaction of this type may lead to the dissociative adsorption of O_2 with probably simultaneous proton addition and valency change of the transition element in the manner represented by Pathway I in figure 1, followed by reduction of the $M(OH)_2$ to regenerate the catalyst site. Sandstede et al. [7,8] have attempted to explain oxygen reduction with square pyramidal Co(II), Fe(II) and Fe(III) complexes as well as on the thiospinels on the basis of such π bonding. Tseung, Hibbs and Tantram [9] have proposed that O_2 reduction on Li-doped NiO changes from a non-dissociative to dissociative mechanism

[1] For reviews see ref. [1,35]. Figures in brackets indicate the literature references at the end of this paper.

above the Neel point (200°C for their ~10-atom % Li doped NiO) in order to explain the increment in catalytic activity in KOH hydrate melts above the Neel temperature.

It is indeed likely that O_2 reduction does proceed by a dissociative adsorption mechanism on some electrocatalysts. Up to date, however, no unambiguous experimental evidence appears to have been presented for O_2 reduction by such a mechanism on either metallic or non-metallic catalyst surfaces in aqueous solutions at moderate temperatures.

With most transition metal catalysts, the most probably structure for O_2 adsorption is the Pauling model [10] in which sp^2 orbitals of O_2 interact with d_{z^2} orbitals of the transition metal. The square pyramidal complexes of Fe(II) and Co(II)[8] which have good activity for O_2 reduction in acid solutions, appear to involve such an end-on interaction on the basis of esr and other evidence [11]. This adsorption of O_2 is expected to be accompanied by at least a partial and probably complete charge transfer to yield a superoxide and then peroxide state, as represented by Pathway II in figure 1. The adsorption of the O_2 on the square pyramidal complexes of Fe(II) and Co(II) may lead directly to the superoxide state. With somewhat similar oxyhemoglobin complexes of iron, various workers have proposed that O_2 binding to the iron involves O_2^- or $O_2^=$ states with Fe in the III valent state [12-14]. The change in valency state of the transition metal coupled with the change in O_2 oxidation state during formation of the O_2 adduct corresponds in principal to the redox electrocatalyst concept proposed by Beck et al. [15,16].

The further reduction of the O_2 beyond the peroxide state requires rupture of the O-O bond. Such can occur in Pathway IIB through the formation of $O^{\cdot}$ or $HO^{\cdot}$ free radicals in solution or the simultaneous reduction-bond cleavage (electrochemical desorption) to yield H_2O or OH^-. Neither of these processes are likely to be sufficiently fast at practical operating potentials for O_2 cathodes but the electrochemical desorption is a better candidate. The free energies of formation of the $O^{\cdot}$ and $HO^{\cdot}$ free radicals in solution are just too high to achieve sufficiently high concentrations for the subsequent homogeneous reactions to proceed at rates corresponding to reasonable current densities at acceptable electrode potentials. Substantial evidence exists for Pathway IIA yielding solution phase peroxide for various metallic and non-metallic electrode surfaces. With non-metallic electrodes such as carbon, graphite and lithiated NiO in aqueous alkaline solutions, significant amounts of peroxide are found in solution and the potential under open-circuit conditions follows the Nernst equation predictions for the O_2-HO_2^- couple [see e.g. ref. 17, 18]. Eventually the peroxide is further reduced at practical O_2 cathodes. The formation of solution phase peroxide as an intermediate, however, is unfortunate since it leads to less favorable operating potentials. With carbon electrodes in alkaline solutions, it is necessary to incorporate a peroxide reduction or decomposition catalyst in the electrode to prevent the buildup to high concentrations of the peroxide within the electrode structure. One possibility is to utilize the spillover effect with the peroxide produced at one site migrating on the surface to an adjacent or nearby site where the peroxide elimination step occurs. This indeed may occur to some extent with high area carbon electrodes containing peroxide elimination catalysts such as Pt or Ag.

Under some circumstances it is possible that the superoxide species $O_2^{\cdot-}$ may desorb to yield the solution phase species. This ion is formed as a reasonably stable entity during O_2 reduction in aprotic solvents [see e.g., ref. 19-22] and probably in carbonate melts [23]. The superoxide ion also has been proposed to be formed in aqueous solutions on Hg [24,25], amalgamated gold [26] and carbon paste [27] cathodes in the presence of surface active agents. Under these circumstances, Divisek and Kastening [24,25] propose that the surfactant molecules displace water molecules from the surface, impeding access of water to the adsorbed $O_2^{\cdot-}$, and thereby inhibiting further reduction. Dubrovina and Nekrasov [26] have proposed that the $O_2^{\cdot-}$ radical may be stabilized through the formation of a complex with the surfactant molecule. In the absence of adsorbed organic species, however, it does not appear that an $O_2^{\cdot-}$ desorption mechanism contributes significantly to the observed current. Rotating disk experiments have rather clearly demonstrated this for graphite [28] and also gold cathodes [29], as will be discussed for the former case later in this lecture.

Pathway III in figure 1 provides an alternate means for bringing about rupture of the O-O bond through the formation of an -O-O- bridge. Such a mechanism may come into play with the proper surface spacing of transition metal atoms or ions in a metal, oxide or thiospinel or in a bimetal complex such as a macrocyclic. The formation of the bridge species

requires proper spacing of the two metal species plus partially filled d_{xz} or d_{yz} orbitals to participate in bonding with the sp^2 orbitals of the oxygen. Macrocyclic transition metal complexes of the type M-O_2-M been synthesized [e.g., see ref. 30, 31, 36, 37] and appear to occur naturally in hemerythrin.

For any of the mechanisms in figure 1, considerable questions exist as to the reversibility of the O_2 adsorption step at the rather high rates involved with practical O_2 cathodes. For O_2 to bond to M^z will generally require the replacement of a water molecule or anion of the electrolyte--a situation which would normally be expected to be unfavorable to O_2 unless the O_2 adduct has a pronounced dipolar character (M^{z+1}-O-O^-) [32, 33]. The reversibility of the formation of such adducts in water and other solvent systems is strongly dependent on the ligands and generally favored in the "picket fence" porphyrins in which the large rather bulky organic groups create an environment more conducive to O_2 uptake [34]. Porphyrins of this type are probably responsible for the relatively good performance of carbon cathodes as O_2 electrodes in blood, but it is doubtful whether they can be rendered sufficiently stable for prolonged use in the strongly acid and alkaline solutions of most fuel cells above 100°C.

At steady state any peroxide formed on the electrode surface must be subsequently further reduced or decomposed. When the O_2 reduction proceeds entirely through a peroxide state on the electrode surface and/or in the solution, the process is usually referred to as "series" whereas when O_2 reduction proceeds simultaneously by a dissociation step without a peroxide state as well as through a peroxide state, the processes are described as "parallel". Peroxide has been detected in the solution phase during O_2 reduction on many metallic and non-metallic electrodes (e.g., Pt, Au, Ag, Pb, Ni, NiO, carbon, graphite) in various aqueous electrolytes at T < 100°C. Consequently little doubt exists that the peroxide mechanism is often functional. Some authors have proposed that reduction also proceeds simultaneously through a dissociative adsorption mechanism as a parallel mechanism. Unfortunately the evidence is for the most part ambiguous.[2]

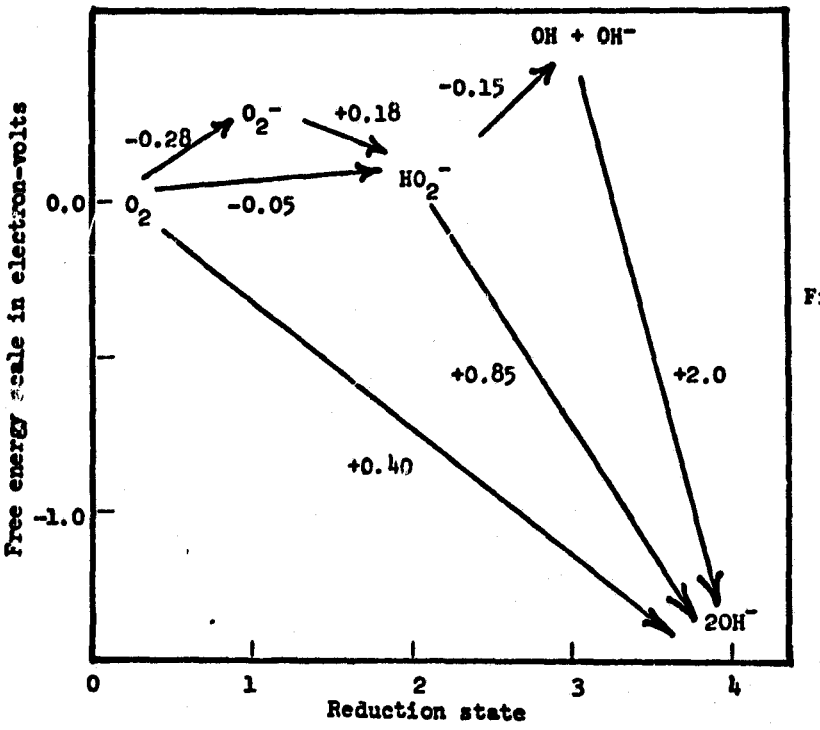

Fig. 2. Free energy relationships for the reduction of oxygen in basic solution at 25°C. Standard reduction potentials in volts are indicated on lines designating steps. Potential for O_2/O_2^- couple from ref. [25]. Multiply ordinates by 23 to obtain free energy in kcal/mol.

[2] Damjanovic, Genshaw and Bockris [39] have proposed that their rotating ring-disk data provide evidence for the parallel mechanism on Pt. Their treatment of the kinetics does not consider the peroxide desorption step. This would explain their results [40] without a parallel mechanism.

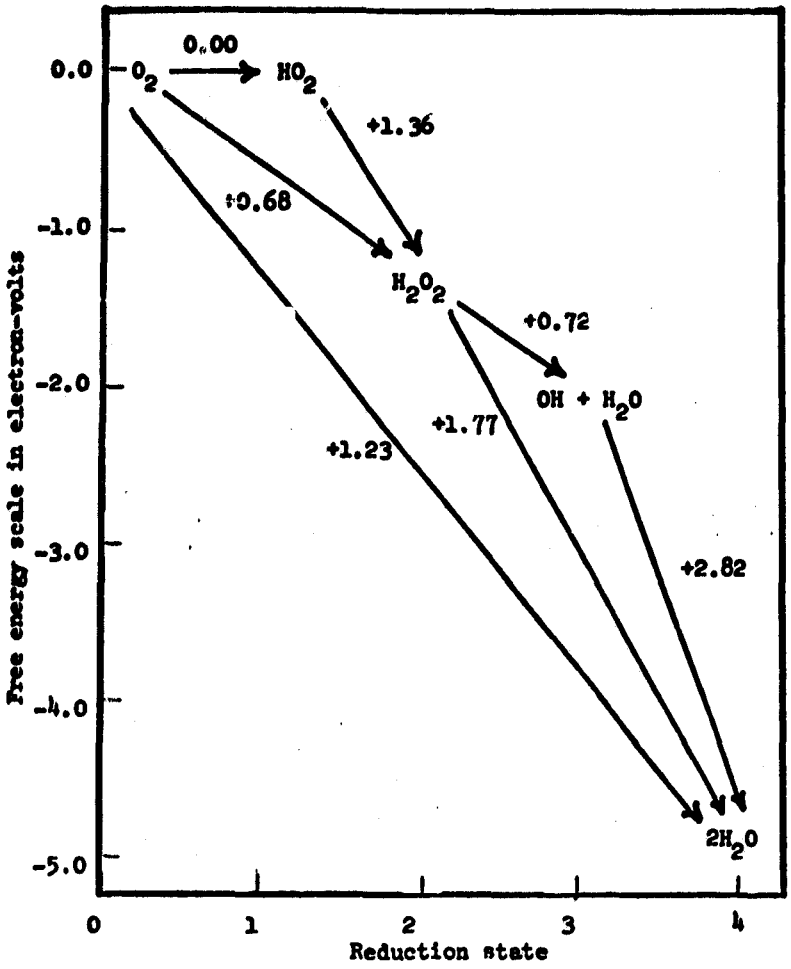

Fig. 3. Free energy relationships for the reduction of oxygen in acid solution at 25°C. Standard reduction potentials in volts are indicated on lines designating steps. Potential for O_2/HO_2^- couple calculated from data for O_2/O_2^- (ref. 25) and pK = 4.88 for $O_2^- - HO_2$ (ref. 38). (Multiply ordinates by 23 to obtain free energy in kcal/mol.)

The question of whether O_2 reduction can proceed by a parallel mechanism is more than just academic. The free energy changes and corresponding standard electrode potentials associated with the various O_2 couples are shown in figures 2 and 3 for alkaline and acid solutions. The standard electrode potential of the O_2-peroxide couple is far less anodic than that for the four-electron O_2 reduction (by +0.45 and -0.53V in alkaline and acid solutions, respectively). Further the O_2-peroxide couple is usually much more reversible than the other steps shown in figures 2 and 3 with the result that the potential is often controlled predominantly by the O_2-peroxide step.

In principle it should be possible for the potential of the O_2-peroxide couple to approach the reversible potential for the four-electron reduction by depressing the peroxide concentration to the equilibrium value for the reaction

$$2HO_2^- = O_2 + 2OH^- \qquad (1)$$

In practice this has not proved possible even with extremely effective peroxide decomposing catalysts under open-circuit conditions because the equilibrium peroxide concentration is extremely low (i.e., 10^{-15}M HO_2^- in 1M caustic). With high area carbon electrodes on which the O_2-peroxide couple has a high exchange current density [e.g., 10^{-4} A/cm^2 (true area)] in alkaline solutions, it has been possible to improve very substantially the performance through the incorporation of very effective peroxide elimination catalysts [see e.g., ref. 41, 68].

3. Summary of Materials Examined as O_2 Electrocatalysts

Table I is a partial list of the various materials which have been examined as O_2 reduction electrocatalysts. Many of the compounds listed in this table have substantial electrocatalytic activity for O_2 reduction in alkaline solutions but do not have sufficient long-term stability. Only a few have significant activity in the concentrated acid solutions and only platinum in ultrahigh area form has combined sufficient activity and stability. A few of these systems will be considered in some detail.

Table 1. Compounds considered for O_2 electroreduction catalysts in the literature.

Type	Example		Literature reference
Metal chelates			
N_2S_2	diacetyl-di(thiophenylbenzhydrazone)[a]	[DT]	7,42,43
N_2O_4	bissalicylaldehyde-o-phenylenediamine[a]	[Pfeiffer]	7,42,43
N_4	tetraphenyl porphyrin[a]	[TP]	7,42,43
	phthalocyanines[a]	[PC]	7,42-44,47
S_4	bisdiphenyldithioethylene[a]		42,43
	polymeric versions of above		42,43
	hemin		48
	Order of activities:		
	for N_4: Fe > Co > Cu > Ni ∿ Mn		
	for N_2O_4: Co > Mn > Fe > Cu > Ni		
	for Co II: $N_2O_4 > N_4 > N_2S_2 > O_4 \sim S_4$		
	for Fe II: $N_4 >> N_2O_2 > N_2S_2 > O_4 \sim S_4$		
Thiospinels			
$Me^aMe_2^bS_4$	Me^a = Mn, Fe, Co, Ni, Cu, Zn		
	Md^b = Ti, V, Cr, Fe, Co, Ni		
	also seleno- and telluro-spinels		
	activity: $Co_3S_4 > Ni_3S_4 > Fe_3S_4$		
Disulfides, diselenides, ditellurides			
	Co compounds active; for Cu, activity is highest with disulfide		
Oxides			
Spinels			
Spinels	$Me^aMe_2^bO_4$: Co_3O_4, Co_2NiO_4, $CoAl_2O_4$ active		52-55
Tungsten bronzes	M_xWO_3		57-60
Perovskites	Sr_xCoO_3 active		9,56
Other oxides:	NiO (lithiated)		9,18
	RuO_2		61
	Au_2O_3		62
Metals			
Pt and Pt family metals, alloys[b]			65-68, 83-85
Au and Au alloys			62,64
Ag			29,40,63
Carbons			
Ion implanted carbon			17,18,28,29,69,86

[a] Cations: Ti, V, Cr, Mn, Fe, Co, Ni, Cu, Zn

[b] The work on Pt is very extensive. For a review see references 75-78.

4. O_2 Electrocatalysis on Carbon and Graphite

On both carbons and graphites of low mineral content, the reduction of molecular O_2 proceeds to hydrogen peroxide in alkaline solution almost quantitatively at low peroxide concentrations. Typical current-voltage curves obtained with the rotating disk technique are shown in figure 4 for the edge and basal planes of stress-annealed pyrolytic graphite in 1M KOH. The hysteresis evident in these slow sweep curves (10 mV/sec) is caused by changes

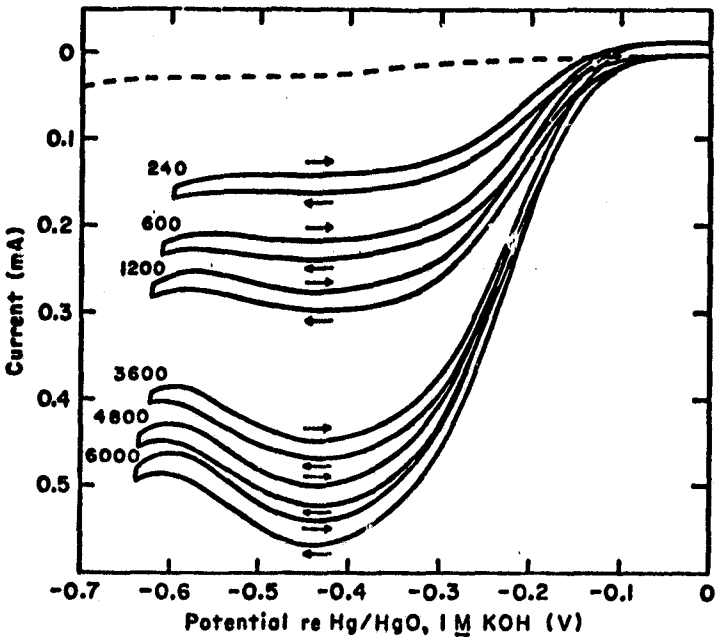

Fig. 4. Reduction of O_2 on high pressure annealed pyrolytic graphite. —— edge orientation, --- cleavage orientation. Electrolyte: 1 M KOH, pressure O_2: 0.97 atm, temperature: 22°C, electrode area: 0.22 cm^2. Rotation rates indicated on curves in rpm. Direction of sweep indicated by arrows. X-ray rocking angle of graphite $\theta_{\frac{1}{2}} = 0.4°$.

in the oxidation state of various groups present on the edge orientation. Isotopic experiments [70] involving O^{18} and the rotating disk experiments [28] indicate the following mechanism in NaOH and KOH solutions:

$$\text{Step I.} \quad S + O_2 \rightarrow S - O_2 \tag{2}$$

$$\text{Step II.} \quad S - O_2 + e^- \rightarrow S - O_2^- \tag{3}$$

$$\text{Step III.} \quad \begin{matrix} S - O_2^- \\ | \\ S - O_2^- \end{matrix} + HOH \rightarrow \begin{matrix} S + C_2H^- + OH^- \\ | \\ S + O_2 \end{matrix} \tag{4}$$

Step II is ordinarily rate controlling with a transfer coefficient of 0.50 but at high current densities, the potential-insensitive Step I becomes controlling. Corroborating evidence for such an O_2^- adsorption step is to be found in the reversible chemisorption of O_2 on carbon from the gas phase, presumably without bond cleavage, as revealed by esr studies [71]. Step III is quite surprising and is definitely a surface reaction rather than a second order solution-phase reaction between superoxide radicals ($O_2^-\cdot$ or $HO_2\cdot$). The fact that Step III is second order in the surface concentration of adsorbed O_2^- indicates that a direct interaction between two adsorbed O_2^- is required for this step. While the kinetic measurements have been carried out principally on various types of graphites, the results for various carbons [17] are sufficiently similar to suggest the same mechanism.

Of particular note is that with single crystal graphite and stress-annealed pyrolytic graphite, the O_2 reduction as well as peroxide oxidation reactions are very inhibited on the basal plane with the exchange current at least three orders of magnitude less on the basal plane than on the edge orientation. Imperfections in the basal plane set a lower limit to the checking of how far the exchange current is depressed on this plane.

This depression of the exchange current on the basal plane may be caused by

1. anisotropic surface-semiconductor properties of the graphite
2. the lack of suitable functional groups or adsorption sites on the basal plane.

The carrier concentration in graphite is rather low near the Fermi level and hence some significant fraction of the applied potential may fall across a space charge region for the basal plane. To check on this, a.c. impedance measurements have been carried out on this plane [72]. The differential capacitance curves and corresponding voltammetry curves are shown in figure 5 for both 1 N NaOH and 1 N H_2SO_4. These curves are in strong contrast to the corresponding curves for the edge orientation [73] which show much structure. The capacitance on the basal plane is much lower than on the edge orientation or on typical metals such as Hg or Au, suggesting that a significant potential drop occurs across a space charge region within the graphite. The potential dependence of the capacitance, however, is close to parabolic rather than the hyperbolic dependence expected for a semiconductor electrode. This may be caused by the high carrier concentration in the graphite; i.e.: $\sim 6 \times 10^{18}$ carriers/cm^3 [74]. Further, the capacitance curves give no indication of specific adsorption, even in the presence of relatively high concentrations of such anions as iodide [72].

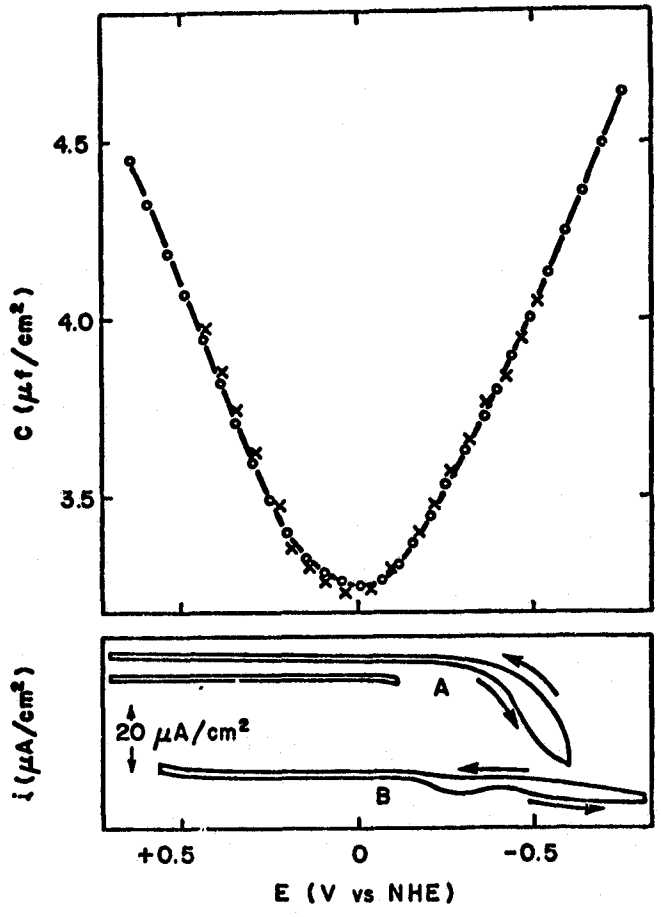

Fig. 5. Capacity-potential and current-potential curves for the basal plane of stress-annealed pyrolytic graphite ($\Delta\theta_{\frac{1}{2}} \cong 0.4°$) in 1 N H_2SO_4 and 1 N NaOH solutions at 25°C and 1000 Hz (sine wave): x 1 N H_2SO_4; o 1 N NaOH. Scan rate for the current-potential curves 0.1 V/sec, direction of sweep indicated by arrows: A) 1 N H_2SO_4; B) 1 N NaOH.

To check further on the extent to which electrode reactions on the basal plane may be impeded by semiconductor effects, the behavior of the $Fe(CN)_6^{3-} - Fe(CN)_6^{4-}$ redox couple has been examined on this surface [28]. The apparent exchange current density is approximately 1/3 of that on the edge (1.1 mA/cm^2 on the basal plane as compared with 3.0 mA/cm^2 on the edge in 0.005 M $K_3Fe(CN)_6$ + 0.005 M $K_4Fe(CN)_6$ + 0.5 M K_2SO_4 at pH = 3 and 26°C). This difference may be caused by a difference in the ratio of true to apparent surface area or ionic double layer effects (different point of zero charge) as well as semiconductor effects but is certainly far less than the two orders of magnitude difference in the exchange current densities for the O_2 reduction on the basal and edge planes.

The most likely explanation for the suppression of O_2 reduction on the basal plane is the lack of suitable adsorption sites for O_2(ads), O_2^- (ads) and O_2H^-(ads) during the reduction. This raises the question as to what particular adsorption sites or functional groups are involved in the O_2 reduction on the edge surface. A large number of functional groups have been proposed to exist on carbon surfaces [79, 80] and some of these should persist on graphite as well as carbon at the potentials for O_2 reduction in alkaline solutions. Even so, it is far from clear which, if any, provide the adsorption sites involved in the O_2 reduction.

Garten and Weiss [81] some years ago proposed that quinone groups are involved in the following way:

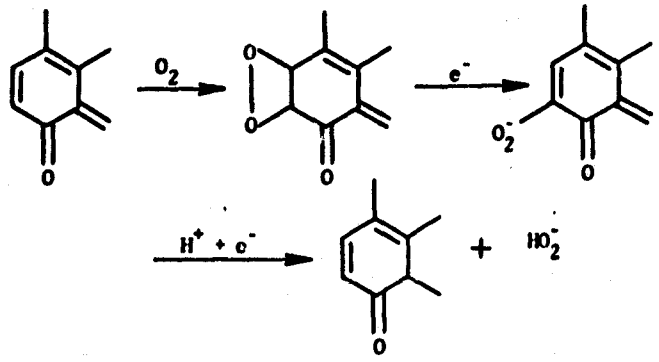

(5)

The O_2 first adds to the olefinic bond associated with the quinone group to form the hydroperoxide or molecular oxide. Electron transfer then occurs to form O_2^-(ads) and subsequently splits off as HO_2^- after a further electron transfer. Steps I and II of this mechanism are compatable with the kinetics but step III is not. The peroxide formation step is second order in O_2^-(ads) and hence appears to involve interaction between two O_2^-(ads) with simultaneous electron transfer either directly or through the carbon substrate. The nature of this interaction is not clear. A similar second order step involving O_2^-(ads) also appears to be involved in O_2 reduction on gold [29, 63].

5. O_2 Electrode Reactions on Nickel Oxide

Oxygen reduction at room temperatures proceeds through a peroxide mechanism on lithiated NiO in alkaline solutions [9, 18, 82]. In O_2-saturated alkaline solutions of HO_2^-, the open-circuit potential of anhydrous NiO produced by various methods corresponds to the thermodynamic value for the $O_2 - HO_2^-$ couple with the proper dependence on HO_2^- activity [18].

The NiO most extensively studied in the author's laboratory [18, 82] is mosaic crystalline anhydrous NiO ([100] orientation) produced by hydrothermal growth on isomorphic MgO from the $NiBr_2 - H_2O$ vapor phase at ~600°C, using the method of Cech and Alessandrini [88]. The mosaic crystals are then doped with 0.1 - 1.0% Li by high temperature infusion (1450-1550°C). This material is a p-type semiconductor and hence processes such as O_2 reduction would be expected to be inhibited. Examination of redox couples such as ferri-ferrocyanide with the rotating disk technique do indicate such cathodic inhibition in acid solutions with the anode branch under combined kinetic and diffusion control [87]. Differ-

ential capacitance measurements in acid solutions indicate that most of the electrode potential change occurs across the space charge region within the NiO(Li) at electrode potentials cathodic to 0.8V vs. standard hydrogen electrode (SHE)[88]. In alkaline solutions, however, the ferri-ferrocyanide couple is no longer cathodically inhibited and both the cathodic and anodic branches are essentially diffusion controlled even at high rotation rates [87]. The flat band potential shifts in alkaline solutions from a positive to quite negative value relative to the reversible potential of this couple with the result that the potential changes occur principally across the Helmholtz layer. The reversible potential for the O_2-peroxide couple, however, is more negative and therefore O_2 reduction even in alkaline solutions is still quite inhibited [82]. The oxidation of HO_2^- to O_2 proceeds more readily but is still much less reversible than on carbon or graphite. Similar results have been observed on lithiated polycrystalline NiO produced by high temperature oxidation of nickel metal in air or O_2 [18].

O^{18} techniques have been used to demonstrate that the O_2 liberated during the oxidation of HO_2^- to O_2 at controlled potential on NiO in alkaline solutions originates only from the HO_2^- [82]. Thus the O-O bond does not appear to be broken during the oxidation process, and presumably also during the reverse reduction of O_2 to HO_2^-.

So far in this lecture, we have only considered the reduction of O_2. Nickel oxide is of some interest from the standpoint of the anodic generation of O_2, however, since nickel electrodes are used in water electrolysis in caustic and these electrodes develop anodic oxide layers under such conditions.

O_2 generation has been examined on mosaic NiO(Li) in acid solutions using O^{18} labelling techniques [90]. The dissolution of NiO in concentrated acid solutions is extraordinarily slow and is under pure kinetic control. After correction for lattice $O^=$ entering the solution through dissolution, a substantial fraction of the anodically generated O_2 has been found to originate from lattice oxygen ($\pm$10% at 1.8V vs. SHE). The proposed mechanism is the falling of p-carriers into surface $O^=$ or OH^- traps. The subsequent formation of O_2 is then coupled to the NiO dissolution process and may proceed as follows:

$$\text{Step I:} \quad 2\,O^{2-} + 2p^+ \rightarrow 2O^- \tag{6}$$

$$\text{Step II:} \quad 2\,O^- + 2H^+ \rightarrow 2\,OH \tag{7}$$

$$\text{Step III:} \quad OH + OH \rightarrow H_2O + 1/2\,O_2 \tag{8}$$

$$\text{Step IV:} \quad 2Ni^{2+}_{lattice} \rightarrow 2Ni^{2+}_{aq} \tag{9}$$

$$2NiO + 2H^+ + 2p^+ \rightarrow 2Ni^{2+}_{aq} + H_2O + 1/2\,O_2 \tag{10}$$

Steps I and II may be a single step or separate steps as shown. Step III undoubtedly involves several component steps. The overall process is independent of the steps. The standard free energy change for the overall process relative to the reaction $2H^+ + 2e \rightarrow H_2$ can be calculated from the standard free energies of formation as listed by Pourbaix [91]; NiO, ΔG_f° = -51.3 kcal/mole; Ni^{2+}, ΔG_f° = -11.53 kcal/mole; H_2O, ΔG_f° = -56.5 kcal/mole. The calculated relative standard free energy change for the overall reaction is +23.1 kcal/mole corresponding to a standard electrode potential of +0.5V.

Alternatively the O_2 formation from lattice oxide may involve two p carriers falling into a O^{2-} surface state; i.e.,

$$\text{Step I:} \quad O^{2-} + 2p^+ \rightarrow O \tag{11}$$

$$\text{Step II:} \quad O \rightarrow 1/2\,O_2 \tag{12}$$

$$\text{Step III:} \quad Ni^{2+}_{lattice} \rightarrow Ni^{2+}_{aq} \tag{13}$$

$$NiO_{lattice} + 2p^+ \rightarrow Ni^{2+}_{aq} + 1/2\,O_2 \tag{14}$$

where Steps I and II are multiple step processes. For the overall process, ΔG° = +39.8 kcal/mole and E° = 0.87V.

The potentials for both of these overall reactions 10 and 14 are cathodic to that for the discharge of O_2 from water. Since the activity of Ni^{2+} is far less than the unit value, the equilibrium potentials may be considerably less anodic than the standard values. This may be the explanation for the observation that at potentials even as small as +0.7V vs. SHE anodic currents were observed for NiO (0.26 atom % Li) in 1 N acid solutions. In the absence of such an anodic process a cathodic current is expected to attend the dissolution of the NiO due to the reduction of lattice Ni^{3+} (resulting from the Li doping) to Ni^{2+} [90].

The voltammetry curve for the [100] interface of the mosaic crystals indicates two peaks (fig. 6) in both acid and alkaline solutions, one at 0.95V vs. SHE (Peak I) and a second at 1.4V (Peak II). Both have a pH dependence of -60 mV/decade over the pH range 0-14. At slow sweep rates ($\leq$ 60 mV/sec), the anodic and cathodic sweep peak potentials coincide, indicating reversibility.

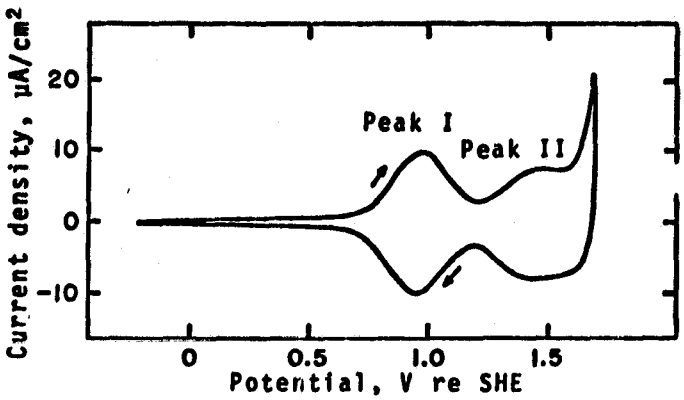

Fig. 6. Linear sweep voltammetry curve at 4.0 V/min for mosiac NiO (0.36 cation % Li) in helium-saturated 1.0 N H_2SO_4 at 25°C. Electrode area: 0.128 cm^2.

Yohe et al. [82] have compared the voltammetry results with the thermodynamic data compiled by Pourbaix [91] and concluded that peaks I and II probably correspond to the oxidation of Ni^{2+} to Ni^{+3} and Ni^{+3} to Ni^{+4}, respectively, coupled with the removal of protons from adjacent oxygen ions. These reactions appear to occur only at the electrode surface since the total charge under both peaks corresponds to less than a monolayer (65%) of the charge for the (100) plane, assuming one electron per Ni^{2+} ion for each peak, and an idealized $(100)_{2+}$ surface orientation with no surface roughness. The difficulty of converting all surface Ni^{2+} ions to a higher valency state is not surprising since complete conversion would probably involve very large surface excess charge. It is even possible that both peaks correspond to the Ni II - Ni III conversion with the marked difference in potential due either to different surface sites with differing charge compensation by surface $O^=$ and OH^- ions or to induced heterogeneity arising from a large increment in the free energy of oxidation for Ni II ions adjacent to an Ni III surface ion.

Another interesting feature is the extraordinarily slow rate of dissolution of the mosaic NiO(Li) in acid electrolytes and the pronounced potential dependence of the solution rate. At room temperatures the dissolution rate in acid solutions (e.g., 6 M H_2SO_4) is typically a few micrograms/cm^2-hr or less, making it possible to make use of this oxide as an electrode over very extended periods of time even in strong acids. To facilitate dissolution rate studies, the dissolution kinetics have been studied in the author's laboratory at temperatures just below the boiling points of the electrolytes. The dissolution rate is entirely under kinetic control [90]. In H_2SO_4 solutions the dissolution rate passes through a maximum as the potential is made increasingly anodic (fig. 7), in accord with the predictions of Engell [92] and Vermilyea [93] when the dissolution is controlled by the transfer of ions across the oxide-electrolyte interface. The maximum should correspond to a shift from control of the dissolution kinetics by the potential energy barrier for cation transfer to control by that for anion transfer across the interface. The theory

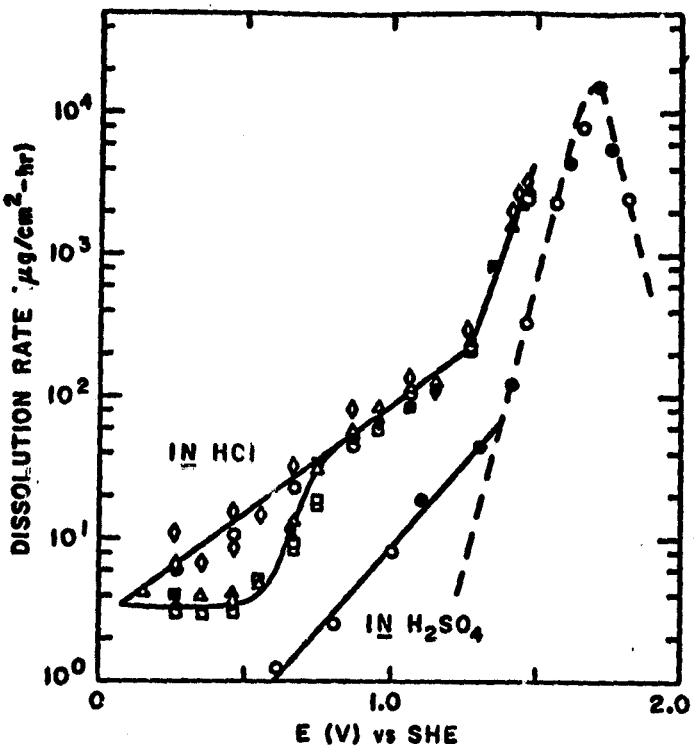

Fig. 7. Dissolution of lithiated nickel oxide in helium-saturated 1 N HCl and 1 N H_2SO_4 solution at 95°C [89]. Symbols corresponding to different group of electrodes:
○● Group 1, $(C_{Li})_{MS}$ = 0.88%; □■△Group 3, $(C_{Li})_{MS}$ = 0.26%;
◇Group 2, $(C_{Li})_{MS}$ = 0.33%; ▲◆Group 4, $(C_{Li})_{MS}$ = 0.12%.
Dashed line: calculated from eq (1) with the following parameters: $\alpha_+ z_+ = 0.62$, $\alpha_- z_- = -0.62$, r_f = 15,000 μg/cm - h, ϕ_f = 1.68 V vs SHE. (Concentrations of Li in cation -%, based on the slopes of the Mott-Schottky plots.)

predicts Tafel linearity on either side of the maximum. It is not possible, however, to identify the specific ionic species being transferred over the potential energy barriers from the observed Tafel slopes, which yield α n (α = transfer coefficient, n = charge of species).

6. O_2 Electrocatalysis on other Oxides

The anodic generation of O_2 has been examined on a number of defect metal oxides, prepared by thermally decomposing a metal salt (usually the chloride) with titanium as the substrate. Potential-current curves obtained by O'Grady and Iwakura in the author's laboratory are shown in figure 8 for a few of these oxides [94]. The current-voltage curves at lower current densities ($<10^{-5}$ A/cm^2) are strongly influenced by the intrinsic changes in valency state of the oxide even though the data were acquired with decreasing current with three minutes at each data point. Since the current densities are apparent values, area differences may have influenced the relative positions of the curves. Of particular importance is the low Tafel slope (~0.04V/decade) for several of the defect oxides (e.g., RuO_x, IrO_x).

The behavior of the corresponding pure metals as O_2 anodes is distinctly different from that of the defect metal oxides in figure 8 even though the metals are oxide coated at the potentials where O_2 generation occurs. Ruthenium metal is not stable as an O_2 anode in 4 M KOH. Active dissolution begins already at ~1.3V vs. RHE.

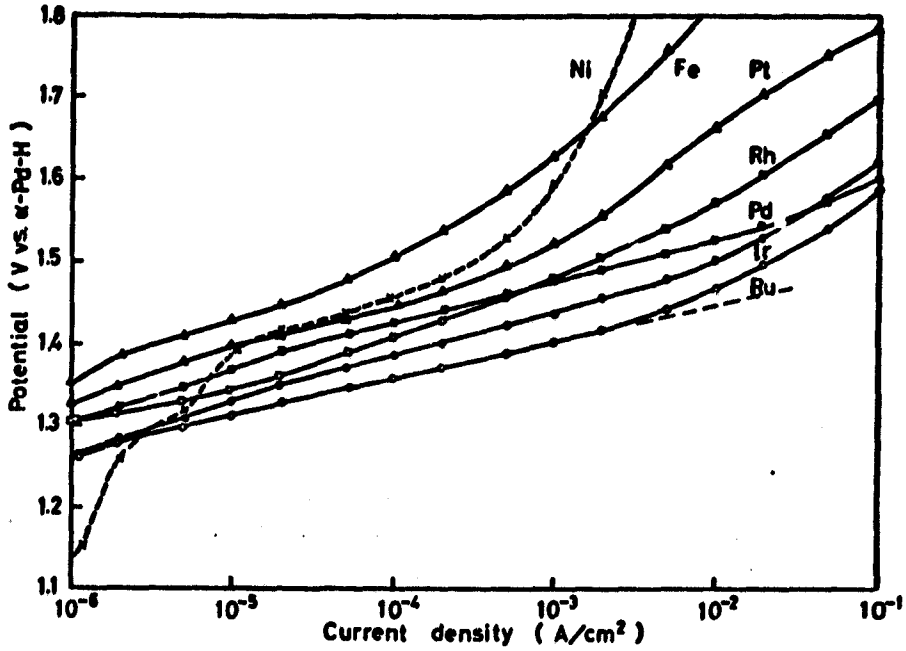

Fig. 8. O_2 generation on various metal oxides. Anodic polarization curves on metal oxides on Ti substrate in O_2-saturated 4 M KOH, obtained with 3 min/point after polarization with increasing current up to 0.1 A/cm² (dashed line represents IR drop corrected curve for RuO_x) [94].

The RuO_x catalyst appears to be similar to that used for the dimensionally stable anodes for Cl_2 generation [97]. This oxide has been investigated in some detail in the author's laboratory [61]. The O_2 generation reaction on RuO_x/Ti is first order in OH^- over the pH range 11 to 14. Unfortunately the stoichiometric number cannot be obtained because of interference from the intrinsic oxidation-reduction reactions of the RuO_2 at low current densities near the reversible potential for the 4-electron reaction.

O'Grady et al. [61] have found[3] that the Tafel slopes are independent of the catalyst loading over the ranges 10^{-8} to 10^{-5} moles Ru/cm² and the apparent exchange current densities are approximately proportional to the catalyst loading over this range. Such a proportion is to be expected since the true-to-apparent area ratio is also approximately proportional to the catalyst loading. The Ti only acts as a substrate and does not have any direct effect on the activity of the RuO_x per unit true area. For RuO_x coverage greater than 10^{-8} moles Ru/cm², ESCA did not indicate any Ti in the RuO_x.

Several of the reaction paths for O_2 generation tabulated by Damjanovic [76] for acid solutions can have Tafel slopes corresponding to $dV/d \ln i = 2RT/3F$ or 0.040 V/decade when modified to a form suitable for alkaline solutions. All have the common feature that the rate controlling step is a second electron rather than first electron transfer. With judicious choice of H_2O vs. OH^- as the reactant in the first and second electron transfer steps or proceeding proton transfer steps, it is possible to have the kinetics also first order in OH^-.

With electrode surfaces involving species with ionic character, O'Grady et al. [61] prefer to write the mechanism in such a way as to indicate the possibility of changes in the effective valency state of the catalyst sites. A simple mechanism compatible with the observed Tafel slope and reaction order is as follows:

[3] The next four paragraphs are quoted from reference 61 with only minor change.

$$\text{Step I:}\quad S^z + OH^- \underset{k_{-a}}{\overset{k_a}{\rightleftharpoons}} (SOH)^z + e^- \text{ (fast)} \tag{15}$$

$$\text{Step II:}\quad (SOH)^z \xrightarrow{k_b} (SOH)^{z+1} + e^- \text{ (slow)} \tag{16}$$

followed by subsequent processes yielding finally O_2 and regenerating the site S^{+z}; for example,

$$\text{Step III:}\quad \begin{matrix} (SOH)^{z+1} & OH^- & S-O\text{-}H\text{--}OH^- & S^z & O & HOH \\ (SOH)^{z+1} & OH^- & S-O\text{-}H\text{--}OH^- & S^z & O & HOH \end{matrix} \tag{17}$$

The sites are probably Ru^{4+} but also could be higher valency state Ru ions. These sites are probably hydrated although the waters of hydration are not shown in the mechanism.

In Step I the site S^z has been proposed by O'Grady et al. to be a Ru ion of the oxide lattice. Step I involves the oxidation of the Ru to a higher valency state with partial transfer of electron charge from the OH species to Ru forming a $(RuOH)^z$ complex. Such a process should require much less energy than the formation of an OH free radical or a rather weakly adsorbed OH radical. Step II involves the further oxidation to $(RuOH)^{z+1}$, possibly followed by the formation of $(RuO)^z$ before proceeding with Step III. The RuO_x electrode surface may have some of the same features as the $Ru(NH_3)_5ORu(NH_3)_4ORu(NH_3)_5^{x7+}$ ion, reported by Earley and Razavi [95, 96] to oxidize OH^- homogeneously to form O_2. These species have the structure Ru-O-Ru-O-Ru^{7+}. Earley and Razavi have pointed out that Ru has a tendency to form species of coordination number 7 and that there are low-lying antibonding π^* orbitals which can accept electron charge from OH^-. Thus the $(RuOH)^z$ intermediate (other species in the inner coordination sphere not shown) seems reasonable."

From the applied standpoint, RuO_x does appear attractive for use as an O_2 anode electrocatalyst. While the exchange currents per unit true area are comparable to Pt in alkaline solutions, the much lower Tafel slope results in significantly lower overpotential at high current densities.

O_2 reduction on RuO_x in alkaline and acid solutions appears to involve a peroxide mechanism [61] although it is possible that "parallel" mechanisms are involved. Pronounced hysteresis and a lack of stability of the oxide have interfered with kinetic studies with the rotating disk technique.

7. Acknowledgment

The experimental data obtained in the author's laboratory and presented herein, have been obtained principally by the following colleagues and students:

Oxygen electrode studies on carbon:	I. Morcos
A.c. impedance measurements on graphite:	J. P. Randin
Redox couples on NiO(Li):	D. Tench, D. Yohe
Dissolution kinetics and O_2 generation on NiO(Li):	C. H. Lee, A. Riga
O_2 electrocatalysis on RuO_x and other defect oxides:	W. O'Grady, C. Iwakura and J. Huang

The author also acknowledges helpful discussions on O_2 electrocatalysis with his colleagues R. K. Sen, W. E. O'Grady and F. Urbach.

This work has been partially supported through grants from the U.S. Office of Naval Research and NASA-Ames.

References

[1] See e.g. McGinnety, J.A., in MTP International Reviews of Science, Inorganic Chemistry Series I, Vol. 5, D. Sharp, ed., Butterworths, London, 1972, p. 229.

[2] Griffiths, J.S., Proc. Roy. Soc. (A) 235, 23 (1956).

[3] Vaska, L., Science 140, 809 (1963).

[4] McGinnety, J., Doedens, R. and Ibers, J., J. Amer. Chem. Soc. 88, 3511 (1966).

[5] e.g., Collman, J., Kubola, M. and Hosking, J., ibid. 89, 4809 (1967).

[6] McGinnety, J., Payne, N. and Ibers, J., ibid. 91, 6301 (1969).

[7] Behret, H., Binder, H. and Sandstede, G., in Proc. of the Symposium on Electrocatalysis, M. Breiter, ed., The Electrochemical Society, Princeton, N.J. 1974, pp. 319-338.

[8] Behret, H., Binder, H. and Sandstede, G., Electrochim. Acta 20, 111 (1975).

[9] Tseung, A, Hobbs, B. and Tantram, A., ibid. 15, 473 (1970).

[10] Pauling, L., Nature 203, 182 (1964).

[11] See e.g., Hoffman, B., Diemente, D. and Basolo, F., J. Amer. Chem. Soc. 92, 61 (1970).

[12] Weiss, J.J., Nature 203, 183 (1964).

[13] Wittenberg, J., Wittenberg, B., Persach, J. and Blumberg, W., Proc. Nat. Acad. Sci. 67, 1846 (1970).

[14] Ochiai, E.I., J. Inorg. Chem. 36, 2129 (1974).

[15] Beck, F. Dammert, W., Heiss, J., Hiller, H. and Polster, R., Z. Naturforsh, 28A, 1009 (1973).

[16] Beck, F., Ber. Bunsenges. physik. Chem. 77, 353 (1973).

[17] Yeager, E., Krouse, P. and Rao, K., Electrochim. Acta 9, 1057 (1964).

[18] Yeager, E. and Kozawa, A., Kinetic Factors in Fuel Cell Systems: The Oxygen Electrode, Proc. 6th AGARD Meeting, Cannes, 1964, Pergamon Press, Oxford, 1965, pp. 769-793.

[19] See e.g., Maricle, D.L. and Hodgson, W.G., Anal. Chem. 37, 1562 (1965).

[20] Sawyer, D.T. and Roberts, J.C., J. Electroanal. Chem. 12, 90 (1966). Goolsby, A.D. and Sawyer, D.T., Anal. Chem. 40, 83 (1968).

[21] Peover, M.E. and White, B.S., Electrochim. Acta 11, 1061 (1966).

[22] Nekrasov, L.N., Pukhanova, L., Dubrovina, N. and Vykhodtseva, L., Elektrokhim. 6, 388 (1970).

[23] Appleby, J., Molten Carbonate Fuel Cells in Conference Proceedings, Fuel Cell Catalysis Workshop, Electric Power Research Institute, Palo Alto, California, EPRI SR-13, Special Report, August 1975, pp. 153-6.

[24] Kastening, B. and Kazemifard, G., Ber. Bunsenges. physik. Chem. 74, 551 (1970).

[25] Divisek, J. and Kastening, B., J. Electroanal. Chem. 65, 603 (1975).

[26] Dubrovina, N.I. and Nekrasov, L.N., Elektrokhim. 8, 1503 (1972).

[27] Brezina, M. and Hofanova-Matejkova, A., J. Electroanal. Chem. 44, 460 (1973).

[28] Morcos, I. and Yeager, E., Electrochim. Acta 15, 953 (1970).

[29] Yeager, E., Oxygen Electrode Kinetics on Various Electrode Surfaces, in Conference Proceedings, Fuel Cell Catalyses Workshop, loc. cit., pp. 49-59.

[30] Ochiai, E.I., Inorg. Nucl. Chem. Letters 10, 453 (1974).

[31] Traylor, T.G. and Chang, C.K., J. Amer. Chem. Soc. 95, 5810 (1973).

[32] Stynes, H.C. and Ibers, J.A., ibid. 94, 5125 (1972).

[33] Brimgar, W., Chang, C., Gerbel, J. and Traylor, T., ibid. 96, 5597 (1974).

[34] Collman, J., Gagne, R., Halbert, T., Marchon, J. and Reid, C., ibid. 95, 7868 (1973).

[35] Valentine, J.S., Chem. Revs. 73, 235 (1973).

[36] Bennett, M.J. and Donaldson, P.B., J. Amer. Chem. Soc. 93, 3307 (1971).

[37] Schaefer, W.P., Inorg. Chem. 7, 725 (1968).

[38] Behar, D., Czapski, G., Rabani, J., Dorfman, L. and Schwarz, E., J. Phys. Chem. 74, 3209 (1970).

[39] Damjanovic, A., Genshaw, M. and Bockris, J., J. Chem. Phys. 45, 4057 (1966).

[40] Damjanovic, A., Genshaw, M. and Bockris, J., J. Electrochem. Soc. 114, 1107 (1967).

[41] Yeager, E., The Sodium Amalgam-Oxygen Continuous Feed Cell, in Fuel Cells, Chapter 7, W. Mitchel, ed., Academic Press, New York City, 1963.

[42] Jahnke, H.F., Schönborn and Zimmerman, G., in Proc. of the Symposium in Electrocatalyses, M. Breiter, ed., The Electrochemical Soc., Princeton, N.J., 1974, pp. 303-319.

[43] Jahnke, H.F., Schönborn and Zimmerman, G., "Organic Dyestuffs as Catalysts for Fuel Cells" in Topics of Current Chemistry, Springer-Verlag, Heidelberg, Germany, 1975.

[44] Jasinski, R., J. Electrochem. Soc. 112, 526 (1965).

[45] Jahnke, H., Ber. Bunsenges. physik. Chem. 72, 1053 (1968).

[46] Heller, H., Polster, R., Beck, F. and Guthke, H., German Patent P 2046-345-1, Sept. 9, 1970.

[47] Savy, M., Bernard, C. and Magner, G., Electrochim. Acta 20, 383 (1975).
[48] Kozawa, A., Zilionis, V.E., Brodd, R. and Powers, R.A., J. Electrochem. Soc. 113, 1470, 1974 (1970).
[49] Kozawa, A., Zilionis, V.E. and Brodd, R.J., ibid. 118, 1705 (1971).
[50] Alt, H., Binder, H. and Sandstede, G., J. Cataly. 28, 8 (1973).
[51] Behret, H., Binder, H. and Sandstede, G., Electrochem. Acta 20, 111 (1975).
[52] Marko, A. and Kordesch, K., U.S. Patent 2,615,932 (1952).
[53] Clark, M., Darland, W. and Kordesch, K., "Carbon Fuel Fell Electrodes", Proc. Annual Power Sources Conference, 18th, Atlantic City, N.J., 1964, pp. 11-14.
[54] Savy, M., Electrochim. Acta 13, 1359 (1968).
[55] King, W. and Tseung, A., ibid. 19, 485 (1974).
[56] Tseung, A. and Bevan, H., J. Electroanal. Chem. 45, 429 (1973).
[57] McHardy, J. and Stonehart, P., in MTP International Reviews of Science, A. Buckingham and J. Bockris, eds., Series Z, Vol. 6, Butterworth, London, 1974.
[58] McHardy, J. and Bockris, J. Electrochem. Soc. 120, 53, 51 (1973).
[59] Randin, J.P., ibid. 120, 373 (1973); 121, 1209 (1974). Electrochim. Acta 19, 87 (1974).
[60] Fischman, J., Henry, J. and Tessore, S., ibid. 14, 1324 (1966).
[61] O'Grady, W.E., Iwakura, C., Huang, J. and Yeager, E., in Proc. of the Symposium on Electrocatalysis, loc. cit., pp. 286-302.
[62] Grevstad, P.E., Final Report, "Development of Advanced Fuel Cell Systems", Pratt and Whitney Aircraft Co., NASA Contract NAS3015339, Nov. 1972.
[63] Zurilla, R. and Yeager, E., "Oxygen Electrode Kinetics on Gold", Technical Report No. 23, Case Western Reserve University, ONR Contract N 0014-67-c-0389, May, 1969.
[64] "New Trends in Catalysis", Part II, Report Pennsylvania Research Associates, Inc., Philadelphia, Pa., NASA Contract NAS7-574, Annl. 1968; "The Role of Metal in Electrochemistry", ibid. Sept. 1970.
[65] Appleby, A.J., J. Electrochem. Soc. 117, 328 (1970).
[66] Vogel, W. and Lundquist, J., ibid. 117, 1512 (1970).
[67] Vogel, W., Lundquist, J. and Bradford, A., Electrochim. Acta 17, 1735 (1972).
[68] Kordesch, K. and Scarr, R., "Low Cost Oxygen Electrodes", Final Report, Union Carbide Corp., Consumers Products Division, Cleveland, Ohio, U.S. Army Contract DAADOZ-71-C-0297, July, 1973.
[69] Yeager, E., IVA Meddelande (Sweden) 134, 89 (1963).
[70] Davies, M., Clark, M., Yeager, E. and Hovorka, F., J. Electrochem. Soc. 106, 56 (1959).
[71] Singer, L. and Spry, W., Bull. Amer. Phys. Soc. 1, 214 (1956).
[72] Randin, J.P. and Yeager, E., J. Electroanal. Chem. 36 257 (1972); J. Electrochem. Soc. 118, 711 (1971).
[73] Randin, J.P. and Yeager, E., J. Electroanal. Chem. 58, 313 (1975).
[74] Klein, C.A., J. Appl. Phys. 33, 3338 (1962). Rev. Mod. Phys. 34, 72 (1962).
[75] Bockris, J. O'M. and Srinivasan, S., Fuel Cells: Their Electrochemistry, McGraw-Hill Book Co., New York City, 1969, pp. 412-468.
[76] Damjanovic, A., in Modern Aspects of Electrochemistry, J. Bockris and B. Conway, eds., Vol. 5, Plenum Press, New York City, 1969.
[77] Appleby, A.J. in Modern Aspects of Electrochemistry, loc. cit., Vol. 9, chapter 5, 1974.
[78] Hoare, J.P., Electrochemistry of Oxygen, Interscience, New York City, 1968.
[79] See e.g., Snoeyink, V.L. and Weber, W.J., in Progress in Surface and Membrane Science, J. Danielli, M. Rosenberg and D. Cadenhead, eds., Academic Press, New York, 1972, pp. 63-120.
[80] Panzer, R.E. and Elving, P.J., Electrochim. Acta 20, 635 (1975).
[81] Garten, V.A. and Weiss, D.E., Rev. Pure Appl. Chem. 7, 69 (1957). See also Garten, V.A. and Eppinger, K., Aust. J. Chem. 12, 394 (1959).
[82] Yoke, D., Riga, A., Greef, R. and Yeager, E., Electrochim. Acta 13, 1351 (1968).
[83] Stonehart, P., Kinoshita, K. and Bett, J.A.S., in Proc. of Symposium on Electrocatalysis, loc. cit. pp. 275-285.
[84] Bett, J.A.S., Lundquist, J.T., Washington, E. and Stonehart, P., Electrochim. Acta, 18, 343 (1973).
[85] Blurton, K.F., Greenberg, P., Oswin, H.G. and Rutt, D.R., J. Electrochem. Soc. 119, 559 (1972).
[86] Voinov, M., Buhler and Tannenberger. H., in Proc. of Symposium on Electrocatalysis, loc. cit., pp. 268-274.

[87] Tench, D.M. and Yeager, E., J. Electrochem. Soc. 121, 318 (1974).
[88] Tench, D.M. and Yeager, E., ibid. 120, 164 (1973).
[89] Cech, R. and Alessandrini, E., Amer. Soc. Met. Trans. Quart. 51, 150 (1959).
[90] Lee, C.H., Riga, A. and Yeager, E., The Dissolution Kinetics of Lithiated NiO in Aqueous Acid Solutions, in Mass Transport Phenomena in Ceramics, A.R. Cooper, and A.H. Heuer, eds., Plenum Publishing Co., New York City, 1975, pp. 489-499.
[91] Pourbaix, M., "Atlas of Electrochemical Equilibria in Aqueous Solutions", Pergamon Press, Oxford, 1966 (English translation by J.A. Franklin).
[92] Engell, H.J., Z. Physik. Chem. N.F. 7, 158 (1956).
[93] Vermilyea, D.A., J. Electrochem. Soc. 113, 106 (1966).
[94] O'Grady, W., Iwakura, C., Huang, J. and Yeager, E., unpublished data.
[95] Earley, J. and Rajavi, H., Inorg. Nucl. Chem. Letters 9, 331 (1973).
[96] Earley, J. and Fealey, T., Inorg. Chem. 12, 323 (1973).
[97] e.g., South African Pat. 68/7371, 68/7482 (1968). German Pat. 2021422 (1969) 2014746, 1915951 (1970). British Pat. 1206863 (1970).

76-ENAS-37

an ASME publication

Oxygen Electrocatalysts for Life Support Systems

W. E. O'GRADY

C. IWAKURA'

E. YEAGER

The Electrochemistry Lab.,
Chemistry Dept.,
Case Western Reserve Univ.,
Cleveland, Ohio

The irreversibility of the oxygen electrode increases by 30 to 60 percent the energy required for water electrolysis over the thermodynamic value in life support systems involving conventional water electrolysis cells. To minimize this voltage loss, high area electrocatalysts, such as platinum metal, are often used for the O_2 anode, but even so, the losses are still very substantial. In an attempt to find more effective electrocatalysts for this application, a number of defect metal oxides have been examined.

'Present address: Department of Applied Chemistry, Faculty of Engineering, Osaka University, Suita, Osaka, Japan.

Contributed by the Aerospace Division of The American Society of Mechanical Engineers for presentation at the Intersociety Conference on Environmental Systems, San Diego, Calif., July 12-15, 1976. Manuscript received at ASME Headquarters April 6, 1976.

Copies will be available until April 1, 1977.

E AMERICAN SOCIETY OF MECHANICAL ENGINEERS, UNITED ENGINEERING CENTER, 345 EAST 47th STREET, NEW YORK, N.Y. 10017

Oxygen Electrocatalysts for Life Support Systems

W. E. O'GRADY C. IWAKURA E. YEAGER

INTRODUCTORY BACKGROUND

In water electrolyzers, ohmic losses and electrode polarization result in substantial loss of efficiency in the use of electrical energy to produce O_2 and H_2. Even in modern water electrolyzers operating below 200 C, the cell terminal voltages at reasonable current densities (> 100 mA/cm^2) usually exceed the reversible (thermodynamic) values[2] by 25 to 50 percent. To achieve acceptable operating efficiencies, it is necessary to restrict the current densities to relatively low values with corresponding increments in the weight, volume, and cost of the electrolyzer.

Some voltage losses, however, are usually desirable within water electrolyzers. The entropy change, ΔS, for the production of H_2 and O_2 from water is negative, and, hence, the electrolysis of water under reversible conditions is endothermic. The ohmic and electrode polarization losses can provide this $T\Delta S$ heat as well as the additional heat to offset heat losses to the surroundings with cells operating above ambient temperatures.

For a water electrolysis cell operating at a cell terminal voltage of E, the heat generated within the cell per mole of O_2 produced is

$$Q = 4F(E - E_{rev}) + T\Delta S = 4FE + \Delta H \qquad (1)$$

where F is the Faraday, E_{rev} is the reversible cell potential, and ΔH and ΔS are the enthalpy and entropy changes for the reaction

$$H_2O(l) \qquad 2H_2 + O_2 \qquad (2)$$

The thermoneutral potential, E_{TN}, is defined as the value of E in equation (1) such that Q = 0. Therefore,

$$E_{TN} = -\Delta H/(4F) \qquad (3)$$

The heat loss from the cell can be reduced to a value low compared to ΔH, and, therefore, the thermoneutral potential represents a reasonable target voltage in reducing various types of voltage losses. For water electrolyses cells with pure liquid water at 25 C fed into the cell and H_2 and O_2 exiting at this same temperature after passing through suitable heat exchangers, the thermoneutral potential is 1.48 v; for 100 C the value is 1.45 v.

While several of the advanced electrolyzer represented in Fig. 1 have cell voltages close t to the thermoneutral potential at low current densities, all exceed this value by appreciable

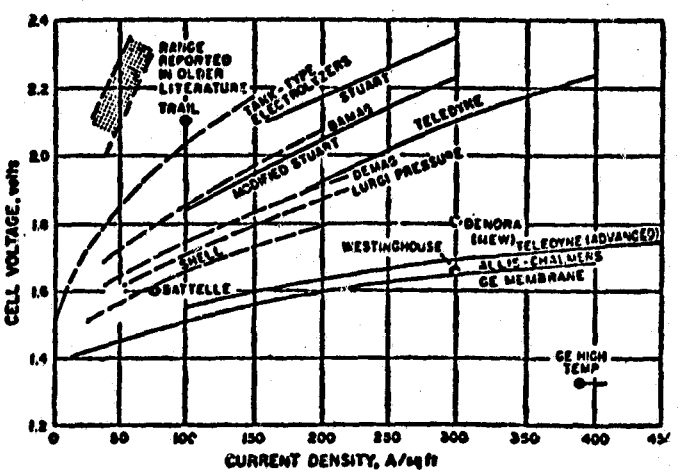

Fig. 1 Cell-operating performances of various advanced electrolyzers (1)

[2] The reversible cell voltage for water electrolysis depends on the electrolyte, pressure, and temperature. For cells for which the mole-fraction of water is >0.9 and the O_2 and H_2 pressures are each ~1 atm, the reversible voltage is 1.23 v at 25 C and 1.17 v at 100 C. For a pressurized electrolyzer with 50 percent (by weight) KOH and O_2 and H_2 pressures of 15 atm, the reversible voltage is 1.03 v at 264 C (2).[3]

[3] Underlined numbers in parentheses designate References at end of paper.

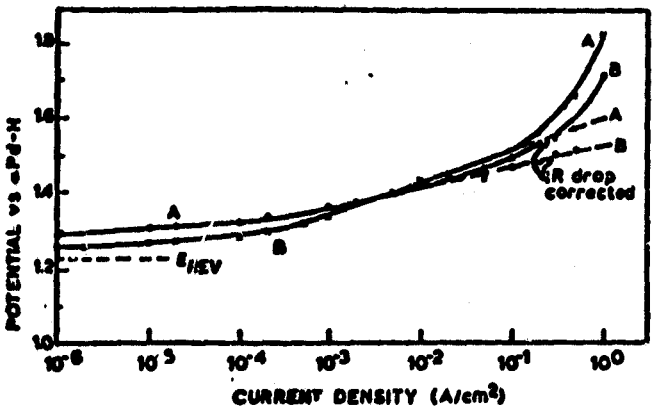

Fig. 2 Anodic polarization curves obtained galvanostatically with decreasing current density (3 min./point) in 4M KOH at 22 C. Curve A. high area Pt. Curve B. RuO_x coated Ti electrode (Ru loading 10^{-5} moles/cm^2). Dashed lines IR drop corrected

amounts at the higher current densities which are attractive in most instances for compact electrolyzers. Thus, even considering the thermoneutral potential, it is attractive to find ways for further reducing voltage losses at high current densities.

PRESENT STATUS OF O_2 ELECTROCATALYSTS FOR WATER ELECTROLYZERS

In most water electrolyzers, polarization at the O_2 anode is the largest source of voltage loss. This polarization arises because of the irreversibility of the electrochemical reactions involved in the formation of O_2 from oxygen of water. Three approaches are available for reducing the electrode polarization at high current densities: (a) electrode surfaces with high intrinsic electrocatalytic activity for the O_2 generation reaction; (b) ultra-high area electrocatalysts; and (c) operation at elevated temperatures. All three approaches have been applied. Nickel has been most extensively used as the O_2 anode surface in water electrolyzers using concentrated NaOH or KOH as the electrolyte. Under operating conditions, a high area oxide film forms on the anode. The overpotentials at reasonable current densities,[4] however, are still high [e.g., 0.4 v at 100 mA/cm^2 at 80 C (2)] unless the cells are operated at temperatures above 175 C. This requires pressurization and furthermore can lead to electrode stability problems.

[4] All current densities are per unit apparent area unless otherwise indicated.

For life support systems for space, high area platinum is presently used for the anode electrocatalyst. This surface has relatively high overpotential at moderate current densities even at normal temperatures (0.3 v at 100 mA/cm^2 at 22 C — see Fig. 2), but the overpotential is still higher than desired and platinum cost can be a problem for some water electrolyzer applications.

CRITERIA FOR O_2 CATALYSIS FOR WATER ELECTROLYZERS

The present research represents an effort to find O_2 anode catalysts superior to high area Pt. In evaluating catalysts, four criteria must be considered:

Electrocatalytic Activity

Over a significant range of current densities, most electrode processes, including the oxygen electrode, follow the Tafel equation; i.e.

$$\eta = E - E_{rev} = B(\log i - \log i_o) \qquad (4)$$

where η is the overpotential, i is the apparent current density, and B is a temperature-dependent constant. The exchange current density, i_o, is usually used as a criteria of catalyst activity. Since i is many orders of magnitude greater than i_o for all presently known O_2 electrocatalysts, it is also important that the slope constant, B, be as low as possible. For the high area Pt electrode represented in Fig. 2, i_o is $\sim 2 \times 10^{-5}$ A/cm^2 while the Tafel slope B is $\sim$0.10 v/decade.

Electronic Conductivity

It is necessary that the catalyst phase have reasonable electronic conductivity. With Pt electrodes, the catalyst phase is an oxide layer of several monolayers formed *in situ*. Present indications (3) are that electron transfer through this film occurs by tunneling and is sufficiently slow to contribute substantially to the oxygen overpotential. With catalyst layers or particles of the order of 10^{-4} cm, the resistivity must be less than 10^3 ohm-cm.

Stability

This requires that the catalyst have very low solubility in the electrolyte, not undergo undesirable changes in valency state, and not be very susceptible to trace poisons. High area catalysts are usually involved, and these must not undergo sintering or Oswald ripening under the cell operating conditions.

Catalyst Cost

For most life-support applications, the catalyst cost is likely to be a secondary consideration provided the catalyst cost does not exceed some reasonable value such as $1.00 per watt of power consumed. Even heavily loaded Pt electrodes are still well below this figure at reasonable current densities. The situation is quite different for commercial water electrolyzers, for which catalyst costs in excess of $0.05 per watt are probably prohibitive.

The present knowledge of O_2 anodic electrocatalysis does not provide a strong basis for deciding which catalyst systems are best candidates for screening. Despite extensive studies of O_2 generation mostly on Pt, the reaction mechanism is still not well established. The O_2 anode is sufficiently irreversible that the back reaction is negligible even at low current densities. This has made it difficult to establish the mechanism for O_2 generation, since only steps up to the rate-controlling one (usually the first electron transfer) can be examined. Measurements near the reversible potentials are impractical because of competing reactions intrinsic to the electrode surface and impurity currents. The extensive kinetic studies of O_2 reduction have not proved very helpful in understanding the anodic process because the reduction occurs at appreciable rates only at potentials very cathodic (by at least 0.5 v) to those for O_2 generation. The surface conditions prevailing at these potentials are not the same, and, therefore, the kinetics and even the pathways can be expected to be different for the anodic and cathodic processes. To complicate the situation further, a large number of pathways are possible for O_2 generation and reduction.

O_2 ELECTROCATALYSIS ON DEFECT METAL OXIDES

Transition metal oxides head the list of promising oxygen anode catalysts since the transition metal ions are expected to interact with various intermediates in the O_2 anodic reaction and many have good electronic conductivity and good stability, particularly in alkaline electrolytes. Rather than forming these oxides anodically *in situ* on the metal electrodes, the oxides have been formed *ex situ* in the present study by thermal decomposition of transition metal salts on a suitable substrate, such as titanium. Oxides so formed have a highly defective structure and high internal pore surface area. Several such oxides have been found to be attractive.

Potential current curves are shown in Fig. 3 for several transition metal oxides on a Ti support electrode. The curves at lower current densities ($< 10^{-5}$ A/cm^2) are strongly influenced by intrinsic changes in valency state of the oxide even though the data were acquired with decreasing current with 3 min. at each data point. Since the current densities are apparent values, area differences may have influenced the relative positions of the curves.

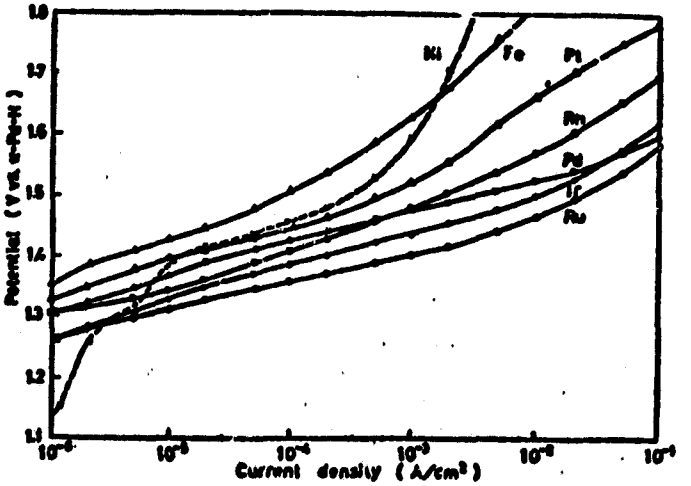

Fig. 3 Polarization curves of various metal oxides on Ti substrate electrodes in O_2-saturated 4M KOH obtained by pseudo-steady-state galvanostatic method (3 min./point). Measured after polarized with increasing current up to 10^{-1} A/cm^2. T = 22 C

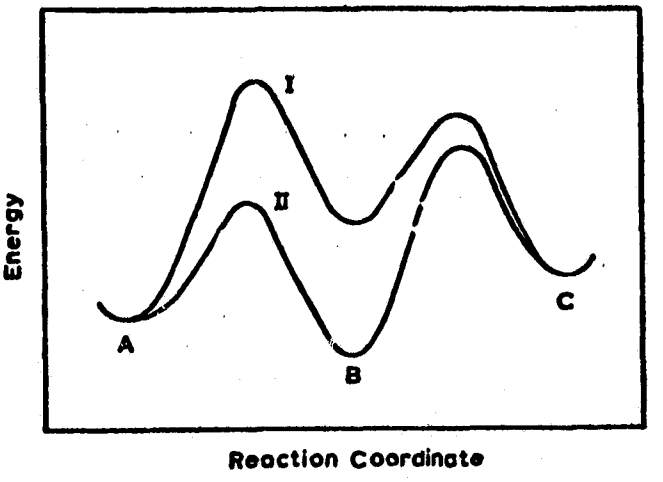

Fig. 4 Effect of stability of adsorbed state B on the energy barriers for the process A→B→C. For the O_2 anode, see equations (11) and (12) for possible intermediates.

Kinetic studies of O_2 generation have usually indicated the first electron transfer step to be rate controlling. If the stability of an adsorbed intermediate (e.g., the OH radical)

formed in this step can be increased, then the rate control may shift to a later step, such as the second electron transfer.[5] With O_2 generation on Pt, the situation appears to correspond to Curve I in Fig. 4. With defect oxides such as ruthenium and iridium oxides, the situation appears to correspond to Curve II. The principal evidence for such is the Tafel slope of 0.04 to 0.05 v/decade exhibited by these oxides in alkaline solutions, as compared with 0.1 to 0.24 v/decade found with Pt.

The behavior of the corresponding pure metals as O_2 anodes is distinctly different from that of the defect metal oxides in Fig. 3 even though the metals are oxide coated at the potentials where O_2 generation occurs. Ruthenium metal is not stable as an O_2 anode in 4 M KOH; active dissolution begins at ~1.3 v versus RHE.

RUTHENIUM OXIDE AS AN O_2 ANODE CATALYST

Of special interest is ruthenium oxide, produced by the thermal decomposition of ruthenium salts on a titanium support. This catalyst combines high electronic conductivity with low oxygen overpotential at high current densities even at room temperature (4). Further it has good stability in high area form in caustic solutions. The exchange current density is comparable to that of platinum, but the Tafel slope is considerably lower (0.04 v per decade of current density) than with platinum (Fig. 2), resulting in lower overpotentials at practical current densities.

Experimental

Oxygen generation on defective RuO_x has been studied in some detail (4). The preparation of this oxide involves the thermal decomposition of $RuCl_3$ on an appropriate metal substrate in a manner similar to that described in the patent literature (5) for the dimensionally stable anodes (DSA) used in the chloralkali industry. Titanium metal was used for the substrate (99.95 percent Ti supplied by Research Organic-Inorganic). After polishing the Ti with emery and thorough cleaning, including degreasing by refluxing in isoproponal vapor, the surface was coated with a solution of reagent grade $RuCl_3$ (Fisher) in 20 percent HCl.

In order to vary the catalyst loading on the electrode surface while maintaining an essentially constant preparative procedure, varying amounts of the original solution (0.1M Ru) were diluted to the same volume, and this solution then applied to the substrate in six repetitive coatings or alternatively the number of coatings varied. After each coating, the solution was dried at a moderate temperature (110 C in a drying oven for 5 min.) and then placed in a preheated furnace at 350 C for 10 min. After the final coating, the temperature of the furnace was raised to 450 C for 1 hr. The catalyst loadings examined in the present work ranged from 10^{-9} to 10^{-5} moles of Ru per cm^2. Other substrate materials have also been examined; namely gold, tantalum, platinum, and nickel. The substrate has no direct effect on the electrocatalytic activity, expressed per unit true area of the RuO_x for catalyst loadings of 10^{-7} to 10^{-5} moles of RuO_x per cm^2 of geometric area. Titanium is preferred to Au, Ta, Pt, or Ni as a substrate because the RuO_x forms a more uniform and adherent layer on Ti.

The majority of the measurements have been carried out with 4M KOH prepared from reagent grade KOH (Baker, 0.2 percent carbonate) and triply distilled water (second stage from alkaline permanganate). For the pH dependence studies, different ratios of 1M KOH and 0.5M K_2SO_4 were used. For the rotating disk experiments, the solutions were pre-electrolyzed in a separate Teflon cell between bright nickel electrodes (7 cm^2 each) at a current density of 1 ma/cm^2 for a minimum of 24 hr with agitation obtained using purified helium gas (6).

O_2 reduction as well as generation were studied on the RuO_x/Ti electrodes using the rotating disk electrode technique. The rotating disk experiments were carried out in an all-Teflon cell (7) consisting of a main compartment containing the working electrode and two separate compartments for the reference and counter electrodes, both of which were Pd-H in the form of Pd diaphragms supplied with H_2 from the back side. The reference compartment was connected to the main working electrode compartment by a Teflon Luggin capillary positioned at 4 mm from the rotating disk electrode surface on the axis of rotation. The electrolyte in the main compartment was usually saturated with purified O_2 gas (6).

A Werking potentiostat, a linear sweep generator, and Houston x-y recorder were used to carry out the electrochemical measurements. The essentially steady-state polarization data were obtained with very slow voltage sweeps (1 mv/sec) and in some instances also with point by point measurements (e.g., 3 min. per point) as a check. The IR drop corrections, needed at higher current

---

5 A specific mechanism is proposed later in the discussion of the results for RuO_x.

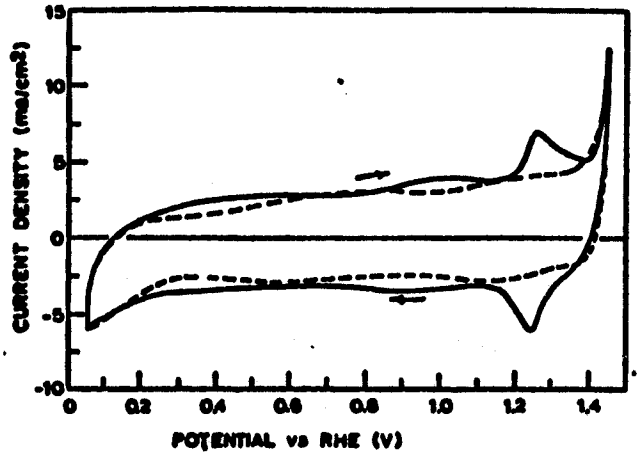

Fig. 5 Cyclic voltammogram for RuO_x on Ti substrate in N_2 saturated 4 M KOH (solid curve) and 2 M $HClO_4$ (dashed curve). Sweep rate: 50 mv/sec; catalyst loading: 1×10^{-5} moles Ru/cm^2; temperature ~ 22 C

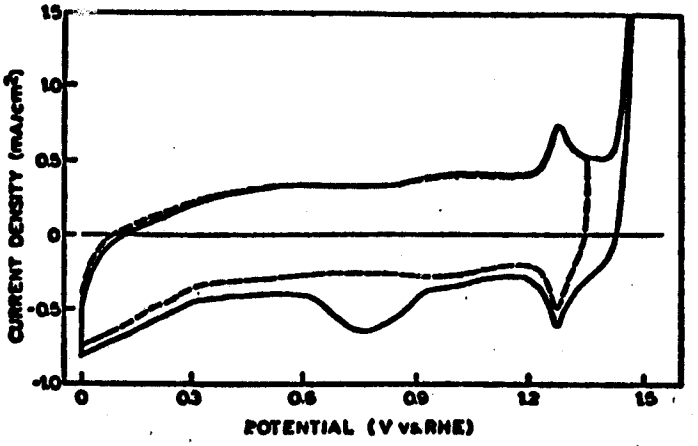

Fig. 6 Effect of anodic sweep limit on the cyclic voltammograms of Ru oxide on Ti electrode in 4M KOH (N_2 saturated). Sweep rate: 10 mv/sec; temperature: ~22 C

densities, were determined using the current interrupter technique with a high pressure hydrogen, mercury-wetted relay to interrupt the current.

Results

Electrochemical Area. The Zn^{2+} ion adsorption technique, developed by Kozawa (8) has been used to obtain an estimate of the ratio of true-to-apparent area for the RuO_x on Ti electrodes. This method is preferred to the usual BET measurements, since pores that may not necessarily be electrochemically accessible may contribute to the BET areas.

The Zn^{2+} adsorption method is based on the concept that the Zn^{2+} will ion exchange with H^+ bound to surface O^-, releasing H^+ into the solution. The assumption is made that the surface coverage with Zn^{2+} is near or at saturation and that the area per Zn^{2+} has a specific value. Kozawa has demonstrated the validity of the method for battery oxides such as MnO_2 with the Zn^{2+} adsorption measured by the decrease in Zn^{2+} concentration in a $ZnCl_2$-NH_4Cl solution and the area taken to be 17 $\mathring{A}^2$ per adsorbed Zn^{2+}.

In the present study, the Zn^{2+} ion adsorption was measured on the RuO_x coated flat titanium electrodes by placing them in a 0.5M NH_4Cl solution containing 0.005M Zn^{+2} at a pH of 7.25. Overnight was allowed for equilibrium and an alloquote of the solution then titrated with EDTA using Erichrome Black T as the indicator.

Using an area of 20 $\mathring{A}/Zn^{2+}$, this method yields a ratio of true-to-apparent surface area of typically 60 to 80 for a catalyst loading of 1×10^{-5} moles Ru/cm^2 of geometric area. Studies of the adsorption isotherms for Zn^{2+} on dispersed RuO_x (without potential control) indicate that the Zn^{2+} adsorption is not at saturation under the aforementioned conditions (9). Therefore, the true-to-apparent surface area ratio measured by the Zn^{2+} adsorption method can only be viewed as lower limiting values.

Using krypton BET, Kuhn and Mortimer (10) found a ratio of 240 for their RuO_x on Ti electrodes. While the technique used to prepare their electrodes is similar to that in the present work, their catalyst loading is not specified. Since more concentrated Ru solutions (0.4M) were used by Kuhn and Mortimer for coating their electrodes, the thickness of the RuO_x coatings on their electrodes may well have been several fold greater.

Voltammetry Curves for RuO_x. Typical slow sweep voltammetry curves are shown in Fig. 5 in N_2-saturated alkaline and acid solutions. Some minor features of the curves in the voltage range 0.6 to 1.0 v are associated with the O_2/H_2O_2 couple. The peak at ~1.3 v in the alkaline solution is only slightly irreversible at the sweep rate of 50 mv/sec. At slower sweep rates (e.g., 10 mv/sec), this peak is essentially reversible with the anodic and cathodic peak potentials coinciding.

This peak, however, has not been observed for RuO_x on nickel or platinum or for the uncoated titanium. Thus, the peak appears to involve the interaction of the RuO_x with the Ti substrate or TiO_y. This peak is much suppressed or almost absent for mixed oxide layers of Ru + Ti as well as Ru + Ir and Ru + Pt, produced by thermal decompo-

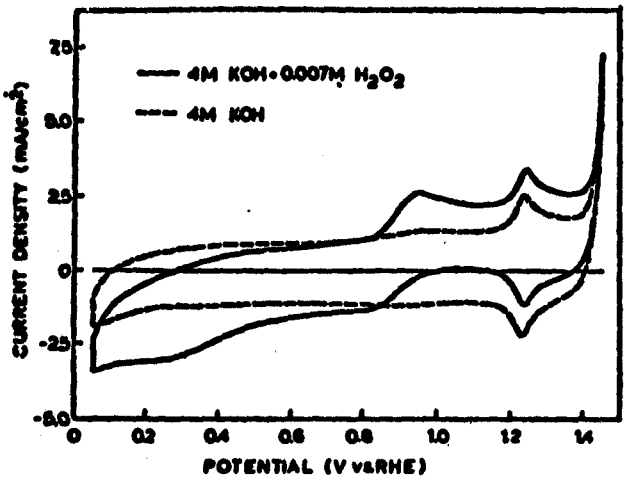

Fig. 7 Effect of hydrogen peroxide on the cyclic voltammograms of Ru oxide on Ti electrode in 4M KOH (N_2 saturated). Sweep rate: 50 mv/sec; temperature: ~22 C

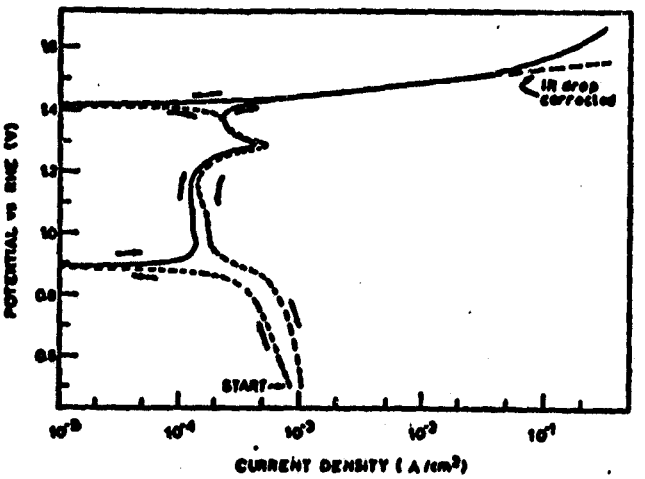

Fig. 8 Current-potential data for RuO_x on Ti. Data obtained with sweep rate of 2mv/sec with rotating disk technique. Electrolyte: 4M KOH (O_2 saturated); catalyst loading: ~1 x 10^{-5}M Ru/cm² (apparent area); rotation rate: 8800 rpm; temp.: ~22 C. Solid curve: anodic current; dashed curve: cathodic current

sition on a Ti substrate.

On the basis of the voltammetry curves, the RuO_x can be reduced and reoxidized over a substantial range of potentials in both acid and alkaline solution. The oxidation and reduction products appear to involve a single phase in view of having the voltammetry current density high over the wide potential range of the sweep rather than having the charge associated with a single voltammetry peak, even at very low sweep rates. The total charge associated with the area under the voltammetry curves in the cathodic or anodic sweeps between 0.1 and 1.4 v is approximately 0.1 C/cm² of apparent area for the electrodes with 1 x 10^{-5} moles Ru/cm², or approximately one-tenth of that required to change the valency state by one electron per Ru atom in the oxide coating.

Kozawa (11) has reported that porous bulk hydrated RuO_2 can be reduced rather reversibly over an extended voltage range when mixed with carbon in both alkaline and acid solutions. The initial open-circuit voltage observed by Kozawa starting with near stoichiometric RuO_2 was + 0.5 v and + 0.8 v versus RHE for the anhydrous and hydrated materials, respectively. Even considering the question of the reversibility of these potential measurements, it appears likely that the O_2 evolution reaction on RuO_x on Ti occurs in a potential range where at least the surface Ru ions of the catalyst are in a higher valency state than + 4.

A large cathodic peak was observed in the voltammetry curves for the RuO_x on Ti electrodes in N_2 saturated KOH solutions in the potential range 0.6 to 0.9 v when the anodic limit of the sweep was extended beyond 1.4 v (Fig. 6). Saturation of the solution with O_2 rather than N_2 increased this peak. The potential range corresponds to that expected to O_2 reduction to HO_2^-. The assignment of this peak to the reduction of O_2 to peroxide was confirmed by adding the H_2O_2 to the solution and observing complementary cathodic and anodic peaks (Fig. 7). Thus, in alkaline solutions, O_2 reduction on RuO_x/Ti electrodes involves solution phase HO_2^- as an intermediate.

ESCA and X-ray Diffraction Measurements. An effort has been made to examine the relationship of catalytic activity to the crystal structure, surface structure, and sample preparation temperatures. X-ray diffraction studies of this material indicate a rutile-type of structure similar to that of single crystal RuO_2. The x-ray results also indicate that the catalytically active material, which is prepared at 450 C, is not a well-crystallized sample. The x-ray lines are displaced from those of RuO_2 as well as being much broader. As the temperature of the sample preparation is increased to 650 C, the lines become narrower and shift toward those of well-crystallized RuO_2, indicating either an increased ordering in the crystals or a growth in crystallite size. A further interesting result from the x-ray data for samples prepared at 650 C is a decrease in the intensity of the lines due to the

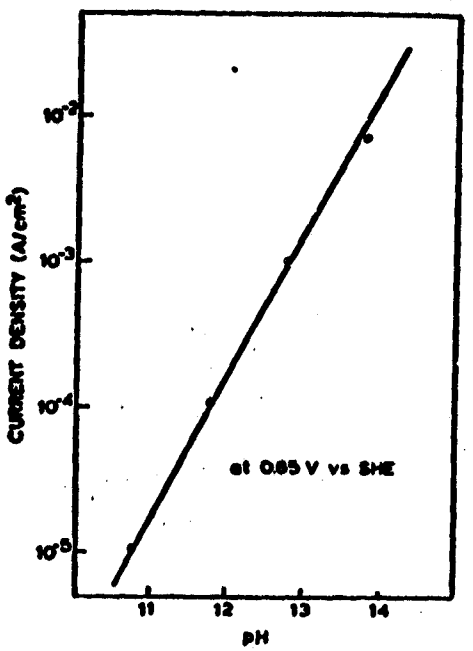

Fig. 9 pH dependence of current density at 0.65V vs SHE. in KOH - K_2SO_4 solutions with K^+ = 1 M; temperature: ~22 C. Stationary electrode

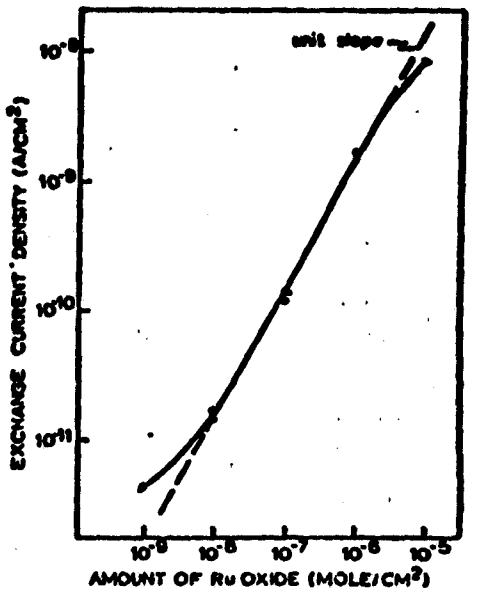

Fig. 10 Exchange current densities for O_2 generation on catalyst loading for RuO_x/Ti electrodes; temperature: ~22 C; electrolyte 4 M KOH

titanium metal substrate with a simultaneous increase in the intensity of the lines due to TiO_2.

ESCA has been used to determine the composition of the catalyst surface. The surface of the catalyst was found to contain ruthenium in the four valent state and oxygen in the form of bound water, hydroxyl and O^{2-}. Some residual chloride was also found. In the samples prepared at low temperatures (e.g., 450 C), there appear to be two forms of chloride while at the higher temperature, only one form.

As the aforementioned changes occur, the catalytic activity falls off. Several explanations are possible including: (a) the catalytic activity may be critically dependent on surface defects and the concentration of such surface defects is greatly reduced upon recrystallization; (b) the growth of large crystals results in a large loss in surface area; and (c) the growth of a non-conducting TiO_2 layer between the metal substrate and the RuO_x layer may lead to ohmic losses and an apparent loss of catalytic activity.

Polarization Measurements. Fig. 8 indicates the log current density versus potential data obtained potentiostatically for a RuO_x/Ti electrode with a very slow sweep (1 mv/sec) in O_2 saturated 4M KOH at a rotation rate of 8800 rpm. The hysteresis evident in this type of plot is very pronounced at low current densities because of the small currents associated with intrinsic changes in the oxidation state of the catalyst even at such slow sweep rates.

The anodic branch for O_2 generation is free of hysteresis effects above 5×10^{-3} A/cm^2 (apparent area) and exhibits a Tafel slope of 0.040 v/decade over three decades after IR drop correction. Measurements in KOH-K_2SO_4 solutions of varying pH with constant K^+ ion concentration indicate a reaction order of 1.0 with respect to OH^- for the O_2 generation reaction over the pH range 11 to 14 (Fig. 9). With the electrode stationary and control of the boundary layer by O_2 bubble evolution, an anodic limiting current density has been observed in the KOH-K_2SO_4 electrolytes, which is directly proportional to the OH^- ion concentration from pH 10 to 14, amounting to ~0.02 A/cm^2 (apparent area) at pH 11.8. Above the limiting current density, the discharge is from water with a Tafel slope of ~0.13 v/decade, indicating a change in mechanism.

Unfortunately, the stoichiometric number cannot be obtained for the O_2 generation reaction in the alkaline solutions because of the interference from the intrinsic electrochemistry of the RuO_x/Ti electrode surface at low current densities near the reversible potential for the four-electron reaction.

The Tafel slopes are independent of the catalyst loading over the ranges 10^{-8} to 10^{-5} moles Ru/cm^2, and the apparent exchange current densities are approximately proportional to the catalyst loading over this range (Fig. 10). Such

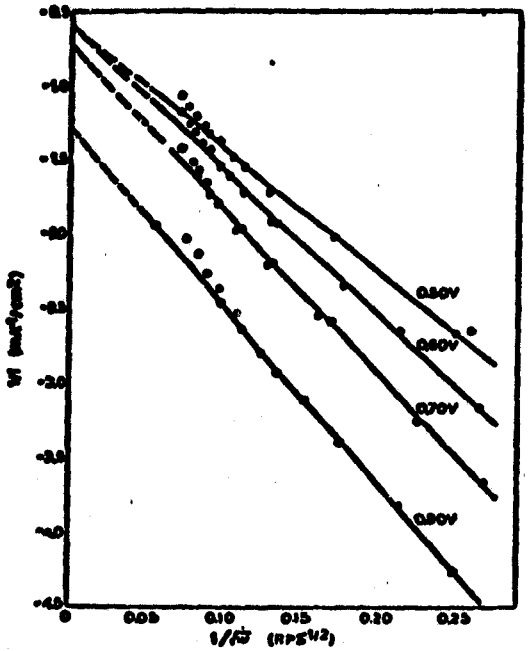

Fig. 12 Simplified representation of series and parallel mechanism involving peroxide

a proportion is to be expected since the true-to-apparent area ratio is also approximately proportional to the catalyst loading.

The current density passes through zero in the anodic sweep and increases very substantially cathodically during the cathodic sweep at approximately 0.90 v as a consequence of the O_2 - HO_2^- reaction. The dependence of the O_2 reduction current density on rotation rate (f) at constant potential indicates that the O_2 reduction is under combined diffusion and kinetic control (Fig. 11).

The rotating disk data can be explained (4) on the basis of the following two reduction processes:

Reaction 1:

$$O_2 + H_2O + 2e^- \xrightarrow{\vec{k}_1} HO_2^- + HO^- \qquad (5)$$

Reaction 2:

$$HO_2^- + H_2O + 2e^- \xrightarrow{\vec{k}_2} 3HO^- \qquad (6)$$

The possibility cannot be ruled out that some of the O_2 may also be reduced by a direct four-electron reduction process:

Reaction 3:

$$O_2 + 2H_2O + 4e \xrightarrow{k_3} 3HO^- \qquad (7)$$

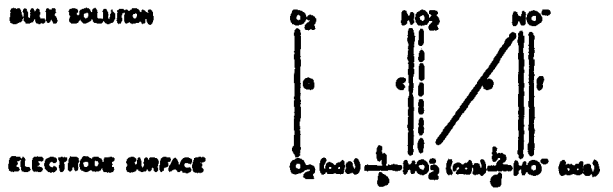

Fig. 11 Dependence of current density on rotation rate for O_2 reduction on the RuO /Ti electrode. Electrolyte: 4 M KOH_2 (O_2-saturated); catalyst loading: 1 x 10^{-5} moles Ru/cm^2; temperature ~ 22 C. (Open and solid circles correspond to two different experiments)

proceeding in parallel with reactions (1) and (2). Further measurements with the rotating ring-disk technique are needed to check this point.

DISCUSSION OF O_2 REDUCTION AND GENERATION KINETICS ON RuO_x/Ti

Since the cathodic and anodic branches for the oxygen electrochemistry on RuO_x/Ti in alkaline solutions are distinctly different, the results for each will be discussed separately.

Cathodic Branch

The parallel and series reaction schemes represented by equations (5) through (7) can be considered as part of the overall scheme shown in Fig. 12 for alkaline solutions. The difference between the series and parallel mechanisms then is just a matter of the reversibility of the adsorption-desorption of HO_2^- (step C). If this step is very irreversible, then the parallel scheme is the more appropriate representation.

The $4e^-$ overall reduction of O_2 may also proceed by a parallel reaction which does not involve a peroxide species on the surface. In view of the strength of the O-O interaction in O_2, this seems rather unlikely.

The assumption has been made in Fig. 12 that the O_2 must be first adsorbed on the electrode prior to the first electron step but the adsorption may be electrochemical; i.e., simultaneous adsorption-electron transfer:

$$O_2 + e^- \rightarrow O_2^-(ads) \qquad (8)$$

or

$$O_2 + HOH + e^- \rightarrow HO_2(ads) + HO^- \qquad (9)$$

A separate O_2 adsorption step, preceding the first electron transfer step, however, provides a convenient potential insensitive step to explain the small dependence of the intercept 1/i on potential in Fig. 11. The possible reduction of O_2

and HO_2^- without adsorption at a position equivalent to the outer Helmholtz plane has not been included in Fig. 12 on the basis that strong interaction is required with the electrode surface for the electron transfers to proceed at a reasonable rate.

Anodic Branch

Several of the reaction paths for O_2 generation tabulated by Damjanovic (12) for acid solutions can have Tafel slopes corresponding to dV/d ln i = 2 RT/3F or 0.040 v/decade when modified to a form suitable for alkaline solutions. All have the common feature that the rate controlling step is a second electron rather than first electron transfer. With judicious choice of H_2O versus OH^- as the reactant in the first and second electron transfer steps or proceeding proton transfer steps, it is possible to have the kinetics also first order in OH^-.

With electrode surfaces involving species with ionic character, the authors prefer to write the mechanism in such a way as to indicate the possibility of changes in the effective valency stat· of the catalyst sites. A simple mechanism compatible with the observed Tafel slope and reaction order is as follows:

Step a:

$$S^z + OH^- \underset{k_{-a}}{\overset{k_a}{\rightleftharpoons}} (SOH)^z + e^- \text{ (fast)} \qquad (10)$$

Step b:

$$(SOH)^z \xrightarrow{k_b} (SOH)^{z+1} + e^- \text{ (slow)} \qquad (11)$$

followed by subsequent processes yielding finally O_2 and regenerating the site S^{+z}; for example,

Step c:

$$(SOH)^{z+1} + (SOH)^{z+1} + OH^- \cdot S\text{—}O\text{-}H\text{--}OH^- \cdot S^z \longrightarrow \begin{matrix} O \\ | \\ O \end{matrix} + HOH + HOH + S^z + OH^- \qquad (12)$$

The sites are probably Ru^{4+}, but also could be higher valency state Ru ions or Ti ions. These sites are undoubtedly hydrated, although the waters of hydration are not shown in the mechanism. With the Step b rate controlling, negligible back reactions and the coverage of $(SOH)^z$ and $(SOH)^{z+1}$ low, the current density is

$$i = 4F \cdot \frac{k_a k_b}{k_{-a}} C_{OH^-} \cdot \exp \frac{(1+\beta_2)FE}{RT} \qquad (13)$$

where E is the electrode potential against an arbitrary pH insensitive reference electrode; k_a, k_{-a}, and k_b are the rate constants for Steps a and b at E = 0; and β_2 is the transfer coefficient for Step b. For the usual value of $\beta_2 = 1/2$, the Tafel slope then is (2RT/3F) (2.30) or 0.040 v/decade with i first order in C_{OH^-}. If Step b is followed by the reaction indicated by Step c, then the stoichiometric number should be 2. Unfortunately, the stoichiometric number is not known experimentally.

In Step a, the site S is a Ru ion of the oxide lattice. Step a involves the oxidation of the Ru to a higher valency state with partial transfer of electron charge from the OH species to Ru forming a $(RuOH)^z$ complex. Such a process should require much less energy than the formation of an OH free radical or a rather weakly adsorbed OH radical. Step b involves the further oxidation to $(RuOH)^{z+1}$, possibly followed by the formation of $(RuO)^z$ before proceeding with Step c. The RuO_x/Ti electrode surface may have some of the same features as the $Ru(NH_3)_5ORu\text{-}(NH_3)_4ORu(NH_3)_5^{7+}$ ion, reported by Earley and Razavi (13, 14) to oxidize OH^- homogeneously to form O_2. These species have the structure Ru-O-Ru-O-Ru^{7+}. Earley and Razavi have pointed out that Ru has a tendency to form species of coordination number 7 and that there are low lying antibonding π^* orbitals which can accept electron charge from OH^-. Thus, the $(RuOH)^z$ intermediate (other species in the inner coordination sphere not shown) seems reasonable.

ACKNOWLEDGMENTS

The authors are pleased to acknowledge the support of this work by NASA-Ames and ONR.

REFERENCES

1 Bockris, J. O'M., in Proceedings of the Cornell International Symposium and Workshop on the Hydrogen Economy, Lirke, S. ed., Cornell University, Ithaca, N. Y., 1975.

2 Miles, M., et al., Electrochemical Society, Vol. 123, 332, 1976.

3 See e.g., MacDonald, J. and Conway, B. E., Proceedings of the Royal Society, Vol. 269, No. 419, 1962; Schultze, J. W. and Vetter, K. J., Electrochim. Acta, Vol. 18, 889, 1973; Damjanovic, A. and Jovanovic, B., J. Electrochem Society, Vol. 123, 374, 1976.

4 O'Grady, W., et al., in Proceedings of the Symposium on Electrocatalysis, Breiter, M. ed., The Electrochemical Society, Princeton, N. J.,

1974, pp. 286-302.

5 See e.g., South African Pat. 68/7371, 68/7482 (1968); German Pat. 2021402(1969); 2014746, 1915951(1970); British Pat. 1206863(1970).

6 Morcos, I. and Yeager, E., Electrochim. Acta, Vol. 15, 953, 1970.

7 Zurilla, R. and Yeager, E., "Oxygen Electrode Kinetics on Gold," ONR. Tech. Rept. 23, Case Western Reserve University, Cleveland, Ohio, 1969.

8 Kozawa, A., J. Inorganics of Nuclear Chemistry, Vol. 21, 315, 1961.

9 Kozawa, C., O'Grady, W. E., and Yeager, E., unpublished research.

10 Kuhn, A. and Mortimer, C., J. Electrochemical Society, Vol. 120, 231, 1973.

11 Kozawa, A., "Electrochemical Reduction of RuO_2," Abstract No. 29, National Meeting Electrochemical Society, Boston, Mass., Oct. 1973.

12 Damjanovic, A., in Modern Aspects of Electrochemistry, Vol. 5, Bockris, J. O'M. and Conway, B. E., eds., Plenum Press, N. Y., 1969, pp. 369-483.

13 Earley, J. and Razavi, H., Inorganics of Nuclear Chemistry Letters, Vol. 9, 331, 1973.

14 Earley, J. and Fealey, T., Inorganics of Chemistry, Vol. 12, 323, 1973.

Electrode surface studies by Leed–Auger*

W. E. O'Grady, M. Y. C. Woo, P. L. Hagans, and E. Yeager

Chemistry Department, Case Western Reserve University, Cleveland, Ohio 44106

(Received 19 October 1976)

The role the electronic and geometric structures of the metal surface play in electrochemical surface reactions remains as yet an unknown factor. In order to investigate these surface contributions to electrochemical reactions, a low-energy-electron diffraction (LEED) and an Auger electron spectrometer (AES) have been combined with an electrochemical thin-layer cell (TLE). The surface to be studied electrochemically is first characterized by LEED–AES and then transferred into a second chamber where it becomes part of the electrochemical thin-layer cell. Electrochemical reactions are then run on this surface. The sample may then be transferred back to the LEED–AES chamber for further characterization. Data on Pt (111) will be presented.

PACS numbers: 82.45.+z, 82.65.My, 82.65.Jv

INTRODUCTION

The hydrogen electrode reaction and the adsorption of hydrogen on platinum are the most extensively studied electrochemical reactions.[1-5] The pathways and corresponding rate constants for the overall electrode reaction are fairly well established.[4-7] Surprisingly, the understanding of the bonding of the adsorbed hydrogen is still incomplete and controversial.[7,8] The source of the multiple hydrogen-adsorption peaks observed in linear sweep voltammetry[9] on both polycrystalline and single-crystal surfaces still awaits explanation. Up to five peaks have been observed in acid electrolytes. The factors which have been proposed to account for the multiple peaks include chemically different adsorption sites on a particular crystallographic surface orientation, a distribution of different crystal-surface orientations even with a given single-crystal orientation, induced heterogeneity associated with the perturbation of adjacent sites by the adsorbed hydrogen itself, and the adsorption of anions which create further surface heterogeneity by blocking some sites and perturbing adjacent sites. The situation is further complicated by the fact that in acid solutions the potential of zero charge (PZC)[10] for Pt falls within the hydrogen adsorption–desorption region. Thus the adsorption–desorption of anions can closely be coupled to the hydrogen adsorption–desorption process.

Single-crystal studies of hydrogen adsorption on Pt should make it possible to resolve at least a part of the question of intrinsic heterogeneity associated with different crystal faces versus sites of different adsorption energies on a given crystallographic plane. Such studies have been attempted and have generally shown only changes of relative peak heights in the voltammetry curves.[11,12] Great uncertainty exists, however, whether unique crystallographic planes were achieved in these studies because of the high probability that the surfaces restructured after introduction into the electrochemical environment. In virtually all instances, electrochemists studying single-crystal platinum have found it necessary to cycle the potential of the electrode to quite high anodic potentials in order to oxidize and desorb various impurities initially present on the surface.[12] This treatment leads to the formation and reduction of an anodic oxide film on the platinum and therefore the probable restructuring upon return to the potential region of hydrogen adsorption.

The present work represents an effort to design an experiment for the study of hydrogen adsorption on single-crystal platinum of known surface structure free of "impurities." LEED and Auger spectroscopy are used to establish the structure and composition of the single-crystal surface, and thin-layer electrochemical techniques are used to electrochemically characterize the surface. The philosophy is that if one starts with a "truly clean" surface it is not necessary to cycle the electrode into potential regions where restructuring will occur before examining the electrochemical adsorption–desorption of hydrogen. Further, during the transfer from the UHV environment of the LEED–Auger system to the electrochemical environment, the sample must be protected from oxygen and other adsorbing species. To this end a special transfer system has been developed.

This paper describes the design of the LEED–Auger electrochemical system, preliminary results obtained with it, and complementary experiments with conventional electrochemical techniques.

EXPERIMENTAL

The LEED–Auger electrochemical system used in this work is shown schematically in Fig. 1(a). It is composed of two all-metal UHV (10^{-8} Pa) systems, one housing the LEED–Auger-electron-spectrometer (AES) and the second housing the electrochemical thin-layer cell and other sample preparation methods. The two chambers are completely isolated by an all-metal bakeable valve through which the sample is transferred.

The LEED–AES is a standard Varian retarding field analyzer. The sample holder is a modified Varian manipulator which allows the sample to be removed for transfer to the second chamber while retaining the features of cooling the sample to 100 K and heating it to 1400 K.

In the second chamber is a liquid-nitrogen-cooled manipulator which allows the sample to be removed for transfer and

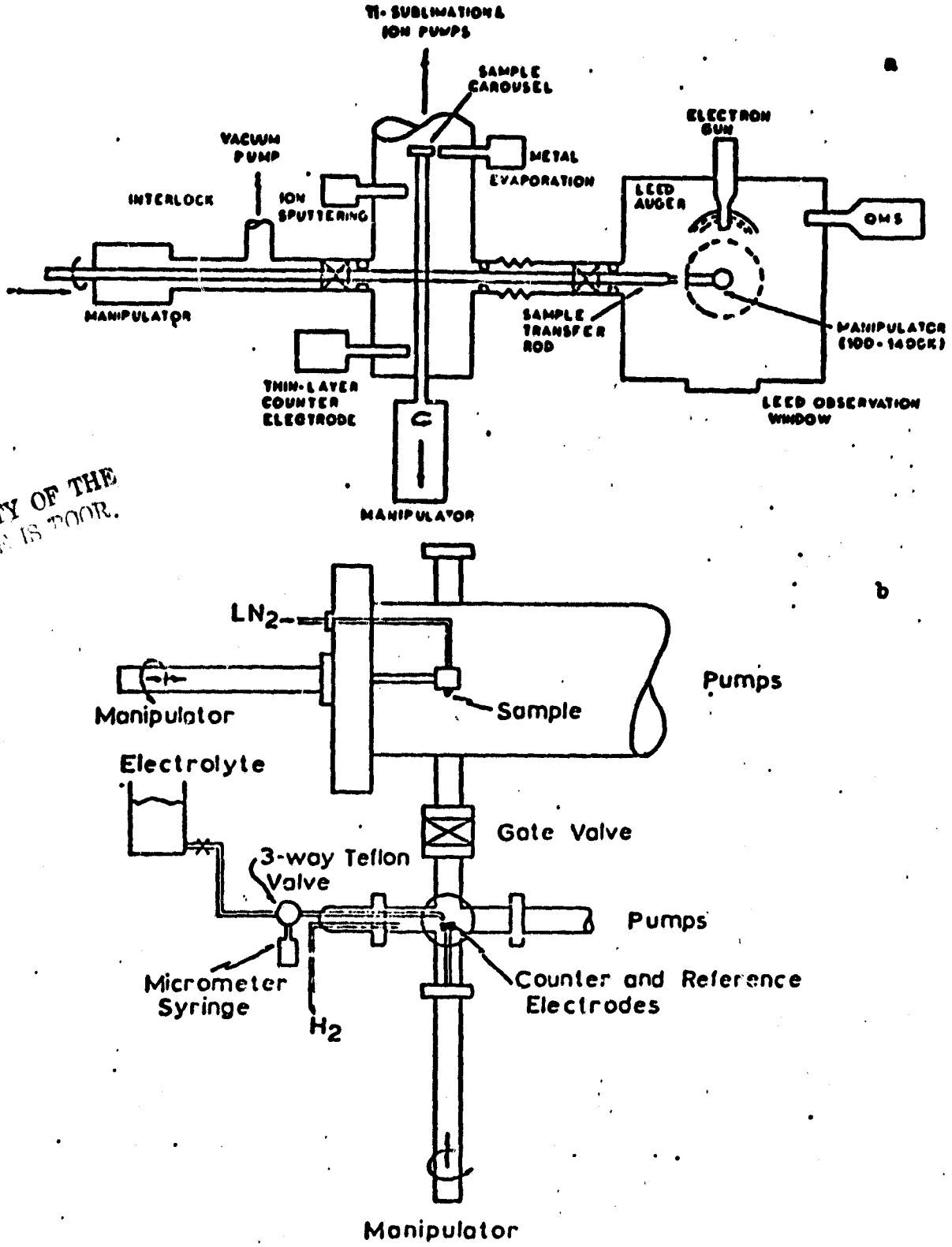

FIG. 1. Schematic drawings of (a) the LEED-Auger-thin-layer electrochemical system and (b) details of the solution injection and thin-layer cell system

also positions the sample for argon-ion sputtering or for use in the thin-layer cell. The transfer of the sample from the LEED-AES chamber to the electrochemical chamber and back is accomplished by a spring clip holder mounted on a wand which is manipulated magnetically from outside of the vacuum system.

Details of the electrolyte injection and thin layer cell system are shown schematically in Fig. 1(b). The electrolyte used in the present experiments was 0.1*N* H_2SO_4 prepared with ultra-pure acid (Baker Ultrex H_2SO_4) and pyrolyzed water after the method of Conway.[13] After deaerating and pre-electrolyzing for 24 h in an all-glass vessel the electrolyte is introduced into the thin-layer cell by an all-Teflon-glass system. The micrometer syringe is filled with electrolyte, the three-way valve is switched, and several microliters of solution are placed on the palladium counter-reference electrode. The

palladium electrode is then brought up through the gate valve into contact with the sample forming the thin-layer cell. Before the electrolyte is brought into contact with the single-crystal electrode, the two electrodes are connected to the potentiostat with a 500-Ω resistor across them and the applied potential adjusted to a value in the double-layer region 400 mV versus reversible hydrogen electrode (RHE). This prevents any possible excursion of the platinum electrode into an oxidizing potential region and hence possible restructuring of the electrode surface.

The choice of the thin-layer technique for these experiments is dictated by several factors. The first is the small volume of electrolyte which is introduced into the cell and hence the vacuum system—only about 10^{-3} ml. The second is the concentration of impurities which may be tolerated. For most impurities to form a monolayer on the surface approximately 10^{-9} mole/cm^2 are required. If the 10^{-9} moles originate from the solution in the cell (10^{-3} ml), the concentration of the impurity which can be tolerated is of the order of 10^{-3} molar (M), which is a high impurity concentration. Hence the thin-layer cell is far less susceptible to impurity contamination than the normal electrochemical experiment. The use of the thin-layer cell in conjunction with LEED-Auger was first suggested by Hubbard.[14] His version of the technique has one severe drawback, and that is the necessity of a capillary connecting the outside reference electrode to the cell inside the vacuum. This problem has been overcome in the present experiments by combining the counter and reference electrodes as a single palladium–hydrogen-alloy electrode.[15] It should be noted that this electrode surface must be as clean as the electrode surface being studied. Therefore the surface of the counter-reference electrode is also cleaned by argon-ion sputtering and then maintained in a hydrogen atmosphere prior to its use.

The experimental procedure used is as follows:

1. The platinum samples are introduced into the sample preparation chamber.
2. The system is evacuated and baked until the pressure after cooling is in the 10^{-8} Pa region.
3. The sample is argon-ion sputtered.
4. The sample is transfered to the LEED–AES chamber and the Auger spectrum is recorded. If it is clean, the sample is annealed at 900° C, the Auger is checked for cleanliness and the LEED pattern observed. If it is not clean, it is resputtered.
5. The sample is then returned to the preparation chamber and positioned in the thin-layer cell.
6. The preparation chamber is brought to atmospheric pressure with purified argon.
7. The electrochemical characterization of the sample is carried out.
8. The preparation chamber is then re-evacuated and the sample returned to the first chamber for further characterization by LEED and Auger.

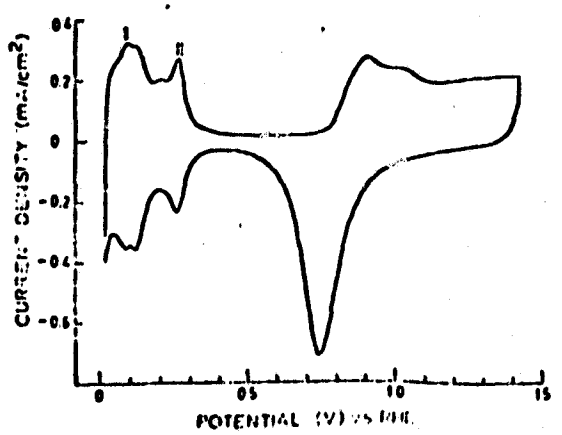

FIG. 2. Voltammogram for polycrystalline Pt in 0.1N H_2SO_4 in a conventional electrochemical cell, sweep rate 100 mV/s.

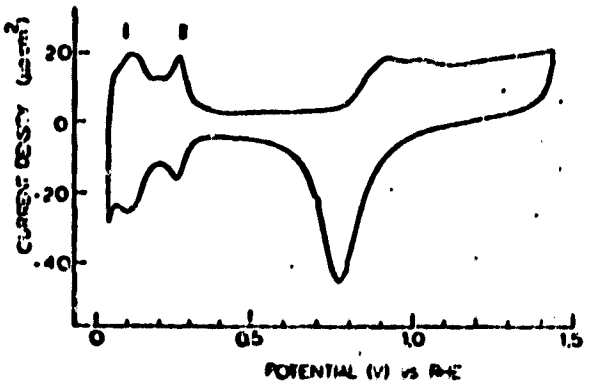

FIG. 3. Voltammogram for polycrystalline Pt in 0.1N H_2SO_4 in a thin-layer cell with Pd–H counter-reference electrode (gap 10^{-4} cm), sweep rate 20 mV/s.

RESULTS

The use of cyclic voltammetry to characterize platinum surfaces is now well documented[12] and a typical scan is shown in Fig. 2 using a conventional electrochemical cell with special precautions to minimize impurities. Prior to the present time however, voltammograms of this quality have generally not been obtained for hydrogen adsorption on Pt using thin-layer techniques (see e.g., Ref. 16). In Fig. 3 is shown a typical cyclic voltammogram obtained on Pt in 0.1N H_2SO_4 using the Pd–H counter-reference electrode in a thin-layer cell. All of the features in both the hydrogen adsorption–desorption region and the oxide formation–reduction region are reproduced. With this verification of the technique it now becomes possible to utilize the thin-layer cell in meaningful studies of hydrogen electrochemistry in combination with LEED and Auger.

In the initial experiments a Pt (111) surface was cleaned completely of carbon and the typical Auger spectrum and the LEED pattern for clean platinum were obtained. However, when this sample was placed in the thin-layer cell, difficulties were encountered in forming a stable electrolyte film between the two electrodes, and hence no reasonable cyclic voltammograms were obtained in these initial experiments. With very clean polycrystalline platinum surfaces Bockris and Cahan[17] found thin films of electrolyte broke up into beads.

A second set of experiments were run on Pt (111), which was cleaned as previously described. Then a carbon layer was deliberately deposited on the surface by irradiating the CO-

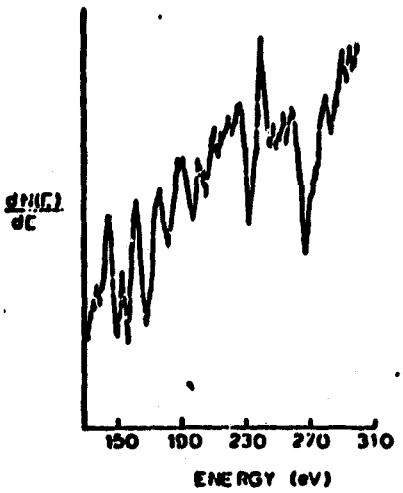

FIG. 4. Auger spectrum for partially cleaned Pt (111).

covered Pt surface with electrons at a temperature of <150°C.[18] It has been suggested that this type of carbon layer is quite uniform on the surface.[18] The Auger spectrum is shown in Fig. 4. The amount of carbon on this surface has been estimated to be 0.3 of a monolayer, following the method of Chang.[19] This sample was then placed in the thin-layer cell and the cyclic voltammogram was obtained for the potential region +0.4–+0.040 V (RHE), as shown in Fig. 5.

The anodic peak corresponds to the near reversible oxidation of the H_2 produced in the electrolyte during the cathodic sweep. Surprisingly, there is no evidence of either weakly or strongly bound hydrogen, peaks I and II, respectively, in Figs. 2 and 3. Note that the current density scale is greatly expanded over that in Figs. 2 and 3.

Several possibilities exist to explain the behavior of hydrogen adsorption in this case: the sites for hydrogen adsorption could be completely blocked by the carbon but this seems unlikely since the carbon is believed to be present well below monolayer amounts. The second possibility is the perturbation of the electronic structure of the Pt surface such that the hydrogen can no longer adsorb. This possibility cannot be ruled out at this time. However, the H_2 oxidation appears to be essentially reversible, which is to be expected on Pt but not on carbon or graphite.[20]

The implication is that hydrogen does not electrochemically adsorb on Pt (111) in appreciable amounts. This remains to be verified but certainly has major implications for the electrochemistry of hydrogen on Pt. Bernasek and Somorjai[21] have found that hydrogen does not adsorb on Pt (111) from the gas phase.

The question may be asked how H_2 can be oxidized nearly reversibly to H^+ ion on Pt (111) if there is no evidence of appreciable amounts of adsorbed hydrogen in the voltammetry curve. Workers concerned with hydrogen overvoltage on platinum[4,5,8] have already postulated that the adsorbed hydrogen involved in the H_2 formation step is at a very low coverage in order to explain the kinetics. The observation of near reversible H_2 oxidation and formation on the Pt (111) despite the absence of hydrogen adsorption peaks is consistent with this view.

An estimate of the double-layer capacity of thin Pt (111) surface, partially covered with carbon, can be made from the change in the current attending the shift from anodic to cathodic sweep. The value obtained is 12μF/cm^2, which appears to be a quite reasonable value.

Efforts are in progress to examine the Pt (111) and other orientations of platinum free of impurities.

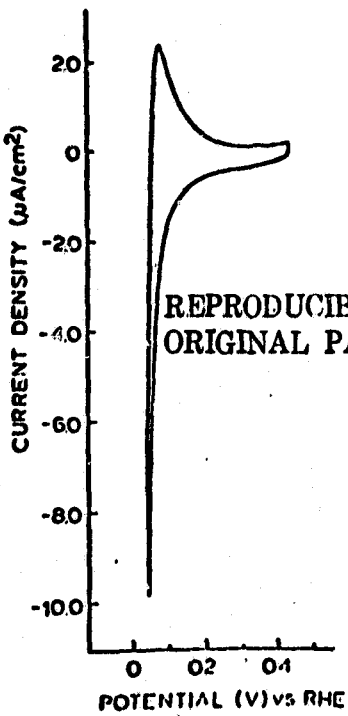

FIG. 5. Voltammogram for Pt (111) in the LEED AES thin-layer electrochemical system in 0.1*N* H_2SO_4, sweep rate 20 mV/s.

*The authors are pleased to acknowledge the support of this research by the ONR, NASA Ames, and the Diamond Shamrock Corp., the latter through a fellowship to one of the authors (M.Y.C.W.).

The authors express thanks to General Motors and Union Carbide for grants that helped with the purchase of equipment.

[1]K. J. Vetter, *Electrochemical Kinetics* (Academic P, New York 1967).
[2]A. N. Frumkin, *Advances in Electrochemistry and Electrochemical Engineering*, *Vol 3* (Wiley, New York, 1963).
[3]L. I. Krishtalik, *Advances in Electrochemistry and Electrochemical Engineering*, *Vol 7*, (Wiley, New York, 1968).
[4]M. Breiter, *Transactions of the Symposium on Electrode Processes*, edited by E. Yeager, (Wiley, New York, 1961), pp. 307–324.
[5]S. Schuldiner, J. Electrochem. Soc. 115, 362 (1968).
[6]J. O'M. Bockris, I. Ammar, and A. Huq, J. Chem. Phys. 61, 879 (1957).
[7]F. Ludwig, R. K. Sen, and E. Yeager (unpublished).
[8]J. C. Huang, W. E. O'Grady and E. Yeager, (unpublished).
[9]S. Srinivasan and E. Gileadi, Electrochim. Acta 11, 321 (1966).
[10]A. N. Frumkin and O. A. Petrii, Electrochim. Acta 20, 347 (1975).
[11]F. G. Will, J. Electrochem. Soc. 112, 451 (1965).
[12]H. Angerstein-Kozlowska, W. B. A. Sharp, and B. E. Conway, in *Proceedings of the Symposium on Electrocatalysis*, edited by M. W. Breiter (Electrochemical Society, Princeton, NJ, 1974) p. 94.
[13]B. E. Conway, H. Angerstein-Kozlowska, W. B. A. Sharp and E. Criddle, Anal. Chem. 45, 1331 (1973).
[14]A. T. Hubbard, Crit. Rev. Anal. Chem. 3, 201 (1973).
[15]Details for the use of the Pd–H counter-reference electrode in a thin-layer cell are to be published elsewhere.
[16]R. F. Lane and A. T. Hubbard, J. Phys. Chem. 79, 808 (1975).
[17]J. O'M. Bockris and B. D. Cahan, J. Chem. Phys. 50, 1307 (1969).
[18]H. P. Bonzel and R. Ku, Surf. Sci. 40, 85 (1973).
[19]C. Chang, Surf. Sci. 48, 9 (1975).
[20]H. E. Zittel and F. J. Miller, Anal. Chem. 37, 200 (1965).
[21]S. L. Bernasek and G. A. Somorjai, J. Chem. Phys. 62, 3149 (1975).

The Effects of Cations and Anions on Hydrogen Chemisorption at Pt

J. C. Huang,* W. E. O'Grady,* and Ernest Yeager*

Case Laboratories for Electrochemical Studies and the Department of Chemistry, Case Western Reserve University, Cleveland, Ohio 44106

Reprinted from JOURNAL OF THE ELECTROCHEMICAL SOCIETY
Vol. 124, No. 11, November 1977
Printed in U.S.A.

The Effects of Cations and Anions on Hydrogen Chemisorption at Pt

J. C. Huang,* W. E. O'Grady,* and Ernest Yeager*

Case Laboratories for Electrochemical Studies and the Department of Chemistry, Case Western Reserve University, Cleveland, Ohio 44106

The adsorption of hydrogen on the platinum electrode has been the subject of extensive investigation [see, *e.g.*, Ref. (1-10)]. Many questions persist, however, as to the true nature of the multiple hydrogen adsorption peaks observed in linear sweep voltammetry studies of single crystal as well as polycrystalline platinum. Up to five peaks have been observed (10) in ultrapure dilute sulfuric acid electrolytes. Factors which have been proposed to account for these multiple peaks include different adsorption sites on a given crystallographic plane, a distribution of surface crystallographic orientations even with a given single crystal macro-orientation, induced heterogeneity associated with the perturbing of adjacent sites by the adsorbed hydrogen itself, and the adsorption of anions which create further surface heterogeneity by blocking some sites and perturbing adjacent sites. The situation is further complicated by the fact that in acid solutions the point of zero charge (pzc) for Pt falls within the hydrogen adsorption-desorption region. Thus the adsorption-desorption of anions can closely couple to the hydrogen adsorption-desorption process.

In considering the role of oxyanions Conway and his co-workers (10) have examined both their own linear sweep voltammetry data and that of others and conclude that anion adsorption changes the relative heights of the hydrogen adsorption peaks but has relatively little effect on the peak potentials, and hence, adsorption energies. On this basis they conclude that the anions principally affect the distribution of adsorbed hydrogen on the surface but do not disturb significantly the adsorption energy for a particular type of site. In examining the dependence of hydrogen adsorption on Pt on the electrolyte, however, we differ with this conclusion and find that ionic adsorption substantially shifts the potentials in addition to the relative heights of the peaks. These effects appear well beyond what can be explained on the basis of simple blocking of hydrogen adsorption sites.

The purpose of this note is to present experimental data to substantiate this view. Despite the relatively large amount of data on ion adsorption effects, we have found it necessary to obtain additional data to more clearly establish the trends. Much of the data in this literature has been obtained by adding various ionic components to sulfuric acid solutions. The HSO_4^- and/or $SO_4^=$ ions, however, are moderately strongly adsorbed on Pt in the hydrogen adsorption region as the present work indicates, and this complicates studies of the adsorption of other ions in this electrolyte. The present study shows that $HClO_4$ and HF are better reference electrolytes for anion studies. The measurements have also been extended to alkaline solutions. Relatively little data have been reported for hydrogen adsorption on Pt in alkaline solutions and even then much of this has been obtained by charging techniques (8, 9) which do not show up well the fine structure in this potential region.

* Electrochemical Society Active Member.

Key words: hydrogen adsorption, platinum, electrosorption, voltammetry, hydrogen electrode.

Experimental

Conventional techniques were used to record the linear sweep voltammograms. For all work herein reported the sweep rate was 100 mV/sec and the voltammograms recorded after several cyclic sweeps. The measurements were made in an all-Teflon cell, consisting of a main working electrode compartment and two separate compartments for the reference and counterelectrodes. The working electrode was a 0.5 cm disk of reference grade Pt (99.999% pure) mounted in Teflon. The reference and counterelectrodes were β-Pd-H using Pd foils charged continuously with purified H_2 from the back side. O_2 was removed from the solution by bubbling purified helium through the cell prior to measurements. The cell was mounted in a N_2-atmosphere box to prevent CO_2 and dust contamination of the electrolyte in the filling of the cell and to eliminate any possible diffusion of O_2 into the cell.

The working electrode surface was first polished with alumina to a mirror finish, washed with distilled water, degreased with spectro grade isopropanol, cleaned with 1:1 volume ratio H_2SO_4-HNO_3 (reagent grade), rinsed with triply distilled water followed by pyrolyzed water, further cleaned with ultrasound in a solution of the same composition as the electrolyte to be used, and then either introduced into the cell or stored in pyrolyzed water. All of these operations were carried out in carefully cleaned Teflon vessels. This procedure was repeated for each new electrolyte.

The acid solutions were prepared with ultrapure acids (Ultrex H_2SO_4 from J. T. Baker, ultrapure 49% HF and 85% H_3PO_4 from Apache Chemicals, ultrapure 70% $HClO_4$ from Ventron Alfa Products) and pyrolyzed water. The latter was prepared according to the procedure described by Conway *et al.* (11). The H_2SO_4, $HClO_4$, and H_3PO_4 solutions were prepared in cleaned glassware and used without further chemical treatment. All HF solutions were prepared in Teflon bottles. The HF solution was first made up as 10*M* and subjected at this concentration to activated charcoal purification, principally to remove trace chloride. Omission of the activated charcoal purification had no significant effect on the results. The solution was then diluted down to desired concentration with pyrolyzed water.

Solutions of 0.1*M* NaOH were also prepared in Teflon bottles and subjected to the activated charcoal purification. A 50% stock solution of NaOH was first formulated from special low carbonate NaOH pellets (J. T. Baker) with triply distilled water. This solution was allowed to stand over several weeks and the solution

decanted many times to remove precipitated Na_2CO_3. The carbonate solubility in 50% NaOH is $\sim 10^{-4}M$ and the carbonate concentration in the 0.1*M* NaOH should be $\sim 5 \times 10^{-7}M$.

Before each measurement, the final solution was preelectrolyzed at a potential of 1.5V between two auxiliary Pt electrodes (4 × 2 × 0.01 cm) within the Teflon cell for at least 24 hr for acid solutions and 48 hr for the NaOH solutions.

Results

Figures 1 and 2 indicate the voltammetry curves for 0.1*M* HF and 0.1*M* $HClO_4$ as well as the effect of adding successively increasing amounts of H_2SO_4 to these electrolytes. Only the hydrogen region is shown for purposes of clarity, but the sweep in the anodic direction was continued out to 1.4V *vs.* RHE. The curves for the HF and $HClO_4$ solutions resemble each other closely. The addition of H_2SO_4 to either of these electrolytes has a substantial effect on the hydrogen adsorption region with respect to the position as well as relative height of the strongly adsorbed hydrogen peak IV [H_{A4}, using the notation of Flo[illegible] *et al.* (10)]. The addition of up to 0.1*M* HF [illegible] H_2SO_4, however, has virtually no effect on the hydrogen adsorption. This implies that undissociated HF as well as F^- are not adsorbed to any significant extent with the presence of SO_4^{2-}. Figure 3 compares the curves for 0.02*M* H_2SO_4 and 0.14*M* HF, both of which have essentially the same pH. The shift in potential and increment in height of peak IV is similar to that noted by Frumkin *et al.* (6) although Fig. 3 shows clearly four peaks for the H_2SO_4 solution while the earlier Soviet work indicated only two. This figure indicates that the principal differences between the HF and H_2SO_4 solution are not due to pH.

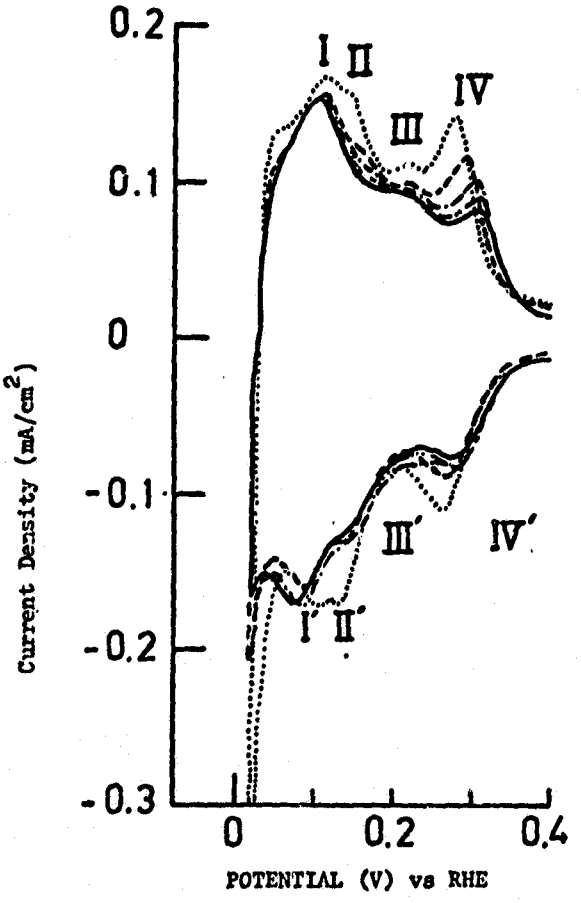

Fig. 1. Voltammograms for Pt in 0.1M HF with various concentrations of H_2SO_4 added. —— 0.1M HF, -·-· 0.1M HF + 5 × 10^{-5}M H_2SO_4, -·- 0.1M HF + 5 × 10^{-4}M H_2SO_4, - - - 0.1M HF + 5 × 10^{-3}M H_2SO_4, ... 0.1M HF + 5 × 10^{-2}M H_2SO_4.

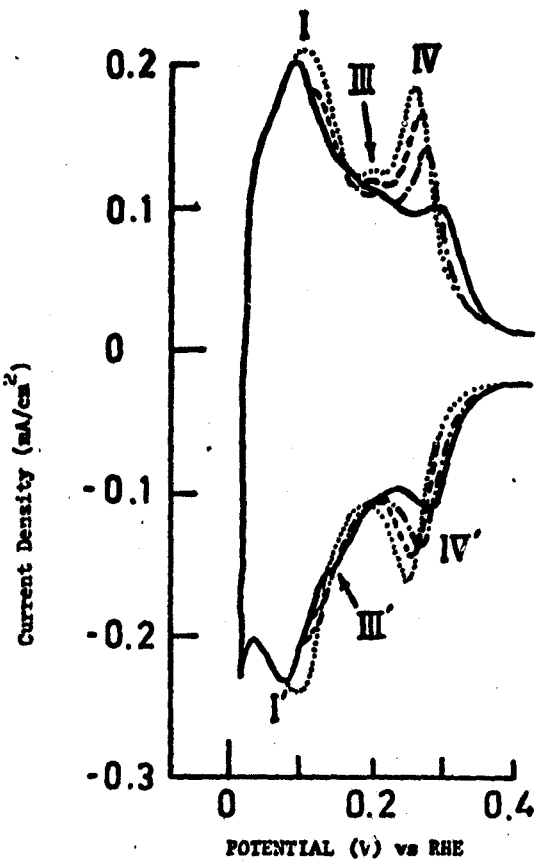

Fig. 2. Voltammograms for Pt in 0.1M $HClO_4$ with various concentrations of H_2SO_4 added. —— 0.1M $HClO_4$, -·- 0.1M $HClO_4$ + 5 × 10^{-4}M H_2SO_4, - - - 0.1M $HClO_4$ + 5 × 10^{-3}M H_2SO_4, ... 0.1M $HClO_4$ + 5 × 10^{-2}M H_2SO_4.

In voltammetry studies of the hydrogen peaks in H_2SO_4 solutions reported in the literature, peaks I, III, and IV have usually been observed in the anodic sweep but only peaks I and IV have shown up in the cathodic sweep. Various explanations have been proposed to explain peak III in the anodic sweep, and particularly why peak III is missing in the cathodic sweep (7, 10, 12-14). In the present work the counterpart of the anodic peak III is evident in the cathodic sweeps in 0.1*M* HF (Fig. 1) and 0.1*M* $HClO_4$ (Fig. 2) although not in the H_2SO_4 solutions (Fig. 3 and 6) or 0.033*M* H_3PO_4, (Fig. 4) which rather closely resembles H_2SO_4. The lack of peak III in the cathodic sweep in the H_2SO_4 and H_3PO_4 solutions is probably due principally to the strong overlap of the other more predominant peaks.

Figures 5 and 6 indicate the effects of HCl additions to 0.1*M* HF and 0.5*M* H_2SO_4. Peak IV in both the HF and H_2SO_4 is shifted substantially in the cathodic direction. The shift amounts to ~120 mV with $10^{-2}M$ HCl in the 0.1*M* HF solution. This shift is quite linear with the log concentration of H_2SO_4 or HCl added to the HF or $HClO_4$ solutions as shown in Fig. 7. Such linearity may arise because of the logarithmic nature of the anion adsorption isotherm.

Cations have much less effect on the hydrogen adsorption on Pt in acid solutions. The addition of chloride-free $(C_2H_5)_4NF$ to the HF solution shifts peak I in the anodic direction and peak IV in the cathodic direction (see Fig. 8), whereas the addition of Cs_2SO_4 to H_2SO_4 only slightly shifts the weak hydrogen adsorption peak I in the anodic direction (Fig. 9). The addition of either 5 × $10^{-3}M$ Na_2SO_4 or 5 × $10^{-3}M$ Li_2SO_4 to 0.05*M* H_2SO_4 has a negligible effect as is

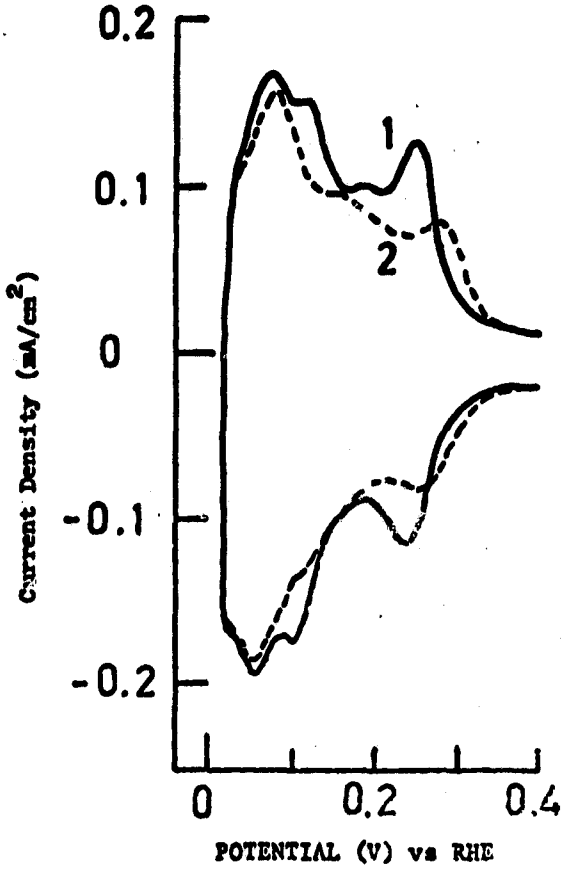

Fig. 3. Voltammograms for Pt in 0.02M H_2SO_4 and 0.14M HF. Curve 1, 0.02M H_2SO_4 and curve 2, 0.14M HF.

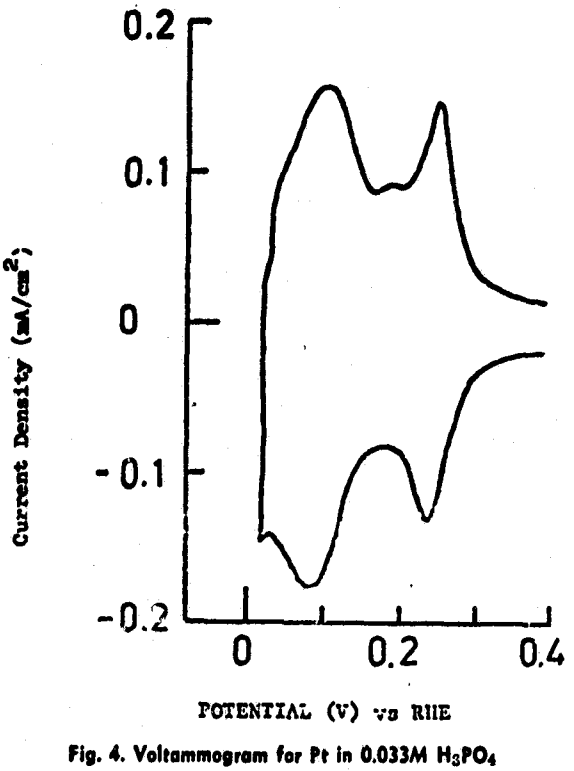

Fig. 4. Voltammogram for Pt in 0.033M H_3PO_4

also the case with the addition of $5 \times 10^{-4}M$ $Ba(ClO_4)_2$ or $5 \times 10^{-4}M$ $Sr(ClO_4)_2$ to the 0.1M $HClO_4$.

The hydrogen adsorption region is quite different in alkaline solutions (see Fig. 10 and 11). Only two peaks (A and B) are clearly observed. Peak C corresponds to

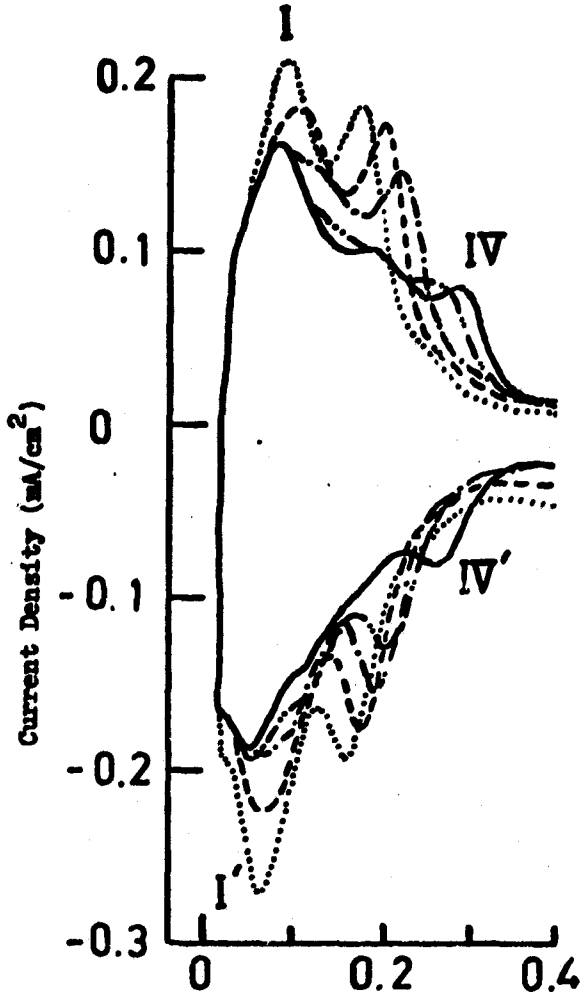

Fig. 5. Voltammograms for Pt in 0.01M HF with various concentrations of HCl added. —— 0.1M HF, –·–· 0.1M HF + 10^{-5}M HCl, –·– 0.1M HF + 10^{-4}M HCl, – – – 0.1M HF + 10^{-3}M HCl, ... 0.1M HF + 10^{-2}M HCl.

the anodic oxidation of solution phase H_2 produced during the cathodic sweep. In contrast to the acid media, the positions and heights of both peaks A and B are substantially influenced by the addition of $Ba(OH)_2$ or $Ca(OH)_2$. The addition of Cl^-, F^-, ClO_4^-, PO_4^{-3}, SO_4^{-2}, or SiO_3^{-2} up to $10^{-3}M$ had no detectable effect and $10^{-3}M$ Br^- had only a slightly perceptible effect. The pzc in the alkaline solutions even in the presence of these various anions is probably still quite anodic to the hydrogen adsorption region, and thus specific adsorption of these anions is small in this region. With a strongly specifically adsorbed anion such as I^- in alkaline solution the effects on the hydrogen adsorption peaks are pronounced (see Fig. 12). Tracking of the peak shifts in position *vs.* height changes, however, is rather difficult with the data in Fig. 12.

Discussion

It is difficult to explain all of the anion and cation effects in acid and alkaline solutions on the basis of a single model for the interaction of the ions with the hydrogen adsorption. The situation is complicated by a lack of a clear understanding of the extent to which various structural features of the electrode surface are responsible for the several hydrogen peaks, *i.e.*, the importance of intrinsic *vs.* induced heterogeneity [see *e.g.*, Ref. (10)]. The addition of various cations and

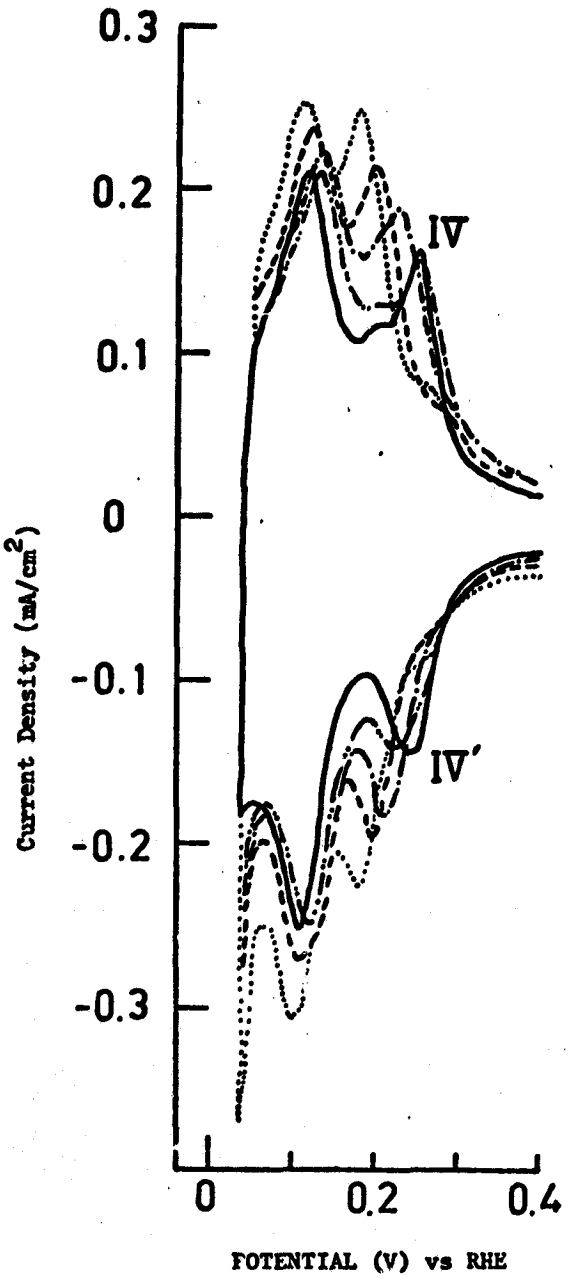

Fig. 6. Voltammograms for Pt in 0.5M H_2SO_4 with various concentrations of HCl added. ——0.5M H_2SO_4, –·–· 0.5M H_2SO_4 + 10^{-5}M HCl, –·– 0.5M H_2SO_4 + 10^{-4}M HCl, – – – 0.5M H_2SO_4 + 10^{-3}M HCl, ... 0.5M H_2SO_4 + 10^{-2}M HCl.

anions to electrolytes such as HF and $HClO_4$ can bring about changes in the structure of the hydrogen adsorption region in the voltammetry curves in a number of ways:

1. *Blocking of sites by anion adsorption and coupling of hydrogen adsorption and anion desorption.*—Specific adsorption of ions, particularly anions, can block sites on which hydrogen otherwise would be adsorbed. For hydrogen to adsorb on these sites requires the desorption of anions with the result that hydrogen adsorption and anion desorption are coupled. Such coupling can be expressed through the following equation

$$yH^+ + X_{ad}^{-(z-\sigma_x)} + (y\sigma_H + \sigma_x)e^- \rightarrow yH_{ad}^{(1-\sigma_H)} + X^{-z}$$

This effect can lead to a shift in the peak potential as well as peak area. Strong anion adsorption makes it more difficult to adsorb hydrogen and hence a shift to more cathodic potentials should occur for the particular peak(s) involved with such coupling.

Evidence for this effect is to be found in Fig. 13, in which the ratio of the charge associated with the strong

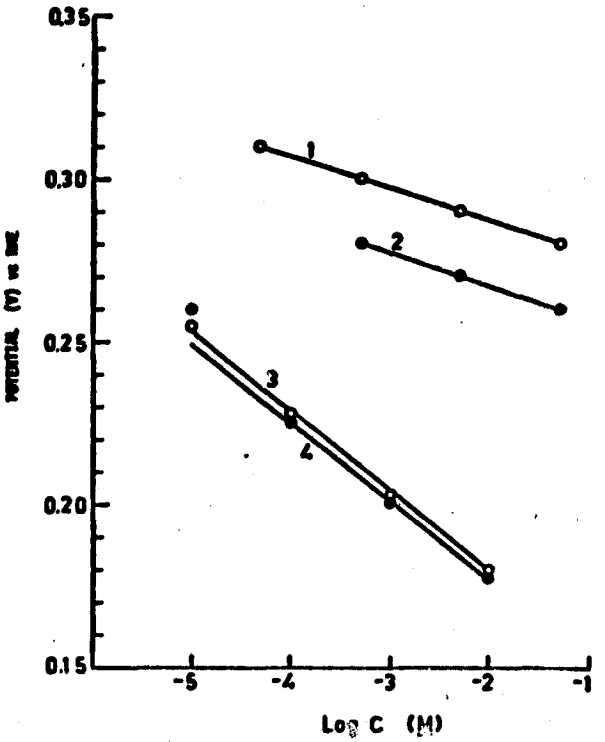

Fig. 7. The shift of strongly bound hydrogen peak potential as a function of the concentration of added anions. Curve 1, 0.1M HF + H_2SO_4; curve 2, 0.01M $HClO_4$ + H_2SO_4; curve 3, 0.1M HF + HCl; curve 4, 0.5M H_2SO_4 + HCl.

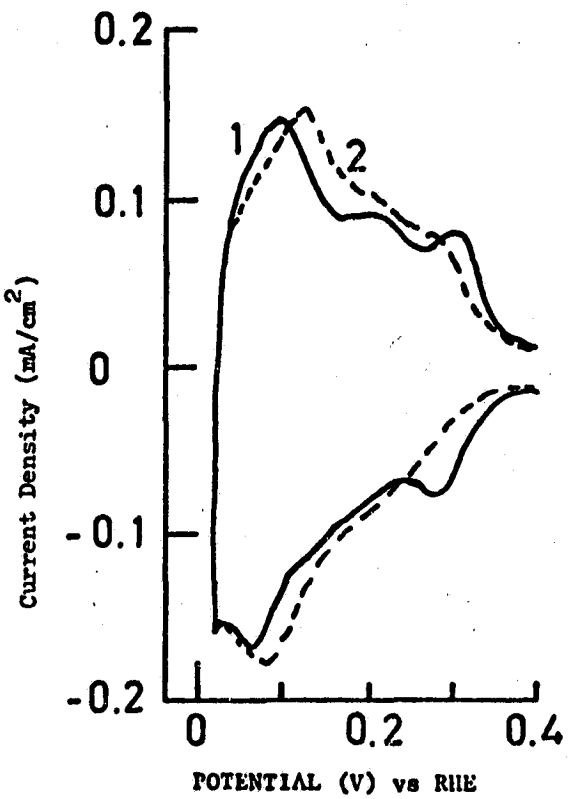

Fig. 8. Voltammograms for Pt in 0.1M HF with $(C_2H_5)_4N^+$ cations added. Curve 1, 0.1M HF and curve 2, 0.01M HF + 5 × 10^{-3}M $(C_2H_5)_4NF$.

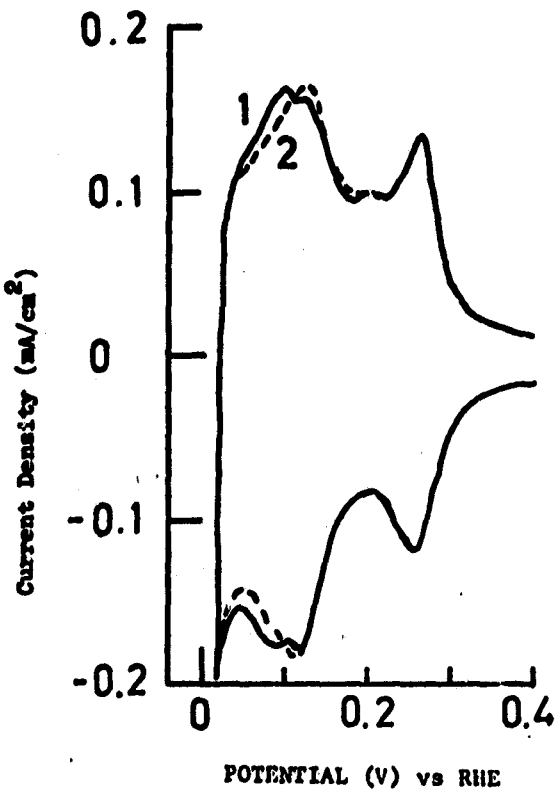

Fig. 9. Voltammograms for Pt in 0.05M H_2SO_4 with Cs^+ cations added. Curve 1, 0.05M H_2SO_4 and curve 2, 0.05M H_2SO_4 + 5 × 10^{-3}M Cs_2SO_4.

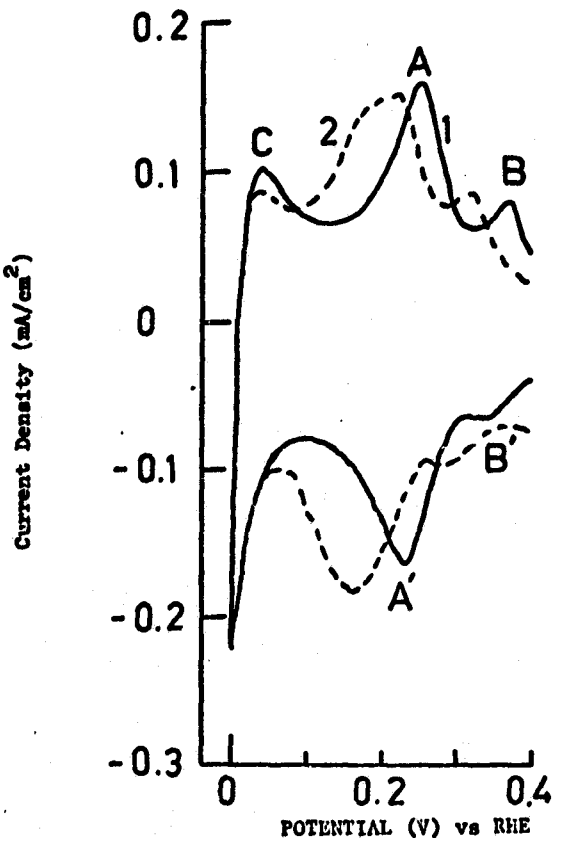

Fig. 10. Voltammograms for Pt in 0.1M NaOH with Ba^{2+} cations added. Curve 1, 0.01M NaOH and curve 2, 0.1M NaOH + 5 × 10^{-3}M $Ba(OH)_2$.

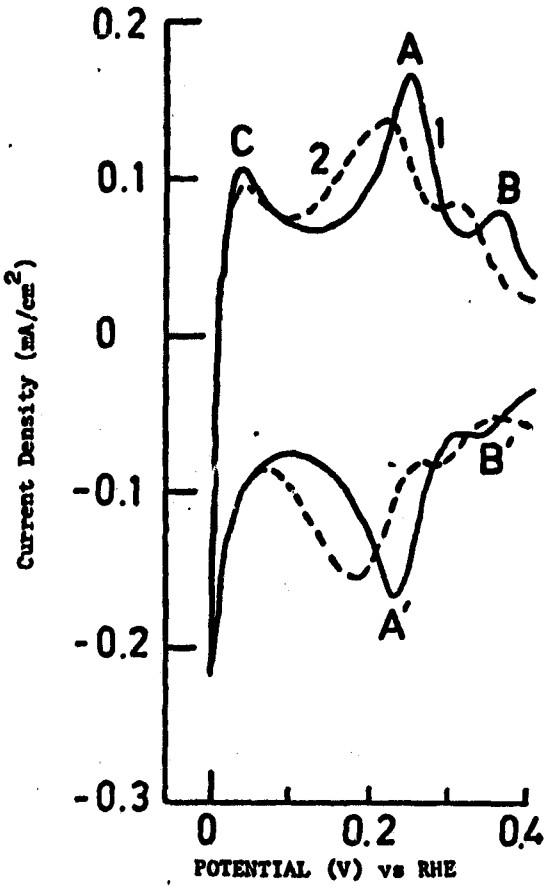

Fig. 11. Voltammograms for Pt in 0.1M NaOH with Ca^{2+} cations added. Curve 1, 0.1M NaOH and curve 2, 0.1M NaOH + 5 × 10^{-3}M $Ca(OH)_2$.

hydrogen adsorption peak to the total charge for hydrogen adsorption is shown to increase linearly with the log of the concentration of sulfate added to the 0.1M $HClO_4$ and HF electrolytes. The specific adsorption of the SO_4^{-2} should follow a Temkin isotherm over this concentration region, and hence the amount of specifically adsorbed sulfate is expected to be a linear function of the log of the concentration of this ion in solution. The linearity in Fig. 13 implies that the charge ratio is linearly dependent on the amount of specifically adsorbed SO_4^{-2}. In principle, the coupling mechanism proposed above should lead to a linear dependence of the charge Q_{IV} under the strong peak *IV* on log $C_{SO_4^{-2}}$ and not the charge ratio Q_{IV}/Q. It is difficult, however, to ensure that the ratio of true-to-apparent electrode area is constant between measurements and hence it has been preferable to plot Q_{IV}/Q. Since the Q_{IV}/Q is rather small compared to unity, a near linear relation is still observed in Fig. 13.

2. *Modification in the hydrogen adsorption energies for sites adjacent to adsorbed anions.*—The adsorption energies for hydrogen on sites adjacent to adsorbed anions are expected to be modified. This effect can occur through changes in the surface electronic structure as well as local changes within the compact double layer, particularly the water dipoles immediately adjacent to the electrode. Such electronic interactions of the anions with hydrogen adsorbed on adjacent sites are similar to those considered by Conway *et al.* (10) in regard to induced heterogeneity. The authors believe this effect to be small except for strongly adsorbed ions such as iodide where very substantial electronic interactions occur between metal surface orbitals and those of the iodide.

3. *Changes in the potential distribution across the interface.*—For ionic double layer effects to have a

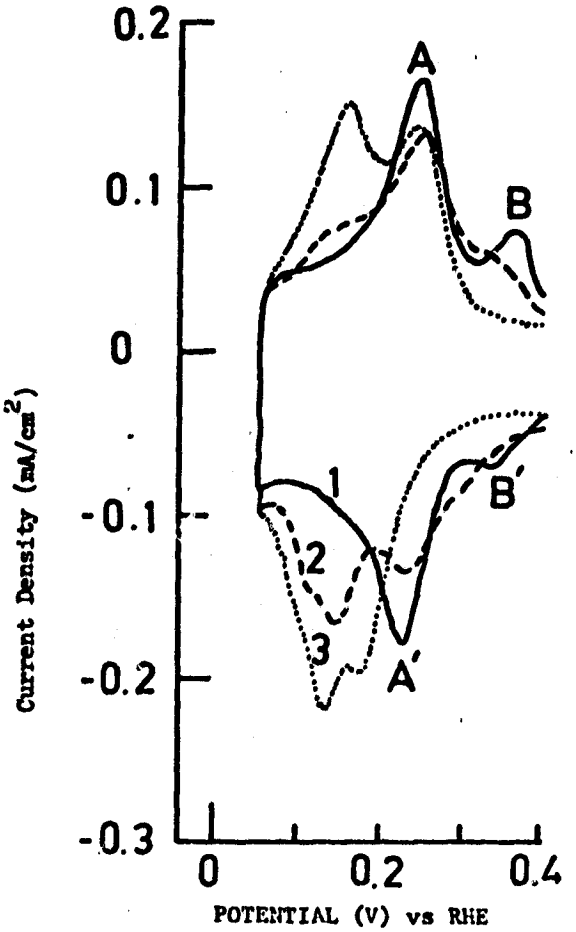

Fig. 12. Voltammograms for Pt in 0.1M NaOH with I^- anions added. Curve 1, 0.1M NaOH; curve 2, 0.1M NaOH + 10^{-5}M NaI; curve 3, 0.1M NaOH + 10^{-3}M NaI.

large influence on hydrogen adsorption requires that the H_{ad} have substantial positive or negative charge. Double layer effect may produce minor shifts in the peak potentials such as observed with some cations in alkaline solutions, but it is doubtful if the M-H dipoles are sufficiently strong to explain the large shifts in the peak potentials observed with anion adsorptions in acid electrolytes.

4. *Surface restructuring.*—During the sweep of the potential into the anodic film formation region, the ions adsorbed on the metal and the anodic film possibly can influence the surface restructuring which occurs during the oxidation and subsequent reduction of the platinum surface. Thus the microstructure and distribution of lattice sites prevailing in the hydrogen adsorption region are probably dependent on the electrolyte composition. This effect can result in changes in the relative peak heights, but should not result in significant shifts in the peak potentials.

Of these various mechanisms for accounting for anion and cation effects, the authors believe that the coupling of the ionic adsorption to the hydrogen adsorption (mechanism 1) is predominant for anion adsorption effects in acid media and that changes in the double layer-potential distributions (mechanism 3) is predominant for the cation adsorption effects on alkaline solutions.

Acknowledgments

The authors are pleased to acknowledge the support of this research by NASA (Ames), and helpful discussions with our colleagues, Drs. B. D. Cahan and R. K. Sen.

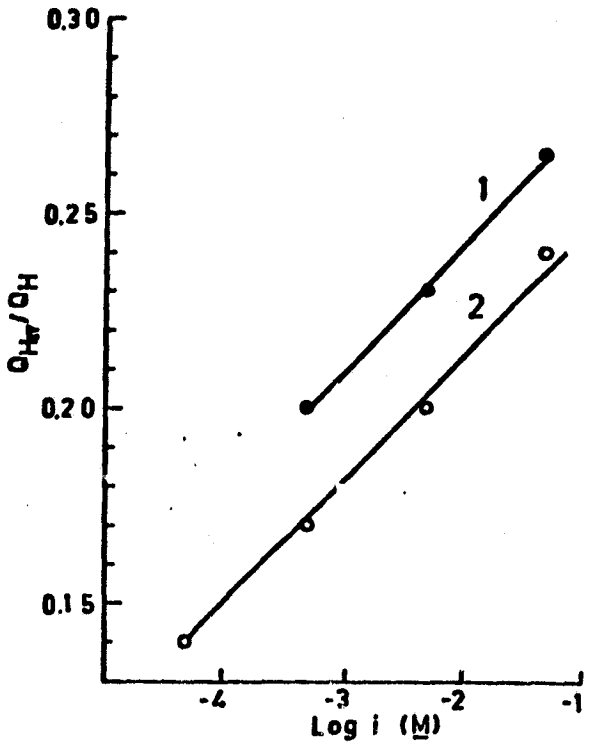

Fig. 13. The plot of the charge under the strongly bound hydrogen peak as a logarithmic function of SO_4^{2-} concentration. The charge is expressed as a ratio $Q_{H_{IV}}/Q_H$ to the total charge for hydrogen chemisorption. Curve 1, SO_4^{2-} in 0.1N $HClO_4$ and curve 2, SO_4^{2-} in 0.1N HF.

Manuscript submitted Sept. 10, 1976; revised manuscript received Jan. 4, 1977.

Any discussion of this paper will appear in a Discussion Section to be published in the June 1978 JOURNAL. All discussions for the June 1978 Discussion Section should be submitted by Feb. 1, 1978.

Publication costs of this article were assisted by Case Western Reserve University.

REFERENCES

1. M. W. Breiter, *Electrochim. Acta*, 8, 925 (1963) and references therein.
2. S. Gilman, *J. Phys. Chem.*, 68, 2098, 2112 (1964).
3. V. S. Bagotzky, Yu B. Vaassilyev, J. Weber, and J. N. Pirtskhalva, *J. Electroanal. Chem.*, 27, 31 (1970).
4. G. D. Azkumbaeva, F. M. Tokabaeva, and D. V. Sokolskii, *Elektrokhimiya*, 6, 777 (1970).
5. S. H. Cadle and S. Bruckenstein, *Anal. Chem.*, 43, 1959 (1971).
6. B. I. Podlovchenko, N. A. Epshtein, and A. N. Frumkin, *J. Electroanal. Chem.*, 53, 95 (1974).
7. K. Kinoshita, J. Lundquist, and P. Stonehart, *J. Catal.*, 31, 375 (1973).
8. A. Hickling, *Trans. Faraday Soc.*, 41, 333 (1945).
9. V. E. Kazarinov, *Z. Phys. Chem. (Leipzig)*, 226, 167 (1964).
10. H. Angerstein-Kozlowska, W. B. A. Sharp, and B. E. Conway, in "Proceedings of the Symposium on Electrocatalysis," M. W. Breiter, Editor, The Electrochemical Society Softbound Symposium Series, Princeton, N.J. (1974) and references therein.
11. B. Conway, H. Angerstein-Kozlowska, W. Sharp, and E. Criddle, *Anal. Chem.*, 45 . 1331 (1973).
12. F. Will, *This Journal*, 112, 451 (1965).
13. M. W. Breiter, "Electrochemical Processes in Fuel Cells," p. 60, Springer-Verlag, New York (1969).
14. P. Stonehart, *Electrochim. Acta*, 15, 1853 (1970).

RECENT ADVANCES IN THE UNDERSTANDING OF ELECTROCATALYSIS AND ITS RELATION TO SURFACE CHEMISTRY

Ernest Yeager

Case Laboratories for Electrochemical Studies and The Chemistry Department, Case Western Reserve University
Cleveland, Ohio 44106

I. INTRODUCTION

Electrosorption plays a key role in electrocatalysis. Little information is available, however, concerning the chemical nature of the interactions of the adsorbed species with the electrode and even less about the adsorption sites. This situation has been detrimental to the development of electrocatalysis as a science. There is a general lack of good molecular level techniques for examining the chemical structure of electrochemical interfaces, analogous to the various spectroscopic techniques which have had such an impact on bulk phase chemistry. In most instances electrochemical techniques provide a sensitive tool for the detection of electrosorption but lack the needed molecular level specificity. Even the charge on electrosorbed species cannot be determined electrochemically because of the difficulty of resolving what fraction of the externally provided charge is transferred to the adsorbed species rather than just residing on the metal surface, compensating the charge of the electrosorbed species and the remainder of the ionic double layer (see e.g., ref. 1-5).

The most promising experimental approach for obtaining such molecular level information is in situ optical spectroscopy. Ultraviolet-visible reflectance spectroscopy and ellipsometric spectroscopy are sensitive to the surface electronic properties. Although a number of electrochemists have made use of these techniques to study electrosorption over the past decade, to date these measurements have provided little further understanding of the electronic features of adsorption. Much of the needed information is contained in the ultraviolet-visible reflectance and ellipsometric data but interpretation is a major problem -- not restricted to electrochemical interfaces.

Vibrational data for adsorbed species would also be very helpful. In situ infrared studies have been carried out (8,9) but have not yielded much information. Solvent absorption is a serious problem. In situ Raman (11,12) and particularly resonant Raman (13), where applicable, appear more promising for adsorbed organic species since solvents such as water are not a problem.

It is unfortunate that the elegant surface physics techniques such as LEED, UPS, XPS and Auger cannot be applied in situ to electrochemical studies. Even so, efforts are in progress to use these techniques in electrochemical studies with special procedures for minimiz-

ing structural changes during the transfer between the electrochemical and high vacuum environments.

The role of adsorbed species and surface layers in electrocatalysis will be reviewed for several electrode systems:

II. THE HYDROGEN ELECTRODE

In recent years, some general insights have been achieved into the relationship of hydrogen electrode kinetics to hydrogen adsorption. For a given mechanism the exchange current density is related to the standard free energy of adsorption of the particular type of adsorbed hydrogen upon which the kinetics depend. This dependence is represented by the familiar volcano shaped curves (14-16), shown in Fig. 1, according to Parsons (14), for the following rate controlling steps:

I.	Discharge:	$H_3O^+ + e^- \rightarrow H_2O + H_{ad}$	(a)
II.	Recombination:	$2H_{ad} \rightarrow H_2$	(b)
III.	Ion-plus atom:	$H_3O^+ + H_{ad} + e^- \rightarrow H_2O + H_2$	(c)

where reaction I may be followed by either II or III. Reaction III may proceed with $(H\text{-}H)^+_{ad}$ as an intermediate; i.e.,

$$H_3O^+ + H_{ad} \rightarrow H_2O + (H\text{-}H)^+_{ad} \qquad (c')$$

$$(H\text{-}H)^+_{ad} + e^- \rightarrow H_2 \qquad (c'')$$

The flat portion of the curves corresponds to the Temkin region of the adsorption isotherm. In constructing the volcano curves the transfer coefficient relating the standard free energy of activation $(\Delta G^\circ)^\dagger$ to the standard free energy change ΔG° has been taken to be 1/2; i.e., $\alpha = \Delta(\Delta G^\circ) = 0.5$. This may be open to question for Reactions II and III. Arguments can be put forth (17), based on Bond's model of non-activated adsorption of type C hydrogen (40), that $(\Delta G^\circ)^\dagger$ approaches ΔG° for Reaction II on some metals. Further it is likely that the activated state for this reaction involves the direct interaction of both hydrogens with the surface rather than an end-on interaction of a H-H intermediate. Consequently, the transfer coefficient α for Reaction III may also approach unity rather than 1/2. Under such circumstances, the volcano curves take on the form (17) indicated in Fig. 2, using a combination of Freiter's data (18) and Ludwig's data (17) (extended to 3M HCl) as a few calibration points.

The experimentally observed behavior of hydrogen overpotential on various metals correlates reasonably well with Fig. 2. Metals such as Hg, Tl, Zn, Cd and Pb which adsorb hydrogen weakly (positive values of ΔG°) have low values for the apparent exchange current density, Tafel

slopes of -2RT/F and Reaction I as rate controlling. Metals such as Pt and the Pt family with ΔG° values close to 0 have high apparent exchange current densities and kinetics which indicate that Reaction II follows Reaction I and is rate controlling. Metals such as Mo, Ta and W which strongly adsorb hydrogen again have low exchange current densities and kinetics which indicate Reaction III follows Reaction I and is rate controlling.

An important implication of the volcano curves is that it is unlikely a catalyst will be found with an exchange current density higher than that for Pt since this metal has ΔG° close to 0. The main thrust of applied research on hydrogen electrocatalysts should be the finding of catalysts with higher exchange currents per unit cost and resistance to poisoning and to loss of area when used in high area forms.

Various authors have examined the discharge step I theoretically, taking into account the possibility of proton tunnelling (for a review, see ref. 20). Bockris and Matthews (21) have proposed the model in Fig. 3. The vertical transition ΔE_0 corresponds to the transfer of an electron from the Fermi level of the metal to the H_3O^+ ion with no change in the reaction coordinate. Radiationless electron transfer (tunnelling) occurs at the intersection of the two Morse curves from the metal to the vibrationally excited H_3O^+. The various electron energy levels in the metal correspond to translation vertically of the Morse curve for the initial state. The principal levels contributing to the discharge current are those within kT of the Fermi level.

Several electrochemists have considered proton tunnelling through the barrier rather than over the barrier. Bockris et al. (21,22) using a symmetrical Eckart barrier have concluded that proton tunnelling is important to hydrogen discharge on Hg and compatible with linear Tafel behavior. Christov (23-25) reached a similar conclusion using symmetrical and asymmetrical Eckhart and parabolic barriers. Conway (26) treated proton tunnelling, assuming the proton to originate from a water molecule immediately adjacent to the surface with a very thin barrier (0.5Å). This model results in high tunnelling probability but high Tafel slopes at low overpotentials and non-linear Tafel behavior at higher overpotentials ($-\eta > 0.5V$), which is contrary to the experimental data for Hg. Conway and Salomon (27) have concluded that proton tunnelling is not important for proton discharge even at temperatures down to -110°C in methanol. (The activation energy is essentially independent of temperature.)

Levich (28) has questioned the validity of using the Gamow tunnelling equation for proton discharge because of complications associated with solvent polarization fluctuations. Bockris and Sen (31) have rebutted this argument by attempting to show that the proton tunnelling occurs in a time considerably less than the 10^{-13}s and hence short compared to the solvent relaxation times.

The Bockris-Matthews model in Fig. 3 does not take into account resonance interactions at the intersection of the Morse curves. Salomon, Enke and Conway (30) and Bockris and Sen (31) have applied the semi-empirical bond-energy bond-order method (BEBO) to calculate the potential energy surface. Bockris and Sen arrive at a value of 15 kcal/mole for the height of the barrier for Hg, which seems reasonable.

Dogonadze, Kuznetsov and Levich (32,33) have treated Reaction I using a quantum statistical mechanical approach which is an extension of their earlier outer sphere electron treatment. The proton as well as electron transfer are assumed to be fast subsystems with the solvent a slow system. Their treatment is interesting but unfortunately does not include the contribution to activation associated with stretching of the H-OH_2 and H-H bonds. The recent quantum statistical mechanical treatment of Kharkats and Ulstrup (34) takes into account not only the bulk solvent polarization contributions but also discrete modes around the reaction centers which they considered to be a solvated $H_9O_4^+$ ion. These authors show that anharmonicity can account for the extended Tafel linearity observed over more than 1V on metals such as Hg.

Hydrogen electrode kinetics are of special interest on Pt because of its high catalytic activity. Various workers (35-37) have found a Tafel slope for the cathodic branch of -RT/2F and high exchange current densities (e.g., $\geq 10^{-2} A/cm^2$). Two explanations have been advanced for this behavior. Schuldiner (35) and Bockris et al. (36) have used a mechanism involving Reactions I and II (discharge followed by atomic recombination) with Reaction II rate controlling. Breiter (38) has proposed pure diffusion control involving dissolved H_2. On the basis of ultrasonic (36) and rotating disk-ring (39,19) measurements, Yeager et al. have proposed that the cathodic process is controlled by combined H_2 diffusion and recombination kinetics. Parsons (14) and Krishtalik (41) have offered theoretical arguments for desorption by Reaction II as rate controlling.

The anodic oxidation of H_2 exhibits first order dependence on H_2 concentration (42) and most workers consider the dissociative adsorption of H_2 (the reverse of Reaction II) as rate-controlling (see e.g., 42-45). Here again, however, the high exchange current density makes it difficult to examine the kinetics without transport of dissolved H_2 to the electrode surface being the predominant control, even with the rotating disk electrode technique (19,42,46), particularly with Pt electrodes which have relatively high area and hence high activity as a result of repeated cycling to anodic potentials prior to the H_2 oxidation measurements.

A problem associated with H_2 formation with the kinetics controlled by Reaction II is that the -RT/2F slope is to be expected with low H(ads) coverage (35). On the other hand, various electrochemical measurements including impedance (e.g. 47), linear sweep voltammetry

(see e.g., 48-51) and charging curves (e.g., 52,53) indicate that total H(ad) coverage is already close to unity at the reversible potential. This problem can be resolved by assuming that two types of H(ads) are involved in the overall electrode process and that the adsorbed hydrogen involved in Reaction II is at low coverage, as suggested by Schuldiner (35,43). The existence of several types of adsorbed hydrogen on Pt appears fairly evident from the various electrochemical measurements of adsorbed hydrogen just cited. Thus the H_2 formation may be represented as follows:

$$H_3O^+ + e^- \rightarrow H_A \qquad (d)$$

$$H_A \rightarrow H_B \rightarrow \cdots H_j \qquad (e)$$

$$H_i + H_j \rightarrow H_2 \qquad (f)$$

where H_i and H_j may or may not be the same; steps d and e are essentially reversible; and one or more of the forms of H(ad) are at high coverage but the sites available for H_i and H_j type adsorption are at low coverage. Considering combined kinetic and diffusion control with Langmuir behavior for H_i and H_j, the current-potential behavior for the anodic as well as cathodic branches is described by the equation

$$\ln[1/(1-\exp\tfrac{2F\eta}{RT})] = -\frac{2F\eta}{RT} + \ln\chi_o \qquad (1)$$

where

$$\frac{1}{\chi_o} = \frac{j}{i_o} + \frac{1}{i_d} \qquad (2)$$

i_d is the anodic diffusion limiting current density for H_2 transport, i_o is the exchange current density for Reaction f, η is the overpotential and the other symbols have their usual meaning. This equation has been tested for Pt by Ludwig et al. (17,19) using the rotating disk technique and fits the data quite well (see Fig. 4). The values of i_o evaluated for Pt in 6.1N HCl for a H_2 pressure of 1 atm at 25°C are $i_o = 8 \times 10^{-3}$ A/cm^2 for Pt not roughened by cycling to anodic potentials.

The question remains open as to what type of adsorbed hydrogen is involved in the desorption reaction f. It is unlikely that H_i and H_j correspond to any of the hydrogen peaks observed by linear sweep voltammetry and other electrochemical techniques on Pt. Nonetheless, it will be helpful to understand the various factors contributing to up to five hydrogen peaks observed in the voltammetry curves. Various explanations have been proposed including different adsorption sites on a given single crystal surface, a distribution of crystallographic surfaces, induced heterogeneity associated with hydrogen adsorption itself (50) and anion adsorption which induces heterogeneity by blocking sites to varying degrees and perturbing adjacent sites (51). The

pronounced dependence of the hydrogen electrosorption on the type and concentration of anion (Fig. 5) indicates that hydrogen adsorption-desorption are coupled to anion desorption-adsorption (51).

In an attempt to resolve this problem, various electrochemists have examined hydrogen electrosorption on single crystal Pt. Will (54) examined the low index planes (100), (110) and (111) and found the same two major peaks on these three orientations although the relative heights depended on the crystal orientation. The single crystal Pt electrodes studied by Will probably did not expose a single crystallographic surface. The distribution of crystallographic surface planes depends on the overall orientation and the extent to which the surface has been cycled to anodic potentials. Will arrived at the conclusion that the strongly adsorbed hydrogen peak IV (Fig. 5) corresponds to the 100 plane and the weakly adsorbed peak I to the (110) plane. Rather analogous results have been reported by Bronel et al. (56) for the (100) and (111) Pt surfaces. These workers used electron microscopy to establish that the surfaces were facet-free. Kinoshita and Stonehart (57) have examined hydrogen adsorption on dispersed Pt as a function of crystallite size and find a dependence which they interpret as further evidence that the multiple peaks result from different surface crystallographic structures.

In contrast, Bagotsky et al. (55) and Conway et al. (50) have concluded from their single crystal Pt studies that there is little difference in the hydrogen adsorption on the (100) (110) and (111) planes. Conway et al. (50) attribute the multiple peaks principally to induced heterogeneity arising from collective long-range electronic interactions.

The probability is high in all of the single crystal studies just cited that the surface prevailing during the electrochemical measurements does not correspond to a single crystal plane. Even if the Pt crystal has only one plane predominant before the electrosorption measurements, these authors generally cycled their electrodes to anodic potentials in the anodic film region to oxidize or desorb interfering surface contaminants and this procedure is likely to cause restructuring.

Recently several groups have attempted to devise techniques which permit the introduction of a single crystal surface of predominantly one plane and free of impurities into an electrochemical environment with a minimum possibility of restructuring and contamination. These include A. Hubbard at the University of California at Santa Barbara (58,59), J. A. Joebstl at Fort Belvoir (60), Lane at United Technology (60) and the author's group at Case Western Reserve University (61). Each group has turned its attention to the (100), (110) and (111) planes of Pt and first establishes that the surface is predominantly one plane using low energy electron diffraction (LEED) and free of surface impurities down to a few percent of a monolayer using Auger

electron spectroscopy.

The results obtained by Ross (62) and in the author's laboratory by O'Grady et al. (63) will be presented in separate papers in this symposium. The key features of the techniques used by O'Grady et al. are vacuum transfer; thin-layer electrochemical cell techniques to avoid contamination; and introduction of the Pt single crystal surfaces into the electrolyte at controlled potentials in the hydrogen adsorption region. In the cyclic voltammetry studies of hydrogen electrosorption, the potential range is restricted to +0.05 to 0.40V vs. RHE to reduce any possible restructuring. The voltammetry curves on the single crystal Pt surfaces retract with repeated cycling, starting with the very first sweep. If the voltage sweep is extended into the anodic film formation region to $\geq$1.4V vs. RHE, the hydrogen adsorption region changes significantly with new peaks appearing or very minor peaks becoming major peaks, depending on the original surface. This is probably the result of restructuring although the possibility exists that oxygen has been irreversibly adsorbed into sites within the surface layer.

On the (100) Pt surface, Hubbard et al. (59), Ross (62) and our group (63) find one predominant peak (Fig. 6) corresponding to the strongly adsorbed hydrogen peak on polycrystalline Pt in acid solutions. The LEED pattern for the Pt (100) indicates a 5 x 20 overlayer mesh (58,64). This surface probably reverts to (1x1) in contract with the electrolyte. On the (111) surface, our group finds only a minor peak corresponding to weakly adsorbed hydrogen while Ross and Hubbard et al. report a major peak. The source of this discrepancy is not fully clear but may be caused by the cycling of the electrode to anodic potentials in the case of Ross' work and possibly also Hubbard et al. Alternatively our (111) Pt surface may have some of the sites blocked by an impurity but on the other hand Auger does not indicate any such impurity. In any event, the presence of only one major peak on the (100) Pt surface provides strong evidence that the principal peaks on polycrystalline Pt correspond to different crystallographic planes.

A number of theorists are presently involved in calculating the relative bond energies for hydrogen and other species on various sites on metal surfaces, using extended Hückel molecular orbital theory, LCAO, and Xα scattering. These types of calculation can contribute substantially to the understanding of electrochemical interfaces. Leban and Hubbard (65) have used extended Hückel molecular orbital theory to predict the most stable sites for various species including H_2O, OH^-, H, the halides and Pt on (111) Pt. The most stable sites for these species are shown in Fig. 7. According to their calculations, the preferred sites for hydrogen adsorption on the (111) surface are in the plane between three adjacent Pt. While substantial questions exist as to the validity of various assumptions in such calculations, nonetheless, they present an important step in the development of a theoretical basis for electrocatalysis. [For a review, see (126,127.)]

C-2

III. THE OXYGEN ELECTRODE

The oxygen electrode reactions are less well understood than for the hydrogen electrode. The pronounced irreversibility of the oxygen electrode reactions at moderate temperatures has severely complicated mechanistic studies. The exchange current densities for the oxgyen electrode are very low -- typically 10^{-10} to 10^{-11} A/cm^2 on an effective catalytic surface such as platinum at room temperature. Consequently the current densities near the reversible potential are generally too low to permit measurements under conditions where the kinetics are sensitive to the reverse as well as forward reactions. Further, the experimentally accessible portions of the cathodic and anodic branches of the polarization curves are sufficiently separated in potential that the surface conditions differ very substantially. Therefore, the cathodic and anodic processes under these conditions are probably not the reverse of each other. To complicate the situation further, the oxygen electrode reactions may proceed through a large number of pathways. This explains why the mechanisms of O_2 generation and reduction are still not fully understood even on platinum, the most extensively used and most studied O_2 electro-reduction catalyst.

Before discussing O_2 electrocatalysis on specific non-metallic surfaces, some of the general features of the possible electrode mechanisms will be considered. O_2 reduction in aqueous solutions requires a strong interaction of O_2 with the electrode surface for the reaction to proceed at a reasonable rate. Three types of models for such interaction have been proposed (66,67). These and the corresponding likely reaction pathways for O_2 reduction are those in Fig. 8. The Griffiths model involves a lateral interaction of the π-orbitals of the O_2 interacting with empty d_{z^2} orbitals of a transition element, ion or metal atom with back bonding from at least partially filled d_{xz} or d_{yz} orbitals of the transition element to the π^* orbitals of the O_2. This type of interaction should lead to a weakening of the O-O bond with a corresponding lengthening of this bond. The Vaska complexes [e.g., $Ir(O_2)Cl(CO)(PPh_3)_2$] appear to form such complexes with O_2 (71,72). These compounds are selective oxidation catalysts for cyclic olefins (73). The formation of a strong metal-to-oxygen interaction results in a weakening of the O-O bond and an increment in the length of this bond (74). Sufficiently strong interaction of this type may lead to the dissociative adsorption of O_2 with probably simultaneous proton addition and valency change of the transition element in the manner represented by Pathway I in Fig. 1, followed by reduction of the $M(OH)_2$ to regenerate the catalyst site. Sandstede et al. (75,76) have attempted to explain oxygen reduction with square pyramidal Co(II), Fe(II) and Fe(III) complexes as well as on the thiospinels on the basis of such π bonding. Tseung, Hibbs and Tantram (77) have proposed that O_2 reduction on Li-doped NiO changes from a non-dissociative to dissociative mechanism above the Neel point (200°C for their ~10-atom % Li-doped NiO) in order to explain the increment in catalytic activity in KOH hydrate melts above the Neel temperature.

With most transition metal catalysts, the most probable structure for O_2 adsorption is the Pauling model (69) in which sp^2 orbitals of O_2 interact with d_{z^2} orbitals of the transition metal. The square pyramidal complexes of Fe(II) and Co(II), which have good activity for O_2 reduction in acid solutions, appear to involve such an end-on interaction on the basis of esr and other evidence (78). This adsorption of O_2 is expected to be accompanied by at least a partial charge transfer to yield a superoxide and then peroxide state, as represented by Pathway II in Fig. 7. The adsorption of the O_2 on the square pyramidal complexes of Fe(II) and Co(II) may lead directly to the superoxide state. With somewhat similar oxyhemoglobin complexes of iron, various workers have proposed that O_2 binding to the iron involves O_2^- or $O_2^=$ states with Fe in the III-valent state (79-81). The change in valency state of the transition metal coupled with the change in O_2 oxidation state during formation of the O_2 adduct corresponds in principal to the redox electrocatalyst concept proposed by Beck et al. (82,83).

The further reduction of the O_2 beyond the peroxide state requires rupture of the O-O bond. Such can occur in Pathway IIB through the formation of O^- or $HO\cdot$ free radicals in solution or the simultaneous reduction-bond cleavage (electrochemical desorption) to yield H_2O or OH^-. Neither of these processes are likely to be sufficiently fast at practical operating potentials for O_2 cathodes but the electrochemical desorption is a better candidate. The free energies of formation of the O^- and $HO\cdot$ free radicals in solution are just too high to achieve sufficiently high concentrations for the subsequent homogeneous reactions to proceed at rates corresponding to reasonable current densities at acceptable electrode potentials. Substantial evidence exists for Pathway IIA yielding solution-phase peroxide for various metallic and non-metallic electrode surfaces. With non-metallic electrodes such as carbon, graphite and lithiated NiO in aqueous alkaline solutions, significant amounts of peroxide are found in solution and the potential under open-circuit conditions follows the Nernst equation predictions for the O_2-HO_2^- couple (see e.g., ref. 84,85) providing the surfaces are free of traces of Pt and other contaminants which catalyze peroxide decomposition or reduction.

Under some circumstances it is possible that the superoxide species O_2^- may desorb to yield the solution-phase species. This ion is formed as a reasonably stable entity during O_2 reduction in aprotic solvents (see e.g., ref. 86-89) and probably in carbonate melts (90). The superoxide ion also has been proposed to be formed in aqueous solutions on Hg (91,92), amalgamated gold (93) and carbon paste (94) cathodes in the presence of surface active agents. Under these circumstances, Divisek and Kastening (91,92) propose that the surfactant molecules displace water molecules from the surface, impeding access of water to the adsorbed O_2^-, and thereby inhibiting further reduction. Dubrovina and Nekrasov (93) have proposed that the O_2^- radical may be stabilized through the formation of a complex with the surfactant molecule. In the absence of adsorbed organic species, however, it does not appear in alkaline solutions that an O_2^- desorption mechanism contributes significantly to the observed current. Rotating disk

experiments have rather clearly demonstrated this for graphite and also gold cathodes (96,97).

Pathway III in Fig. 8 provides an alternate means for bringing about rupture of the O-O bond through the formation of an -O-O-bridge. Such a mechanism may come into play with the proper surface spacing of transition metal atoms or ions in a metal, oxide or thiospinel or in a bimetal complex such as a macrocycle. The formation of the bridge species also requires that the two metal species have partially filled d_{xz} or d_{yz} orbitals to participate in bonding with the sp^2 orbitals of the oxygen. Macrocyclic transition metal complexes of the type M-O_2-M have been synthesized (e.g., see ref. 98-101) and appear to occur naturally in hemeythrin.

For any of the mechanisms in Fig. 8, considerable questions exist as to the reversibility of the O_2 adsorption step at the rather high rates involved with practical O_2 cathodes. For O_2 to bond to M^z will generally require the replacement of a water molecule or anion of the electrolyte -- a situation which would normally be expected to be unfavorable to O_2 unless the O_2 adduct has a pronounced dipolar character ($M^{z+}O\text{-}O^-$) (102,103).

At steady state any peroxide formed on the electrode surface must be subsequently further reduced or decomposed. When the O_2 reduction proceeds entirely through a peroxide state on the electrode surface and/or in the solution, the process is usually referred to as "series" whereas when O_2 reduction proceeds simultaneously by a dissociation step without a peroxide state as well as through a peroxide state, the processes are described as "parallel". Peroxide has been detected in the solution phase during O_2 reduction on many metallic and non-metallic electrodes (e.g., Pt, Au, Ag, Pb, Ni, NiO, carbon, graphite) in various aqueous electrolytes at $T < 100°C$. Consequently little doubt exists that the peroxide mechanism is often functional.

Various workers have used the rotating disk-ring electrode to examine the kinetics of O_2 reduction on a number of metal and non-metal surfaces and particularly to establish whether the series or parallel schemes are applicable. Damjanovic, Genshaw and Bockris (104) proposed that a potential dependent intercept for the plot of i/i_R vs. $1/\sqrt{\omega}$ plot constituted evidence for the parallel mechanism (i=disk current, i_R=ring current, ω=angular rotation rate). The kinetic analysis by Damjanovic et al., however, did not consider a potential dependent electrodesorption of peroxide. When such is included in the analysis, it is found that the series mechanism can also yield a potential dependent intercept (105-107). Wroblowa et al. (106) has called attention to the fact that the correlation of the intercept of the i/i_R vs. $1/\sqrt{\omega}$ plot with the slopes at various potentials can serve as a diagnostic test for the parallel mechanism.

Electrode surfaces on which O_2 reduction proceeds predominantly by the series mechanism through a peroxide intermediate include gold (97, 105,113), graphite and various carbons (84,109-111) including glassy carbon (112). The parallel mechanism appears operative on Pt (108, 114,117), Ir (124), Rh (114), Pt-Rh alloys (116) and Pd (114,115).

Much more complete kinetic data are available for the two-electron O_2 reduction to peroxide on a surface such as gold than for the overall four electron reduction to water or OH^- on a surface such as Pt. The rotating disk-ring studies of Zurilla et al. (97,105) in alkaline solutions have yielded a stoichiometric number (2.0) and Tafel slopes and reaction orders for the forward and reverse reactions which support the following mechanism (97,105):

$$O_2 + e^- \rightarrow O_2^-(ads) \qquad (g)$$

$$2O_2^-(ads) + H_2O \rightarrow HO_2^- + O_2 + OH^- \qquad (h)$$

with reaction g rate controlling and reaction h fast. Reaction h may be multistep. These reactions involve adsorbed O_2^- and not the corresponding solution phase for radicals. Evidence for such can be deduced as follows (97): if a solution phase dismutation reaction equivalent to reaction h were involved, then it must occur within the Nernst boundary layer; otherwise the rotating disk experiments could not indicate two electrons per O_2 reaching the electrode surface. On the other hand, an upper limit can be set for the O_2^- concentration in the solution adjacent to the electrode on the basis of the reversible potential for the O_2/O_2^- couple. Further an upper limit for the second-order solution phase dismutation reaction is known from radiation chemistry studies. This permits an upper limit to be set for the current density compatible with reaction h as a solution phase process. The values so calculated are typically three orders of magnitude below the experimental values (97,118). Thus reaction h must be a heterogeneous one.

The further reduction of HO_2^- to OH^- is first order in HO_2^- and the rate constant has very little potential dependence. This suggests a chemical step preceding the electron transfer as rate controlling; e.g.

$$HO_2^- + H_2O \rightarrow 2OH(ads) + OH^- \qquad (i)$$

In both acid and alkaline solutions hydrogen peroxide is generated during O_2 reduction on Pt. The O_2 reduction to H_2O or OH^- by a parallel pathway not involving H_2O_2 or HO_2^- is predominant on reduced Pt in the absence of adsorbed impurities (108,114,117). A Tafel slope of -RT/F is observed in the region corresponding to the start of anodic film formation where Conway et al. (50) and others (119) assign the structure in the linear voltammetry curves to essentially reversible OH adsorption; i.e., 0.8 to 0.95V vs. RHE. At more cathodic potentials the slope shifts to -2RT/F or a transfer coefficient of 1/2. Similar

behavior has been observed in ~85% H_3PO_4 (108,120-122). Damjanovic et al. (117) have explained this behavior on the basis of the dissociative adsorption of O_2. Specifically Damjanovic et al. (117,124) proposed two possible pathways, expressed for alkaline solutions as follows:

Mechanism I:

$$M + O_2 \rightarrow 2M\text{-}O \quad (j)$$

$$2[M\text{-}O + e^- \rightarrow M\text{-}O^-] \quad (k)$$

$$2[M\text{-}O^- + H_2O \rightarrow MOH + OH^-] \quad (l)$$

$$2[MOH + e^- \rightarrow M + OH^-] \quad (m)$$

Mechanism II:

$$M + O_2 \rightarrow 2M\text{-}O \quad (n)$$

$$2[M\text{-}O + H_2O \rightarrow M\text{-}O\text{-}H\text{-}OH\ ] \quad (o)$$

$$2[M\text{-}O\text{-}H\text{-}OH + e^- \rightarrow M\text{-}O\text{-}H\text{-}OH^-] \quad (p)$$

$$2[M\text{-}O\text{-}H\text{-}OH^- \rightarrow M\text{-}OH + OH^-] \quad (q)$$

$$2[M\text{-}OH + e^- \rightarrow M + OH^-] \quad (r)$$

Mechanism I is similar to that proposed by Krasilshchikov (123) in 1963. With Mechanism I, Damjanovic et al. propose reaction l as rate controlling at low cathodic overpotentials and l. rate controlling at high cathodic overpotentials, thus accounting for the shift in slopes. With Mechanism II, reaction q is rate controlling at low cathodic overpotentials and reaction p at high overpotentials.

Tarasevich (114) has proposed a different pathway for O_2 reduction to water that involves adsorption of O_2 without charge transfer; i.e.,

Mechanism III:

$$M + O_2 \rightarrow M\text{-}O_2 \quad (s)$$

$$M\text{-}O_2 + e^- + M + H_2O \rightarrow MO + MOH + OH^- \quad (t)$$

with the peroxide reaction coupled as follows:

$$M\text{-}O_2 + e^- \rightarrow M\text{-}O_2^- \quad (u)$$

$$M\text{-}O_2^- + e^- + M + H_2O \rightarrow M + HO_2^- + M\text{-}OH^- \quad (v)$$

Tarasevich (114) assumes that the slow steps for both the overall $4e^-$ reduction and the peroxide mechanism are the first electron transfer relations t and v. Tarasevich then considers the effects of surface coverage of M-O and M-OH on the kinetics of these steps assuming that $M\text{-}O_2$ coverage is low and assuming Temkin type behavior with respect to M-O and M-OH. The transition from the low to higher Tafel slope results as M-O coverage becomes significant. The potential region which Tarasevich assigns to M-O formation on Pt, however, is attributed by

Conway et al. (50) and our group (119) to reversible adsorption of MOH^-. The basic concept that the shift in Tafel slope is associated with the reduction of the anodic film, however, appears correct, as has also been proposed by Damjanovic and Genshaw (125).

Time restrictions prevent a discussion of O_2 electrogeneration catalysis.

In summary, the science of electrocatalysis is still in its infancy but there are promising signs on the horizon for more rapid growth, the most significant of which is that theorists, surface physicists and inorganic chemists joining forces with electrochemists to attack this area as part of the overall field of heterogeneous catalysis.

ACKNOWLEDGMENT:

The preparation of this paper has been made possible through support from the U. S. Office of Naval Research and NASA-Ames.

REFERENCES

1. W. Lorenz, Z. Phys. Chem. 248, 161 (1971); 252, 374 (1973); 253, 243 (1973).
2. K. J. Vetter and J. W. Schultze, Ber. Bunsenges. Phys. Chem. 76, 920 (1972)
3. J. W. Schultze and K. J. Vetter, J. Electroanal. Chem. 44, 63 (1973); 53, 67 (1974); Electrochim. Acta 19, 230 (1974).
4. J. W. Schultze and F. D. Koppitz, Electrochim. Acta 21, 327 (1976).
5. A. Frumkin, B. Damaskin and O. Petrii, J. Electroanal. Chem. 53, 57 (1974); Elektrokhim. 12, 1 (1976).
6. J. D. E. McIntyre in "Optical Techniques in Electrochemistry", Vol. 9, R. H. Muller, ed., Advances in Electrochemistry and Electrochemical Engineering, J. Wiley and Sons, New York City, 1973.
7. G. Blondeau and E. Yeager, Progress in Solid State Chemistry 11, 153 (1976).
8. A. Reed and E. Yeager, Electrochim. Acta 15, 1345 (1970).
9. D. Laser and M. Ariel, J. Electroanal. Chem. 41, 381 (1973).
10. K. Egumi, H. Moyazaki and T. Kubota, J. Phys. Chem. 74, 2397 (1970).
11. M. Fleischmann, P. Hendra and A. J. McQuillan, Chem. Phys. Letters 26, 163 (1974).
12. A. J. McQuillan, P. J. Hendra and M. Fleischmann, J. Electroanal. Chem. 65, 933 (1975).

13. C. Hagen and E. Yeager, unpublished data for p-nitroso-dimethyl analine; to be submitted for publication.

14. R. Parsons, Trans. Faraday Soc. 54, 1053 (1958).

15. B. Conway and J. O'M. Bockris, J. Chem. Phys. 26, 532 (1957).

16. L. Krishtalik, Elektrokhim. 2, 616 (1966).

17. F. Ludwig and E. Yeager, "Hydrogen Overpotential on Platinum", Tech. Report 21, U.S. Office of Naval Research Contract N00014-67-C-0389, Case Western Reserve University, Cleveland, Ohio 1 February 1968.

18. M. Breiter, Electrochim. Acta 7, 25 (1962).

19. F. Ludwig, R. K. Sen and E. Yeager, Elektrokhim., in press.

20. R. K. Sen, E. Yeager and W. E. O'Grady, Annual Rev. Phys. Chem. 26, 287 (1975).

21. J. O'M. Bockris and D. B. Matthews, Proc. Roy. Soc. London A292, 479 (1966); J. Chem. Phys. 44, 298 (1966).

22. J. O'M. Bockris, S. Srinivasan and D. B. Matthews, Disc. Faraday Soc. 39, 239 (1965).

23. S. G. Christov, Z. Elektrochem. 62, 567 (1958).

24. S. G. Christov, Electrochim. Acta 4, 306 (1961).

25. S. G. Christov, J. Res. Inst. Catal., Hokkaido Univ. 16, 169 (1968).

26. B. E. Conway, Can. J. Chem. 37, 178 (1959).

27. B. E. Conway and M. Salomon, J. Chem. Phys. 41, 3169 (1964). See also ibid. 68, 2009 (1964); Ber. Bunsenges. Physik. Chem. 68, 331 (1964).

28. V. G. Levich in "Physical Chemistry, An Advanced Treatise", H. Eyring, D. Henderson and W. Jost, eds., Vol. 9B, Chap. 12, Academic Press, New York City, 1970.

29. R. K. Sen, Ph.D. Thesis, University of Pennsylvania, 1972.

30. M. Salomon, C. Enke and B. E. Conway, J. Chem. Phys. 43, 3989 (1965).

31. R. K. Sen and J. O'M. Bockris, Chem. Phys. Letters 18, 166 (1973).

32. R. R. Dogonadze, A. M. Kuznetsov and V. G. Levich, Elektrokhim. 3, 739 (1967).

33. R. R. Dogonadze, A. M. Kuznetsov and V. G. Levich, Electrochim. Acta 13, 1075 (1968).

34. Yu. I. Kharkats and J. Ulstrup, J. Electroanal. Chem. 65, 555 (1975).

35. S. Schuldiner, J. Electrochem. Soc. 99, 488 (1952); 106, 891 (1959); 108, 985 (1961).

36. E. Yeager, T. Oey and F. Hovorka, J. Phys. Chem. 57, 268 (1953).

37. J. O'M. Bockris, I. Ammar and A. Huq, J. Phys. Chem. 61, 879 (1957).

38. M. Breiter, "Transactions of the Symposium on Electrode Processes", E. Yeager, ed., J. Wiley and Sons, New York City, 1961, pp 307-324.

39. F. Ludwig, E. Yeager and C. Lozier, Rev. Polarography (Japan) 14, 94 (1967).

40. G. Bond, "Catalysis by Metals", Academic Press, New York City, 1962, pp. 68-69, 93-98, 174-179.

41. L. J. Krishtalik, in "Advances in Electrochemistry and Electrochemical Engineering", Vol. 7, p. Delahay, ed., J. Wiley and Sons, New York City, 1970.

42. M. P. Makowski, E. Heitz and E. Yeager, J. Electrochem. Soc. 113, 204 (1966).

43. S. Schuldiner, J. Electrochem. Soc. 110, 332 (1963); 115, 362 (1968).

44. V. A. Gromyko, Yu. B. Vassilyev and V. S. Bagotzky, Elektrokhim. 8, 914 (1972).

45. W. Vogel, J. Lundquist, P. Ross and P. Stonehart, Electrochim. Acta 20, 79 (1975).

46. V. S. Bagotzky and N. V. Osetrova, J. Electroanal. Chem. 43, 233 (1973).

47. M. Breiter, H. Kammermaier and C. Knorr, Z. Elektrochem. 57, 6, 399 (1953).

48. R. Woods, J. Electroanal. Chem. 49, 217 (1974).

49. S. Srinivasan and E. Gileadi, Electrochim. Acta 11, 321 (1966).

50. H. Angerstein-Kozlowska, W. B. A. Sharp and B. E. Conway in "Proceedings of the Symposium on Electrocatalysis", M. W. Breiter, ed., The Electrochemical Society, Princeton, N. J., 1974, p. 94.

51. J. C. Huang, W. E. O'Grady and E. Yeager, J. Electrochem. Soc., in press.

52. A. N. Frumkin in "Advances in Electrochemistry and Electrochemical Engineering", Vol. 3, Chap. 5, P. Delahay and C. Tobias, eds., J. Wiley and Sons, New York City, 1963.

53. M. Breiter, G. Knorr and W. Volkl, Z. Elektrochem. 59, 681 (1955).

54. F. Will, J. Electrochem. Soc. 112, 451 (1965).

55. V. S. Bagotzky, Yu. B. Vassilyev and J. I. Pyshnograeva, Electrochim. Acta 16, 2141 (1971).

56. G. Bronel, M. Hain, J. Pesant and G. Peslerbe, Surface Sci. 61, 297 (1976).

57. K. Kinoshita and P. Stonehart, Electrochim. Acta 20, 101 (1975).

58. R. M. Ishikawa and A. T. Hubbard, J. Electroanal. Chem. 69, 317 (1976).

59. A. T. Hubbard, J. A. Schoeffel and H. W. Walter, "Ethylene Hydrogenation and Related Reactions on Single Crystal and Polycrystalline Pt Electrodes", National Meeting, American Chemical Society, New Orleans, Mar. 1977, Abstract COLL. 142.

60. J. A. Joebstl, "Surface Characterization of Electrocatalysts by LEED, Auger Electron Spectroscopy and Related Techniques", First Chemical Congress of North American Continent, Mexico City, Nov. 30-Dec. 5, 1975. Abstract: PHSC-18.

61. J. A. Joebstl, "Surface Research for Development of New Electrocatalysts for Acid Electrolyte Fuel Cells", Army Research Conference, Fort Belvoir, 1976.

62. P. N. Ross, "Electrocatalytic Properties of Single Crystal Pt Surfaces in Aqueous Acid Electrolytes", in Proceedings of the Symposium on Electrode Materials and Processes for Energy Conversion and Storage, National Meeting, The Electrochemical Society, Philadelphia, May 8-13, 1977. Paper No. 343.

63. W. E. O'Grady, M. Y. C. Woo, P. Ll Hagans and E. Yeager, "Electrochemical Hydrogen Adsorption on the Pt (111) and (100) Surfaces", loc. cit. Paper No. 335.

64. W. E. O'Grady, M. Y. C. Woo, P. L. Hagans and E. Yeager, J. Vac. Sci. Technol. 14, 365 (1977).

65. M. A. Leban and A. T. Hubbard, J. Electroanal. Chem. 74, 253 (1976).

66. e.g., J. A. McGinnety, in MTP International Reviews of Science, Inorganic Chemistry Series I, Vol. 5, D. Sharp, ed., Butterworths, London, 1972, p. 229.

67. J. S. Valentine, Chem. Reviews 73, 235 (1973).

68. J. S. Griffiths, Proc. Roy. Soc. (A) 235, 73 (1956).

69. L. Pauling, Nature 203, 182 (1964).

70. E. Yeager, "Mechanisms of Electrochemical Reactions on Non-Metallic Surfaces", in Electrocatalysis on Non-Metallic Surfaces, NBS Special Publication 455, 1976, pp 203-219.

71. L. Vaska, Science 140, 809 (1963).

72. J. McGinnety, R. Doedens and J. Ibers, J. Amer. Chem. Soc. 88, 3511 (1966).

73. e.g., J. Collman, M. Kubola and J. Hosking, ibid. 89, 4809 (1967).

74. J. McGimpsey, N. Payne and J. Ibers, ibid. 91, 6301 (1969).

75. H. Behret, H. Binder and G. Sandstede, in Proc. of the Symposium on Electrocatalysis, M. Breiter, ed., The Electrochemical Society, Princeton, N. J. 1974, pp. 319-338.

76. H. Behret, H. Binder and G. Sandstede, Electrochim Acta 20, 111 (1975).

77. A. Tseung, B. Hobbs and A. Tantram, ibid. 15. 473 (1970).

78. See e.g., B. Hoffman, D. Diemente and F. Basolo, J. Amer. Chem. Soc. 92, 61 (1970).

79. J. J. Weiss, Nature 203, 183 (1964).

80. J. Wittenberg, B. Wittenberg, J. Parnach and W. Blumberg, Proc. Nat. Acad. Sci. 67, 1846 (1970).

81. E. I. Ochiai, J. Inorg. Chem. 36, 2129 (1974).

82. F. Beck, W. Dammert, J. Heiss, H. Hiller and R. Polster, Z. Naturforsh, 28A, 1009 (1973).

83. F. Beck, Ber. Bunsenges. Physik. Chem. 77, 353 (1973).

84. E. Yeager, P. Krouse and K. Rao, Electrochim. Acta 9, 1057 (1964).

85. E. Yeager and A. Kozawa, "Kinetic Factors in Fuel Cell Systems: The Oxygen Electrode", Proc. 6th AGARD Meeting, Cannes, 1964, Pergamon Press, Oxford, 1965, pp. 769-793.

86. See e.g., D. L. Maricle and W. G. Hodgson, Anal. Chem. 37, 1562 (1965).

87. D. T. Sawyer and J. C. Roberts, J. Electroanal. Chem. 12, 90 (1966).

88. M. E. Peover and B. S. White, Electrochim. Acta 11, 1061 (1966).

89. L. N. Nekrasov, L. Pukhanova, N. Dubrovina and L. Vykhodtseva, Elektrokhim. 6, 388 (1970).

90. J. Appleby, "Molten Carbonate Fuel Cells" in Conference Proceedings, Fuel Cell Catalysis Workshop, Electric Power Research Institute, Palo Alto, California, EPRI SR-13, Special Report, August 1975, pp. 153-6.

91. B. Kastening and G. Kazemifard, Ber. Bunsenges. Physik. Chem. 74, 551 (1970).

92. J. Divisek and B. Kastening, J. Electroanal. Chem. 65, 603 (1975).

93. N. I. Dubrovina and L. N. Nekrasov, Elektrokhim. 8, 1503 (1972).

94. M. Brezina and A. Hofanova-Matejkova, J. Electroanal. Chem. 44, 460 (1973).

95. I. Morcos and E. Yeager, Electrochim. Acta 15, 953 (1970).

96. E. Yeager, "Oxygen Electrode Kinetics on Various Electrode Surfaces", in Conference Proceedings, Fuel Cell Catalysis Workshop, loc. cit., pp. 49-59.

97. R. W. Zurilla, R. K. Sen and E. Yeager, J. Electroanal. Chem. Soc., submitted for publication.

98. E. I. Ochiai, Inorg. Nucl. Chem. Letters 10, 453 (1974).

99. T. G. Traylor and C. K. Chang, J. Amer. Chem. Soc. 95, 5810 (1973).

100. M. J. Bennett and P. B. Donaldson, J. Amer. Chem. Soc. 93, 3307 (1971).

101. W. P. Schaefer, Inorg. Chem. 7, 725 (1968).

102. M. C. Stynes and J. A. Ibers, ibid. 94, 5125 (1972).

103. W. Bringar, C. Chang, J. Gerbel and T. Traylor, ibid. 96, 5597 (1974).

104. A. Damjanovic, M. Genshaw and J. O'M Bockris, J. Chem. Phys. 70, 3761 (1966).

105. R. Zurilla and E. Yeager, "Oxygen Electrode Kinetics on Gold", Technical Report 23, U.S. Office of Naval Research Contract N0014-67-C-0389, Case Western Reserve University, Cleveland Ohio, May 1969.

106. N. S. Wroblova, Y. D. Pan and G. Razumney, J. Electroanal. Chem. 60, 195 (1976).

107. M. R. Tarasevich, K. A. Radyushkina, V. Yu. Filinovski and R. Kh. Burshtein, Elektrokhim. 6, 1522 (1970).

108. J. C. Huang, R. K. Sen and E. Yeager, "Oxygen Reduction on Pt in 85% H_3PO_4", National Meeting, The Electrochemical Society, Philadelphia, May 8-13, 1977, paper 300. Extended abstracts, pp. 762-3.

109. M. O. Davies, M. Clark, E. Yeager and F. Hovorka, J. Electrochem. Soc. 106, 56 (1956).

110. I. H. Morcos and E. Yeager, Electrochim. Acta 15, 953 (1970).

111. M. R. Tarasevich, F. Z. Sabirov, A. P. Mertsalova and R. Kh. Burshtein, Elektrokhim. 6, 1522 (1970).

112. R. J. Taylor and A. A. Humffray, J. Electroanal. Chem. 64, 63, 85, 95 (1975).

113. M. R. Tarasevich, K. A. Radyushkina, V. Yu. Filinovskii and R. Kh. Burshtein, Elektrokhim. 6, 1522 (1970).

114. M. R. Tarasevich, ibid. 9, 599 (1973).

115. M. R. Tarasevich and V. S. Vilinskaya, ibid. 8, 1489 (1972); 9, 98 (1973); 9, 1187 (1973).

116. M. R. Tarasevich and K. A. Radyushkina, ibid. 7, 248 (1971).

117. A. Damjanovic, M. A. Genshaw and J. O'M. Bockris, J. Electrochem. Soc. 114, 466 (1967); 114, 1107 (1967).

118. R. K. Sen, J. Zagal and E. Yeager, Inorganic Chem., submitted for publication.

119. J. Horkans, B. D. Cahan and E. Yeager, Surface Sci. 46, 1 (1974).

120. W. M. Vogel and J. T. Lundquist, J. Electrochem. Soc. 117, 1512 (1970).

121. A. J. Appleby, ibid. 117, 328 (1970).

122. H. R. Kunz and G. A. Gruver, ibid. 122, 1279 (1975).

123. A. I. Krasilshchikov, Zhur. Fiz. Khim. 37, 531 (1963).

124. A. Damjanovic, A. Dey and J. O'M. Bockris, Electrochim. Acta 11, 791 (1966). See also J. Electrochem. Soc. 113, 739 (1966).

125. A. Damjanovic and M. A. Genshaw, Electrochim. Acta 15, 1281 (1970).

126. G. Blyholder, in Modern Aspects of Electrochemistry, No. 8, Chapt. 1, J. O'M. Bockris and B. E. Conway, eds., Plenum Press, New York City, 1972.

127. R. P. Messmer, "Theoretical Models of Chemisorption on Metal Surfaces" in Proceedings of the Symposium on Electrode Materials and Processes for Energy Conversion and Storage, The Electrochemical Society, May 1977. Paper No. 333.

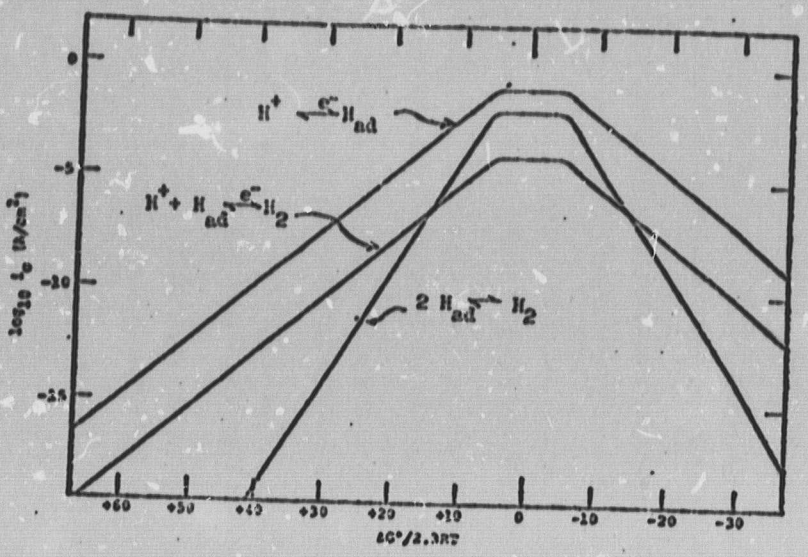

Fig. 1. Exchange currents at the hydrogen electrode and the standard free energy of adsorption of hydrogen.

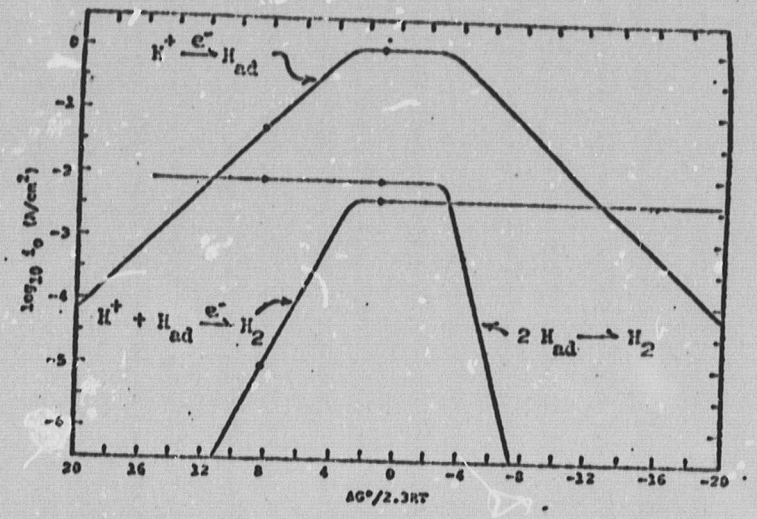

Fig. 2. Volcano curves in 3M HCl with $\alpha_I = 0.5$; $\alpha_{II} = 1$; $\alpha_{III} = 1$. [Ludwig and Yeager(17)].

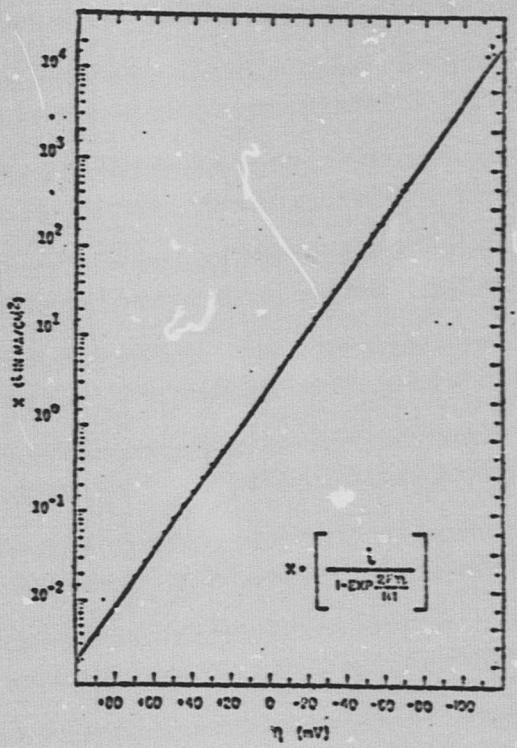

Fig. 4. Hydrogen electrode kinetics on Pt(19). Rotating Disk technique. Rotation rate: 187 Hz; T = 25 C; 6.1 M HCl. IR corrected. [see eqs. 1, 2 in text.]

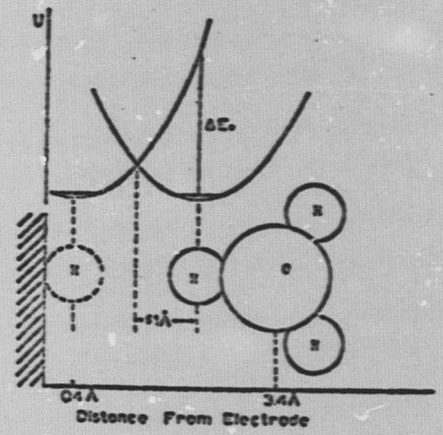

Fig. 3. Bockris-Matthews model for proton discharge (21).

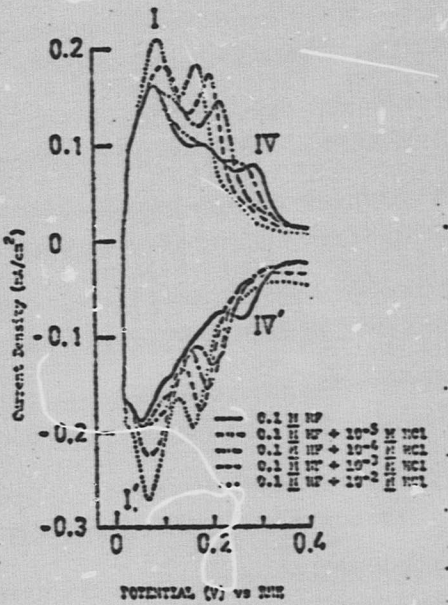

Fig. 5. Voltammograms for Pt in 0.1N HF plus HCl [Huang et al.(51)]

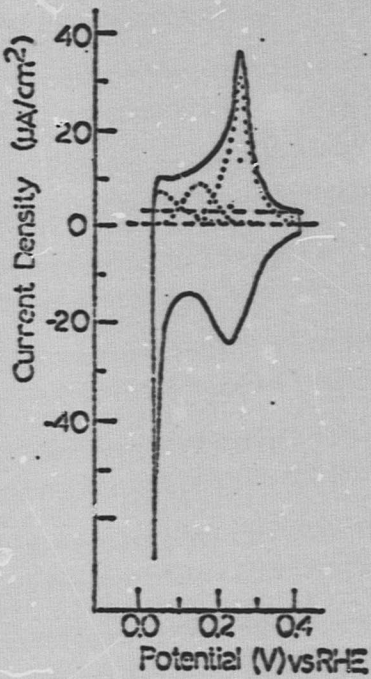

Fig. 6. Voltammogram for clean Pt(100-5x1) in 0.1N H_2SO_4. Sweep rate: 50mV/s.

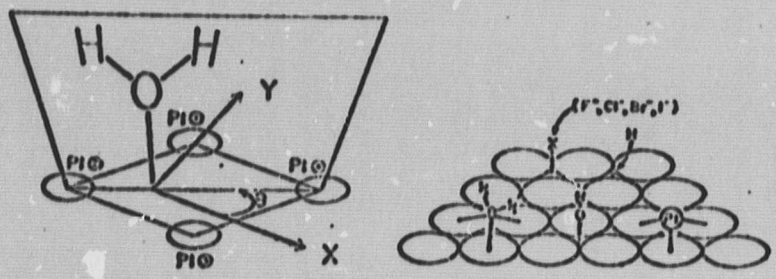

Figure 7. Adsorption sites on Pt (111) for various species. [Leban and Hubbard (65)].

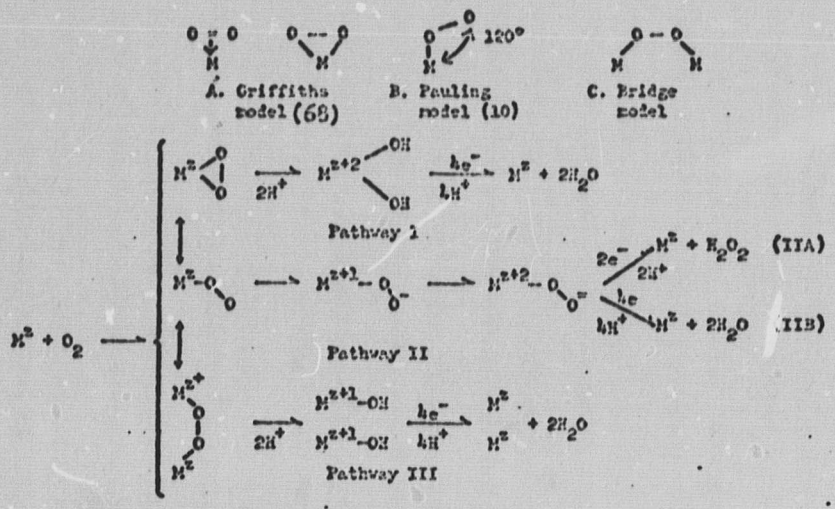

Figure 8. Reaction pathways for O_2 electroreduction. [Yeager (70)].

ELECTROCHEMICAL HYDROGEN ADSORPTION ON THE Pt (111) AND (100) SURFACES

W. E. O'Grady, M.Y.C. Woo, P.L. Hagans and Ernest Yeager
Case Laboratories for Electrochemical Studies
and Chemistry Department, Case Western Reserve
University, Cleveland, Ohio 44106

Hydrogen adsorption on platinum electrodes is of particular interest to electrochemists because of the important role it plays in the electrocatalytic behavior of this metal. Hydrogen is deposited at underpotentials on Pt, giving rise to multiple peaks in the cyclic voltammograms of both polycrystalline (1) and single crystal platinum (1,2). A typical voltammetry curve for polycrystalline platinum under ultra clean conditions in H_2SO_4 is shown in Figure 1. Various workers have proposed explanations for these peaks which include: different adsorption sites on a particular crystallographic surface orientation; induced heterogeneity associated with the perturbation of adjacent sites by the adsorbed hydrogen itself (1); and the adsorption of anions which create further surface heterogeneity by blocking some sites and perturbing adjacent sites (3). The situation is further complicated by the fact that in acid solution the potential of zero charge (PZC) for Pt falls within the hydrogen adsorption-desorption region. This leads to a pronounced dependence of the hydrogen electrosorption on the type and concentration of anion in the electrolyte. Furthermore, it indicates that the hydrogen adsorption-desorption is coupled with anion desorption-adsorption (3).

The questions of intrinsic heterogeneities associated with different crystal faces and site variation on a given crystallographic orientation should be amenable to study on single crystal surfaces. Previous studies have generally shown changes only in the relative peak heights in the voltammetry curves while retaining most of the peaks observed on polycrystalline Pt (1,2). It is very unlikely that unique crystallographic surfaces have been examined previously. Prior to the observation of the electrochemical adsorption of hydrogen it is customary to cycle the electrode to anodic potentials in order to desorb and oxidize impurities initially present on the Pt surface. At these anodic potentials the Pt surface is oxidized and when the surface is subsequently reduced during the hydrogen adsorption measurements the surface is restructured.

Uncertainties concerning the surface structure in Pt single crystal studies can be virtually eliminated by preparing clean single crystal surfaces in ultra high vacuum, where the surface structure is determined by LEED and the surface composition monitored by Auger electron spectroscopy. These samples are then transferred into an electrochemical environment avoiding contamination and oxidation of the surface. The possibility of chemical restructuring of the surface is minimized by never allowing the electrode to see potentials anodic to the hydrogen adsorption region. The problem of impurities

originating from the electrolyte phase can be virtually eliminated through the use of the thin-layer electrochemical cell technique which was first suggested by Hubbard (4).

This paper describes the design of the LEED-Auger-thin layer electrochemical (TLE) system and our results on Pt(111) and Pt(100) surfaces.

EXPERIMENTAL

The LEED-Auger-TLE system used in this work is shown schematically in Figure 2a. The all-metal UHV 10^{-10}torr(10^{-8}Pa) system has two individually pumped chambers which are completely isolated by an all-metal bakeable valve through which the sample may be transferred. The LEED-Auger electron spectrometer is housed in one chamber and the electrochemical thin-layer cell and other sample preparation methods are housed in the other.

The LEED-AES is a standard Varian 4-grid retarding-field analyzer. The sample holder is a modified Varian manipulator which allows the sample to be removed for transfer to the second chamber while retaining the features of cooling the sample to 100K and heating it to 1200K.

In the second chamber is a liquid-nitrogen-cooled manipulator which allows the sample to be removed for transfer and also positions the sample for argon-ion sputtering or for use in the thin-layer cell. The transfer of the sample from the LEED-AES chamber to the electrochemical chamber and back is accomplished by a spring-clip holder mounted on a wand which is actuated magnetically from outside the vacuum system.

The samples are prepared by spark cutting a slice about 1mm thick from a Pt single crystal (obtained from Materials Research Corporation) after it has been oriented ($\pm 0.5°$) by Laue X-ray back scattering. The samples are spot welded to a 1 mil Pt foil, mechanically polished and finally they are spot welded to the transferable Mo sample holder. Just prior to placement in the vacuum system the samples are etched briefly in aqua regia.

After the samples are transferred into the vacuum system the surfaces are cleaned by prolonged argon-ion bombardment (energy ~350 eV) and then annealed at 900C to obtain a sharp LEED pattern. The primary surface contaminant is carbon which diffused to the surface from the bulk of the Pt metal. The Auger spectrum from a clean Pt surface as shown in Figure 4 and is identical to those published previously (7).

The electrolyte injection and thin-layer cell are shown schematically in Figure 2b. The 0.1 N H_2SO_4 electrolyte was prepared using ultrapure acid (Baker Ultrex H_2SO_4) and pyrolyzed water which was prepared following the method of Conway(5). This solution was deaerated and pre-electrolyzed for a minimum of 24 hours in an all-glass vessel before it was introduced into the thin-layer cell by an all Teflon-glass system. Several microliters of solution are placed on the palladium counter-reference electrode with the micrometer syringe and then the palladium

electrode is brought up through the gate valve into contact with the Pt sample to form the thin-layer cell. Prior to the electrolyte being brought into contact with the single crystal electrode, the two electrodes are connected to the potentiostat with a 500 ohm resistor across them and the potential applied to a value in the double-layer region 400 mV (RHE). This prevents any possible excursion of the Pt electrode into oxidizing potential regions which may lead to restructuring of the electrode surface.

There are two important considerations which lead to the choice of the thin-layer technique for these experiments. The first is that the small volume of electrolyte used in the cell will introduce a minimum amount of electrolyte into the vacuum system, only about 10^{-3}ml. The second is the ubiquitous problem of impurities in the electrolyte. Approximately 10^{-9} mole/cm^2 of impurities are required to form a monolayer on the surface. If these 10^{-9}moles of impurities arose completely from the solution in the cell (10^{-3}ml), the concentration of the impurity which could be tolerated is of the order of 10^{-3} molar (M) which is a high impurity concentration. Hence the thin-layer cell is far less susceptible to impurity contamination than the conventional electrochemical cell. The normal operation of a thin-layer cell requires a capillary connection to an external reference electrode. It is a difficult problem to introduce this capillary into the vacuum system and maintain the vacuum integrity of the system. This problem has been overcome in our experiments by combining the counter and reference electrodes as a single palladium-hydrogen alloy electrode. Also, the counter-reference electrode surface must be as clean as the electrode surface being studied. In order to insure this, the counter-reference electrode is cleaned by argon ion sputtering and then is maintained in a hydrogen atmosphere prior to its use.

The procedure followed in these experiments is as follows:

1. The platinum single crystal samples are introduced into the sample preparation chamber.
2. The system is evacuated and baked until the pressure after cooling is in the 10^{-10}torr region.
3. The sample is argon-ion sputtered.
4. The sample is transferred to the LEED-AES chamber and the Auger spectrum is recorded. If it is clean, the sample is annealed at $\sim$ 900C, the Auger spectrum is run again and the cleanliness is checked and the LEED pattern observed. If the surface is not clean, the entire process is repeated until a clean surface is obtained.
5. After cleaning, the sample is returned to the preparation chamber and positioned in the thin-layer cell.

6. The preparation chamber is brought to atmospheric pressure with ultrapure argon.

7. The electrochemical characterization of the sample is carried out.

8. The preparation chamber is then re-evacuated and the sample returned to the first chamber for further examination by Auger and LEED.

RESULTS

The use of cyclic voltammetry to characterize the adsorption and desorption of hydrogen on platinum is now well documented (1,2, 3). A typical voltammogram of polycrystalline Pt in 0.1 N H_2SO_4 is shown in Figure 1. This scan was obtained using conventional electrochemical methods taking special precautions to minimize impurities (3). This voltammogram contains all of the fine structure which has been found for platinum in clean H_2SO_4 solutions (1,3). Voltammograms showing this characteristic structure, especially in the hydrogen adsorption/desorption region, have generally not been obtained using thin-layer electrochemical techniques (see e.g. 6). In Figure 3 is shown a typical voltammogram for polycrystalline Pt in 0.1 N H_2SO_4, observed both in the hydrogen adsorption-desorption region and in the oxide formation-reduction region. Hence it is possible to utilize the Pd-H alloy electrode as a combined counter-reference and to study hydrogen adsorption-desorption phenomena in this thin layer electrochemical cell.

Figure 5 shows the electrochemical adsorption of hydrogen on clean Pt(111) in 0.1 N H_2SO_4 obtained on the first scan. The scan begins at +0.4 V (RHE) going cathodic, toward smaller values of potential and shows a hydrogen adsorption peak (b) at ~0.10 V and then hydrogen evolution at ~ 0.05 V. The scan then reverses and proceeds in the anodic direction, showing first a pronounced peak due to the oxidation of solution phase H_2 produced during the initial cathodic portion of the sweep and then a peak (a) at ~0.12 V due to the desorption of hydrogen. The charge under the anodic peak is estimated to be about 25$\mu C/cm^2$. Assuming 15.0×10^{14} atoms/cm^2 on the Pt(111) surface and one hydrogen atom per Pt atom gives a coverage of about 0.1. This rather minor coverage may arise from several sources. Although the Pt(111) gave very sharp diffraction spots and a rather low background intensity, this does not insure that the surface has a high degree of perfection. This ability to determine the perfection of the surface lattice from visual observation of the LEED patterns has received severe criticism (8) and it has been shown that the intensity distribution of the various spots in the pattern as a function of the electron energy must be studied in order to make any definitive statements concerning the surface lattice perfection (8,9). At this time we cannot make any comment

on what the real contribution of imperfections might be. Samples which have been well annealed at high temperature as the samples in this study were, usually exhibit a highly defect-free surface (8). A second possible factor, which could be contributing, is the edges of the single crystal sample. In our earlier report (10) it was indicated that the electrolyte did not spread properly on the clean Pt(111). The suggestion here is that the electrolyte has spread over the edges of the crystal and the area at the edges is contributing the minor hydrogen adsorption observed here.

The second explanation for the hydrogen adsorption seems the more plausible at this time. Gas phase studies indicate that hydrogen does not readily adsorb on clean Pt(111) (7,11). However, increased imperfection in the Pt(111) surface created either by sputtering without annealing (14) or by using stepped surfaces (15) leads to increased hydrogen adsorption as measured by flash desorption.

Figure 6 shows the first sweep obtained on Pt(100) in 0.1 N H_2SO_4 in the hydrogen electrosorption region. Again the scan was begun at 0.4 V(RHE) and swept cathodic, giving a hydrogen adsorption peak at ~ 0.2 V and then hydrogen evolution at ~ 0.05 V. In the reverse scan proceeding in the anodic region, an initial contribution from H_2 oxidation is observed and then the very pronounced hydrogen desorption peak is observed at ~ 0.28 V. The charge ratio $Q_{cath}/Q_{anod} \approx 1$ and amounts to ~ 60μC/cm^2. Assuming 13.1 x 10^{14} atoms/cm^2 on the Pt(100) surface and one hydrogen atom per Pt atom gives a coverage of 0.3. The position of this peak corresponds to the peak which is normally attributed to the strongly adsorbed form of hydrogen. There may be some slight contribution of weakly adsorbed hydrogen in this scan but further efforts are required to completely establish this possibility. Flash desorption results in the gas phase on Pt(100) (12,13) show this surfact to be covered by about 0.3 monolayer of hydrogen at room temperature, in very good agreement with the electrosorption results presented here.

The effects of cycling have also been examined. The voltammogram for Pt(111) after cycling to an anodic limit of 1.4 V(RHE) for ten cycles is shown in Figure 7. A definite increase in the amount of adsorbed hydrogen is seen. The weakly adsorbed peak has grown and become more defined and a definite peak has begun to appear at the position of the strongly adsorbed hydrogen.

This set of results on Pt(111) and Pt(100) indicate that the surface orientation has a pronounced effect on hydrogen adsorption. The effect of even slight cycling upon these surfaces is dramatic leading to increased hydrogen adsorption as seen in the changes of peak heights as well as the addition of peaks at new potentials for a given surface. The necessity of conducting experiments at this level of purity becomes much more apparent in the light of the present results. In order to establish the details, extensive work

is required, especially on the effects of cycling and the role of imperfections in adsorption. The latter problem will be studied by using stepped surfaces. These experiments are presently underway in this laboratory.

ACKNOWLEDGMENT:

The authors are pleased to acknowledge the support of this research by ONR, NASA-Ames and the Diamond Shamrock Corp., the latter through a fellowship to one of the authors (M.Y.C.W.). The authors express thanks to General Motors and Union Carbide for grants that helped with the purchase of equipment.

REFERENCES

1. H. Angerstein-Kozlowska, W.B.A. Sharp and B. E. Conway, in Proceedings of the Symposium on Electrocatalysis, ed. M.W. Breiter. (Electrochemical Society, N.J. 1974). p. 94.

2. F. G. Will, J. Electrochem. Soc., 112 , 451 (1965).

3. J. C. Huang, W. E. O'Grady and E. Yeager, J. Electrochem. Soc., in press.

4. A. T. Hubbard, Crit. Rev. Anal. Chem., 3, 201 (1973).

5. B.E. Conway, H. Angerstein-Kozlowska, W. B. A. Sharp and E. Criddle, Anal. Chem., 45, 1331 (1973).

6. R. F. Lane and A. T. Hubbard, J. Phys. Chem., 79, 808 (1975).

7. S. L. Bernasek and G. A. Somorjai, J. Chem. Phys., 62, 3149 (1975).

8. F. Jona, Surface Sci., 8, 478 (1967).

9. R. Heckingbottom, Surface Sci., 17, 394 (1969).

10. W. E. O'Grady, M.Y.C. Woo, P.L. Hagans and E. Yeager, J. Vac. Sci. Technol. 14, 365 (1977).

11. B.E. Nieuwenhuys, Surface Sci., 59, 430 (1976).

12. K. E. Lu and R. R. Rye, Surface Sci., 45, 677 (1974).

13. F. P. Netzer and G. Kneringer, Surface Sci., 51, 526 (1975).

14. K. Christmann, G. Ertl and T. Pignet, Surface Sci., 54, 365 (1976).

15. K. Christmann and G. Ertl, Surface Sci., 60, 365 (1976).

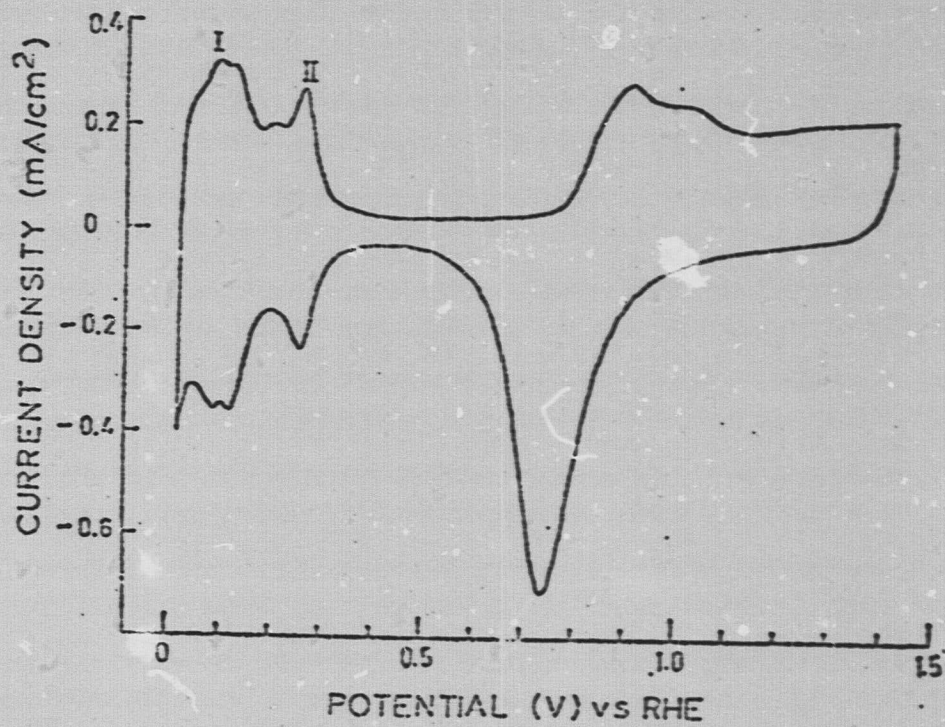

Figure 1. Voltammetry curve for polycrystalline Pt in 0.1 N H_2SO_4. Sweep rate 100 mV/sec. Peaks I to IV: hydrogen electrosorption region. Structure at more anodic potentials is anodic film formation and reduction.

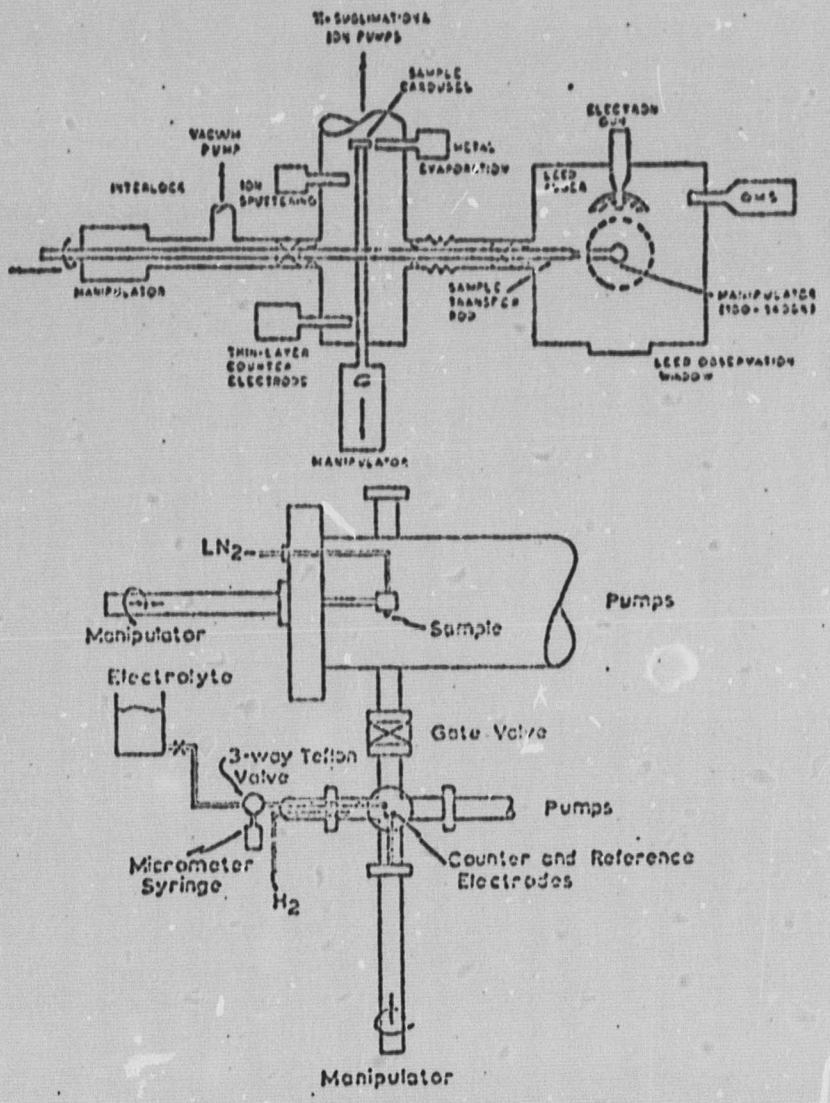

Figure 2. Schematic drawings of (a) the LEED-Auger-thin layer electrochemical system and (b) details of the solution injection and thin-layer cell system.

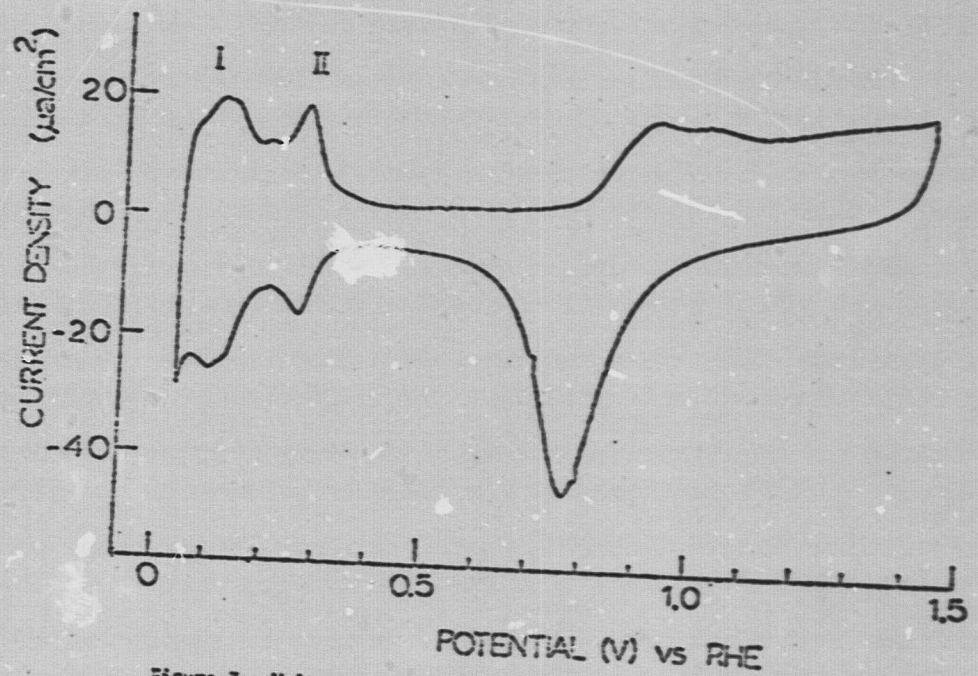

Figure 3. Voltammetry curve for polycrystalline Pt in 0.1 N H_2SO_4 in a thin-layer cell with a Pd-H counter-reference electrode (gap 10^{-3} cm); sweep rate 20mV/sec.

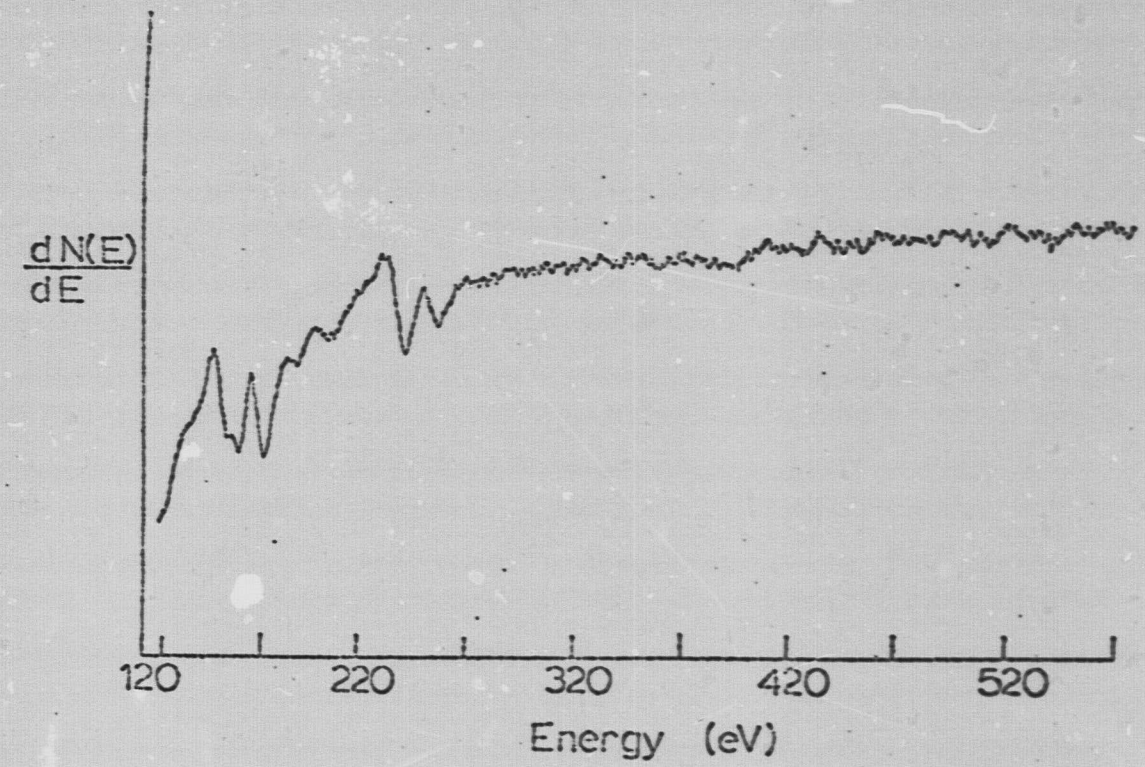

Figure 4. Auger spectrum for clean platinum.

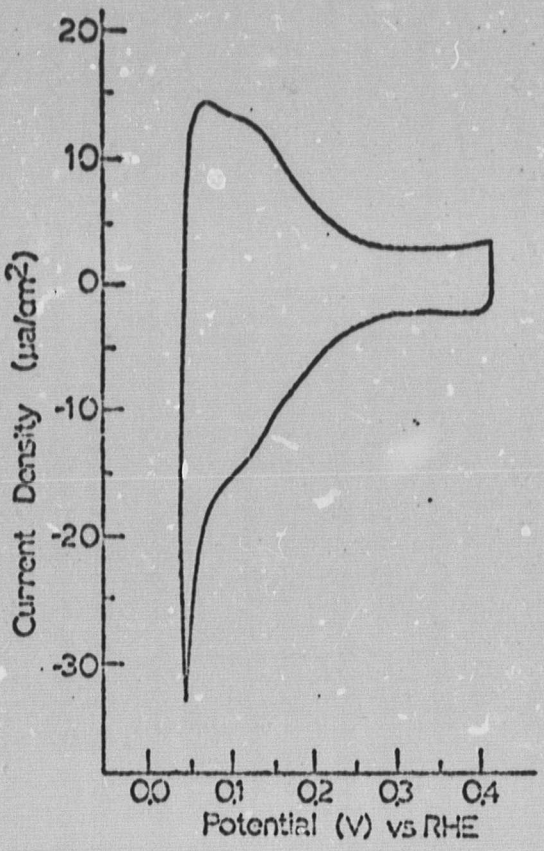

Figure 5. Hydrogen electrosorption on clean Pt(111) in 0.1 N H_2SO_4 using the LEED-AES-thin-layer electrochemical system. Sweep rate 100 mV/sec.

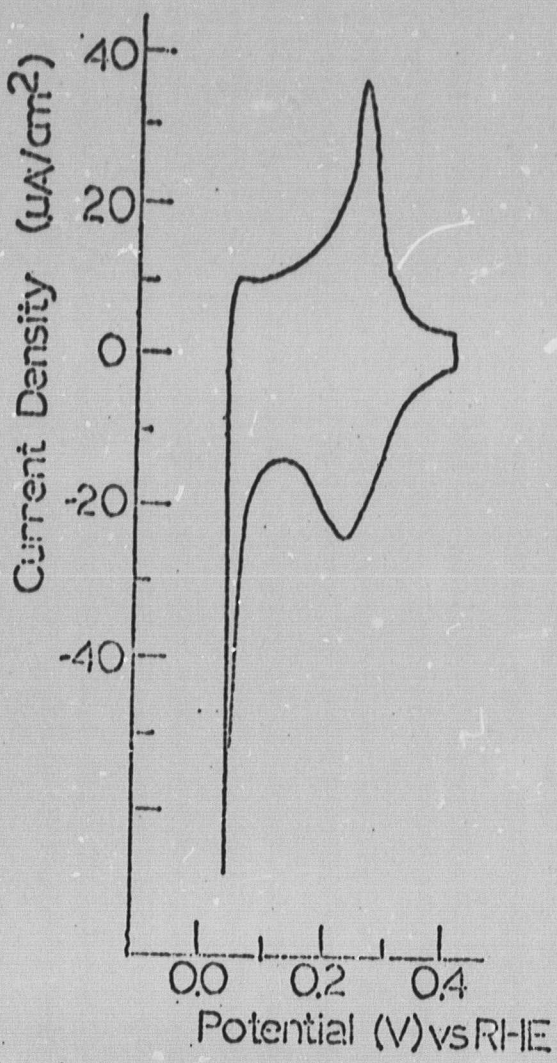

Figure 6. Hydrogen electrosorption on clean Pt(100) (5 x 20) in 0.1 N H_2SO_4 using the LEED-AES-thin-layer electrochemical system. Sweep rate 50 mV/sec.

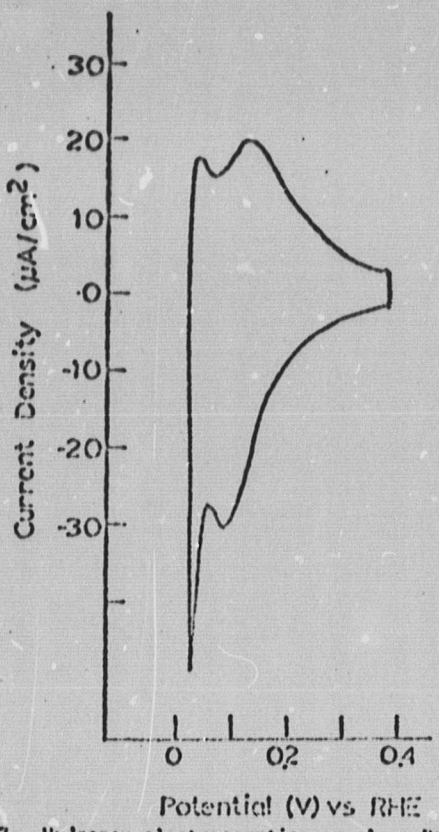

Figure 7. Hydrogen electrosorption on clean Pt(111) in 0.1 N H_2SO_4 after ten cycles using the LEED-AES-thin-layer electrochemical system. Sweep rate 50 mV/sec.

Hydrogen Adsorption on Single Crystal Platinum

E. Yeager,* W. E. O'Grady,* M. Y. C. Woo,* and P. Hagans*

Case Laboratories for Electrochemical Studies and Department of Chemistry, Case Western Reserve University, Cleveland, Ohio 44106

Various electrochemists (1-5) have examined the role of surface structure in electrocatalysis but the results have not been highly conclusive. Recently more sophisticated efforts have been made to determine the role of crystal orientation (6-8). This note reports the results of studies of H electrosorption on Pt(111), (100) and (110) as well as the effect of cycling the potential of polycrystalline Pt.

The LEED-Auger-electrochemical system used in these studies has been described elsewhere (6). The Pt surfaces were cleaned by argon ion sputtering at 350eV and annealed at 900°C to obtain sharp LEED patterns. The principal surface contaminant is carbon which diffuses to the surface from the bulk of the Pt. This procedure was repeated a number of times until no further C or other impurity was detectable in the Auger spectrum (sensitive to ~0.01 monolayer). The same procedure was used for polycrystalline Pt without the LEED examination. The sample was next transferred under vacuum into a second vacuum chamber which was back-filled with ultra-pure argon (99.9999%, further purified by Ti gettering). The sample was then examined electrochemically in a thin-layer cell with an a Pd-H counter electrode in 0.05M H_2SO_4, prepared with ultra-pure acid (Baker Ultrex H_2SO_4) and pyrolyzed water. The Pt was brought into contact with the electrolyte under controlled potential (0.4V vs. RHE) to minimize the possibility of surface reconstruction.

Figure 1 presents the voltammetry curves for Pt(100) and (111) obtained on the first cathodic scan, starting at 0.4V (RHE) and the reverse anodic sweep. H_2 formation is observed in the cathodic sweep at ~0.05V and the complementary H_2 oxidation peak in the anodic sweep. The (111) surface exhibits a small H peak in the anodic and cathodic sweeps at ~0.10V. The charge under the anodic peak is estimated to be ~7μC/cm^2. Assuming 1.5.0 x 10^{14}atoms/cm^2 on Pt(111) and one H per Pt atom, this corresponds to a low coverage of ~0.03. The first sweep on the Pt(110) surface also exhibits a quite small H peak at ~0.1V and is similar to that for Pt(111). This is not surprising since a (2x1) LEED pattern was obtained for the Pt(110) surface as a result of a reconstructed surface composed of Pt(111) facets (9).

The first sweep for the Pt(100) surface indicates a much larger H peak at ~0.25V, corresponding to more strongly adsorbed H. Although the anodic and cathodic peaks differ in width, the charge ratio Q(cath)/Q(anod)=~1 and the charge is ~50μC/cm^2. Assuming 13.1 x 10^{14} atoms/cm^2 on the Pt(100) surface, this corresponds to a coverage of ~0.3. There may also be a small contribution from weakly adsorbed H. The LEED pattern for the clean Pt (100) surface indicated a (5x1) overlayer as reported in the literature (10) but this surface probably reconstructed to (1x1) upon introduction into the electrolyte.

The H coverages on these surfaces are surprisingly low compared to those found in conventional electrochemical experiments on polycrystalline Pt. The 0.3 coverage for strongly adsorbed H on Pt(100), however, compares favorably with flash desorption studies (11) in the gas phase on Pt(100) which also yield coverages of ~0.3 at room temperature. The low coverage (~0.03) for the weakly adsorbed H peaks on the Pt(110) and (111) may not be associated with these surfaces but rather edge effects in the thin-layer cell. They may also arise from portions of the surface which are not the orientation indicated by the LEED pattern. The LEED patterns are sharp and up to literature standards but this does not necessarily insure a very high degree of surface perfection. Samples annealed at high temperatures as in the present study, however, usually have relatively defect free surfaces (12). A third possibility is that the low coverage is the result of surface contamination. This is unlikely in view of the extensive precautions to prevent contamination. Reexamination of the surfaces with Auger after the electrochemical measurements was complicated by the non-volatility of the

---

Electrochemical Society Member

ey words: hydrogen adsorption, platinum ingle crystal, LEED, Auger.

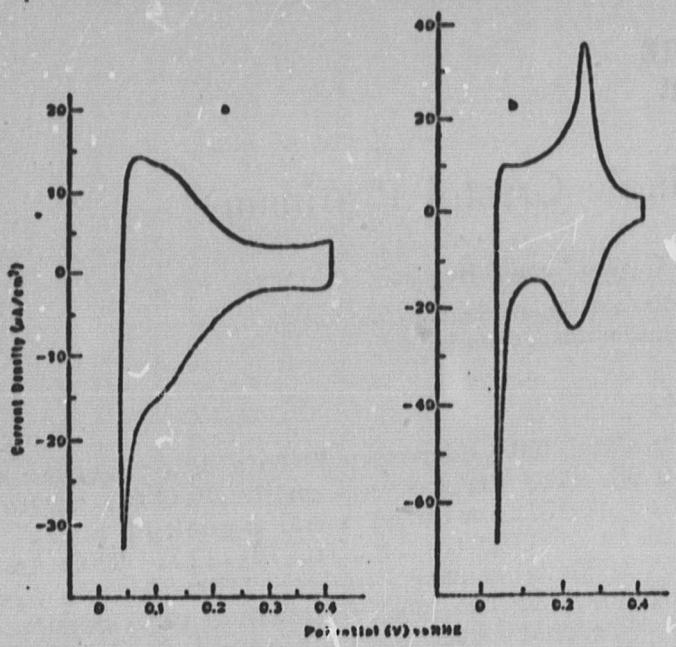

Fig. 1. Voltammograms for a) clean Pt(111) - (1x1) and b) clean Pt(100) - (5x1) in 0.05M H_2SO_4. Sweep rate: a) 100mV/s; b) 50mV/s.

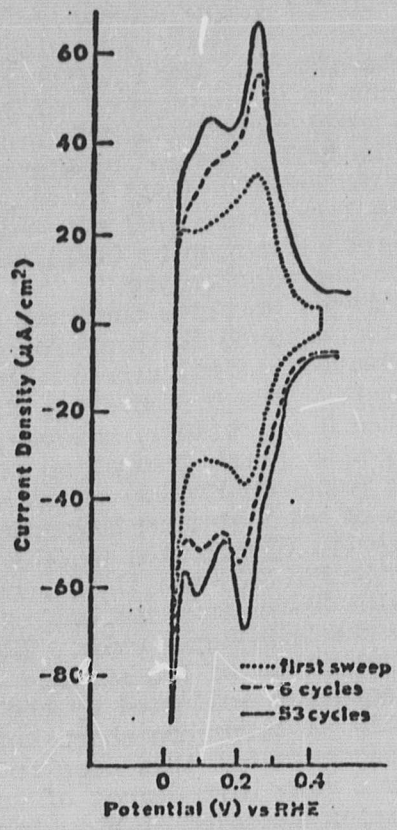

Fig. 2. Voltammograms for polycrystalline Pt in 0.05M H_2SO_4. Sweep rate: 100mV/s.

Manuscript received Nov. 22, 1977; revised manuscript received Dec. 7, 1977.

electrolyte. Post-Auger measurements indicated large sulfur peaks from the sulfate electrolyte and only a minor C peak. On the basis of the ratio of the C to Pt peaks, the C coverage was less than ~0.1 monolayer.

In Figure 2 is shown the initial scan in 0.5M H_2SO_4 for polycrystalline Pt. The scan was begun at 0.4V and swept cathodically. A predominate H peak appears at ~0.25V corresponding to stronger adsorbed H with only a minor contribution due to the weakly adsorbed hydrogen. The high temperature annealed poly crystalline Pt resembled quite closely the (100) surface. Cycling of the polycrystallin Pt out to 1.3V in the anodic film region lead to increases in the areas of the H peaks already present as well as the development of additional peaks. After 53 cycles the voltammogram begins to take on the appearance normally found in conventional studies of Pt. The most likely explanation is the reconstruction of the Pt surface.

Acknowledgement.-- This research has been supported by ONR, NASA-Ames and the Diamond Shamrock Corporation, the latter through a fellowship to one of the authors (M.Y.C.W.). The authors express thanks to the General Motors and Union Carbide Corporations for grants which helped with the purchase of equipment.

REFERENCES

1. F. G. Will, This Journal, 112, 451 (1965).
2. S. Schuldiner, M. Rosen, and D. R. Flinn, ibid., 117, 1251 (1970).
3. V. S. Bagotzky, Yu. B. Vassiliev, and I. I. Pyshnograeva, Electrochim. Acta, 16, 2141 (1971).
4. K. Kinoshita and P. Stonehart, ibid., 20, 101, (1975).
5. H. Angerstein-Kozlowska, W. B. A. Sharp, and B. E. Conway, in Proceedings of the Symposium on Electrocatalysis, ed. M. W. Breiter, (Electrochemical Society, N.J. 1974), p.94.
6. W. E. O'Grady, M. Y. C. Woo, P. L. Hagans, and E. Yeager, J. Vac. Sci. Technol., 14, 365 (1977).
7. P. N. Ross, Jr., J. Electroanal. Chem., 76, 139 (1977).
8. R. W. Ishikawa and A. T. Hubbard, ibid., 69, 317 (1976).
9. R. Ducros and R. P. Merrill, Surface Sci., 55, 227 (1977).
10. e.g., G. A. Somorjai, "Principles of Surface Chemistry," Chapt. 1, Prentice-Hall, New York (1972).
11. K. E. Lu and R. R. Rye, Surface Sci., 45, 677 (1974).
12. F. Jona, ibid., 8, 478 (1967).

Publication costs of this article were assisted by Case Western Reserve University.

NON-TRADITIONAL APPROACHES TO THE STUDY OF SOLID-ELECTROLYTE INTERFACES: PROBLEM OVERVIEW

by

Ernest Yeager
Case Laboratories for Electrochemical Studies
and the Chemistry Department
Case Western Reserve University
Cleveland, Ohio 44106

I. INTRODUCTION

.Electrochemistry is undergoing a renaissance, a key feature of which is the attracting of scientists to this area from other disciplines. This renaissance has been partially stimulated by the importance of electrochemistry to energy conversion and storage. Equally important are indications that electrochemistry has reached a critical stage where rapid development of the science is likely to occur over the next decade.

During the early part of this century, much of the thermodynamics of electrochemistry as a whole was put in place but electrochemical kinetics and electrocatalysis remained an art rather than a science. Reproducibility of kinetic measurements in electrocatalysis studies was a particular problem but over the past two decades electrochemists have gained sufficient control over the various experimental factors to achieve reasonably reproducible results even with surface demanding reactions. Substantial theoretical developments have also occurred over the last two decades in the areas of electron and proton charge transfer at electrochemical interfaces. Further, the impact of the various surface chemical physics techniques, both in situ and ex situ to the electrochemical environment, is starting to be felt in electrocatalysis. The potential for major strides in the science of electrocatalysis using non-traditional methods over the next decade is great and provides the rationale for this conference.

II. MODELS FOR THE SOLID-ELECTROLYTE INTERFACE

The ionic double layer on the solution side of an electrochemical interface consists of two regions, a compact layer immediately adjacent to the electrode and a diffuse ion layer extending into the solution phase. Most of the potential drop between the two bulk phases is usually across the compact layer. Figure 1 presents a model of the compact layer as proposed by Bockris et al. [1]. Adjacent to the electrode surface is a layer of water molecules whose structure and orientation depend on the specific interaction with the electrode surface as well as the electric field. In electrolytes such as NaCl, the cations interact rather strongly with the immediately adjacent water molecules and the inner hydration sphere is retained as the cation approaches the electrode surface even when the electrode is quite negative relative to the solution. Thus, in the plane of closest approach to the electrode surface (the outer Helmholtz plane) cations are usually separated by one or two water molecules from the surface except at quite cathodic potentials. In contract, most anions interact rather weakly with water and their limiting distance of closest approach often corresponds to direct contact as shown in Fig. 1. This is referred to as specific ionic adsorption and the plane through the centers of these ions in their limiting position is known as the inner Helmholtz plane. Anions may be retained in this plane even when the electrode is negatively charged because of favorable interaction with the surface.

The potential distribution across the interface averaged parallel to the surface is shown in Figs. 2 and 3 without and with specific adsorption [5]. Potential gradients of $\sim 3 \times 10^7$ V/cm are easily reached in the compact layer when the electrode is at a potential remote to the point of zero charge on the electrode relative to the electrolyte. These potential gradients play an important role in the electrochemical processes at the interface.

The theoretical treatments of the potential distribution across the diffuse layer are simple only for dilute solutions (<0.01M)(see e.g. ref. 7). At higher

concentrations, account must be taken of solvent dielectric saturation and discreteness, the finite size of the ions, and the polarizability of the ions. The treatments become quite sophisticated [2-4,6,7], including the use of cluster theory [2]. At concentrations greater than 1.0M, the Debye length approaches the dimensions of a solvated ion and the diffuse layer is no longer "diffuse". No fully quantitative description is available for such concentrated electrolytes. The potential drop across the layer, however, becomes small at high electrolyte concentrations and therefore less important to the overall behavior of the interface.

For electrochemical reactions, the plane x_2 is often considered as the pre-reaction state for non-specially adsorbed reactants. Electrochemists have developed methods for estimating the potential ϕ_2 and then calculating the concentrations of ionic reactants in this plane [5,7]. In kinetic studies of electrochemical reactions, the experimentalist often adds a large concentration of a "supporting" electrolyte whose ions are not involved in the reactions in order to keep ϕ_2 numerically small.

When specific adsorption occurs, the situation is far more difficult. There is really no fully quantitative treatment to calculate ϕ_1. The surface concentration and coverage, however, can often be determined by both electrochemical [7] and other methods such as optical reflectance [8].

Various multiple state models have been proposed for the structure of the compact layer and particularly the solvent adjacent to the surface, including the three-state models of Damaskin and Frumkin [9,10] and Bockris and Habib [12] and the four-state models of Parsons [11]. The four states according to Parsons's treatment are shown in Fig. 4 and involve single water dipoles oriented towards and away from the surface and clusters consisting of three water molecules with net dipoles also towards and away from the surface.

The most extensively used experimental test of various models for the compact layer is the differential electrode capacitance. There is a divergence of views as to just how well the experimental capacitance data fit the models [14-20]. These

models of the compact layer, however, in general do not adequately take into account the electronic properties and discrete structure of the electrode surface or the interaction of the water adjacent to the electrode with other water molecules. Without such, it is unlikely that any treatment of the compact layer will provide an adequate basis for understanding the properties of the interface. The truncation of the conduction band orbitals at the electrode surface results in an evanescent wave extending into the interface. When the charge on the metal is changed, the extent to which the evanescent wave extends out from the metal surface changes (see Fig. 5). The water molecules and other species in the compact layer feel the tail of the electron density distribution. Even if there is no strong localized orbital interaction, the distance of approach of the solvent molecules and solvent dipole interactions at the surface will be changed. Furthermore, at high positive charge on the electrode, the extension of the tail of the s- conduction band into the interface will probably regress to the point that the more tightly bound d orbitals will no longer be well shielded at the interface. This is likely to result in a significant change in the interaction of the solvent molecules with the electrode surface.

III. CHARGE TRANSFER PROCESSES ACROSS THE METAL-ELECTROLYTE INTERFACE

Electron transfer processes at metal-electrolyte interfaces may be divided into two classes:

1. electron transfer to and from the outer Helmholtz plane
2. electron transfer to and from the inner Helmholtz plane

With the former (C and C' in Fig. 6), the electron is transferred from the conduction band in the metal at an energy within $\sim \pm kT$ of the Fermi level to the reacting species in the outer Helmholtz plane and vice versa. The interaction of the solution phase reactant with the metal surface is weak.

Since the electron transfer is non-radiative, it is necessary for the tunnelling process to occur without a change in the energy of the system within the restraint of the uncertainty principle. This in turn requires that the metal-reacting species-solvent system be pre-stressed to a condition wherein the energy of the overall system

is the same with the electron either in the metal conduction band or an orbital of the reacting species. This constitutes the activated state. In this activated state, the resonance stabilization is weak and the electron transfer may be described as non-adiabatic or only weakly adiabatic. The barrier through which the electron tunnels in the activated state involves the solvent molecules separating the metal and the outer Helmholtz plane. Only virtual states are expected to be involved in this barrier. Following the electron transfer, the reactant-solvent system relaxes back to a minimum potential energy state.

When the reacting species is in the inner Helmholtz plane (A in Fig. 6), the interaction of the electron orbitals of the reacting species with the metal is far stronger. Pronounced resonance splitting occurs in the activated state and the electron becomes delocalized in the activated state with the process adiabatic.

In addition to these two cases, it is possible to have a reacting species (B in Fig. 6) in the outer Helmholtz plane interact with an ionic species in the inner Helmholtz plane which serves as a bridge for the electron transfer. The barrier for the electron transfer may now have a real electron state of accessible energy. This can result in a higher electron transmission probability through the barrier in the activated state and under favorable conditions even substantial resonance splitting. Bridging ions in the inner Helmholtz plane may lead to a much higher concentration of the reacting species in the outer Helmholtz plane if the charge of the reacting species is of opposite sign.

Marcus [21-25] has treated the first case using classical statistical mechanics to calculate the free energy of activation. His treatment of electron transfer at the electrochemical interface is very similar to that for homogeneous electron transfer between two reacting species in solution. He sets the rate constant for the heterogeneous electron transfer equal to

$$k = \kappa Z \exp - (\Delta G^*/kT) \qquad (1)$$

where κ is the electron transmission coefficient in the activated state, Z is the frequency factor analogous to the collosion number in homogeneous second order

kinetics and ΔG^* is the free energy of activation involved in the prestressing of the system prior to the radiationless electron transfer. Marcus gives for the contributing terms to ΔG^* the following:

$$\Delta G = \Delta G_e^{\ddagger} + \Delta G_o^{\ddagger} + \Delta G_i^{\ddagger} + \Delta G_s^{\ddagger} \qquad (2)$$

where $\Delta G_e^{\ddagger}$ is the electrical work term associated with bringing the reacting species to the outer Helmholtz plane, $\Delta G_i^{\ddagger}$ is the reorganizational free energy contribution from the inner coordination sphere of the reacting species, $\Delta G_o^{\ddagger}$ is the corresponding term for other solvent molecules surrounding the reacting species and $\Delta G_s^{\ddagger}$ is an entropy term associated with any change in the electron spin before and after the electron transfer. Marcus treats the distribution of activated states corresponding to electron transfer from or to the various electronic energy levels in the metal near the Fermi level as the equivalent of a single activated state corresponding to the Fermi level. Bond stretching contributions from the inner coordination sphere are included through $\Delta G_i^{\ddagger}$ [25, see also ref. 26,27]. Marcus takes into account the interaction of the image forces in the metal on the solvent polarization in the $\Delta G_o^{\ddagger}$ term. Within the frame work of classical statistical mechanics, it is impossible to calculate the transmission factor κ and hence Marcus assumes the process to be weakly but sufficiently adiabatic for $\kappa \leq 1$, but without substantial resonance stabilization in the activated state.

Comparison of the Marcus treatment with experimental data indicates at least order of magnitude agreement for electron transfer reactions at metal electrodes when the reacting species is in the outer Helmholtz plane [21, 39-41].

Levich, Dogonadze and Kuznetsov (LDK) [28-32] have used quantum statistical mechanics to treat non-adiabatic homogeneous and heterogeneous electron transfers and have been able to calculate κ as a function of distance of approach. The basic equation in their treatment for the reduction current in the heterogeneous electron transfer is

$$i = e\int\int c(x)m(\varepsilon)\rho(\varepsilon)W(\varepsilon,x)\, d\varepsilon\, dx \qquad (3)$$

where $\rho(\varepsilon)$ is the density of electronic states in the metal, $\rho(\varepsilon)$ is the Fermi-

Dirac distribution function, and $W(\varepsilon,x)$ is the transition probability for the system to be transformed from the initial to final state. The latter is calculated with first order perturbation theory, using the Franck-Condon principle and using the Born-Oppenheimer approximation to separate the electronic and nuclear wave functions.

In their early treatment of $W(\varepsilon,x)$, LDK considered the reacting ion with its inner coordination sphere as a frozen system which did not contribute to the activation process. They reasoned that the relevant vibration modes of the inner coordination sphere were such that $h\nu \gg kT$, and hence, to excite them from the ground vibrational state would require too many multiphonon interactions to have a reasonable probability of their excitation. This reasoning, however, does not take into account the possibilit of vibrational energy being stored in much softer modes associated collectively with the outer and inner coordination sphere solvent (particularly bond bending modes). With random phasing, this vibrational energy is then transferred into inner sphere stretching modes which could then contribute very substantially to the activated state. Many workers [21,26,33-36] have called attention to the importance of the inner sphere contributions, which within the frame work of the Marcus theory often results in $\Delta G_i^{\ddagger}$ being larger than $\Delta G_o^{\ddagger}$. Dogonadze and his co-workers [37,38], however, still appear to hold the view that vibrational modes with $h\nu \gg kT$ are not directly involved in the activation process and their effects on the rates involve only the pre-experimental factor. Schmickler [44] and Schmidt [45,46] have attempted to include inner coordination spheres in the LDK treatment.

For an one electron transfer process such as $Fe^{3+} + e \rightleftharpoons Fe^{2+}$ with equal concentrations of Fe^{2+} and Fe^{3+}, both the Marcus and LDK type treatments lead to a potential dependence for the current density of the form

$$i = Fk_o c \left[\exp -\beta \frac{F}{RT}(E-E_o) - \exp(1-\beta)\frac{F}{RT}(E-E_o)\right] \qquad (4)$$

where k_o is the standard rate constant, c is the concentration of either the Fe^{3+} or Fe^{2+}, E_o is the standard reversible electrode potential, F is the Faraday, and β is known as the transfer coefficient. Both theories predict a value of $\beta = 0.5$

provided the electrode potential E is not varied too far either positively or negatively from the reversible value. In practice β is constant over a much wider potential range than expected. This has been partially explained by introducing non-parabolic terms in the LDK treatment.

Theoretical effort have also been directed to the bridge-assisted electron transfer reactions, both heterogeneous and homogeneous. The principal theoretical work in this area is by the Dogonadze group [42.43), who have used second order perturbation theory to calculate the transition probability factor $W(\varepsilon,x)$. This has involved the rather doubtful assumption, however, that there is no strong interaction between the electronic states of the reacting species in the outer Helmholtz plane, the bridging species in the inner Helmholtz plane and the metal electrode.

IV. PROTON TRANSFER ELECTRODE REACTIONS

The discharge of protons to form H_2 is among the most studied electrochemical reactions in which the electrode surface has a pronounced catalytic effect. The first step in this process is the discharge of the proton from either a hydronium ion in acid aqueous electrolytes or a water molecule in neutral or basic electrolytes to form an adsorbed H; i.e. $H_3O^+ + e \rightleftharpoons H(ads) + H_2O$. For metal such as Hg, this step is rate controlling. Various authors have attempted to calculate the potential energy surfaces for this reaction using various models for the pre-reaction state of the hydronium ion at the electrode surface and the activated state. Bockris and Matthews [47.48] have proposed the model in Fig. 7 in which the central oxygen of the hydronium ion resides at a distance of $\sim$ 3.4A from the electrode surface just prior to the transfer of the proton to the adsorbed state on the metal surface. These workers have then attempted to construct the potential energy surface from the Morse curves, assuming that in the activated state the electron is transferred from the conduction band of the metal to the proton by tunnelling. Bockris and Sen [49] and

Salomon et al. [50] have considered resonance splitting due to strong interaction in the activated state, using the bond energy bond order (BEBO) method of Paar and Johnson [51].

Instead of transmission of the proton over the barrier shown in Fig. 7, various authors [48,52-56] over a number of years have considered the possibility of proton tunnelling through the barrier using various potential barriers.

Both theoretical and isotopic experimental evidence appear to favor proton tunnelling as responsible for a substantial fraction of the current associated with proton discharge on some metals such as Hg where the barrier for discharge is high.

Dogonadze, Kuznetsov and Levich (DKL) [57,58] have attempted to treat the proton discharge reaction using a theoretical approach similar to that involved in their treatment of electron transfer outer Helmholtz plane reactions. They invoke the assumption that the probability of exciting the $[H - OH_2]^+$ and M-H stretching modes in the activated state is sufficiently unlikely to be neglected since $h\nu >> kT$. They then consider the proton and electron to be a fast subsystem with the solvent as the slow system. In the DKL treatment activation occurs by solvent fluctuations. The neglect of the various vibrational modes in the hydronium ion and the M-H bond, however, does not appear proper for reasons similar to those mentioned earlier in conjunction with the DKL electron transfer treatment.

Aside from the question of transmission over the barrier vs. tunnelling, such treatments are seriously compromised by the lack of sufficient information concerning the sites involved in the proton adsorption on the electrode surface and solvent interactions at this surface.

V. TYPES OF INFORMATION NEEDED TO UNDERSTAND SOLID-ELECTROLYTE INTERFACES

The traditional approaches to the study of electrochemical interfaces involve the thermodynamic characterization of the interface and its response to perturbation from equilibrium conditions in terms of current-charge-potential measurements [59].

A wide range of both steady state and transient perturbation techniques have been used. Such techniques are often very sensitive to the microscopic features of the interface and particularly to the presence of adsorbed species at even a small fraction of a monolayer species that may be present as residual impurities as well as intentionally added. Today, however, the electrochemist in fundamental studies has been able to achieve well controlled conditions where impurity adsorption is negligible and in fact where the only species immediately adjacent to the electrode surface is the solvent itself. This is the electrochemical equivalent of the ultra high vacuum of the surface physicist.

The difficulty with these electrochemical methods is that despite good sensitivity they lack sufficient molecular specificity. They do not indicate on what sites a particular species is adsorbed, the nature of the interactions with the substrate and usually not even the charge on the adsorbed species. Often the electrosorption of a species on to the electrode surface is attended by gross chemical changes in the species and electrochemical methods alone do not usually reveal the nature of these changes.

To illustrate, consider the adsorption of hydrogen on platinum. The voltammetry curve shown in Fig. 8 was obtained by measuring the current while sweeping the applied potential cyclically between limits. The hydrogen adsorption occurs during the sweep from 0.3 to 0.0V (cathodic direction) while the hydrogen desorption occurs during the reverse sweep (anodic direction) over this same range. [The structure at more positive potentials (>0.6V) is due to the formation of an anodic film involving an adsorbed oxygen species and its subsequent very irreversible reduction.] Up to five hydrogen peaks have been deconvoluted from the desorption sweep [60]. This hydrogen desorption curve is somewhat analogous to the thermal desorption curves for hydrogen on platinum at the solid-gas interface. The electrochemical desorption, however, approaches reversible behavior at slow sweep rates and involves the formation of hydronium ions $(H_3O)^+$ while the thermal desorption is usually irreversible and leads

to H_2 molecules. In each instance, the weakly bound hydrogen is desorbed first. At the electrochemical interface, the hydrogen desorption may be attended by some rearrangement of the water structure at the interface, depending on the type of hydrogen adsorption site. The energetics of hydrogen electrochemical adsorption-desorption reflect not only the bonding of the hydrogen to surface sites but also the interaction of water with these sites and the adsorbed hydrogen.

In a sense, the voltammetry curves are a form of energy spectroscopy with the potential a relative measure of the enenrgy of the adsorbed species in various states on the surface. The resolution is sufficient to resolve several peaks in Fig. 8. The question is then what causes these peaks: Are they due to adsorption on different crystal surfaces, different sites on a given crystal plane, induced heterogeneity or competitive adsorption of other species such as anions? Single crystal studies using LEED quality surfaces and special techniques for the transfer from the high vacuum to electrochemical environments provide evidence that the multiple peak structures in Fig. 8 are associated principally with different crystallographic planes [103-108].

A particularly interesting phenomenon is the underpotential deposition (UPD) of mono- and submonolayers of metal atoms on a foreign metal substrate. The formation of such layers is termed underpotential electrodeposition because the layers are formed at potentials quite positive to those for the deposition of the bulk metal of the layer. UPD occurs because of a favorable interaction of the UPD species with the substrate. One approximate indication of the strength of such interactions is the difference in the work function of the substrate metal and that of the layer in bulk form [61-64]. The correlation is quite good, even though the work function is a bulk property and the electronic properties of the UPD species may not well approximate those of the corresponding bulk metal. In fact, there is still some uncertainty as to what extent the UPD species may retain significant ionic character in various instances. More than electrochemical methods are needed to establish the nature of the electronic interactions. In situ UV-visible optical

methods are particularly promising and have already yielded significant information [65-68].

The UPD adsorption-desorption curves on single crystal surfaces contain peaks or spikes some of which are particularly sharp; for example with lead on the Au (111)-(1 x 1) one peak component is of the order of 5 mV (Fig. 9). These single crystal studies were carried out with instrumentation described in Section VI of this paper [110]. Such sharp peaks may be caused by order-disorder transitions and in some instances condensation into patches with probably some registration between the atoms of the layer and the substrate. They are quite specific to the particular low index surfaces.

In contrast the adsorption-desorption of species such as the halide ions on noble metals such as gold [69-71] yields very broad peaks with half widths often of several tens of a volt. This can be explained on the basis of unfavorable interactions between the adsorbed species.

While the voltammetry curves provide information concerning the adsorption isotherm, this is not sufficient to understand electrosorption and its role in various electrochemical processes where the processes depend strongly on the catalytic properties of the electrode surface. Microscopic level information is needed concerning the surface electronic states, bonding, configuration, adsorption sites and vibrational properties for adsorbed species and the state of the solvent adjacent to the electrode surface. How do we obtain such?

VI. OVERVIEW OF NON-TRADITIONAL EXPERIMENTAL APPROACHES

Much progress has been made in recent years in studies of the chemical physics of solid-vacuum interfaces using various electron photon and ion physics techniques. On the other hand, in most bulk phases the chemist today is almost routinely able to pin down the structure of quite complex molecules principally through the use of the

optical spectroscopies and nuclear magnetic resonance spectroscopy coupled with conventional chemical methods. So, far the only spectroscopies which have found edtensive use for in situ studies of electrochemical interface are UV-visible reflectance spectroscopy and Raman, the latter very recently. These optical methods are quite promising but to date their impact on the understanding of the electrochemical interface has been only moderate. The lectures and papers scheduled for this conference, however, provide evidence of a great surge of progress in understanding optical phenomena at electrochemical interfaces and gaining useful information concerning such interfaces.

There are three experimental approaches to obtaining molecular level information concerning electrochemical interfaces and processes occurring thereat:

A. direct in situ spectroscopic measurements;

B. ex situ measurements on the electrode surface before and after electrochemical measurements; and

C. complementary ex situ experiments at solid-vacuum and solid-gas interfaces designed to provide insight concerning the interaction of various species with electrode surfaces.

A. In situ spectroscopic techniques

Table I lists the majority of the presently used in situ spectroscopic techniques for the study of electrochemical interfaces. Various windows exist for electromagnetic radiation in solvents such as water, i.e. X-ray, UV-visible and for very limited paths certain parts of the infrared. Consequently optical spectroscopy lends itself to in situ studies. The majority of the UV-visible and infrared studies make use of intensity changes upon reflection from the electrochemical interface in the external or internal attenuated total reflection modes. With the external mode both specular and diffuse reflection techniques have been used. The reflectance changes attending the change of electrode potential are small but still quite easily measured with modern signal detection-processing techniques. These reflectance techniques have yielded information concerning surface charge, adsorption isotherms, the state of water in the compact double layer, transitions in under-

potential deposited layers, surface roughness and the electronic properties of anodic films and passivation layers on metals as well as semiconductor-electrolyte interfaces (for reviews, see ref. 73-75). Ellipsometric spectroscopy using automatic instrumentation [76,77] is a particularly powerful technique for obtaining information concerning the collective dielectric properties of the interface and adsorbed layers as a function of wavelength and potential and the effective optical thickness of these layers [76,77]. The critical need in this area is for theoretical treatments of the collective optical properties of the metal-electrolyte interface and adsorbed species at the monolayer so as to provide a quantitative frame work within which to interprete such optical measurements. With layers which are much thicker than monolayer dimensions (e.g. passivation layers on active metals), a simple three layer optical model involving two continuous phases with an intermediate thin layer appears to be adequate [77.78].

Since the early observations of unusually strong Raman signals for pyridine adsorbed on silver by Fleischmann, Hindra and their students at Southampton [79-85], great interest has developed in Raman studies of adsorbed species on electrode surfaces. Indeed this conference has fifteen papers in thia area, principally directed to possible mechanisms for the large surface enhanced Raman signals observed with most adsorbed molecules on silver and also copper. Several explanations have been offered for the surface enhancement and it is likely that more than one mechanism is involved. With adsorbed species exhibiting intrinsic resonance Raman, very strong signals have been observed on other metals such as bright platinum electrodes (see e.g. ref. 86,87). Although the Raman signals may only be observable with certain electrode surfaces, this technqiue is expected to prove of much importance to electrochemistry in providing much needed in situ vibrational data. With adsorbed species on semiconductor-gas interfaces such as ZnO and TiO_2, surface enhanced Raman signals have been observed as the incident laser radiation approaches the band gap [88].

With probe molecules exhibiting strong intrinsic resonance Raman such as para

nitrosodimethylanaline, it has been possible to establish whether they are adsorbed on Lewis acid or base sites by examining changes in their Raman signal [88-90]. So far this technique has only been applied to solid-gas interfaces but it should be applicable also to solid-electrolyte interfaces.

Aside from the implications of various photoelectrochemical processes for solar energy conversion, they afford interesting information concerning band bending in semiconductor electrodes, surface states and other electronic features of the interface. A number of papers in the conference are concerned with this area. Photoemission from metals into electrolytes has also been studied by electrochemists (see e.g. 91,92).

Mössbauer spectroscopy has been applied to in situ studies of various layers on electrode surfaces containing appropriate elements to serve as either emitters or absorbers. From the Mössbauer spectra, under favorable conditions it is possible to gain insight into spin states and nearest neighbor interactions. Particularly interesting results have been obtained for electrochemical passivation layers on iron [93] and iron transition metal macrocyclic catalyst layers on electrode surfaces such as carbon [94,95].

When the potential across an electrochemical interface is a.c. modulated, both shear and compressional acoustical waves are generated. The shear waves result from the modulation of the a.c. interfacial tension and are detected in the solid electrode phase with a shear sensitive transducer attached to the back side of the electrode [96.97]. The compressional waves are readily detected in the electrolyte phase with a hydrophone [98.99]. With solid metal electrodes, these compressional waves are produced by the a.c. modulation of the volume of the ionic double layer--particularly the compact double layer. With semiconductor electrodes, intrinsic and field induced piezoelectric properties may result in large compressional components in the electrolyte phase and both shear and compressional components in the solid electrode phase. Both the shear and compressional acoustoelectrochemical effects are quite sensitive to adsorbed species at the electrode surface and can be used to

follow the adsorption-desorption of such. Quantitative measurements of the compressional effect on metal electrodes should yield dV/dE (where V is the volume, E is the applied potential) and hence be of special interest in testing double layer models.

Electrospin spin resonance has been used to detect various free radicals in the electrolyte phase (see e.g. 100-102) and in principal can be used to examine radicals adsorbed on electrode surfaces by proper location and configuration of the electrode in the microwave cavity of the spectrometer

Two techniques that appear promising for in situ studies of electrochemical interfaces and particularly catalyst and passivation layers are extended X-ray absorption fine structure (EXAFS)[a] and nuclear magnetic resonance. In both instances it will probably be necessary to use high area electrodes such as dispersed ultra small metal particles on a high area carbon support or metal blacks. With the in situ EXAFS, it is worthwhile to consider fluorescence yield as well as the more conventional absorption measurements.

With the recent developments in NMR of solids using magic angle spinning and various spin decoupling techniques, it should be possible to obtain the fine line NMR spectra of adsorbed species on electrodes even at the monolayer level using very high surface area electrocatalysts.

B. Ex situ Techniques

The electron and ion spectroscopies listed in Table II can be used to characterize electrode surfaces including single crystal systems before and after electrochemical measurements. The critical question is whether the electrode surface can be transferred from the ultra high vacuum environment to the electrochemical environment and vice versa without substantial restructuring of the surface as well as chemical changes and contamination. Several research groups (see e.g. 103-109)

---

[a]The various features of EXAFS as applied to interface studies will be summarized by P. Eisenberger in Lecture G6.

have carried out electrochemical measurements such as hydrogen electrosorption and lead underpotential electrodeposition on noble metal single crystal surfaces which have been prepared and characterized with LEED/in ultrahigh vacuum or RHEAD. Special precautions have been used to minimize the possibility of restructuring during the transfer into the electrolyte. The approach used in the author's laboratory for accomplishing such is as follows [110]. Clean single crystal platinum or gold surfaces of known orientation are prepared by repeated sputtering with argon and high temperature annealing in an ultra high vacuum chamber (A in Fig. 10). The surfaces are examined with LEED and Auger spectroscopy in ultra high vacuum ($\sim 10^{-10}$ Torr) and then transferred into a second vacuum chamber (B in Fig. 10) also at $\sim 10^{-10}$ Torr without removal from the vacuum environment by means of a magnetically operated transfer wand, Ultrapure argon is then admitted to this vacuum container. A second parallel electrode surface with a drop of electrolyte is then brought close to the single crystal surface to form a thin layer electrochemical cell with a gap of $\sim 10^{3}$cm. This second electrode is choosen so as to serve both as a counter and potential reference electrode. The use of the thin-layer cell technique results in a high area to volume of electrolyte ratio and hence much less sensitivity of the single crystal surface to impurities in the electrolyte (e.g. a 10^{-5}M of a typical ionic impurity corresponds to $\sim 10^{-2}$ of a monolayer even if all adsorbed on the electrode surface). Following the electrochemical measurements, the electrodes are separated. With an electrolyte such as aqueous dilute HF, the electrolyte can be completely vaporized at room temperature as the argon is pumped out. The single crystal electrode is then re-transferred into the LEED-Auger chamger and the surface re-examined.

This system was used to obtain the voltammetry data in Fig. 10 for lead underpotential deposited on single crystal gold from a 0.1M HF solution containing 10^{-4}M Pb with an α-Pd/H counter reference electrode. The LEED patterns following the electrochemical treatment indicate relatively complex behavior, which depends on

the single crystal surface and the potentials to which the electrode has been expanded [110]. When the single crystal gold surfaces are introduced into the electrolyte and removed at potentials somewhat anodic to those for UPD of lead, the LEED patterns resemble the original patterns. With even the Au(100) surface with its initial (5x20) overlayer, there is still evidence of the (5x20) pattern after this apparently mild electrochemical treatment. On the other hand, if more than 0.1 of a monolayer of Pb is formed on this surface, only the (1x1) pattern is observed. With depositions of substantial fractions of a monolayer of lead, restructuring involving substrate atoms appears to occur at least on some gold surfaces. There are interesting similarities between this work and that of Rhead et al. [111,112] on vapor deposited lead on single crystal gold.

C. Complementary ex situ experiments

The electrochemical interface can not be simulated even approximately with solid-vacuum interfaces. Nonetheless, studies of the adsorption of water, oxygen various organic molecules and other species at such interfaces can provide information of help in understanding electrochemical interfaces. The interaction of water with such metals as gold and platinum is relatively weak at electrochemical interfaces and hence, some similarities are expected between the behavior of various adsorbed neutral species such as hydrogen atoms and organic species on these metals in the electrochemical and vacuum environments. Such comparisons are most likely to be valid when the electrochemical interface is near the potential of zero charge and the potential gradient at the interface is small.

Particular types of information which can prove useful to the electrochemist include the energetics of the adsorption process, types of adsorption sites, configuration, electronic and vibrational properties of the adsorbed species and chemical modifications of the adsorbate attending the adsorption process. Most electrochemists concerned with various electrocatalysis processes already pay considerable attention

to solid-gas catalytic literature and this trend is likely to increase over the coming decade.

Acknowledgement:

The author is pleased to acknowledge the support of the U.S. Office of Naval Research and NASA for some of the experimental work in the author's laboratory described in this paper.

REFERENCES

1. J. O'M. Bockris, M. A. Devanathan and K. Muller, Proc. Roy. Soc., A274 (1963) 55.

2. C.A. Barlow, Physical Chemistry, An Advanced Treatise, Vol. IX A, Chapter 2, H. Eyring, D. Henderson and W. Jose, eds., Academic Press, New York City, 1970.

3. R. Payne, J. Electroanal. Chem., 41, (1973) 277.

4. R. Payne, ibid. 41, (1973) 309.

5. E. Yeager, J. de Physique 38,(1977) C5-1.

6. F. B. Buff and F.H. Stillinger, J. Chem. Phys., 39, (1963) 1911.

7. P. Delahay, The Double Layer and Electrode Kinetics, Interscience Publishers, New York City, 1965.

8. R. Adzic, E. Yeager, and B.D. Cahan, J. Electroanal. Chem., 85, (1977) 267.

9. B.B. Damaskin and A.N. Frumkin, Electrochem. Acta 19, (1974) 173.

10. B.B. Damaskin, J. Electroanal. Chem. 75, (1977) 359.

11. R. Parsons, J. Electroanal. Chem., 59, (1975) 229.

12. J. O'M. Bockris and M. A. Habid, Electrochim. Acta, in press.

13. D.C. Grahame, J. A. Chem. Soc., 76, (1954) 4819.

14. J.A. Harrison, J.E.B. Randles, and D.J. Scheffrin, J. Electroanal. Chem., 48, (1973) 359.

15. J. O'M. Bockris and M.A. Habid, J. Electroanal. Chem., 65,(1975) 473.

16. R.N. Reeves, Modern Aspects of Electrochemistry, Vol. 9, J. O'M. Bockris and B.E. Conway, eds., Plenum Press, New York City, 1974.

17. R.J. Watts-Tobin, Philos. Mag. 6, (1961) 133.

18. A.W. Verkroost, M. Sluyters-Rehbach, and J.H. Sluyters, J. Electroanal. Chem., 24, (1970) 1.

19. R. Payne, J. Electroanal. Chem. 113, (1966) 999.

20. R. Payne, Trans. Faraday Soc. 64, (1968) 1638.

21. R.A. Marcus, Ann. Rev. Phys. Chem., 15, (1964) 155.

22. R.A. Marcus, J. Chem. Phys. 24, (1956) 966.

23. R.A. Marcus, J. Chem. Phys., 26,(1957) 867.

24. R.A. Marcus, Can. J. Chem., 37,(1959) 155.

25. R.A. Marcus, Discus. Faraday. Soc., 29, (1960) 21.

26. N.S. Hush, Trans. Faraday Soc., 57, (1961) 557.

27. N.S. Hush, J. Chem. Phys., 28, (1958) 962.

28. V.G. Levich and R.R. Dogonadze, Dokl. Acad. Nauk SSSR 124, (1959) 123.

29. R.R. Dogonadze and Y.A. Chizmadzhev, Dokl. Acad. Nauk SSSR 144, (1962) 1077.

30. R.R. Dogonadze, A.M. Kuznetsov and A.M. Chexmadzhev, Zh. Fiz. Khim., 38, (1964) 1195.

31. V.G. Levich and R.R. Dogonadze, Coll. Czech. Chem. Commun., 29, (1961) 193.

32. V.G. Levich, Advances in Electrochemistry and Electrochemical Engineering, Vol. 4, Chapter 5, D. Delahay and C. Tobias, eds., Interscience Publishers, New York City (1966).

33. R.J. Marcus, B.J. Zwolinski and H. Eyring, Chem. Rev., 55, (1955) 157.

34. E. Sacher and K.J. Laidler, Modern Aspects of Electrochemistry, Vol. 3, Chapter 1, J. O'M. Bockris and B.E. Conway, eds., Plenum Press, New York City, 1964.

35. A.J. Appleby, J. O'M. Bockris, R.K. Sen and B.E. Conway, MTP - International Review of Science and Technology, J. O'M. Bockris, ed., Butterworths Publishers, London, 1972.

36. J. O'M. Bockris, R.K. Sen and B.E. Conway, Nature Phys. Sci., 240,(1972) 143.

37. R.R. Dogonadze, Reactions of Molecules at Electrodes, Chapter 3, N.S. Hush, ed., J. Wiley and Sons, New York City, 1971.

38. M.A. Vorotyntsev, V.M. Katz and A.M. Kuznetsov, Elektrohhimiya, 7,(1971) 1.

39. R.K. Sen, E. Yeager and W.E. O'Grady, Ann. Rev. Phys. Chem., 26, (1975) 287.

40. N. Sutin, Ann. Rev. Phys. Chem., 17, (1966) 119.

41. A.A. Vlcek, Sixth International Conference on Coordination Chemistry, S. Kirschner, ed., Macmillan, New York City, 1961, pp. 590-603.

42. R.R. Dogonadze, J. Ulstrup and Y.I. Kharkats, J. Electroanal. Chem., 39, (1973) 47.

43. R.R. Dogonadze, J. Ulstrup and Y. I. Kharkats, J. Electroanal. Chem., 43, (1973) 161.

44. W. Schmickler, Ber. Bunsinges, Phys. Chem., 77,(1973) 991.

45. P.P. Schmidt, J. Chem., Soc. Faraday Trans. II, 69, (1973) 1104.

46. P.P. Schmidt, Z. Naturforsch, A29, (1974) 880.

47. J. O'M. Bockris and D.B. Matthews, Proc. Roy. Soc. London, A292, (1966) 479.

48. J. O'M. Bockris and D.B. Matthews, J. Chem. Phys., 44, (1966) 298; see also J. O'M. Bockris and D.B. Matthews, Modern Aspects of Electrochemistry, Vol. 6, Chapter 4, J O'M. Bockris and B.E. Conway, eds., Plenum Press, New York City, 1971.

49. R.K. Sen, Ph.D. Thesis, University of Pennsylvania, 1972.

50. M. Salomon, C. Enke and B.E. Conway, J. Chem. Phys., 43, (1965) 3989.

51. C. Paar and H. Johnson, J. Am. Chem., Soc., 85, (1963) 2544.

52. B. Topley and H. Eyring, J. A. Chem. Soc., 55, (1933) 5058.

53. C.E.H. Bawn and G. Ogden, Trans. Faraday Soc., 30, (1934) 432.

54. B.E. Conway, Can. J. Chem., 37, (1959) 178.

55. S.G. Christov, Z. Elektrochem., 62, (1958) 567.

56. S.G. Christov, Electrochim. Acta 4, (1961) 306.

57. R.R. Dogonadze, A.M. Kuznetsov and V.G. Levich, Elektrokhimiya, 3, (1967) 739.

58. R.R. Dogonadze, A.M. Kuznetsov and V.G. Levich, Electrochim. Acta 13, (1968) 1025.

59. See e.g. E. Yeager and J. Kuta, Physical Chemistry, An Advanced Treatise, Vol. IXA, Chapter 4, H. Eyring, D. Henderson and W. Jost, eds., Academic Press, New York City, 1970.

60. H. Angerstein-Kozlowska, W.B.A. Sharp and B.E. Conway, Proc. Symposium on Electrocatalysis, M.W. Breiter, ed., The Electrochemical Society, Princeton, N.J., 1974, 94.

61. H. Gerischer, D.M. Kolb and J.K. Sass, Advances in Physics, 27, (1978) (3) 437-492.

62. D.M. Kolb, Advances in Electrochemistry and Electrochemical Engineering, Vol. 11, H. Gerischer and C. Tobias, eds., Wiley, New York City, (1978) 125.

63. H. Gerischer, D.M.Kolb and M. Przasnyski, Surface Science 43, (1974) 662.

64. D.M. Kolb, M. Przasnyski and H. Gerischer, J. Electroanal. Chem., 54, (1974) 25.

65. R. Adzic, E. Yeager and B.D. Cahan, J. Electrochem. Soc., 121, (1974) 474.

66. A. Bewick and B. Thomas, J. Electroanal. Chem., 70,(1976) 239; 84,(1977) 127; 85, (1977) 329.

67. D.M. Kolb, J. de Physique, Colloque. No. 5, Supplement 11, 38, (1977) C5-167.

68. J. Horkans, B.D. Cahan and E. Yeager, J. Electrochem. Soc., 122, (1975) 1585.

69. R. Adzic, E. Yeager and B.D. Cahan, J. Electroanal. Chem., 85,(1977) 267.

70. W.K. Paik, M.A. Genshaw and J. O'M. Bockris, J. Phys. Chem., 74,(1970) 4266.

71. V.S. Bagotzkii, V.B. Vassilyev, J. Weber and J.N. Pirtskhalaua, J. Electroanal. Chem., 27,(1970) 31.

72. A. Bewick and B. Thomas, J. Electroanal. Chem., 65, (1975) 911.

73. J.D.E. McIntyre, Advances in Electrochemistry and Electrochemical Engineering, Vol. 9, Chapter 2, R.H. Mueller, ed., J. Wiley and Sons, New York City, 1973.

74. G. Blondeau and E. Yeager, Prog. Solid State Chem., 11, (1976) 153.

75. D.M. Kolb, Advances in Electrochemistry and Electrochemical Engineering, Vol. 11, Chapter 2, H. Gerischcer and C.W. Tobias, eds., J. Wiley and Sons, New York City, 1978.

76. B.D. Cahan and R.F. Spanier, Surface Sci., 16, (1969) 166.

77. B.D. Cahan, Surface Sci., 56, (1976) 354.

78. D.J. Wheeler, B.D. Cahan, C.T. Chen and E. Yeager, Passivity of Metals, R.P. Frankenthal and J. Kruger, ed., The Electrochemical Society, Princeton, N.J., 1978 p. 546-563.

79. M. Fleischmann, P.J. Hendra and A.J. McQuillan, J. Chem. Soc., Chem. Commun., 3, (1973) 80.

80. M. Fleischmann, P.J. Hendra and A.J. McQuillan, Chem. Phys. Lett. 26, (1974) 163.

81. A.J. McQuillan, P.J. Hendra and M. Fleischmann, J. Electroanal. Chem., 65 (1975) 933.

82. M. Fleischmann, P.J. Hendra, A.J. McQuillan, R.L. Paul, and E.S. Reid, J. Raman Spect., 4 (1976) 269.

83. R.P. Cooney, E.S. Reid, P.J. Hendra and M. Fleischmann, J. Am. Chem. Soc., 99 (1977) 2002.

84. R.P. Cooney, P.J. Hendra and M. Fleischmann, J. Raman Spect., 6 (1977) 264.

85. R.P. Cooney, M. Fleischmann and P.J. Hendra, J. Chem. Soc. Chem. Commun., 1 (1977) 235.

86. G. Hagan, B. Simic-Glavaski and E. Yeager, J. Electroanal. Chem., 88 (1978) 269.

87. D.L. Jeanmaire and R.P. Van Duyne, J. Electroanal. Chem., 84 (1977) 1.

88. J.F. Brazdil, Resonance Raman Spectroscopy of Adsorbed Species at Solid-Gas Interfaces. Ph.D. Thesis, Case Western Reserve University, Cleveland, 1980.

89. Y. Yamamoto and H. Yamada, J. Chem Soc. Faraday Trans.I, 74 (1978) 1562.

90. H. Yamada and Y. Yamamoto, J. Chem. Soc. Faraday Trans. 75 (1979) 1215.

91. A.M. Brodskii and Yu. V. Pleskov, Progress in Surface Science, S.G. Davison, ed., Pergamon Press, Oxford, 1972.

92. J.K. Sass and H.J. Lewering, J. de Physique, Colloque No. 5, Supplement 11, 38 (1977) C5-277.

93. W.E. O'Grady and J. O'M. Bockris, Surface Sci. 38 (1973) 249.

94. A.J. Appleby and M. Savy, Electrocatalysis on Non-Metallic Surfaces, A.D. Franklin, ed., National Bureau of Standards, Special Publication 455, 1976, p. 241.

95. H. Meier, V. Tschirwitz, E. Zimmerhackl, W. Albrecht and G. Zeitler, J. Phys. Chem. 81 (1977) 712.

96. A. Ya. Gokhshtein, Electrokhim. 2 (1966) 1204.

97. F. Borsay and E. Yeager, J. Acoust. Soc. Am. 59 (1978) 596.

98. F. Borsay and E. Yeager, Trans SAEST, 12 (1977) 179.

99. R. E. Malpas, R.A. Fredlein and A.J. Bard, J. Electroanal. Chem. 98 (1979) 339.

100. C.D. Jaeger and A.J. Bard, J. Phys. Chem. 63 (1979) 3146.

101. B. Kastening, Advances in Analytical Chemistry and Instrumentation, Vol. 10, H.W. Nurnberg, ed., John Wiley and Sons, New York City, 1974, pp. 421-494.

102. T.M. McKenney, Electroanalytical Chemistry. Vol. 10, A.J. Bard, ed., Marcel Dekker, New York City, 1979.

103. E. Yeager, W.E. O'Grady, M.Y.C. Woo and P. Hagans, J. Electrochem. Soc. 125 (1978) 346.

104. W.E. O'Grady, M.Y.C. Woo, P.L. Hagans and E. Yeager, Electrode Materials and Processes for Energy Conversion and Storage, J.D.E. McIntyre, S. Srinivasan and F.G. Will, eds., The Electrochemical Society, Princeton, NJ, 1977, p. 172.

105. A.T. Hubbard, R.M. Ishikawa and J. Kalekaau, J. Electroanal. Chem. 86 (1978) 271.

106. R.N. Ross, J. Electroanal. Chem. 76 (1977) 139.

107. R.N. Ross, J. Electrochem. Soc. 126 (1979) 67.

108. R.M. Ishikawa and A.T. Hubbard, J. Electroanal. Chem. 69 (1976) 317.

109. H.O. Beckmann, H. Gerischer, D.M. Kolb and Gunter Lehmpfohl, Faraday Symposium 12, Electrosorption, Nucleation and Phase Formation, The Chemical Society, London, 1977, p. 51.

110. P. Hagans, LEED-Auger-Thin Layer Electrochemical Studies of the Underpotential Deposition of Lead onto Gold Single Crystal Surfaces. Ph.D. Thesis, Chemistry Dept., Case Western Reserve University, Cleveland, 1980.

111. J.P. Biberian and G.E. Rhead, J. Phys., F: Metal Phys. 3 (1973) 675.

112. J. Perdereau, J.P. Biberian and G.E. Rhead, J. Phys., F: Metal Phys. 4 (1974) 798.

LIST OF FIGURES

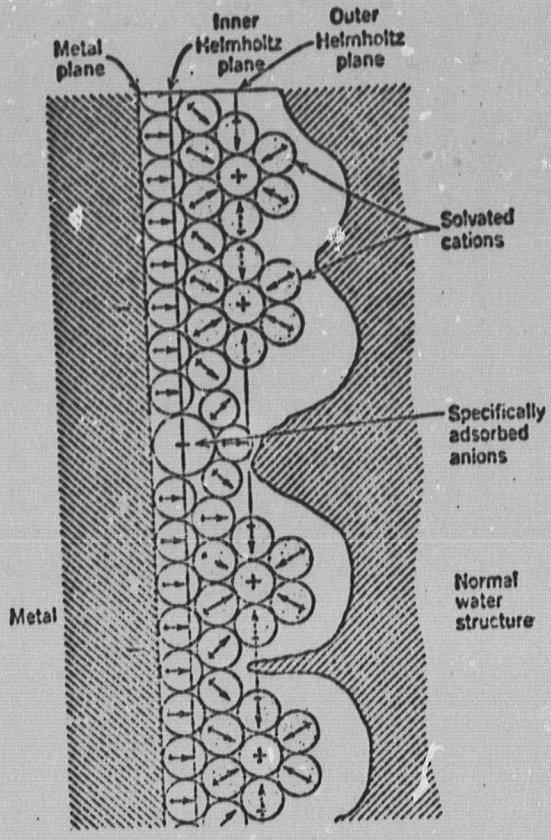

Figure 1. Model for the ionic double layer [Bockris, Devanathan and Muller (1)].

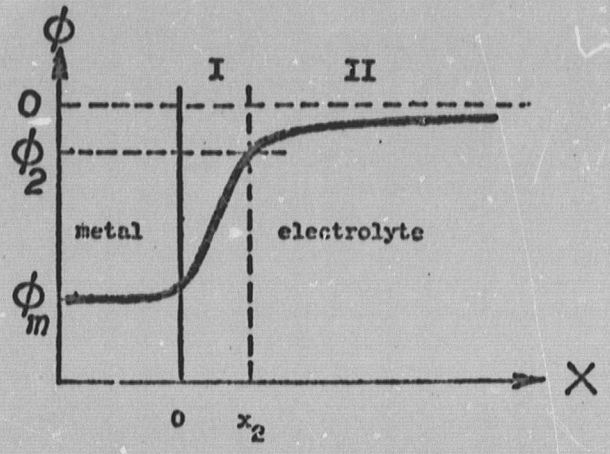

Figure 2. Potential distribution across the metal-electrolyte interface in the absence of specific adsorption.
Region I: Compact layer
Region II: Gouy-Chapman diffuse layer
Plane x_2: outer Helmholtz plane.

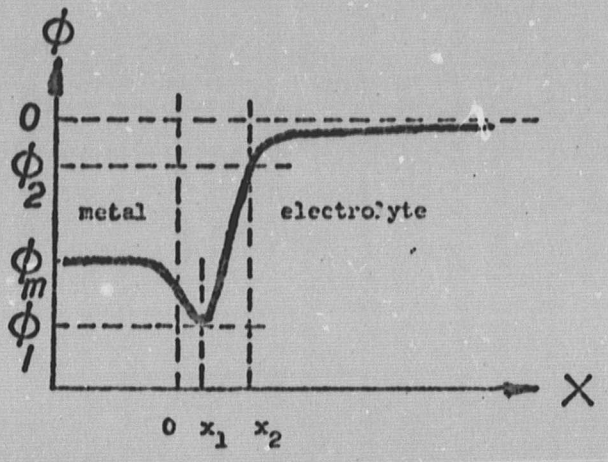

Figure 3. Potential distribution across the metal-electrolyte interface with specific ionic adsorption.

x_2: plane of closest approach without specific adsorption

x_1: plane of closest approach of specifically adsorbed ion.

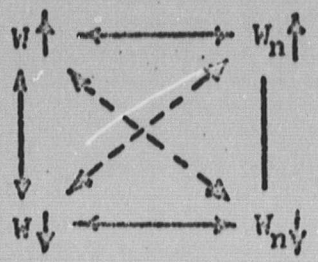

Figure 4. Parsons' four state version (11) of the Damaskin-Frumkin model of water in the compact layer (9,10).

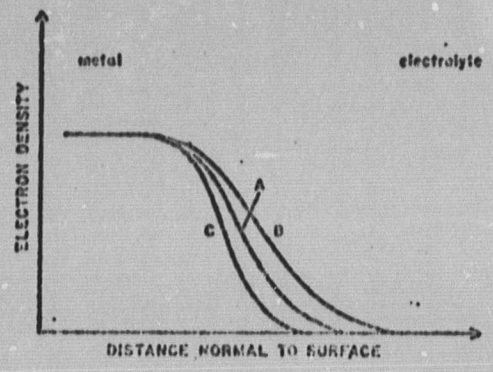

Figure 5. Electron density versus distance at a metal electrode surface. Curve A: at potential of zero charge (pzc). Curve B: cathodic to pzc. Curve C: anodic to pzc.

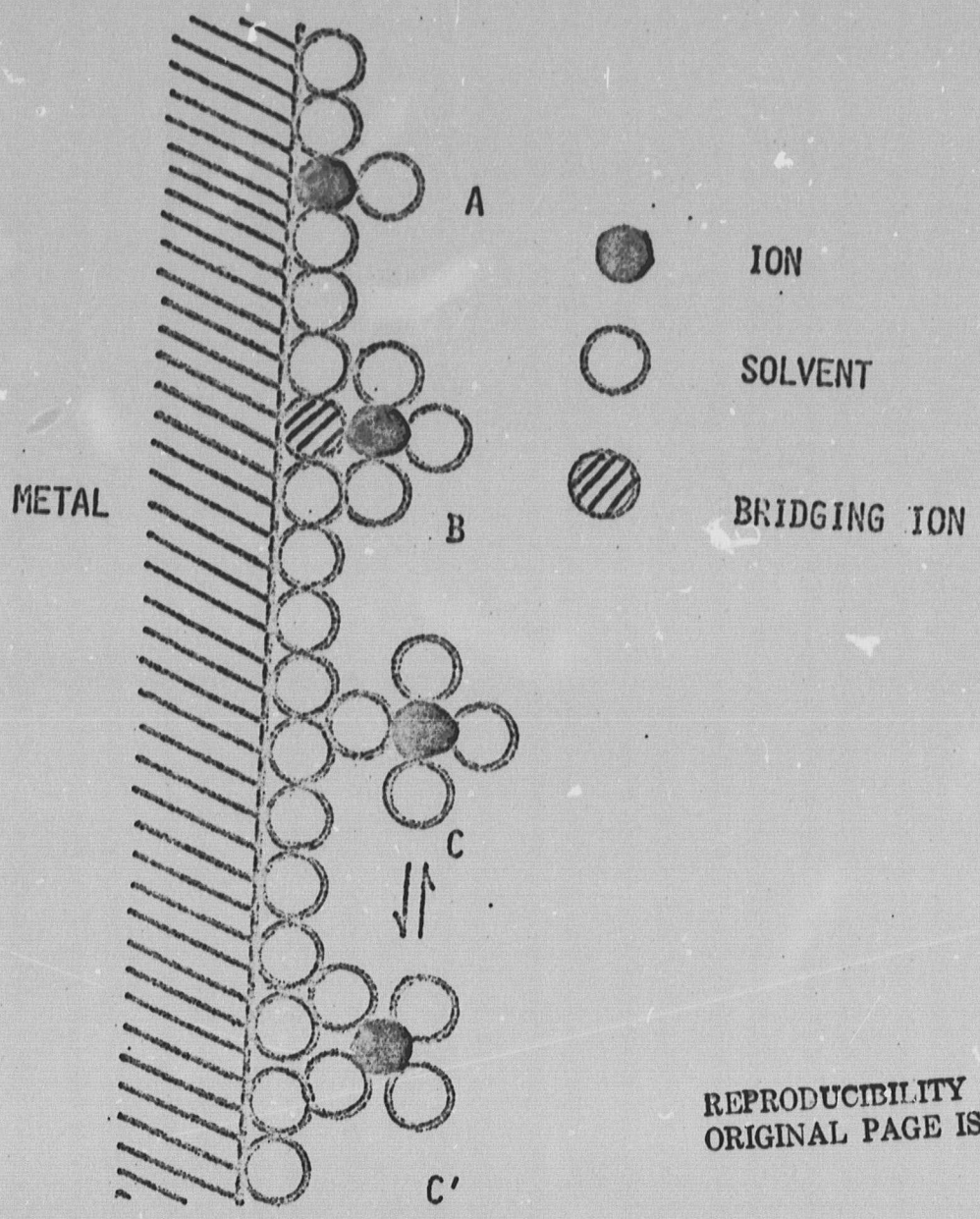

Fig. 6 Positions of reacting ions in electron transfer reactions at metal electrolyte interfaces.
A. specifically adsorbed species; B. bridged species; C,C'. species in outer Helmholtz plane

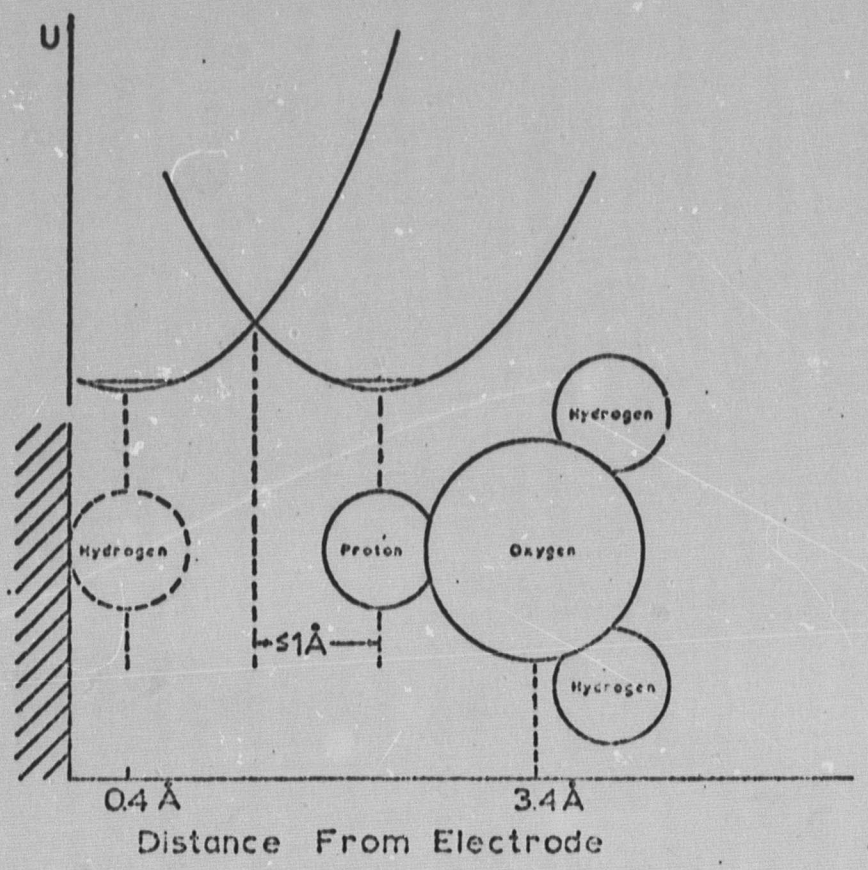

Figure 7. Potential energy surfaces for proton discharge in the Bockris-Matthews model (48).

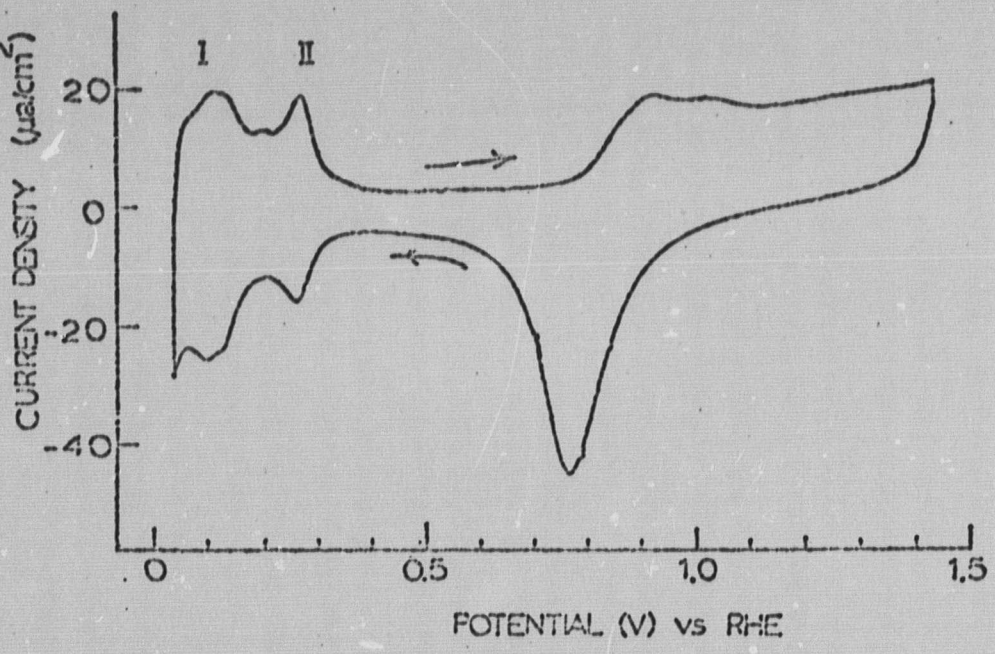

Figure 8. Voltammetry curve for polycrystalline platinum in a thin-layer electrochemical cell with an α-Pd/H counter-reference electrode (104). Potentials are expressed relative to the reversible hydrogen electrode. Electrolyte: 0.05 M H_2SO_4; electrolyte gap: 10^{-3} cm; temperature: ~25°C; voltage sweep rate: 20 mV/s.

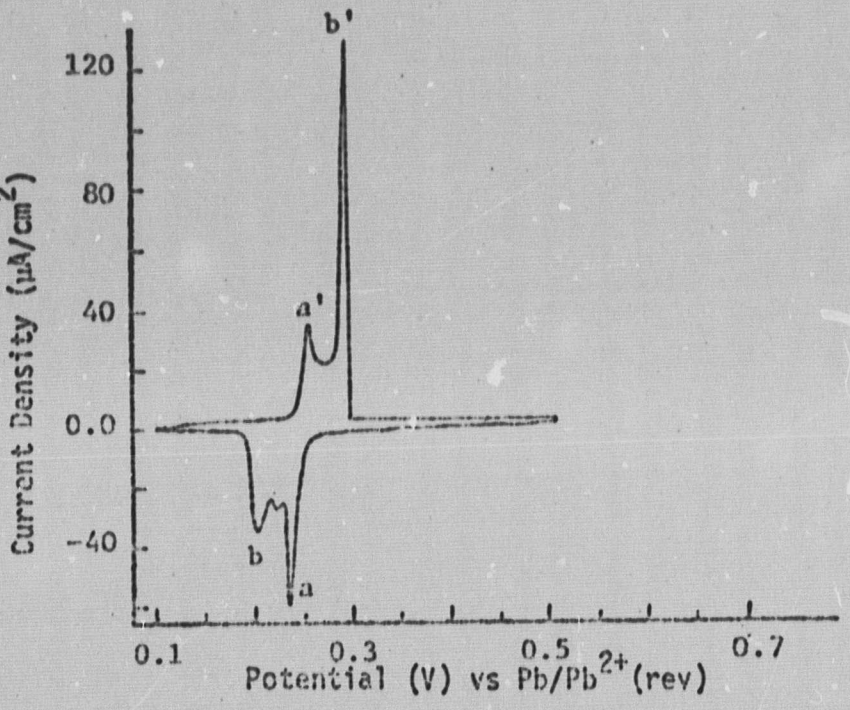

Figure 9. Voltammetry curve for the underpotential deposition of lead in Au(111)-(1x1) in 0.1 M HF + 1 mM $Pb(NO_3)_2$, using a thin layer cell. Gap: 10^{-3} cm; sweep rate: 20 mV/s; temperature: ~ 25°C.

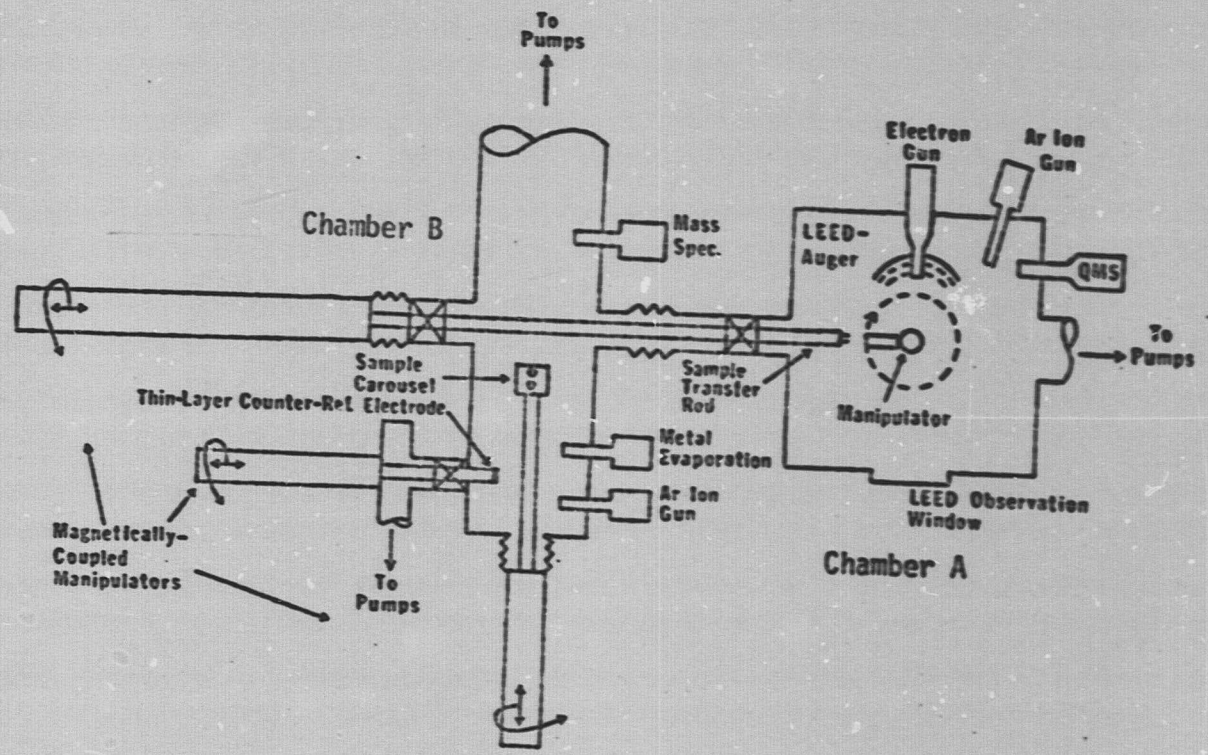

Figure 10. The LEED-Auger-thin layer electrochemical cell system at Case (110).

TABLE I. NON-TRADITIONAL IN SITU TECHNIQUES FOR THE STUDY OF SOLID ELECTROLYTE INTERFACES

PRESENT

I. Optical

A. UV-visible, infrared

- specular reflectance spectroscopy: external, internal
- ellipsometry - as a spectroscopic tool
- diffuse reflectance spectroscopy
- photoacoustic spectroscopy

B. Raman spectroscopy

C. Photoassisted processes, including photoemission

II. Mössbauer spectroscopy

III. Acoustoelectrochemical measurements

- shear wave generation
- compressional wave generation

IV. Electron spin resonance

PROMISING POSSIBILITIES

V. EXAFS

VI. NMR

- broadline
- high resolution

TABLE II. EX SITU TECHNIQUES FOR THE STUDY OF ELECTRODE SURFACES

I. Electron Physics

X-ray photoelectron spectroscopy (XPS)
Ultraviolet photoelectron spectroscopy UPS)
Auger spectroscopy
Electron energy loss spectroscopy
Low energy electron diffraction (LEED)
Reflection high energy electron diffraction (RHEED)
Inelastic electron tunnelling
Transmission electron microscopy - diffraction

II. Ion Beams

Ion scattering spectroscopy
Secondary ion mass spectroscopy